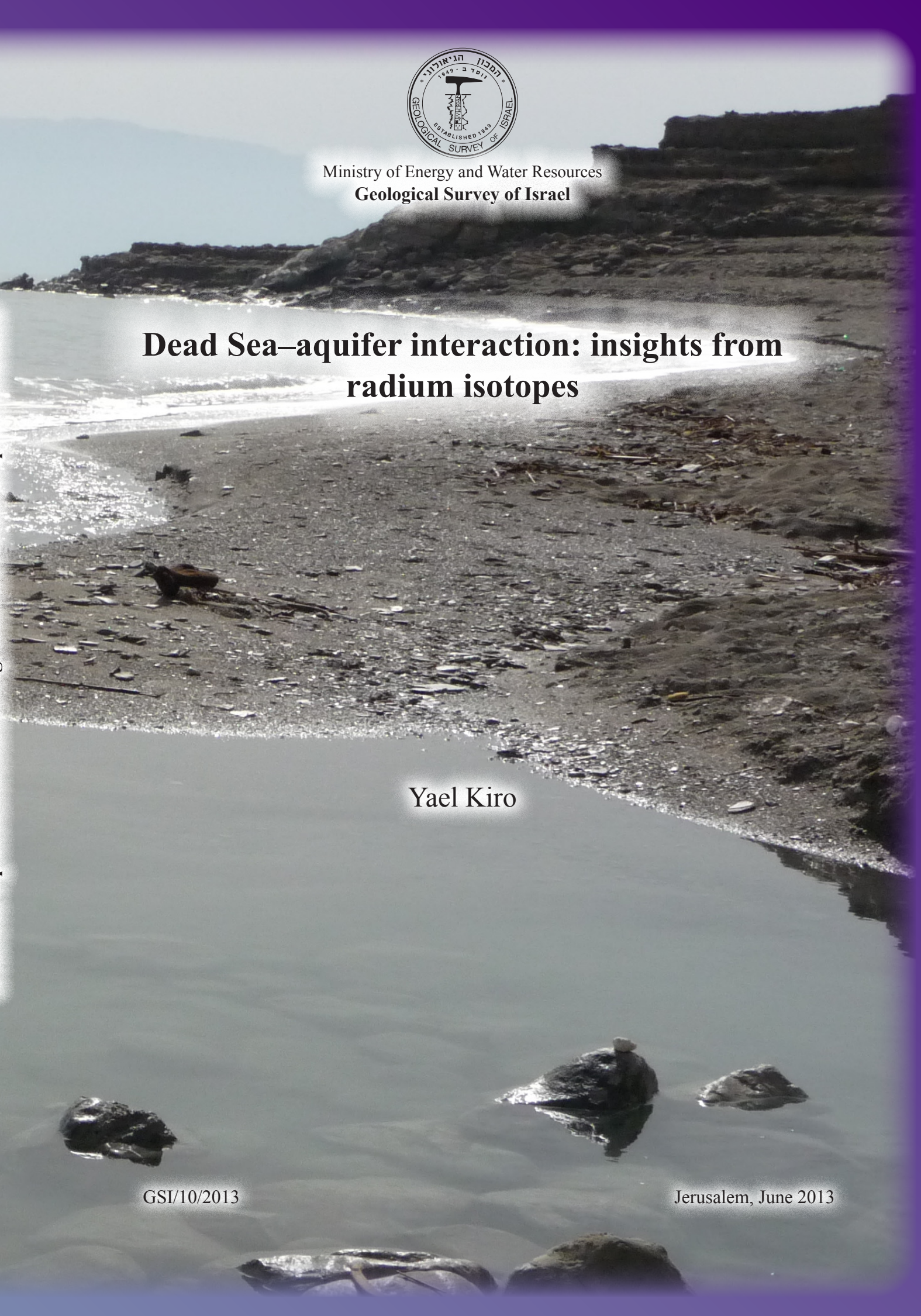


Ministry of Energy and Water Resources
Geological Survey of Israel

Dead Sea–aquifer interaction: insights from radium isotopes

Yael Kiro

GSI/10/2013

Jerusalem, June 2013

Ministry of Energy and Water Resources
Geological Survey of Israel

Dead Sea–aquifer interaction: insights from radium isotopes

Yael Kiro

This thesis was submitted for the degree "Doctor of Philosophy" to the senate of the Hebrew University of Jerusalem, Israel.

The study was carried out under the supervision of:
Prof. Abraham Starinsky, The Institute of Earth Sciences, The Hebrew University, Israel
Dr. Yoseph Yechieli, Geological Survey of Israel
Dr. Yishai Weinstein, Department of Geography and Environment, Bar-Ilan University, Israel

Report GSI/10/2013 Jerusalem, June 2013

Acknowledgments

First, I would like to thank my advisors, Prof. Yosseph Yechieli, Dr. Yishai Weinstein and Prof. Abraham Starinsky, for their knowledgeable guidance and kind support and for encouraging me to explore new ideas and to develop them into well-defined concepts.

Special thanks also to the dissertation committee, Prof. Yehoshua Kolodny, whose door was always open and always welcomed me to discuss anything and for his insightful ideas, Prof. Boaz Lazar and Dr. Ittai Gavrieli for many fruitful discussions and constructive suggestions.

Thanks to Prof. Amitai Katz and Prof. Mordechai Stein for many fruitful discussions about the geochemistry of the Dead Sea. Thanks to Prof. Yigal Erel for very constructive and fruitful discussions about water–rock interaction. Thanks to Dr. Nadav Lensky for the cruises in the Dead Sea lake and for fruitful discussions about the Dead Sea limnology. Thanks to Dr. Mariana Stiller for reviewing part of this thesis and contributing many good suggestions. Thanks to Dr. Efrat Morin for many useful discussions and helping with the mass balance model. Thanks to Dr. Yair Rosenthal for fruitful discussions.

I would like to warmly thank all the students that helped me at the counting lab and in the field: Mor Feldman, Avishai Abbo, Hagar Hauzer and Yael Neumeier who helped me with sample measurements. Many thanks to Haim Hemo, Shlomo Ashkenazi, Hallel Lutzky and Iyad Swaed for accompanying me in the field.

Warm thanks to the GSI lab staff - Dr. Ludwik Halicz, Dr. Olga Yoffe, Dina Stiber and Natalya Teplyakov for the trace and major element measurements. I wish to thank William C. Burnett and Kirstin Eller (FSU) for the ^{228}Ra measurements by γ-spectrometry.

Thanks to Chana Netzer-Cohen, Bat-Sheva Cohen and Nili Almog of the Israel Geological Survey for their assistance with the graphic work throughout my studies.

Thanks to Yoav Rosenberg and Itay Reznik for many fruitful discussions about the geochemistry of the Dead Sea. I especially would like to thank Yoav for his assistance with measurements.

I am thankful to Yosi Sherer, who was always available, taught me and helped me a lot

in the lab. Thanks to Andrei Podelko who swiftly solved any electronic problem in the lab.

Very warm thank to the Institute of Earth Sciences staff – Batya Moshe, Magiuy Perkin, Dikla Hanukkah, Shoshana Bousheri and Keren Shoshana who was always kind and helpful with any request.

Thanks to the teachers of the Institute of Earth Sciences who advised and taught me throughout my PhD studies – Ari Matmon, Ronit Kessel, Oded Navon, Jonathan Erez, Boaz Luz and Yehuda Enzel.

I am much indebted to the opportunity to take part in and Sylvia Hoffman Leadership and Responsibility Fellowship Program, for the financial support and for the opportunity to take part in a unique program which enriched me with another dimension of my PhD studies. I would like to thank the program directors, Amalya Oliver, Ehud de Shalit, Roi Baer and Lital Myers and all of my friends from the extended "Hoffman family".

I am grateful for the financial support granted by the Wolf foundation, Rieger-JNF fellowship, BSF travel grant and the Israel Association of University Women.

I would like to thank all of my close friends at the institute of earth sciences for their companionship and moral and practical support: Uri Ryb, Navot Morag, Yehuda Shalem, Reuven Belmaker, Yair Rinat, Shalev Siman-tov, Yona Geler, Elad Levanon, Imri Oz, Eyal Wurgaft, Zvika Steiner, Yael Levinson, Daniel Palchan, Netta Shalev, Galit Sharabi, Orly Goren, Tamar Ryb and Olga Zlatkin.

I want to thank my parents and my sister and brother: Sara, Shmuel, Ruti and Avner for their moral support and unwavering support of my research. I thank my mother in particular for her great help with my three children.

Thanks to Rachel, Yiftah and Nitai, children, for their patience.

Last, I would like to thank my husband, Doron Feldman, without whom I couldn't have done all of this. Thanks for taking care of the children and home, allowing me to focus my attention on my research. Thanks for his patience, support and love.

Abstract

Seawater circulation in coastal aquifers, a major component of submarine groundwater discharge (SGD), is now widely recognized as a major process affecting trace element and nutrient mass balances in coastal areas. Estimates of SGD vary over several orders of magnitude (1-10^6 m^3/y per meter shoreline). These estimates are sensitive to fresh–saline SGD ratios and to the temporal and spatial scales of the circulation, which range from wave setup and tidal-driven small-scale circulation through seasonal scale and up to the large-scale dispersive circulation along the fresh–saline water interface. In oceanic settings most circulation types occur together, making it hard to define the contribution and effect of each process.

The Dead Sea system is an excellent natural field lab for studying seawater–groundwater interaction and large-scale circulation due to the absence of tides and to the minor role played by waves. During Dead Sea water circulation in the aquifer several geochemical reactions occur, ranging from the short-term adsorption-desorption reactions and up to the long-term precipitation and dissolution reactions. All of these processes affect the trace element distribution in the saline groundwater and may also affect the chemical composition of the Dead Sea. This study focuses on seawater circulation in the aquifer and highlights the significance of the relationship between the circulation and water–rock interaction time scales in terms of the potential affect on elemental mass balances.

Na/Cl ratios and ^{228}Ra ($t_{1/2}$=5.75 y) vary in the saline groundwater and were used to estimate the velocities of Dead Sea water circulating in the coastal aquifer. Na/Cl decrease during the past few decades in the Dead Sea was used in order to estimate the velocity of the circulated Dead Sea water inflow from the lake into the aquifer. Dead Sea water enters the aquifer with low activities of ^{228}Ra ($\sim$1 dpm/L), which increase gradually with distance from shore until it reaches equilibrium with the aquifer sediments (steady-state activities of $\sim$30 dpm/L). The rate of ^{228}Ra accumulation in the circulated Dead Sea water may be used to determine groundwater velocity. Both methods show that the saline water flow from the lake into the aquifer and the calculated velocities are several meters per year (1–6 m/y).

The hypersaline water of the Dead Sea (TDS of 340 g/L) is supersaturated with barite

and celestine, which appears to precipitate during Dead Sea water circulation in the aquifer, reducing barium (from 5 to 1.5 mg/L), strontium (from 350 to 300 mg/L) and the long-lived ^{226}Ra (from ~147 to ~60 dpm/L) in the saline groundwater. Redox-controlled reactions also affect the chemistry of the circulated Dead Sea water, causing a decrease in uranium from 2.4 to 0.1 μg/L, an increase in Fe from 1 to 13 mg/L and an increase in Mn from 7 to 9 mg/L.

Based on the calculated velocities, rate constants were calculated for certain reactions applying steady-state one-dimensional mass balances along the hypesaline groundwater flow path from the lake into the aquifer. The order of the rate constants of the Dead Sea aquifer was found to be: $k_{SO_4} > k_U > k_{Ba} = k_{Sr} = k_{Ra} > k_{Mn} > k_{Fe}$.

The sequence of the redox-controlled reactions is different from that described in other oceanic setting, resulting in a faster removal of U relative to the contribution of Fe and Mn. This may be explained by adsorption of oxidized U or by the different microbiology of the Dead Sea system.

A detailed survey of the radium sources around the Dead Sea shows that the radium isotopic ratio of groundwaters in the Dead Sea is affected by the Th/U ratio of the aquifer rocks, the groundwater age and flow mechanism. Groundwater from the east and the west of the Dead Sea has different isotopic ratios. ^{228}Ra/^{226}Ra and ^{224}Ra/^{223}Ra ratios are higher in the east due to the higher Th/U ratio in the sandstone aquifer. ^{226}Ra/^{223}Ra and ^{224}Ra/^{228}Ra ratios in young groundwater (such as the circulated Dead Sea water) or in recently mixed groundwater (such as in the fresh–saline transition zone or in the Kane and Samar springs) deviate from secular equilibrium while older groundwater (such as at Ein Feshkha, Ein Qedem and in the eastern catchment of the Dead Sea) contain secular equilibrium ratios of the radium isotopes and may be an indication of the longer period of water–rock interaction.

^{222}Rn activities are significantly high in most of the Dead Sea groundwater, and may be in excess of 100% of the ^{222}Rn produced by the aquifer rocks, suggesting a major contribution by adsorbed ^{226}Ra. The highest activities are found in the thermal brines, both at the east and west of the Dead Sea and in Ein Feshkha which may be related to the increase in adsorbed ^{226}Ra due to the decrease in salinity or water temperature (during the ascent of thermal brines).

In the fresh–saline transition zone, the short-lived radium isotopes (^{223}Ra and ^{224}Ra) and ^{222}Rn have a half-life of several days and are produced relatively fast from the aquifer sediments, which is their main source, reaching steady-state activities in several weeks. The short-lived radium isotopes increase with salinity nonlinearly, while ^{222}Rn is related with

salinity by a second-order polynomial, where the maximal ^{222}Rn concentration is in the intermediate salinities (∼2500 dpm/L). These relationships of the short-lived isotopes with salinity can all be explained by a linear relationship between the adsorption distribution coefficients of radium (K) and salinity.

While the short-lived isotopes are only an indication of the relationship between K and salinity, the linear relationship between the long-lived ^{226}Ra and salinity, given the dynamic conditions of the Dead Sea level drop, constrains the absolute value of K.

In order to study the behavior of all radium isotopes in dynamic conditions of a coastal aquifer, a multi-species density-dependent groundwater flow model (SUTRA-MS) was used. The simulations calculated the change in radium distribution in the dynamic system of the Dead Sea, where the lake level drops at a rate of 1 m/y. The effect of K on the distribution of each of the radium isotopes during lake level changes depends on the isotope half-life. The response of the short-lived radium isotopes is not affected by K while the response of ^{226}Ra is retarded when the retardation factor ($R = K + 1$) is large. Therefore, the relationship between ^{226}Ra and salinity, which is linear, constrains the maximal value of K and should allow a response of the ^{226}Ra distribution to the lake level drop. Hence, the value of K in the circulated Dead Sea water and in the fresh groundwater should be up to 0.6 and 100, respectively. These values of K cannot cause the observed decrease in ^{226}Ra from ∼147 to ∼60 dpm/L and therefore support the conclusion of barite/celestine precipitation. The K's obtained here for fresh water are lower than those found in other studies, as well as in some fresh/brackish springs next to the Dead Sea (e.g. Ein Feshkha springs).

The decrease in ^{226}Ra and the increase in ^{228}Ra in the circulation process provide a robust method to assess the extent of the Dead Sea water circulation in the aquifer. Using the lake radium concentration from the 1970's, it is estimated that the circulation under steady-state conditions of the lake is on the order of 320 million m^3/y (∼2 million m^3/y per km shoreline). This volume of water does not affect the water budget but has a great potential of affecting trace element concentrations in the Dead Sea, suggesting that long-term seawater circulation is significant to oceanic mass balances as well.

Contents

List of Figures ix

List of Tables xi

1 Introduction 1

1.1 Groundwater flow dynamics in coastal aquifers . . . 1
1.2 Submarine groundwater discharge . . . 3
1.3 The Dead Sea . . . 4
1.3.1 The Dead Sea water chemistry and evolution . . . 5
1.3.2 Hydrogeology of the Dead Sea basin . . . 6
1.4 Radon and radium isotopes in natural water . . . 7
1.4.1 Radon and radium in the Dead Sea system . . . 9
1.5 Research Goals . . . 10

2 Methods 12

2.1 Sampling . . . 12
2.2 Radium adsorption onto MnO_2-coated acrylic fibers . . . 12
2.3 Radium and radon isotope measurements . . . 14
2.3.1 ^{222}Rn and ^{226}Ra . . . 14
2.3.2 ^{223}Ra and ^{224}Ra measurements . . . 16
2.3.3 ^{228}Ra measurements . . . 16
2.4 Major and trace element measurements . . . 17
2.5 Modeling radium distribution in dynamic density-dependent flow conditions 18

3 Groundwater ages and reaction rates during seawater circulation in the Dead Sea aquifer 19

3.1 Introduction . . . 19

3.1.1 Radon and Radium isotopes . . . 20
3.1.2 The Dead Sea hydrological system . . . 21
3.2 Methods . . . 22
3.3 Results and discussion . . . 23
3.3.1 Groundwater ages and flow velocities . . . 24
3.3.2 Reaction rates in the hypersaline groundwater . . . 30
3.3.3 Processes in the fresh-saline transition zone . . . 37
3.4 Summary . . . 42

4 Modeling radium distribution in coastal aquifers during sea level changes: The Dead Sea case (GCA, 2012) 44

5 Radon and radium in the hydrological system of the Dead Sea 63
5.1 Introduction . . . 63
5.1.1 The behavior of radon and radium isotopes in groundwater . . . 64
5.1.2 The Dead Sea hydrological and geochemical system . . . 65
5.2 Methods . . . 68
5.3 Results . . . 69
5.3.1 $^{228}Ra/^{226}Ra$ and $^{224}Ra/^{223}Ra$ ratios . . . 69
5.3.2 $^{226}Ra/^{223}Ra$ and $^{224}Ra/^{228}Ra$ ratios . . . 71
5.3.3 ^{226}Ra, ^{223}Ra and ^{222}Rn relationship . . . 73
5.3.4 ^{222}Rn in the Dead Sea system groundwaters . . . 73
5.4 Discussion . . . 77
5.4.1 Radium isotope composition and Th/U ratio of the aquifer rocks . . . 77
5.4.2 The source of ^{222}Rn to the Dead Sea system groundwater . . . 78
5.4.3 Groundwater age and secular equilibrium ratios of radium isotopes . . . 79
5.4.4 The mass balances of ^{226}Ra, ^{223}Ra and ^{222}Rn . . . 81
5.4.5 The adsorption of radium . . . 83
5.4.6 The thermal brine of Ein Qedem . . . 84
5.5 Summary and conclusions . . . 86

6 The role of long-term aquifer seawater circulation in elemental mass balances: a lesson from the Dead Sea 87
6.1 Introduction . . . 87
6.1.1 Radium isotopes . . . 88

6.1.2 The Dead Sea system . . . 88
6.2 Methods . . . 89
6.3 Results and discussion . . . 90
6.3.1 Radium in the Dead Sea . . . 90
6.3.2 Dead Sea Water Circulation in the Aquifer . . . 92
6.3.3 Radium Mass Balance in the Dead Sea . . . 95
6.4 Implications . . . 101
6.4.1 The Dead Sea trace element mass balances . . . 101
6.4.2 Long-term circulation in coastal aquifers . . . 101
6.5 Conclusions . . . 103

7 Summary and conclusions **104**

Appendices **107**

A SGD estimates from different studies **108**

B ^{228}Ra mass balance in the groundwater including co-precipitation with barite **114**

C Additional data of samples **116**

D ^{226}Ra and ^{228}Ra activities in the Dead Sea **121**

E ^{226}Ra and ^{228}Ra activities in circulated Dead Sea water **125**

Bibliography **126**

List of Figures

1.1 The dispersive seawater circulation in the aquifer 2
1.2 Types of seawater circulation 3
1.3 The decay chain of U and Th series. 8

2.1 Location map. (a) Regional, (b) Dead Sea map (c) Arugot alluvial fan. . . . 13
2.2 Adsorption efficiency on MnO_2-coated fibers of diluted Dead Sea water. The error bars represent the analytical error. 14
2.3 Calibration plot of ^{226}Ra standards for using the RAD7. 15
2.4 Results of bubbling test in the RAD7. 15
2.5 The growth of ^{228}Th due to the decay of ^{228}Ra. 17
2.6 ^{226}Ra measurements using the γ-spectrometry method compared with the emanation technique 18

3.1 Groundwater composition cross sections in Arugot alluvial fan aquifer 27
3.2 The change in Na/Cl ratio in the Dead Sea water during the past fifty years 28
3.3 Calculated and measured ^{228}Ra activities in circulating Dead Sea water . . . 30
3.4 Concentrations of ^{226}Ra, Ba and Sr in the hypersaline groundwater with distance from shore 33
3.5 (a) Sulfate concentrations in the circulating Dead Sea water with distance from shore, (b) the relationship betewwn sulfate and salinity in groundwater of the Dead Sea coastal aquifer. 35
3.6 Concentrations of Fe, Mn and U in the circulated Dead Sea water 36
3.7 Degree of saturation of barite in the fresh–saline groundwater transition zone 38
3.8 ^{224}Ra activities versus salinity in groundwater 39
3.9 Excess ^{222}Rn over salinity in the Dead Sea aquifer groundwater 40

5.1 The relationship between ^{228}Ra and ^{224}Ra activities in the Dead Sea groundwater 70

5.2 The relationship between ^{226}Ra and ^{223}Ra activities in the Dead Sea groundwater. 70
5.3 ^{228}Ra/^{226}Ra and ^{224}Ra/^{223}Ra ratios in groundwater around the Dead Sea . . 71
5.4 ^{228}Ra/^{226}Ra vs. ^{224}Ra/^{223}Ra ratio in groundwater around the Dead Sea . . . 72
5.5 A ternary diagram of ^{226}Ra, ^{223}Ra and ^{222}Rn with plotted groundwater samples demonstrating processes affecting the relationship between these three isotopes 73
5.6 ^{226}Ra/^{223}Ra and ^{224}Ra/^{228}Ra ratios along a flow path 85

6.1 ^{226}Ra and ^{228}Ra profiles in the Dead Sea during the meromictic period of the Dead Sea and at present 91
6.2 Cross sections of Arugot alluvial fan groundwater (salinity and trace elements) 93
6.3 Ba and ^{226}Ra versus density at the fresh–saline transition zone 94
6.4 A summary of the sources and sinks of radium in the Dead Sea 103

List of Tables

2.1 Efficiencies of the different channels in RaDeCC 16

3.1 Major elements and composition of the Dead Sea water and of the groundwater from the adjacent aquifer 25
3.2 Activities of radon and radium isotopes in the Dead Sea water and groundwater 26
3.3 Trace element concentrations in the Dead Sea water and groundwater 31
3.4 Degrees of saturation of barite celestine and gypsum in the Dead Sea and in the groundwater 34

5.1 Radium and radon activities and ratios in water around the Dead Sea 74
5.2 Radium isotopic ratios in Ein Qedem and estimated velocity 84

6.1 Averaged concentrations of trace elements and radium isotopes in the circulated Dead Sea water and in the lake 91
6.2 Radium and barium in the main water sources of the Dead Sea. 95
6.3 Model parameters and output. 96
6.4 Sources and sinks of radium in the Dead Sea 97
6.5 Input and output by decay of radium in the Dead Sea 99
6.6 Inventory and fluxes of several trace elements, based on the concentrations in table 6.1, due to Dead Sea water circulation in the aquifer. 101

A.1 SGD estimates from different studies 109

C.1 Groundwater samples parameters and major element concentrations. 117
C.2 Concentrations of trace elements in the Dead Sea groundwater. 120

Chapter 1

Introduction

The dissertation is written in a format of individual chapters and is divided into seven parts: introduction, methods, four chapters that are based on articles and summary and conclusions. Chapter 4 was published in *Geochimica et Cosmochimica Acta* in 2012, while chapter 3 has been submitted and 6 is ready for submission to peer-reviewed journals. Due to this structure there are some repetitions in the text, mainly in the general sections.

Chapter 3 describes the geochemical processes during Dead Sea water circulation in the aquifer and derives the groundwater velocity and the rates of the geochemical processes. Chapter 4 deals with the response of the distribution of the radium isotopes to the Dead Sea lake level drop, and provide estimations of the adsorption–desorption partition coefficient of radium and its dependence on salinity. Chapter 5 describes the results of radium analysis of a detailed survey of the water sources around the Dead Sea and interpretation of the radium composition of these water sources. Chapter 6 details the radium mass balance of the Dead Sea, which is based on the results in chapters 3 and 5, and provide the estimation of the annual volume of Dead Sea water circulation in the aquifer.

1.1 GROUNDWATER FLOW DYNAMICS IN COASTAL AQUIFERS

Generally, in a coastal aquifer, fresh groundwater flows above saline water, which penetrates the aquifer due to density differences. The two water bodies are separated by a fresh–saline transition zone. In steady-state, the flow dynamics and configuration of this system is mainly affected by the density differences, the hydraulic gradient, hydraulic conductivity, porosity, hydrodynamic dispersion and other hydrological parameters (Henry, 1964).

The fresh-saline interface occurs as a transition zone due to dispersive mixing of the fresh groundwater that flows above the saline groundwater body. The inflow of seawater into

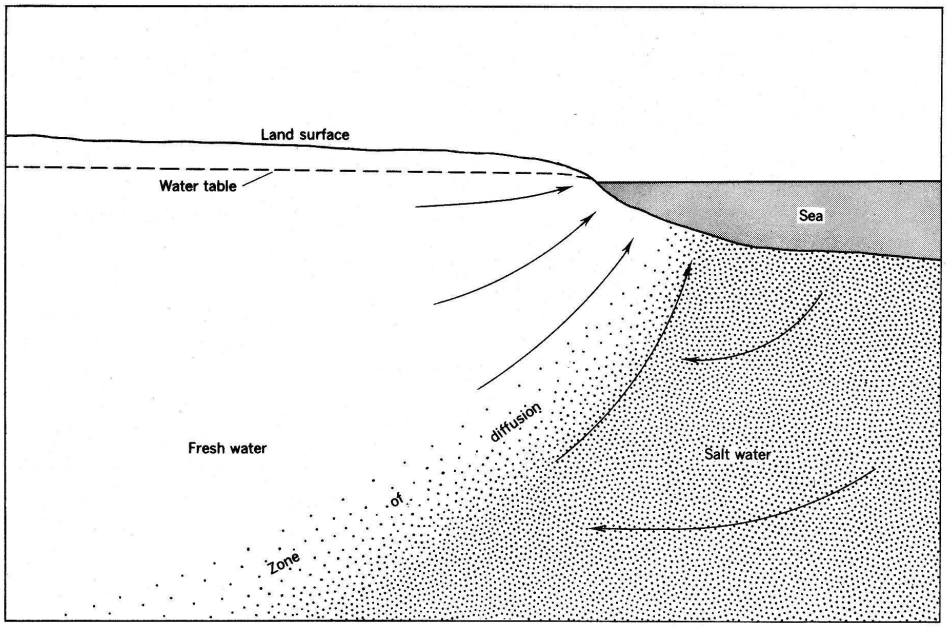


Figure 1.1: The dispersive seawater circulation in the aquifer (Cooper, 1959).

the aquifer due to the density differences and the outflow of saline groundwater toward the sea through the transition zone cause saline water circulation in the aquifer (Cooper, 1959, Figures 1.1, 1.2).

Together with this basic dispersive circulation there are other types of seawater circulation in the aquifer driven by sea level changes or seasonal changes in the groundwater system that vary by their spatial and temporal scales. Tides and waves drive nearshore circulation in the aquifer (Longuet-Higgins, 1983; Robinson et al, 1998; Li et al, 1999), while deeper circulation occurs due to tidal pumping (Li et al, 1999). Seasonal scale of seawater circulation in the aquifer also occurs due to changes in sea level or in the groundwater system (Michael et al, 2005) and a small-scale circulation in a rippled continental shelf permeable sand driven by waves or currents, which may be deep, has also been shown (Webb and Theodor, 1972; Reimers et al, 2004, Fig. 1.2).

All circulation types were widely studied, mainly by modeling, both analytically and by numerical simulations (e.g. Henry, 1964; Li et al, 1999; Michael et al, 2005; Robinson et al, 2006; Kiro et al, 2008). However, being not readily accessible and difficult to observe, seawater circulation was hardly studied in the field. When studied, it was usually limited to the small-scale circulation types (e.g. Michael et al, 2005; Reimers et al, 2004; Charette and Sholkovitz, 2006) and was either about the reactions taking place in the fresh–saline transition zone (the *subterranean estuary*, Charette and Sholkovitz, 2006) or about the volumes

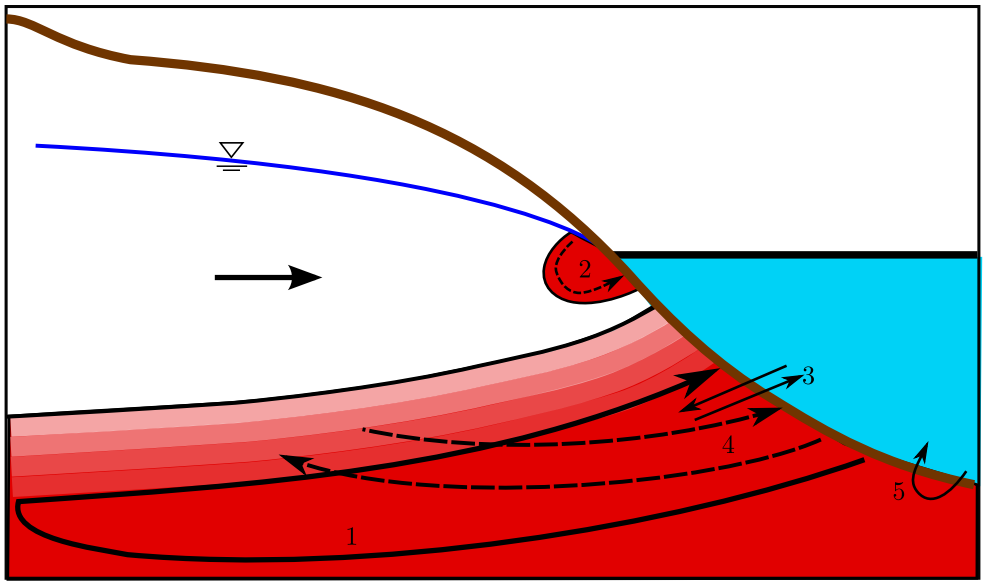


Figure 1.2: Types of seawater circulation. 1) dispersive circulation (Cooper, 1959). 2) nearshore circulation driven by tides and waves (Longuet-Higgins, 1983; Robinson et al, 1998; Li et al, 1999). 3) Tidal pumping (Li et al, 1999). 4) Seasonal changes in the groundwater system or the sea level (Michael et al, 2005). 5) Advective solute transport in rippled continental shelf sands driven by waves or currents (Webb and Theodor, 1972; Reimers et al, 2004).

of water involved (Moore, 1996; Moore et al, 2008).

1.2 SUBMARINE GROUNDWATER DISCHARGE

Submarine Groundwater Discharge (SGD) is now widely recognized as a major coastal process and is an important factor in coastal water mass balances (e.g. Simmons, 1992; Moore, 1996). SGD is assessed by various methods, including hydraulic gradient models or standard water balance considerations, as well as seepage meter measurements (Simmons, 1992) and radioisotope tracers such as radon (e.g. Burnett and Dulaiova, 2003; Weinstein et al, 2007b) and radium isotopes (e.g. Moore, 1996). SGD estimates vary over several orders of magnitude, between 1 and 10^6 m^3/y per meter shoreline (Appendix A), representing the natural spatial variability in hydrological, geological and climatological parameters (Burnett et al, 2001; Taniguchi et al, 2002; Gallardo and Marui, 2006).

SGD is composed of fresh (terrestrial) groundwater and circulated seawater including the circulation types mentioned in section 1.1. The largest fresh SGD estimates are in humid areas and under large river outlets (e.g., Taniguchi et al, 2008; Dowling et al, 2003, Appendix A). Nonetheless, most SGD is of circulated seawater, which may also be significant to mass balances of certain elements in the ocean (Moore et al, 2008).

The effect of SGD (both marine and terrestrial) in oceanic mass balances was hardly studied. SGD was shown to contribute Ca, Ba and Sr to the Bengal Basin in the same order of magnitude as river fluxes suggesting reevaluation of Sr isotopes in the oceanic budgets (Basu et al, 2001; Dowling et al, 2003). Also, Charette and Sholkovitz (2006) pointed out the importance of seawater circulation as an uranium sink. Though, the volumes of water are not large (compared with river fluxes), however, due to the enhanced water–rock interaction, they may have the potential to affect the budgets of certain elements in the ocean.

The motivation for the current study lies in the fact that in order to understand the actual effect and contribution of SGD to the ocean, one should carefully study the various circulation types, their temporal and spatial scales and their sensitivity to hydrological parameters. The effect of seawater circulation on seawater chemistry should be directly dependent on the circulation time scale, where long-term circulation has a greater potential to affect water composition, due to the longer water–rock interaction.

The Dead Sea and its coastal alluvial aquifer, with a very shallow fresh–saline transition zone provides a unique opportunity for a detailed study of seawater circulation. The insignificance of waves and the absence of tides allow a focused study of the long-term (tens of years) dispersive seawater circulation and to study its potential impact on trace element mass balances.

1.3 THE DEAD SEA

The Dead Sea is a terminal lake located in a deep pull-apart basin along the Dead Sea Transform fault which drains groundwater and surface water from a wide area. The deepest point in the lake is about -720 m. It is a terminal hypersaline lake with a current area of 620 km^2 and a drainage basin of 40,000 km^2. The lake level has been dropping from -390m in the 1930's (Klein and Flohn, 1987) to ~ -427m at the end of 2012, with a steeper decline since the 1960's reaching a rate of 1.1 m/y during the last few years. This level decline is the result of the increased utilization of water in the northern part of the basin, particularly the creation of the Israeli National Water Carrier in the 1960's and of the Jordanian Jordan Valley (King Abdullah) Canal in the 1970's. The Israel Dead Sea Works and the Jordanian Arab Potash Company significantly added to this negative balance by increasing the evaporation from the lake. Altogether, these changes in water management resulted in a decrease of the average annual inflow to the lake from 1600–2000 million m^3 in the early 1900's (Klein, 1998; Neumann, 1958; Salameh and El-Naser, 1999) to a current 265–335 million m^3 (Lensky et al, 2005). Assuming the present climate conditions, the evaporation is expected to decrease due

to a decrease both in surface area and in the evaporation rate, a result of the increasing salinity (Yechieli et al, 1998; Krumgalz et al, 2000). Calculations show that the Dead Sea is expected to reach steady state in about 300 years at a level of around -550m (Yechieli et al, 1998).

Until 1979, the Dead Sea was meromictic with an upper water mass that received inflows from sources such as rivers, springs and submerged groundwater and a lower water mass which remained isolated due to its higher salinity. In 1959 the pycnocline was at a depth of 40m and there was a significant density difference between the lower and upper water masses (1.233 kg/L and 1.205 kg/L, respectively). The declining lake level and the negative water balance caused an increase in the density of surface water which lead to a gradual increase in the depth of the pycnocline during the 1970's and eventually to a complete overturn in 1979 (Steinhorn et al, 1979; Steinhorn, 1985). Since then, the lake changed to a monomictic regime (Anati et al, 1987; Lensky et al, 2005). Estimates of the duration of meromixis in the lake range between 170 to 320 years (Assaf and Nissenbaum, 1977; Stiller and Chung, 1984; Chung and Craig, 2004).

Based on energy and mass balances, the annual influx to the Dead Sea is calculated today to be 265–335 million m^3, of which 60 million m^3 at most is sublacustrine inflow (Lensky et al, 2005). Other estimations of fluxes from specific sources into the Dead Sea include 60–150 million m^3/y from the Jordan River (Holtzman et al, 2005) and 150–270 million m^3/y from other inflows around the Dead Sea (Israel Hydrological Service, Salameh and El-Naser, 1999).

1.3.1 The Dead Sea water chemistry and evolution

The composition of the Dead Sea water is Ca-chloride (Starinsky, 1974) with a current salinity of 340 g/L and low Na/Cl ratio compared to that of normal ocean water (0.21 vs. 0.86, respectively). This composition is the result of the evaporation of seawater, which intruded the rift valley, followed by halite precipitation, and dolomitization of carbonates along the fault escarpment. The Na/Cl ratio is still decreasing due to the present precipitation of halite in the lake (Gavrieli, 1997).

The Dead Sea is supersaturated with respect to gypsum ($\Omega = 1.42$), anhydrite ($\Omega = 1.94$), barite ($\Omega = 11.75$) and celestine ($\Omega = 2.48$, Reznik et al, 2009). Despite the supersaturation of barite and celestine in the Dead Sea brine, it seems that they do not precipitate in the lake, not even after the Dead Sea evaporates up to a degree of evaporation of 4 (Zilberman-Kron, 2008).

1.3.2 Hydrogeology of the Dead Sea basin

There are three main aquifers in the Dead Sea region: The Lower Cretaceous Kurnub aquifer, the Upper Cretaceous Judea aquifer and the Quaternary alluvial aquifer (Arad and Michaeli, 1967; Yechieli et al, 1995). The latter is adjacent and in direct hydraulic contact with the Dead Sea, and was the main focus of this study. It mainly consists of clastic sediments deposited in fan deltas (gravel, sand, and clay) and of lacustrine sediments (clay, aragonite, gypsum, and salt). The alternations between gravel and clay create several sub-aquifers that differ in their groundwater level and chemical composition. The alluvial aquifer is bounded on its west by normal faults, which set Cretaceous carbonate rocks of the Judea Group against Quaternary alluvial and lacustrine sediments. The freshwater recharge of the alluvial aquifer is through lateral flow from the Judea Group aquifer, which is replenished in the highlands 10–30km to the west and by flash floods. Direct rain on this aquifer is negligible because of the arid climate in the Dead Sea region.

The extremely high density of the Dead Sea induces a very shallow transition zone between the fresh and saline water. According to the Ghyben-Herzberg approximation, the depth of the transition zone is 4.35 times the groundwater elevation, compared to 40 times in aquifers next to the ocean (Yechieli, 2000).

The groundwater system in the alluvial aquifer reacts relatively fast (a few days) to level changes in the Dead Sea (Yechieli et al, 1995), even though the response is variable in accordance with aquifer parameters and with the variability in the slope of the lake (Yechieli et al, 1995). For example in the Tureibe region, groundwater level declines at a lower rate compared to the Dead Sea level drop (Yechieli et al, 2007b), while at Wadi Arugot the decline rate is similar to that of the Dead Sea (Kiro et al, 2008). The saline groundwater also responds to the Dead Sea level drop. Field data and simulations show that the fresh–saline interface drops and widens over time. According to the simulations, the lake level drop increases the fresh and saline groundwater inflow into the Dead Sea, while the flow of Dead Sea water into the aquifer decreases (Kiro et al, 2008).

Saline springs are common along the Dead Sea coast. At the western part of the lake, the discharge is concentrated along a coastline of ∼3km at the Qedem-Shalem area (Stern, 2010). The brines discharge in this area was estimated by 10^7 m^3/y (B. Rophe, Hydrological Service, pers. Comm., Stern, 2010). The salinity of these brines is about half that of the Dead Sea water and their composition is somewhat different. It is characterized by higher SO_4 concentration (∼ 1000 compared with ∼ 400 mg/L), as well as higher Na/Cl (∼ 0.35) and Ca/Mg ratios (Gavrieli et al, 2001). brines of This type were also found in boreholes

along the alluvial aquifer (Yechieli et al, 1996; Kiro, 2006; Yechieli et al, 2007a). It has been suggested that these brines infiltrated the subsurface during a high stand of an older lake that occupied the Dead Sea basin, and therefore represent a previous stage in the evolution of the Dead Sea brines (Yechieli et al, 1996). The relatively high temperature of some of these brines (∼45°C) suggests an ascent from a depth of ∼1000m via faults in the Dead Sea rift (Gavrieli et al, 2001; Shalev et al, 2007; Stern, 2010). The rate of brine discharge to the Dead Sea was estimated by hydrological simulations to be significantly larger in recent years due to the drop in the lake level (Shalev et al, 2007).

Matmon (1995) suggested that the discharge mechanism of the thermal springs is driven by fresh water from the Judea Mountains. However, it has recently been suggested that the main driving force is the circulation of lake water via faults. The rate of this fault-related circulation is not clear and could range between hundreds to thousands of years (Shalev and Yechieli, 2007).

There are several hot springs discharging to the rivers east of the Dead Sea (in Jordan) including Zarka Ma'in, Wadi El Hidan, Wadi Ibn-Hamad, Wadi Wadia, and Wadi Hasa. These springs usually discharge from the sandy Kurnub aquifer and the groundwater salinity is relatively low (Salameh, 1996).

1.4 RADON AND RADIUM ISOTOPES IN NATURAL WATER

There are four naturally-occurring radium isotopes (the radium quartet), with half-lives ranging from 3.7 days to 1600 years (Fig. 1.3). Two of them, the ^{226}Ra and ^{223}Ra, are the radioactive chain products of uranium isotopes (^{238}U and ^{235}U, respectively), while ^{228}Ra and ^{224}Ra are chain products of ^{232}Th. Three of the isotopes (^{226}Ra, ^{224}Ra and ^{223}Ra) disintegrate into radon daughters (^{222}Rn, ^{220}Rn and ^{219}Rn, respectively), while ^{228}Ra decays to ^{224}Ra via ^{228}Th (and the short-lived ^{228}Ac). In the aquifer and in surface water bodies, all the radium isotopes are produced by the decay of insoluble thorium parents, which are adsorbed on sediment grains or on suspended material. In freshwater, radium is mainly tightly bound to the surface of sediment grains (e.g., Webster et al, 1995; Sturchio, 2001; Gonneea et al, 2008; Lazar et al, 2008), while in saline water the radium is much more soluble and readily undergoes ion exchange with other adsorbed cations (e.g., Krishnaswami et al, 1991).

^{222}Rn (half-life 3.82 days) is a noble gas, which is produced by the decay of ^{226}Ra and disintegrates into ^{218}Po. It has been shown to be a very powerful tool in tracking groundwater discharge to the sea (Burnett and Dulaiova, 2003; Weinstein et al, 2007b).

In terms of hydrological and oceanographic applications, the short-lived isotopes ^{224}Ra

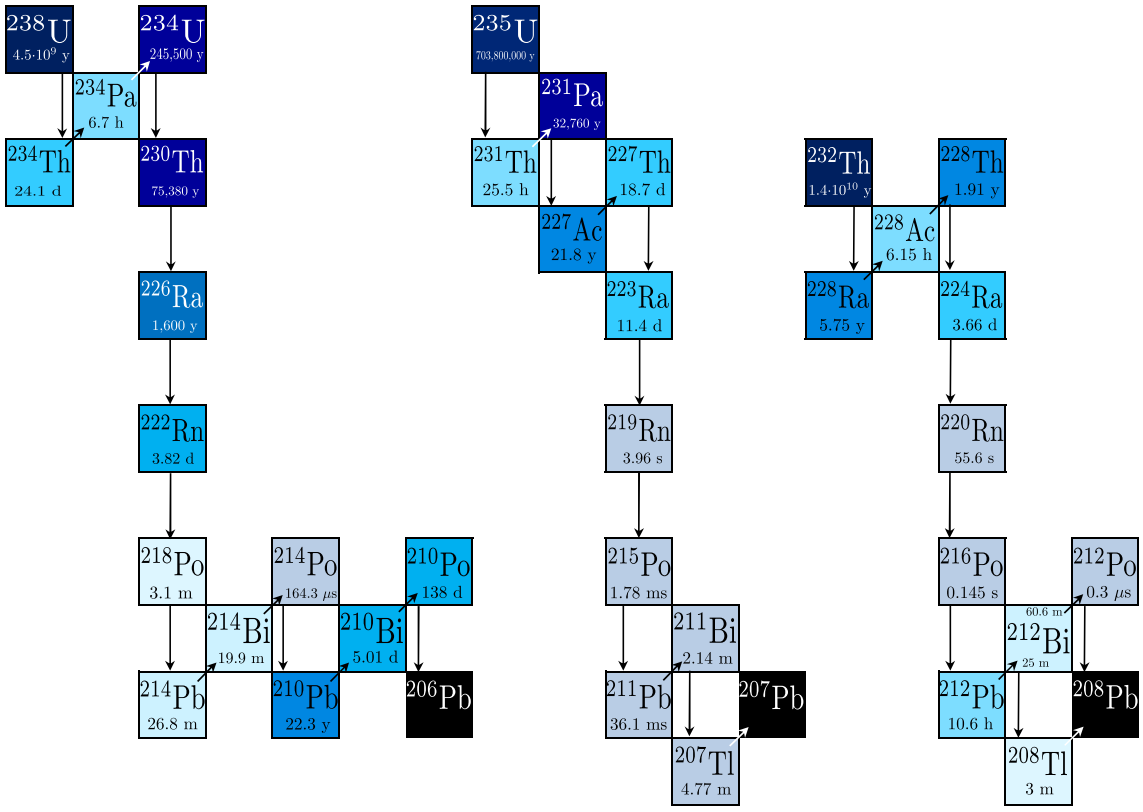


Figure 1.3: The decay chain of U and Th series.

and ^{223}Ra (half-lives of 3.66 and 11.4 days, respectively) are used for studying short term processes such as coastal mass balances and mixing with the open sea (e.g., Moore, 1996; 2000; Shellenbarger et al, 2006), while ^{226}Ra (half-life of 1,600 years) may be used for long-period studies such as residence times in the ocean and lakes (Broecker et al, 1967; Stiller and Chung, 1984).

Usually, both radium isotopes and radon are enriched in groundwater compared to sea water and are used as a tracer for SGD (e.g., Cable et al, 1996b; Moore, 1996; Corbett et al, 1999; Kelly and Moran, 2002). A combined study of radon and radium isotopes may allow the detection of the type (terrestrial or seawater) of the discharging groundwater, as radium activity depends on water salinity (e.g. Krishnaswami et al, 1991; Weinstein et al, 2007b), while radon is usually enriched in both fresh and saline groundwater (e.g. Mulligan and Charette, 2006) or in fresh groundwater only (e.g. Weinstein et al, 2007a).

Due to their different half-life and lack of fractionation during water–rock interaction, radium isotopes may be a useful tool for characterizing and quantifying different hydrological and geochemical processes with different time-scales.

1.4.1 Radon and radium in the Dead Sea system

The Dead Sea is extremely enriched in radium relative to most natural water. The ^{226}Ra activity in the Dead Sea is 1,800 times that of Pacific surface water (∼0.08 dpm/L) and almost 400 times (∼0.35 dpm/L) that of Pacific deep water (Chan and Chung, 1987; Chung and Craig, 2004; Mazor, 1962; Stiller and Chung, 1984). The ^{226}Ra activities before the 1979 overturn were 141 and 121 dpm/L in the upper and lower water masses, respectively, and after the overturn they were 137 dpm/L (Chan and Chung, 1987; Stiller and Chung, 1984). These values yield the same ^{226}Ra inventory in the Dead Sea (Chan and Chung, 1987). The activity of ^{228}Ra in the Dead Sea (Somayajulu and Rengarajan, 1987) is also higher by 2–3 orders of magnitude compared to the ocean (∼0.005 dpm/L, Broecker and Peng, 1982). The ^{228}Ra activity during the meromictic stage was 1.57 dpm/L in the upper water mass, 0.13–0.22 dpm/L at a depth of 175m and 0.42 at depth of 275 m. It was suggested that the higher bottom water values are due to diffusion from bottom sediments or influx of submarine springs (Somayajulu and Rengarajan, 1987).

The activities of ^{226}Ra and ^{228}Ra in the onshore springs range from 20 to 750 and 1.9 to 472 dpm/L, respectively (Gilboa, 1963; Mazor, 1962; Moise et al, 2000). Stiller and Chung (1984) suggested that the inventory of ^{226}Ra in the lake was built up a long time ago and that it is now in steady state with a relatively low input from the Jordan River (1–2 dpm/L;

Stiller and Chung, 1984), from other runoffs and from onshore and submerged springs. They estimated a total inflow of $8.4 \cdot 10^{12}$ dpm/y, balanced by the slow decay rate of the ^{226}Ra in the lake and a minor co-precipitation with aragonite. Chan and Chung (1987) and Chung and Craig (2004) suggested scavenging via adsorption on particles as an additional possible sink for the radium, but they also agree that the main sink of radium in the lake is by radioactive decay. Activities of ^{222}Rn are also very high in springs around the Dead Sea (Moise et al, 2000) reaching 19,000 dpm/L in Ein Qedem and 59,000 dpm/L in Ein Feshkha, which is not supported by ^{226}Ra. Radon was hardly studied in the Dead Sea itself. Chung and Craig (2004) reported excess radon of about 18 dpm/L in the deep layer before overturn, which is probably due to recoil and diffusion from the bottom sediments.

The steady-state model of Stiller and Chung (1984) does take into account the ^{228}Ra activities in the lake and does not include submerged discharge of groundwater around the Dead Sea, circulated saline water and the water sources on the eastern shore of the Dead Sea, which may be significant. In this study, the radium mass balance (for both ^{226}Ra and ^{228}Ra) in the Dead Sea is recalculated using new data and including the Dead Sea water circulation in the aquifer.

1.5 RESEARCH GOALS

The overall aim of this study is to use the Dead Sea as a natural laboratory for studying long-term dispersive seawater circulation in the aquifer and its potential effect on oceanic and lacustrine element budgets. This includes:

1. Determining and timing geochemical processes of water–rock interaction (adsorption–desorption, precipitation, redox) affecting trace element concentrations during Dead Sea water circulation in the aquifer.

2. Quantifying the long-term Dead Sea water circulation in the aquifer and its effect on the Dead Sea elemental mass balances.

3. Understanding the geochemistry of radon and radium in the Dead Sea system in order to develop a method for quantifying the time scale and magnitude of Dead Sea water circulation in the aquifer.

This was done by measuring radon and radium isotopes in the Dead Sea and in its water sources, and studying the chemistry (including radon and radium isotopes) of the fresh–saline transition zone and the circulated Dead Sea water in the aquifer, at different distances

from the Dead Sea shore and after different periods of water–rock interaction. Due to their different half-lives, the radium isotopes are sensitive to processes with different time scales and are a suitable tool for achieving the above goals.

Chapter 2

Methods

2.1 SAMPLING

Water samples were taken from the Dead sea and the main water sources around the lake (Fig. 2.1). The Dead Sea water was sampled from a vertical profile 8km offshore (Fig. 2.1, eg300 - 31.5030°N/35.4712°E) using Niskin bottles and surface water were sampled along a transect from the Dead Sea shore up to 8km (100 m, 1 km, 4 km). The water sources to the Dead Sea included the Jordan River, groundwater and brines discharging along the western shore of the Dead Sea and springs brines and streams at the eastern catchment of the Dead Sea. Circulated Dead Sea water and the fresh–saline transition zone were studied from boreholes. Groundwater samples of various salinities were collected from several depths in boreholes mainly at Wadi Arugot alluvial fan area (Fig. 2.1). Sampling took place after pumping three times the borehole volume in order to clean the borehole and obtain a representative sample of the aquifer's water. Water samples for major elements were collected in plastic bottles, and samples for trace elements were collected in 125ml LDPE bottles after running through a 0.45μ filter and acidified to pH $\sim$2. Water samples for ^{226}Ra and ^{222}Rn analysis were sampled in 0.5L vacuumed glass bottles, while water samples for short-lived radium isotopes (^{228}Ra, ^{223}Ra and ^{224}Ra) were collected in 3-20L plastic containers, followed by running the water through 0.45μ filter and extracting the radium onto MnO_2-coated acrylic fibers (Moore and Arnold, 1996).

2.2 RADIUM ADSORPTION ONTO MNO_2-COATED ACRYLIC FIBERS

The adsorption efficiency of radium on the MnO_2-coated fibers was calculated by comparing the activity of ^{226}Ra adsorbed on the fibers and that in water of the same sample, both

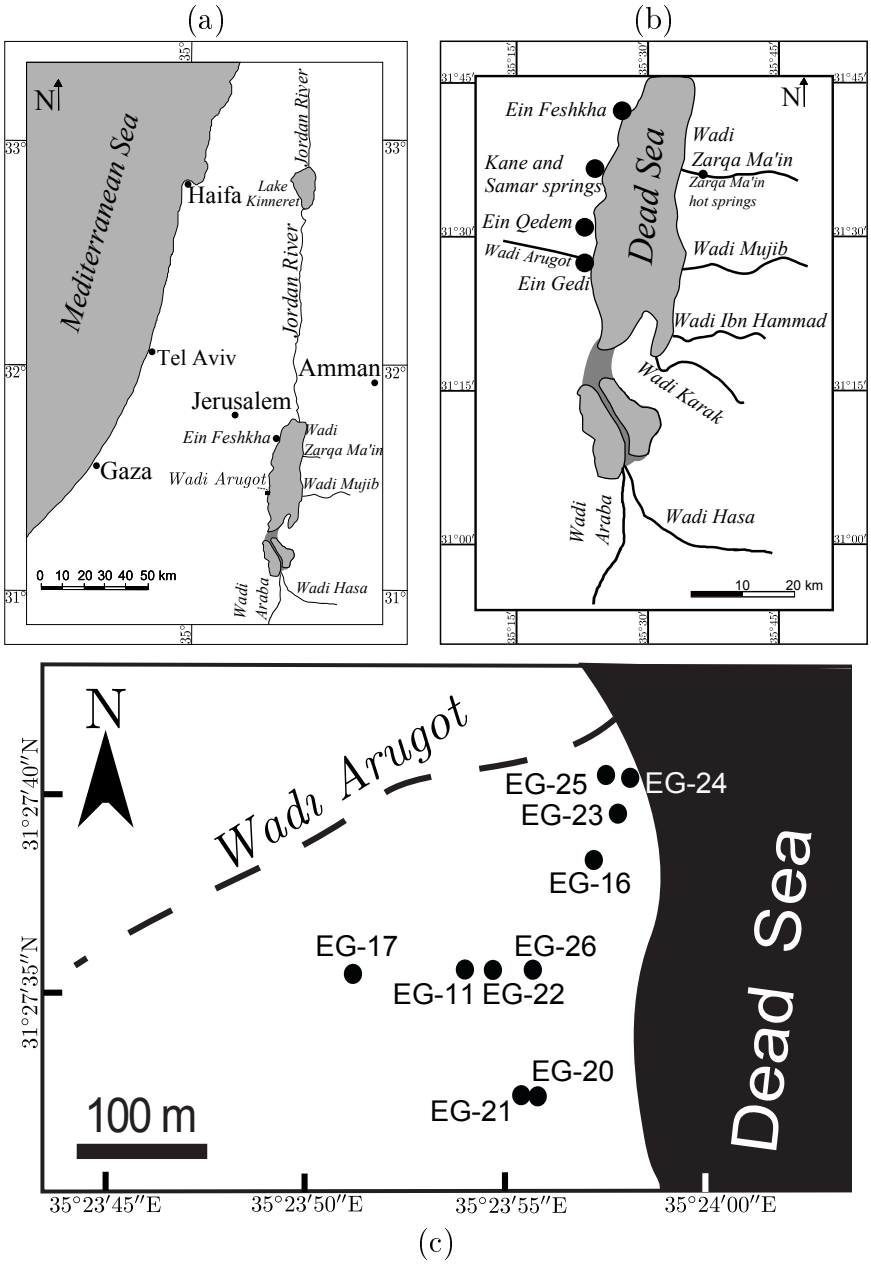


Figure 2.1: Location map of water sources around the Dead Sea. (a) Regional map, (b) Map of the Dead Sea and (c) the main groundwater study area of the Arugot alluvial fan, including borehole locations.

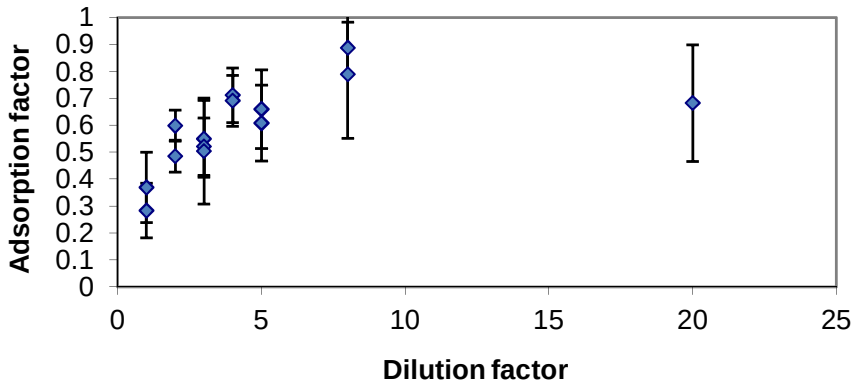


Figure 2.2: Adsorption efficiency on MnO_2-coated fibers of diluted Dead Sea water. The error bars represent the analytical error.

measured with the extraction system. The adsorption of radium from Dead Sea water, was found to be of low efficiency (5–15%), which is due to the very high ionic strength of this water. Therefore, the Dead Sea water and other brines were diluted by 5 to 20 times, which increased the adsorption efficiency to 30–80% (Fig. 2.2). Nevertheless, it was still quite variable. Therefore, the efficiency was determined for each sample, and the activity (of all isotopes) was corrected accordingly.

2.3 RADIUM AND RADON ISOTOPE MEASUREMENTS

2.3.1 ^{222}Rn and ^{226}Ra

^{222}Rn and ^{226}Ra were measured both using RAD7 and the Lucas cells.

RAD7

Analyses of ^{222}Rn and ^{226}Ra were done by the radon-in-air RAD7 spectrometer (DURRIDGE Co.). The RAD7 measures ^{222}Rn by detecting the α decay of its daughter ^{218}Po. The RAD7 is used with the RAD-H_2O application, where the ^{222}Rn is bubbled out of the water sample and is recirculated through the RAD7. Measurement start after ^{222}Rn approaches secular equilibrium with its daughter ^{218}Po. The samples are re-measured for ^{226}Ra after three weeks, the time needed to attain secular equilibrium with the ^{222}Rn.

Because of the high viscosity of the Dead Sea water, the ordinary 250cc sampling bottles can not be used due to the penetration of sample water into the tubing. Thus, Erlenmeyer flasks with relatively large head space were used. The efficiency was defined by ^{226}Ra standards as dpm=0.0709 cpm (Fig. 2.3), while the counts were those of the ^{218}Po (window A).

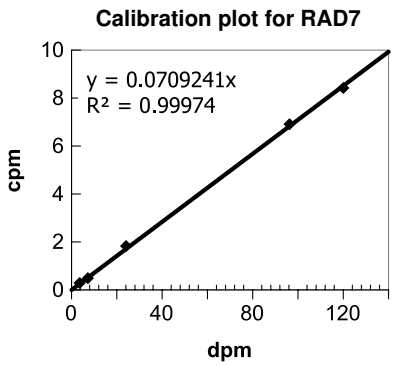


Figure 2.3: Calibration plot of ^{226}Ra standards for using the RAD7.

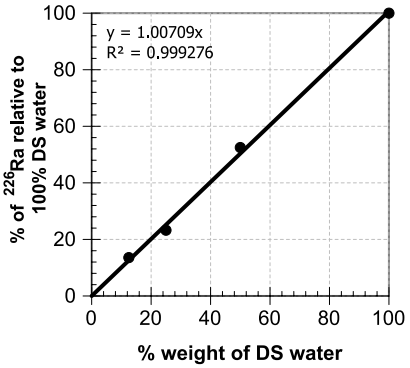


Figure 2.4: Results of bubbling test in the RAD7.

Another test was performed to determine the yield of radon extraction from the Dead Sea water. This was done by diluting a specific amount of Dead Sea water to variable degrees and measuring the ^{226}Ra activity with the RAD7. The results of this experiment show that the yield does not change with salinity and thus, that the RAD-H_2O procedure is effectively bubbling out all the radon from the Dead Sea water samples (Fig. 2.4).

The Rn emanation and Lucas cells system

^{222}Rn was extracted via helium bubbling and was adsorbed onto a cooled charcoal column. The radon gas was then transferred to a counting (Lucas) cell after heating the column to 450°C (Mathieu et al, 1988). Radon disintegrations were counted using a counting system (Applied Techniques, Model AC/DC-DRC-MK 10-2). ^{226}Ra was measured after incubation for at least three weeks in order to allow the ^{222}Rn to reach secular equilibrium with the ^{226}Ra.

The same ^{226}Ra standards (3.6–96 dpm) in the Erlenmeyer flasks were used for both systems, keeping similar efficiencies in each of the systems over time. One standard (52.5

Table 2.1: Efficiencies of the different channels in RaDeCC according to the standards of ^{232}Th and ^{227}Ac.

channel	^{224}Ra efficiency	standard deviation	number of standard measurements	^{223}Ra efficiency	standard deviation	number of standard measurements
1	0.52	0.02	15	0.29	0.03	16
2	0.54	0.04	28	0.27	0.03	16
3	0.55	0.03	17	0.3	0.03	26
4	0.5	0.03	17	0.28	0.02	10

dpm) of ^{226}Ra on MnO_2 fibers in a column was made, yielding the same efficiency (2.5) of the water standards in the Lucas cells system.

2.3.2 ^{223}Ra and ^{224}Ra measurements

The short-lived radium isotopes (223 and 224) were measured by a delayed coincidence counter (RaDeCC, Moore and Arnold, 1996). The short-lived daughters of the radium isotopes, ^{219}Rn and ^{220}Rn, which are produced by recoil from the Mn fibers, are swept into a scintillation cell where alpha decay of the radon nuclides and their polonium daughters (^{215}Po and ^{216}Po, respectively) occurs. The scintillations are translated into electronic signals, and these are sent to a delayed coincidence circuit, which electronically discriminates the paired decays of 219 and 215 (thus 223) from those of 220 and 216 (thus 224, Giffin et al, 1963; Moore and Arnold, 1996). ^{222}Rn and the short-lived radium isotopes were corrected for the time difference between the sampling and measurement. Chance coincidence of ^{224}Ra and ^{223}Ra was calculated according to Giffin et al (1963).

Standards of 1.53 dpm ^{227}Ac and 4.89 dpm ^{232}Th were of prepared from solutions in secular equilibrium supplied by Jan Scholten (IAEA). The efficiencies according to each standard in each channel were measured once every 1–2 months and are detailed in Table 2.1.

2.3.3 ^{228}Ra measurements

^{228}Ra was measured by two methods: by the delayed coincidence counter (RaDeCC) and by gamma spectrometry. The measurements by gamma spectrometry were done in W.C. Burnett lab (FSU, Tallahassee, FL) after ashing the Mn fibers which reduces the sample mass by approximately 90%. ^{228}Ra is determined by counting its daughter ^{228}Ac (Dulaiova and Burnett, 2004). The measurements using RaDeCC followed the procedure of Moore (2008). It was measured on the same fibers used for determining the ^{224}Ra. The samples were measured at least twice ($>$ 1 month and $>$ 6 months) after the first measurement of ^{224}Ra

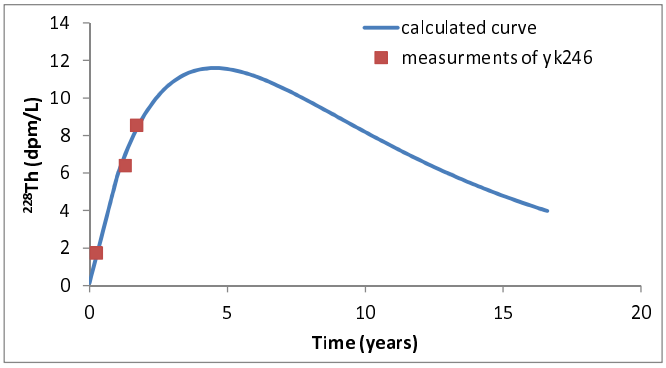


Figure 2.5: An example of the activity of ^{228}Th over time due to the decay of ^{228}Ra on the MnO_2-coated fibers. In this case the curve is fitted to yk246 sample measurements, the activity of ^{228}Ra is 20 dpm/L and the initial adsorbed ^{228}Th is 0.15 dpm/L.

to allow for the growth of ^{228}Th from the adsorbed ^{228}Ra (Fig. 2.5). ^{228}Ra concentration was calculated according to the growth rate of ^{228}Th as described in Moore (2008).

Both methods were used but no intercalibration was done. However, the variability of ^{228}Ra in samples from the same source is larger than the variability between the two methods, the methods agree with each other and fit activities from previous studies (e.g. Somayajulu and Rengarajan, 1987; Moise et al, 2000). This issue is referenced in the text (e.g. see section 3.3.1). Figure 2.6 presents a comparison between ^{226}Ra activities on the Mn fibers measured by γ-spectrometry and by the emanation technique. Part of the fibers in some of the samples from the measurements on October 2011 were lost, however, the ^{228}Ra was determined from the ^{226}Ra/^{228}Ra ratio in the γ-spectrometry and the ^{266}Ra activity in the water sample, taking into account that these samples are with low credibility. Only few samples were measured by γ-spectrometry (yk3, yk9, EG22-29.5, yk70, yk83, yk110, yk366, yk367, yk390, yk392) and the rest of them by the RaDeCC.

2.4 MAJOR AND TRACE ELEMENT MEASUREMENTS

Samples were analyzed for major and trace elements in the labs of the Geological Survey of Israel using Perkin Elmer Optima 3300 ICP-AES for cations, Dionex ICS-2000 Ion Chromatograph for anions and Perkin Elmer Sciex Elan-DRC-e ICP-MS for the trace elements.

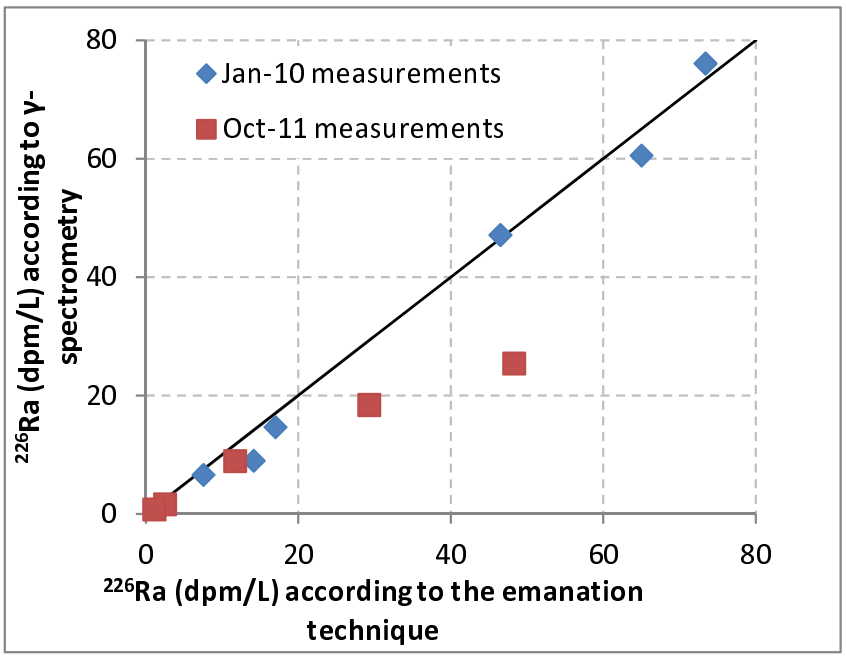


Figure 2.6: ^{226}Ra measurements on the Mn fibers using the γ-spectrometry method compared with the emanation technique.

2.5 MODELING RADIUM DISTRIBUTION IN DYNAMIC DENSITY-DEPENDENT FLOW CONDITIONS

SUTRA-MS (Hughes and Sanford, 2005) was used in order to calculate the distribution of radium isotopes in the density-dependent flow field of the Dead Sea aquifer during its level drop. The flow field was calculated by coupling the flow and solute transport equations. The radium isotope distributions were calculated according to the flow field during the continuous Dead Sea lake level drop. Details about the governing equations and the numerical methods of the model are given in Voss (1984) and Hughes and Sanford (2005).

The solute mass balance equation includes zero and first order production coefficients and an equilibrium adsorption process which may behave according to a linear, Langmuir or Freundlich isotherm (Voss, 1984). An additional modification was made in order to adapt the code to the high salinity conditions of the Dead Sea, by supporting a salinity-dependent adsorption distribution coefficient (K_d).

Chapter 3

Groundwater ages and reaction rates during seawater circulation in the Dead Sea aquifer

3.1 INTRODUCTION

Seawater circulation in aquifers has been recently recognized as a major process in the mass balances of coastal areas (e.g. Simmons, 1992; Moore, 1996; Charette and Sholkovitz, 2006). The spatial and temporal scales of seawater circulation vary between the small-scale, short-term, such as wave- and tidal-driven (Robinson et al, 1998; Li et al, 1999) through seasonal scale (Michael et al, 2005) and up to the large-scale, long-term density-driven dispersive circulation (Cooper, 1959).

Unlike the short-term circulation, which was studied by several authors both by simulations and in the field (e.g. Li et al, 1999; Michael et al, 2005; Charette and Sholkovitz, 2006), the long-term dispersive circulation has been studied only by hydrological simulations (e.g. Lee and Cheng, 1974; Smith, 2004; Kiro et al, 2008), while it was hardly studied in the field (Kiro et al, 2012). Moreover, simulations of saline water circulation are very sensitive to the model parameters (e.g. dispersivities, anisotropy and permeability; Smith, 2004; Kiro et al, 2008), and therefore the simulation-calculated velocities should be treated cautiously.

The Dead Sea system provides a unique opportunity to study the long-term dispersive seawater circulation due to the absence of tides and significant waves and to the very shallow fresh–saline transition zone, which is the result of the extreme high density of the Dead Sea water.

Groundwater systems adjacent to saline water bodies (lakes or the ocean) are usually

of mixed salinities, in which fresh water flows above saline water, with a fresh–saline water transition zone in between. This mixed aquifer zone is also referred to as the *subterranean estuary* (Moore, 1999). The special conditions of various salinities in this environment result in water–rock interactions, which affect the concentrations of nutrients, trace metals, radium isotopes and other radioisotopes in coastal waters (e.g., Moore, 1996; Charette and Sholkovitz, 2002; Kelly and Moran, 2002). Charette and Sholkovitz (2006) studied the geochemical processes, affecting trace element concentrations in the subterranean estuary of Waquiot Bay, northeastern US. They described the chemical reactions that control the studied trace element distributions as redox-controlled and adsorption–desorption processes which may also be inter-dependent. The residence time of the groundwater in the Waquiot Bay subterranean estuary is relatively short (days to weeks, Charette and Sholkovitz, 2006), therefore long-term water–rock interactions probably do not play a major role in this environment. The longer-term circulation in the Dead Sea aquifer (years to tens of years, bellow) allows the tracking of both short- and long-term processes.

Groundwater age is determined by various methods such as CFC's, ^{3}H, and $^{3}H/^{3}He$ for young groundwater (Plummer et al, 1993), while ^{14}C (Mook, 1980), and ^{4}He accumulation rate (e.g. Marine, 1979) are used for older groundwater. Seawater intrusion has also been dated using ^{14}C (e.g. Sivan et al, 2005; Yechieli et al, 2009), however dating hypersaline brines is more complex and only preliminary work was done (Avrahamov et al, 2010).

Any radionuclide that is produced from the aquifer solids and that its behavior during water–rock interaction is known may be used as a groundwater dating tool. Two important considerations are the ability to track the changes in the radionuclide concentrations along the flow path and that the radionuclide half-life fits the time scale of the groundwater flow.

The objective of this study is to determine groundwater ages and velocities, as well as the rates of water–rock interactions that occur during Dead Sea water circulation in the aquifer. In order to do so, we develop here two novel dating approaches for seawater circulating in the aquifer. While the Na/Cl ratio is unique to the Dead Sea system, the method based on ^{228}Ra may be applied elsewhere.

3.1.1 Radon and Radium isotopes

Due to their different half-lives, radium isotopes may be used as a powerful dating tool which may be further used for the determination of the rates of geochemical processes. There are four naturally occurring radium isotopes, with half-lives ranging from 3.7 days to 1600 years. Two of them, ^{226}Ra and ^{223}Ra, are the radioactive progeny of uranium isotopes (^{238}U and

^{235}U, respectively), while ^{228}Ra and ^{224}Ra are decay products of ^{232}Th. ^{228}Ra decays to ^{224}Ra via ^{228}Th (and the short-lived ^{228}Ac). ^{226}Ra disintegrate into ^{222}Rn, which is a dissolved gas. All four radium isotopes are produced from aquifer solids and in surface water bodies by the decay of their insoluble parents on particulate matter. In fresh water, radium is mostly tightly bound to the surface of sediment grains (e.g., Webster et al, 1995; Gonneea et al, 2008; Lazar et al, 2008) while in saline water radium is much more soluble and readily undergoes ion exchange with other adsorbed cations (e.g., Krishnaswami et al, 1991; Moore, 2000; Sturchio, 2001). The adsorption distribution coefficient (K_d) of radium in the hypersaline water of the Dead Sea was found to be very low (maximum 0.06 L/Kg), while it increases with decreased salinity (up to ~ 1 in the fresh groundwater, Kiro et al, 2012).

Several studies modeled radium and other uranium series nuclides using a one dimensional mass balance equation in order to characterize the effect of different parameters and hydrological conditions on the concentrations of the radionuclides (Davidson and Dickson, 1986; Tricca et al, 2001). Krest and Harvey (2003) also used the same mass balances in order to quantify recharge and discharge in wetland sediments.

3.1.2 The Dead Sea hydrological system

The Dead Sea is a terminal hypersaline lake with salinity of 340 g/L. Its chemical composition is Ca-chloride with a low Na/Cl ratio compared with ocean water (0.21 and 0.86, respectively). This composition is derived from ancient brines, which are the residues of seawater that intruded the rift valley and went through evaporation and halite precipitation (Starinsky, 1974). Other processes of water–rock interaction, such as the dolomitization of carbonates in the adjacent aquifer, have further altered the original composition.

The Dead Sea is highly enriched with radium relative to most natural water bodies. The Dead Sea activities of both ^{226}Ra ($\sim$147 dpm/L, Stiller and Chung, 1984; Kiro et al, 2012) and ^{228}Ra (1–2 dpm/L, Somayajulu and Rengarajan, 1987; Kiro et al, 2012) are 2–3 orders of magnitude higher than in the ocean. Dead Sea water is also supersaturated with respect to gypsum, anhydrite, barite and celestine ($\Omega = 1.42, 1.94, 11.75$ and 2.48, respectively, Reznik et al, 2009). Nevertheless, it seems that neither barite nor celestine precipitate in the lake, not even after the Dead Sea water evaporates by a factor of 4 (Zilberman-Kron, 2008). However, during seawater circulation in the aquifer, Ba, ^{226}Ra and Sr are evidently removed from the Dead Sea water, probably mainly due to barite and celestine precipitation (Kiro et al, 2012).

The Dead Sea water level has been decreasing during the past fifty years, due to human

intervention in its water budget, reaching a decline rate of more than 1 m/y. In accordance with the lake level drop, its major element composition also changed since the 1970's due to halite precipitation and mixing with end brines released from the Dead Sea potash industries. Na/Cl ratio decreased from 0.3 to 0.21, while Mg/K ratio increased from 9 to 9.8 (Gavrieli, 1997; Reznik et al, 2009).

This study focuses on the alluvial aquifer adjacent to the Dead Sea which is in direct hydraulic contact with the lake along most of its shoreline. It mainly consists of clastic fan delta deposits (gravel, sand and clay) intercalated with lacustrine sediment (e.g., clastics, aragonite, gypsum and salt). Direct recharge by precipitation is negligible (precipitation $<$100 mm/y), and the main recharge is by lateral flow from the Cretaceous carbonate aquifer on its western border (2–3km from the lake), which is replenished at the highlands 10–30km away, as well as by flash floods.

The fresh–saline groundwater transition zone in the Dead Sea aquifer is very shallow due to the high density of the Dead Sea water. According to the Ghyben–Herzberg approximation, the depth of the transition zone in the Dead Sea coastal aquifer is 4.35 times the groundwater elevation (Yechieli, 2000), compared to 40 times in aquifers next to the ocean.

The hydraulic relationship between the Dead Sea and the alluvial aquifer is manifested in a relatively rapid groundwater level response (several days) to level changes in the Dead Sea (Yechieli et al, 1995). The response rate varies according to the aquifer hydraulic parameters and lake bathymetry near the coast and may reach the same rate as the lake level drop (Kiro et al, 2008). The fresh–saline transition zone also responds to the lake level drop by deepening of the transition zone and by enhancement of the fresh water inflow. Nevertheless, the Dead Sea water circulation, which is the subject of this study, persists during the lake level drop (Kiro et al, 2008).

3.2 METHODS

Groundwater samples of various salinities were collected from several depths in boreholes located 5, 10, 40 and 80 meters from the Dead Sea shore inland at the Wadi Arugot alluvial fan area (Fig. 2.1). Sampling took place after purging by pumping three times the borehole volume. Water samples for major elements were collected in plastic bottles, and samples for trace elements were collected in 125ml LDPE bottles after running through a 0.45μ filter and acidified to pH $\sim$2. Water samples for ^{226}Ra and ^{222}Rn analysis were sampled in 0.5L vacuumed glass bottles, while water samples for short-lived radium isotopes (^{228}Ra, ^{223}Ra and ^{224}Ra) were collected in 3-20L plastic containers, followed by running the water through

0.45μ filter and columns and extracting the radium onto MnO_2-coated acrylic fibers (Moore, 1996).

Major and trace element concentrations were measured in the labs of the Geological Survey of Israel using Perkin Elmer Optima 3300 ICP-AES for cations, Dionex ICS-2000 Ion Chromatograph for anions and Perkin Elmer Sciex Elan-DRC-e ICP-MS for the trace elements.

^{222}Rn was extracted via helium bubbling and was adsorbed onto a cooled charcoal column. The radon gas was then transferred to a counting (Lucas) cell after heating the column to 450°C (Mathieu et al, 1988). ^{226}Ra was measured after incubation for at least three weeks in order to allow the ^{222}Rn to reach secular equilibrium with the ^{226}Ra.

The short-lived radium isotopes (223 and 224) were measured by a delayed coincidence counter (RaDeCC, Moore and Arnold, 1996). Chance coincidence of ^{224}Ra and ^{223}Ra was calculated according to Giffin et al (1963).

^{228}Ra was also measured by the delayed coincidence counter (RaDeCC) on the same fibers used for the determination of ^{224}Ra. The samples were measured at least twice ($>$ 1 month and $>$ 6 months) after the first measurement of ^{224}Ra to allow for the growth of ^{228}Th from the adsorbed ^{228}Ra. ^{228}Ra concentration was calculated according to the growth rate of ^{228}Th as described in Moore (2008).

The adsorption efficiency of radium on the MnO_2-coated fibers was calculated by comparing the activity of ^{226}Ra adsorbed on the fibers and that in water of the same sample, both measured with the radon extraction system (above). The adsorption of radium from the Dead Sea water was found to be of low efficiency (5–15%), which is due to the very high ionic strength of this water. Therefore, the Dead Sea water was diluted 5 to 20 times, which increased the adsorption efficiency to 30–80%. Nevertheless, efficiency was still quite variable, therefore it was determined per each sample, and the activity (of all isotopes) was corrected accordingly.

The degree of saturation of minerals (Ω) and activities of dissolved ions in the solutions were calculated using PHREEQC with the Pitzer database. Radium chemical activities were calculated according to the extension to the Pitzer database developed by Rosenberg et al (2011).

3.3 RESULTS AND DISCUSSION

The chemistry and activities of radon and radium isotopes in the groundwater from the Wadi Arugot alluvial fan (Fig. 2.1) are presented in Tables 3.1 and 3.2 together with lake water

composition. The groundwater samples are mainly of two types. The first is the hypersaline, circulating Dead Sea water, characterized by Cl concentrations of 219–232 g/L (Fig. 3.1a) and density of 1.23–1.24 kg/L, while the other group is that of the transition zone, where Cl concentrations are 41–219 g/L (Fig. 3.1a) and densities are 1.05–1.22 kg/L. We note that at this proximity to the Dead Sea shore there is no actual fresh groundwater. This is due to the very shallow transition zone and the continuous lake level drop.

3.3.1 Groundwater ages and flow velocities

The age of circulated seawater is the time elapsed since the ocean or lake water entered its bottom sediments and into the aquifer. We present here two novel methods for assessing groundwater velocity and its age. The first method is specific to the Dead Sea system since it relies on the lake level decline during the past several decades and the consequent gradual change in the lake water Na/Cl ratio due to halite precipitation. On the other hand, the second method derives velocities and ages using the ^{228}Ra activities, which may be applicable to other sea–aquifer systems.

Na/Cl ratios

Figure 3.1a shows, by means of chloride contours, the transition zone in the Dead Sea aquifer between the relatively fresh groundwater and the Dead Sea circulated water. The Na/Cl ratio changes along the transition zone from 0.27 to 0.37 (Fig. 3.1b) due to mixing of low Na/Cl ratio Dead Sea water with aquifer brines with higher Na/Cl ratio (Kiro, 2006). However, the Na/Cl ratio also changes within the hypersaline Dead Sea circulating groundwater below the transition zone (from 0.27 to 0.21 Fig. 3.1). This is the result of the decrease in the Na/Cl ratio in the Dead Sea during the past 50 years due to halite precipitation in the lake (Gavrieli, 1997, Fig. 3.2) and to the continuous flow of Dead Sea water into the aquifer during this period.

The Na/Cl ratio of groundwater next to the Dead Sea can be translated into ages using the documented history of this ratio in the lake (Fig. 3.2) and assuming that it is conservative while traveling in the aquifer (because halite is close to saturation). According to this method, groundwater ages in boreholes 5–10m inland are several years (Na/Cl=0.21), and it reaches 20 and 30 years (Na/Cl=0.25 and 0.27) at 40 and 80 meters inland, respectively. This yields a saline groundwater circulation velocity of 1.5 to 4 m/y during the last few decades.

Table 3.1: Major elements and composition of Dead Sea and groundwater of the adjacent aquifer. Reaction errors are up to 2%.

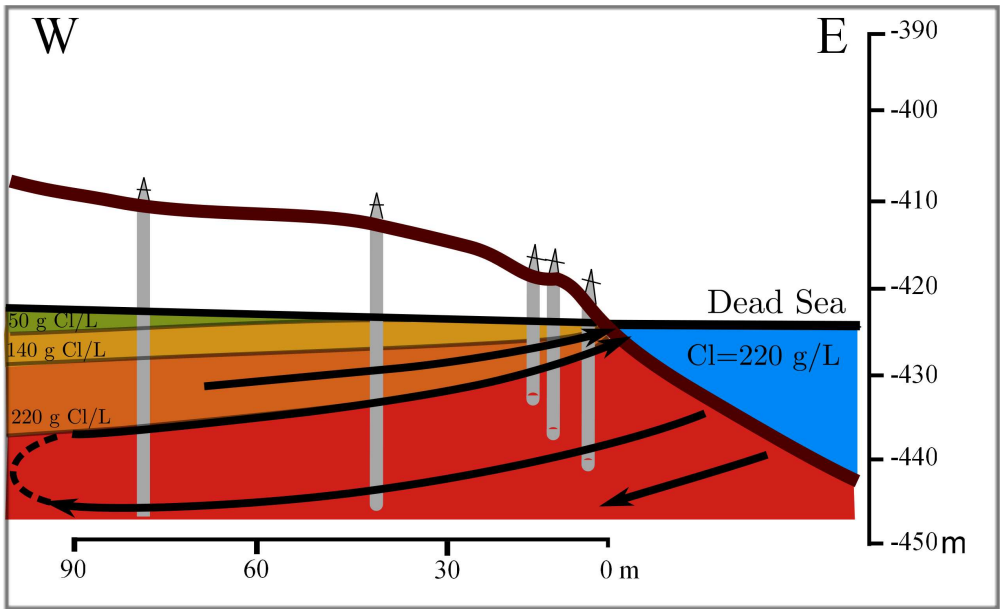
Sample	Location	date	Dist. from shore inland (m)	Elev. (m)	Depth in borehole (m)	Water table elev. (m)	Na (g/L)	K (g/L)	Ca (g/L)	Mg (g/L)	Cl (g/L)	SO_4 (mg/L)	Br (g/L)	Density (kg/L)	Temp. °C	Na/Cl (eq./eq.)
Dead Sea[a]	lake	1983					38.2	7.66	17.8	44.1	223	440	5.3	1.232		0.264
Dead Sea[b]	lake	2008					31	8	19	47	230	393	5.1	1.238		0.21
yk400	EG24	21/03/11	5	-424.6	2.8	-424.4	29.4	4.9	11.8	26.7	148		3.4	1.1587	27.7	0.306
yk401	EG24	21/03/11	5	-439.8	18	-424.4	31.2	8.2	19	49.4	230		6	1.24	28.2	0.209
yk413	EG24	13/06/11	5	-425.0	3.25	-424.6	32.4	7	17.9	42.8	216	356	5.4	1.221	31.7	0.231
yk414	EG24	13/06/11	5	-431.8	10	-424.6	32	7.6	19.4	47.5	229	277	6.1	1.2364	33.4	0.215
yk415	EG24	13/06/11	5	-440.8	19	-424.6	31.1	7.6	19.6	48.2	232	243	6.1	1.2369	32.1	0.207
EG24-10	EG24	01/02/12	5	-431.8	10	-425.5	30.3	7.8	17.4	46	223	231	6.4	1.24	26.8	0.21
EG24-19	EG24	01/02/12	5	-440.8	19	-425.5	30.7	8	18.3	47.8	224	232	4.9	1.24	26.8	0.211
yk3	EG16[c]	21/01/08	10	-420.8	6.05	-420.7	13.6	2.3	5.9	11.6	67		1.6	1.073	23.9	0.313
yk6	EG16[c]	21/01/08	10	-421.8	7.05	-420.7	27.9	4.6	10.9	25.7	142		5.8	1.149	24.3	0.303
yk9	EG16[c]	21/01/08	10	-426.2	11.5	-420.7	33.8	7.8	17.5	44.4	224		5.8	1.236	24.9	0.233
yk416	EG23	13/06/11	10	-426.2	6.32	-424.6	37.6	6.1	15.5	36.2	196	456	4.7	1.2059	31.5	0.296
yk417	EG23	13/06/11	10	-429.8	10	-424.6	32.9	7.5	19.1	46.7	228	238	6	1.2363	32.8	0.223
yk418	EG23	13/06/11	10	-434.3	14.5	-424.6	31.2	7.4	19.3	46.8	223	238	6.1	1.2368	31.4	0.216
yk419	EG23	13/06/11	10	-439.3	19.5	-424.6	31.4	7.5	19.5	47.3	231	234	6.3	1.2391	30.7	0.21
EG23-6.8	EG23	01/02/12	10	-426.6	6.8	-425.4	22.6	3.5	8.4	19	110	1108	2.6	1.12	24.1	0.317
yk402	EG25	21/03/11	13	-424.1	2.75	-424.1	17.6	2.8	6.7	13.7	82		1.8	1.0891	28	0.333
yk412	EG25	13/06/11	13	-424.9	3.5	-424.4	19.5	2.9	8	15.8	95	1762	2.1	1.102	31.2	0.318
yk410	EG25	13/06/11	13	-425.9	4.5	-424.4	29.9	4.7	12.2	26.8	151	968	3.5	1.164	31.4	0.304
yk411	EG25	13/06/11	13	-431.4	10	-424.4	33.5	7.5	18.7	45.9	229	288	5.8	1.23	29.9	0.225
EG25-5.12	EG25	01/02/12	13	-426.5	5.12	-425.2	18.5	2.9	7	15.7	91	984	2.1	1.1		0.314
yk420	EG26	13/06/11	40	-424.4	17.8	-423.8	12.4	1.8	5.2	8.7	56.5	3089	1.3	1.0648	32.7	0.338
yk421	EG26	13/06/11	40	-436.6	30	-423.8	37.2	7.2	17.4	42.9	226	268	5.7	1.2317	31.2	0.254
yk422	EG26	13/06/11	40	-441.6	35	-423.8	37.4	7.2	17.6	43.3	220	251	5.7	1.2334	29.2	0.262
EG26-22	EG26	01/02/12	40	-428.6	22	-424.6	30.1	4.5	10.5	24.3	142	945	3.3	1.15	28.8	0.327
yk11	EG11[c]	21/01/08	80	-420.7	15.9	-419.9	10.5	1.8	4.8	8.4	51		1.2	1.056	27.1	0.317
yk12	EG11[c]	21/01/08	80	-423.9	19	-419.9	28.6	4.7	11.1	25.5	142		3.5	1.147	27.8	0.311
yk113	EG11[c]	22/06/09	80	-423.4	18.5	-421.4	15.9	2.5	6.5	12.6	73	2300	1.6	1.08	32.8	0.336
yk240	EG11[c]	13/06/10	80	-424.4	19.5	-422.3	14.8	2.2	5.9	11.3	68	2333	1.5	1.074	31	0.336
yk13	EG22[c]	21/01/08	80	-432.3	26.5	-420.2	38.4	7.4	16.8	41.6	221		5.6	1.228	26.3	0.268
EG22-29.5	EG22[c]	24/03/09	80	-435.3	29.5		38.1	7.3	16.4	41.2	219		5.7	1.23		0.269
yk122	EG22[c]	22/06/09	80	-425.8	20	-421.6	29.4	4.4	11.3	24	136	1000	3	1.143	32.9	0.334
yk123	EG22[c]	22/06/09	80	-433.8	28	-421.6	39.1	7.2	15.8	39.8	212		5	1.22	32.2	0.285
yk241	EG22[c]	13/06/10	80	-426.8	21	-422.5	28.2	4.2	10.3	23.1	137	1074	3.1	1.143	35.1	0.319
yk242	EG22[c]	13/06/10	80	-431.1	25.3	-422.5	32.8	5.3	13	29.9	169	675	3.9	1.174	34.3	0.3
yk243	EG22[c]	13/06/10	80	-435.3	29.5	-422.5	38.1	7.3	16.6	41.3	219	296	5.4	1.22	32.6	0.268
yk244	EG22[c]	13/06/10	80	-427.8	22	-422.5	24.8	3.6	9.1	19.8	117	1362	2.6	1.124	33.8	0.326
EG22-19.7	EG22	31/01/12	80	-425.5	19.7	-424.5	9.8	1.6	3.9	6.7	41	3417	1	1.05	29.7	0.365
EG22-22	EG22	31/01/12	80	-427.8	22	-424.5	23.9	3.3	8.2	17.5	106	1656	2.3	1.11	29.4	0.35
EG22-29	EG22	31/01/12	80	-434.8	29	-424.5	34.5	5.6	12.6	30.4	169	624	4.2	1.17	28.3	0.316
yk111	EG21[c]	22/06/09	80	-425.9	20	-422.1	30.2	4.5	11	24.2	139		2.9	1.147	31.5	0.336
yk112	EG21[c]	22/06/09	80	-434.9	29	-422.1	38.5	7.7	16.6	42.3	219		5.1	1.229	31	0.271
yk247	EG21[c]	13/06/10	80	-424.8	18.9	-423.0	18.6	2.8	7.2	14.5	87	1922	2	1.095	33.8	0.331
yk248	EG21[c]	13/06/10	80	-428.2	22.3	-423.0	32.2	4.8	11.7	26.4	152	849	3.5	1.161	34.7	0.327
yk249	EG21[c]	13/06/10	80	-431.5	25.6	-423.0	36.4	5.9	14.3	32.2	184	553	4.4	1.192	34.6	0.304
yk250	EG21[c]	13/06/10	80	-435.5	29.6	-423.0	38.3	7.4	16.5	41.8	220	253	5.5	1.225	33.2	0.268
yk110	EG20[c]	22/06/09	80	-469.9	64	-421.7	38.1	8.1	17.3	44.4	227		5.3	1.235	27.6	0.259
yk245	EG20[c]	13/06/10	80	-451.6	45.7	-422.6	36.3	7.5	17.2	42.9	224	250	5.5	1.228	31.5	0.25
yk246	EG20[c]	13/06/10	80	-468.9	63	-422.6	36	7.5	17.3	42.8	220	233	5.5	1.233	31.2	0.252
EG20-55	EG20	01/02/12	80	-460.9	55	-424.7	35.7	7.6	16	42.8	219	238	5.9	1.23	23.6	0.252
EG17-35	EG17	28/06/04	150	-431.5	35		41	7.5	16.7	42.9	221		5.5			0.287
EG17-38	EG17	16/05/05	150	-434	38		38.9	7.5	17.2	44.9	221		5.2			0.271
EG17-50	EG17	24/06/04	150	-446.5	50		35.3	7.7	17.1	46	222		5.4			0.245

[a] Gavrieli (1997) [b] Reznik et al (2009) [c] Cl concentrations from Kiro et al (2012)

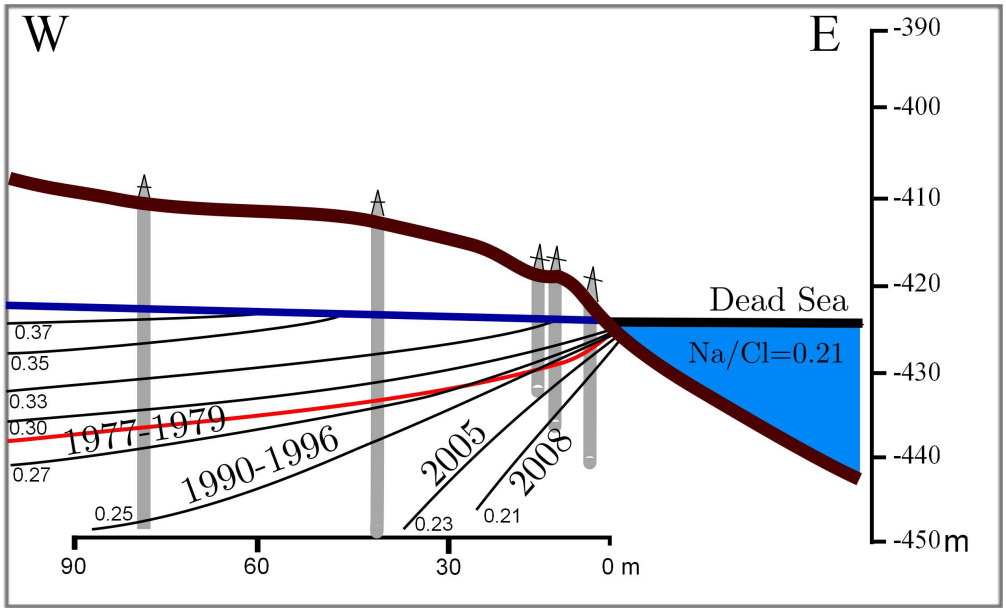
Table 3.2: Activities of radon and radium isotopes in the Dead Sea water and groundwater. Errors on ^{226}Ra and ^{222}Rn measurements are 5% and those of ^{228}Ra, ^{224}Ra and ^{223}Ra are 10%.

Sample	Cl (g/L)	Dist. from shore inland (m)	^{226}Ra (dpm/L)	^{228}Ra (dpm/L)	^{223}Ra (dpm/L)	^{224}Ra (dpm/L)	^{222}Rn (dpm/L)	^{224}Ra/ ^{228}Ra	^{226}Ra/ ^{223}Ra	^{224}Ra/ ^{223}Ra	^{228}Ra/ ^{226}Ra	^{222}Rn/ ^{223}Ra
Dead Sea - 1983	223		138[a]									
Dead Sea - 2008	230		146[b]									
yk400	148	5	27	4.6	8.3	22		4.8	3.3	2.7	0.17	
yk401	230	5	96	1.3	7.9	9.3		7.2	12.2	1.2	0.01	
yk413	216	5	46	9.9	16	39	482	4	2.9	2.5	0.21	31
yk414	229	5	128	5.5	19	27	325	4.8	6.8	1.4	0.04	17
yk415	232	5	133	0.9	15	14	428	15.3	9	1	0.01	29
yk3[c]	67	10	16		5	8	1423		3.2	1.6		285
yk6[c]	142	10	22	6.8[d]	17	26	2324	3.8	1.3	1.5	0.31	137
yk9[c]	224	10	101	<4	31	39	300	>9.8	3.3	1.3	<0.04	10
yk416	196	10	39	8.4	14	27	173	3.2	2.7	1.9	0.22	12
yk417	228	10	94	2.1	23	44		20.8	4.1	1.9	0.02	
yk418	223	10	103	19.9	58	68		3.4	1.8	1.2	0.19	
yk419	231	10	97	2.1	22	50	771	23.8	4.3	2.2	0.02	35
EG23-6.8	110	10										
yk402	82	13	13	1.3	5.2	13		10	2.5	2.5	0.1	
yk412	95	13	20	3.3	13	34	2405	10.3	1.5	2.6	0.17	185
yk410	151	13	36	12	13	37	1164	3.1	2.8	2.8	0.33	90
yk411	229	13	96	17	15	27		1.6	6.4	1.8	0.18	
yk420	56.5	40	13	3	10	27	56	9.8	1.3	2.7	0.21	6
yk421	226	40	65	25	17	35		1.4	3.8	2.1	0.39	
yk422	220	40	62	24	26	108		4.5	2.4	4.1	0.39	
yk11[c]	51	80	6	1.3[d]	2.8	7	1286	5.4	2.1	2.5	0.22	459
yk12[c]	142	80	29	7.5[d]	7.5	15		2.0	3.9	2	0.26	
yk113[c]	73	80	10	1.8[d]	1.5	1.9	1462	1.1	6.7	1.3	0.18	975
yk240[c]	68	80	14	5.8[d]	5	12	1096	2.1	2.8	2.4	0.41	219
yk13[c]	221	80	39	9.4[d]	17	40	689	4.3	2.3	2.4	0.24	41
EG22-29.5[c]	219	80	60	16	4.8	20	2417	1.3	12.5	4.2	0.27	504
yk122[c]	136	80	30	11[d]	3.7	6.8	1324	0.6	8.1	1.8	0.37	358
yk123[c]	212	80	52	8[d]	13	18	976	2.3	4	1.4	0.15	75
yk241[c]	137	80	16	4.6[d]	5.3	8.8	1406	1.9	3	1.7	0.29	265
yk242[c]	169	80	11	9[d]	8.6	17	1243	1.9	1.3	2	0.82	145
yk243[c]	219	80	80	10[d]	5.2	19	2060	1.9	15.4	3.7	0.13	396
yk244[c]	117	80	14	5.2[d]	4.7	11	1267	2.1	3	2.3	0.37	270
yk111[c]	139	80	46	3.2[d]	0.9	2.5	2433	0.8	51.1	2.8	0.07	2703
yk112[c]	219	80	54	14	4.1	8.8	2299	0.6	13.2	2.1	0.26	561
yk247[c]	87	80	16	3.9[d]	1.8	6.3	2652	1.6	8.9	3.5	0.24	1473
yk248[c]	152	80	26	7.8[d]	3.2	9		1.2	8.1	2.8	0.3	
yk249[c]	184	80	41	5.8[d]	4.9	11	1801	1.9	8.4	2.2	0.14	368
yk250[c]	220	80	72	16[d]	8.9	27	1195	0.9	8.1	3	0.4	134
yk110[c]	227	80	68	27	5.8	11	501	0.4	11.7	1.9	0.4	86
yk245[c]	224	80	62	33[d]	26	52		1.6	2.4	2	0.53	
yk246[c]	220	80	75	20[d]	17	34	439	1.7	4.4	2	0.27	26

[a] Chan and Chung (1987), data from 1979 [b] Kiro et al (2012) [c] Ra data from Kiro et al (2012) [d] This study



(a)



(b)

Figure 3.1: Groundwater composition cross sections in Arugot alluvial fan aquifer. (a) Salinity (Cl concentrations) contours showing the circulated Dead Sea hypersaline water zone (red) and the fresh–saline transition zone (orange to green); (b) Na/Cl contours, the area beneath the red line contains circulated Dead Sea water and the area between it and the water table (blue line) is the fresh–saline transition zone. Notice that actually there is no fresh groundwater zone close to the Dead Sea.

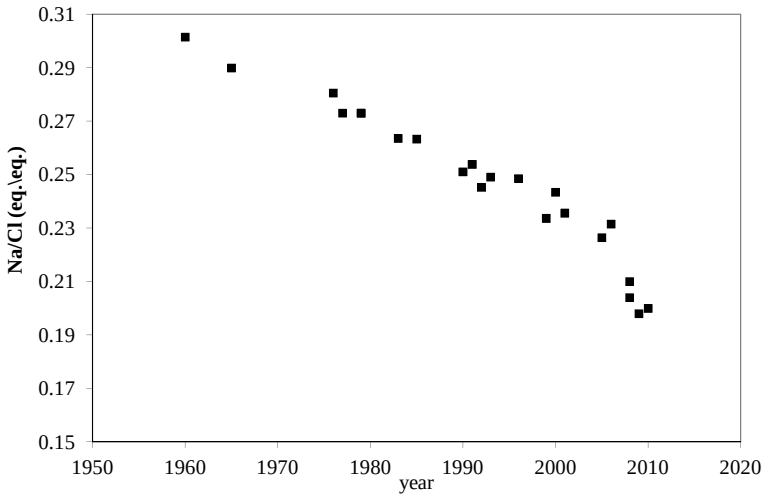


Figure 3.2: The change in Na/Cl ratio in the Dead Sea water during the past fifty years (after Gavrieli, 1997; Reznik et al, 2009).

Groundwater age by radium isotopes

^{228}Ra activities in borehole water along a transect perpendicular to the Dead Sea are shown in Fig. 3.3. ^{228}Ra is increasing with distance from shore, evidently due to contribution from the aquifer solids. ^{224}Ra is also high compared with that in the Dead Sea water (36 ± 25 and 0.5–2.5 dpm/L), and ^{224}Ra/^{228}Ra ratio varies between 0.6 and 23.5 (Table 3.2). Based on the short half-life of ^{224}Ra (3.66 days), we assume that all the water sampled in the hypersaline zone, starting 5m from the lake (Table 3.2), already attained steady-state concentrations. The reason for the high variability in ^{224}Ra activities is its sensitivity (due to its short half-life) to aquifer compositional heterogeneity, which may affect both K (less relevant in the hypersaline environment) and ^{224}Ra production rate.

As shown by the Na/Cl method, hypersaline water ages in the studied boreholes are years to a few tens of years. This is compatible with the half-life of ^{228}Ra, which is 5.75 y. In the hypersaline environment, radium adsorption is negligible (i.e. $K \sim 0$, Kiro et al, 2012), leaving the half-life of the isotope as the most important parameter in the determination of its concentration in groundwater.

The groundwater age or velocity can be obtained by the ^{228}Ra mass balance:

$$\frac{\partial C}{\partial t} = -\nabla \cdot \mathbf{v}C + \nabla \cdot \mathbf{D}\nabla C - \lambda(K+1)C + P - S \tag{3.1}$$

where C[dpm/L] is ^{228}Ra activity in groundwater, t[T] is time, $\mathbf{v}$[L/T] is velocity, $\mathbf{D}$[L^2/T]

is dispersion, λ[1/T] is the decay constant, P[dpm/(L · T)] is the production rate of ^{228}Ra from the aquifer solids by recoil and dissolution and K is a dimensionless adsorption partition coefficient given by $K = C_s/C$ where C_s[dpm/L] is the activity of ^{228}Ra on the solid surface expressed as equivalent concentration in water. S is the rate of ^{228}Ra co-precipitation with barite (see discussion of ^{226}Ra in section 3.3.2).

The one-dimensional solution for ^{228}Ra concentration along the saline-water flow path, assuming steady state ($\frac{\partial C}{\partial t} = 0$), negligible hydrodynamic dispersion (the Na/Cl data indicate that the transport is more advective than dispersive) and negligible co-precipitation with barite ($S = 0$, see Appendix B and Fig. 3.3 where ^{228}Ra activity with and without co-precipitation are compared) is:

$$C(x) = \frac{P}{\lambda(K+1)}\left(1 - e^{-\frac{\lambda(K+1)x}{v_x}}\right) + C_0 e^{-\frac{\lambda(K+1)x}{v_x}} \tag{3.2}$$

where v_x[T/L] is the velocity along the saline groundwater flow path, x[L] is the distance from the shore inland and C_0[dpm/L] is the activity of ^{228}Ra at the lake boundary.

According to this equation, ^{228}Ra increases as the saline groundwater flows inland until it reaches a steady-state concentration (Fig. 3.3), which represents the equilibrium between prodcution, decay and adsorption. The known parameters are ^{228}Ra concentrations and the distance from the lake (x). Assuming ^{224}Ra attained steady state a very short while (~3 weeks, based on its 3.66 days half-life) after entering the aquifer, we defined ^{228}Ra steady-state concentration as 1–0.67 the ^{224}Ra concentrations (Davidson and Dickson, 1986).

Since ^{224}Ra is quite variable, we used the mean of all samples measured in the hypersaline water zone (Table 3.2), which is 36 dpm/L, assuming this averages the aquifer heterogeneity effect. Accordingly, the steady-state concentration of ^{228}Ra should vary between 24 and 36 dpm/L, while the best fit is for 28 dpm/L (^{224}Ra/^{228}Ra=1.3, Fig. 3.3).

Calculated ^{228}Ra activities for the hypersaline groundwater ($K = 0$), are shown in Fig. 3.3 with distance from shore. The velocities that fit the field data from the Dead Sea hypersaline water zone are 1–6 m/y. With $K > 0$, the calculated velocities that fit the field data are larger (e.g. $v = 30$ m/y for $K = 10$, eq. 3.2). The similarity to the Na/Cl velocities obtained above supports the use of the very low K of Kiro et al (2012).

The velocities obtained by both methods are also consistent with hydrological simulations (Kiro et al, 2008) and with radiocarbon data (Avrahamov et al, 2010), and it further allows the assessment of the overall rates of geochemical processes that occur during Dead Sea water circulation in the aquifer. In the following discussion, we will use an approximate average

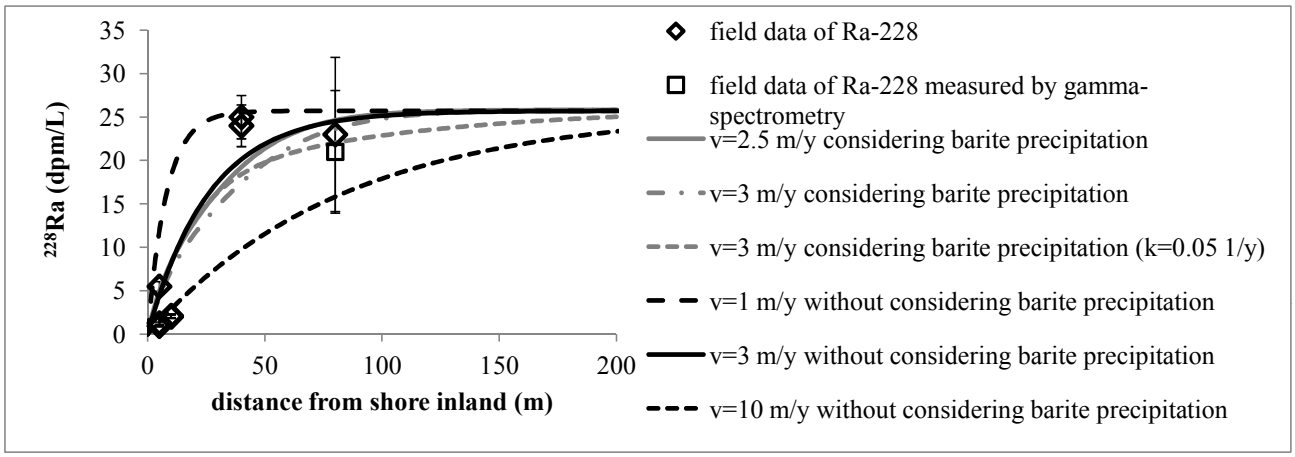


Figure 3.3: Calculated and measured ^{228}Ra activities in circulating Dead Sea water (hypersaline groundwater) with distance from shore. The activity at 80m is an average of several samples from different boreholes in which some were measured by γ-spectrometry (Kiro et al, 2012) and the others were measured by RaDeCC (section 3.2). The error bars are for the analytical error, while the 80m bars include the standard deviation of the samples (Table 3.2). The calculated curves are according to equation 3.2 and the equation in Appendix B, which includes the co-precipitation of ^{228}Ra with barite. ^{224}Ra/^{228}Ra steady-state ratio is assumed to be 1.4 and $k = 0.22$ y^{-1} is used for barite precipitation (Appendix B).

velocity of 3 m/y for the hypersaline, circulated Dead Sea water zone of the aquifer.

It should be noted that the saline groundwater velocities obtained here are during the Dead Sea lake level drop. Kiro et al (2008) have shown that while Dead Sea water circulation in the aquifer persist during the lake level drop, it is slower than during steady-state conditions. Assuming the saline groundwater circulation reaches a distance of 200 meters from the shore (Kiro et al, 2008), the estimated time interval of the whole circulation during lake level drop is around 130 y, while under steady state lake level, it should be much shorter – around 15 years (an order of magnitude larger, Kiro et al, 2008).

3.3.2 Reaction rates in the hypersaline groundwater

During the circulation of the Dead Sea water in the aquifer, the concentration of several elements changes relative to their initial concentration in the lake. Ba, ^{226}Ra, U, Sr, SO_4, Rb, Li, Si and Mo decrease, while the short-lived radium isotopes, Fe and Mn increase (Table 3.3). In the following section we discuss the kinetics of water–rock reactions that affect the concentrations of some of these elements in the circulated Dead Sea hypersaline groundwater based on the above calculated groundwater velocity.

Table 3.3: Trace element concentrations in Dead Sea water and groundwater. Errors are up to 5%.

Sample	Cl (g/L)	Sr (mg/L)	Br (g/L)	Ba (mg/L)	Mn (mg/L)	Fe (mg/L)	U (μg/L)	Mo (μg/L)	Li (mg/L)	Rb (mg/L)	B (mg/L)	Si (mg/L)
Dead Sea - 1983	223		5.3	4.5[b]								
Dead Sea - 2008	230	361	5.1	4.9	7[d]	1[d]	2.4[e]	27	17.9[f]	2[f]	63.8[f]	71.7[f]
yk400	148	216	3.4	1.2	5.3		1.2		11	1.3		4
yk401	230	360	6	4.1	6.7		0.6		17	1.9		1.5
yk413	216	305	5.4	2.2	6.7	7	1.4		10.9	1.3		
yk414	229	334	6.05	3.5	7.8	<1	0.9		12.9	1.4		
yk415	232	338	6.1	4	7	<1	0.7		12.7	1.4		
EG24-10	223	370	6.4	3.6	7.9	<0.5	<1	5.7	20.0	1.1	57.9	2.9
EG24-19	224	386	4.9	4.3	7.3	<0.5	<1	12.5	24.2	1.3	70.8	2.9
yk3[g]	67	105	1.6	0.36								
yk6[g]	142	201	5.8	1								
yk9[g]	224	317	5.8	2.3								
yk416	196	263	4.7	1.3	6.5	13	1.1		9	1.1		
yk417	228	330	6	3.2	8.4	2	0.9		12	1.4		
yk418	223	330	6.1	3.1	7.3	4	0.5		12	1.3		
yk419	231	333	6.3	3.3	7.6	4	0.4		12	1.4		
EG23-6.8	110	170	2.6	1.7	5.9	12	3	50	14	0.9	50	9
yk402	82	120	1.8	0.5	2.1		1.4		6	0.7		15
yk412	95	133	2.1	0.6	2.3	11	1.3		5.2	0.6		
yk410	151	206	3.5	0.9	4.3	11	0.7		7.9	1		
yk411	229	322	5.8	2.8	7.9	3	0.7		12.5	1.4		
EG25-5.12	91	142	2.14	1.3	4.2	3.6	2	6	13	0.7	47	7.5
yk420	56.5	84	1.3	0.4	1.5	2	2.1		2.9	0.4		
yk421	226	295	5.7	1.4	9.3	13	<0.1		11.1	1.3		
yk422	220	300	5.7	1.4	8.8	12	<0.1		10.6	1.3		
EG26-22	142	217	3.3	1.2	4.8	9.3	<1	2	16	1	58	8
yk11[g]	51	85	1.2	0.36								
yk12[g]	142	203	3.5	1.2								
yk113[g]	73	116	1.6	0.48								
yk240[g]	68	103	1.5	0.5	1.8	2	0.7					
yk13[g]	221	303	5.6	1.7								
EG22-29.5[g]	219	295	5.7	1.5								
yk122[g]	136	206	3	1								
yk123[g]	212	294	5	1.3								
yk241[g]	137	190	3.1	1	3.9	5	0.2					
yk242[g]	169	234	3.9	1.2	5.3	7.5	0.09					
yk243[g]	219	297	5.4	1.6	9.4	19	0.07					
yk244[g]	117	163	2.6	0.85	3.2	3.5	0.27					
EG22-19.7	41	77	1	0.3	1	1.2	<1	5	6	0.4	38	24
EG22-22	106	167	2.3	0.7	2.5	3	<1	<1	13	0.8	50	9
EG22-29	169	266	4.2	1.5	6.8	9.2	<1	20	20	1.2	65	6
yk111[g]	139	203	2.9	0.96								
yk112[g]	219	310	5.1	1.3								
yk247[g]	87	126	2	0.58	2.3	3	0.54					
yk248[g]	152	209	3.5	1.05	4.4	6.4	0.17					
yk249[g]	184	252	4.4	1.25	5.5	7.4	0.11					
yk250[g]	220	306	5.5	1.4	9.3	12.5	<0.05					
yk110[g]	227	320	5.3	1.5								
yk245[g]	224	307	5.5	1.5	9.5	11	0.12					
yk246[g]	220	307	5.5	1.5	9.4	11	0.13					
EG20-55	219	340	5.9	1.5	8.2	7.5	<1	6	26	1.5	72	3
EG17-35	221	315	5.5									
EG17-38	221	305	5.2									
EG17-50	222	320	5.4									

[a] Gavrieli (1997) [b] Chan and Chung (1987), data from 1979 [c] Reznik et al (2009) [d] This study [e] Haase-Schramm et al (2004)

[f] Zilberman-Kron (2008) [g] Ba data from Kiro et al (2012)

Precipitation of sulfate minerals

Precipitation of barite (and/or celestine) and the co-precipitation of radium with barite does occur in experiments with supersaturated solutions (e.g. Langmuir and Riese, 1985; Rosenberg et al, 2011) even over a time scale of hours (e.g. Christy and Putnis, 1993). However in the Dead Sea water, being suppersaturated with barite by a factor of ~ 12 (Table 3.4), barite does not naturally precipitate, even after further evaporation (Zilberman-Kron, 2008). On the other hand, Kiro et al (2012) showed by reactive-transport modeling that adsorption alone could not be responsible for the sharp decrease in ^{226}Ra and Ba concentrations in the aquifer (Fig. 3.4) and suggested that it is the result of barite and/or celestine precipitation. This probably happens due the large solid surface area (e.g. Reznik et al, 2011) combined with the relatively long residence time in the aquifer. In this section, we discuss the kinetics of radium and barium removal by barite or celstine precipitation in the Dead Sea aquifer.

Assuming steady state and no hydrodynamic dispersion, the overall rate of removal or contribution of an element due to precipitation or dissolution could be one-dimensionally described as:

$$\frac{\partial C}{\partial x} = -\frac{k(C - C_{sat})}{v_x} \tag{3.3}$$

where $C[M/L^3]$ is the element concentration, $C_{sat}[\mathrm{M/L^3}]$ is the element concentration in the apparent saturation (the concentration where the element does not changes anymore with distance from shore), $x[\mathrm{L}]$ is the distance from shore, $k[1/\mathrm{T}]$ is the first-order rate constant $v_x[\mathrm{L/T}]$ is the groundwater velocity.

The solution for this equation is:

$$C(x) = (C_0 - C_{sat})e^{-\frac{k}{v_x}x} + C_{sat} \tag{3.4}$$

where $C_0[\mathrm{M/L^3}]$ is the initial concentration of the element in the lake.

Using 3 m/y as the groundwater velocity the removal rate of Ba and ^{226}Ra (k), or the first-order precipitation rate of barite/celstine, is 0.22 $\mathrm{y^{-1}}$.

Barite hardly precipitates in other subterranean estuaries, where Ba and Ra are usually being contributed (rather than removed) to the groundwater by desorption even in cases where the groundwater is supersaturated with barite up to a factor of six (e.g. Shaw et al, 1998; Moore, 1999; Charette and Sholkovitz, 2006). The relatively small k of barite pre-

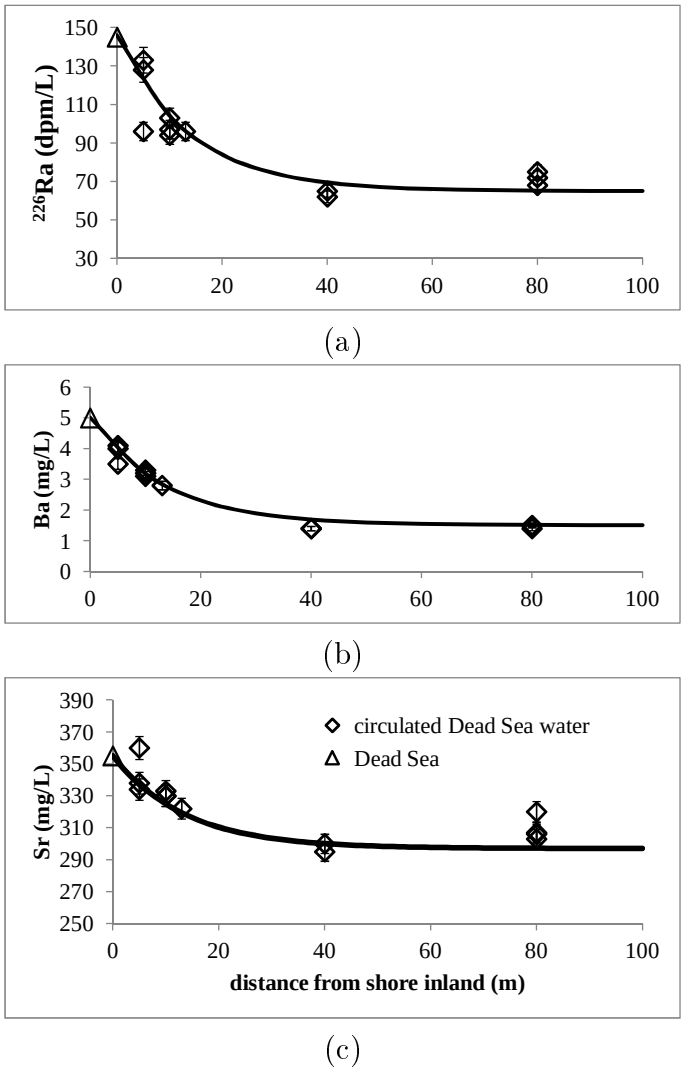


Figure 3.4: (a) ^{226}Ra, (b) Ba and (c) Sr concentrations in the hypersaline groundwater with distance from shore. The solid curve is calculated according to eq. (3.4).

Table 3.4: Degrees of saturation of barite celestine and gypsum in the Dead Sea and in the groundwater. Calculations were done using PHREEQC with the Pitzer database and at 30°C (more details in section 3.2).

Sample	Ω_{barite}	$\Omega_{celestine}$	Ω_{gypsum}
Dead Sea - 1983	11.4		1.3
Dead Sea - 2008	12.2	2.5	1.4
yk413	4.2	1.5	1
yk414	6.2	1.7	1
yk415	6.5	1.6	0.9
EG24-10	6.8	1.3	0.7
EG24-19	7.2	1.4	0.7
yk416	2.7	1.2	0.9
yk417	4.8	1.4	0.8
yk418	4.4	1.3	0.8
yk419	5	1.4	0.9
EG23-6.8	5.8	0.7	0.6
yk412	2.9	1.1	1
yk410	5.8	2	1.2
yk411	5.2	1.7	1
EG25-5.12	4.1	0.5	0.5
yk420	4.9	1.1	1.2
yk421	2.2	1.3	0.8
yk422	1.9	1.1	0.7
EG26-22	3.7	1.1	0.8
yk113	3.7	1	1
yk240	4.1	0.9	0.9
yk122	3.2	1	0.9
yk241	3.5	1	0.9
yk242	2.5	1.1	0.9
yk243	2.7	1.4	0.8
yk244	3.6	0.9	0.9
EG22-19.7	4.9	1.2	1.2
EG22-22	3.6	1.1	0.9
EG22-29	3.6	1.2	0.8
yk247	3.6	0.9	0.9
yk248	3	1	0.9
yk249	2.8	1.2	0.9
yk250	2	1.2	0.7
yk245	2.2	1.3	0.8
yk246	1.9	1.1	0.7
EG20-55	2	1.2	0.6

cipitation (time scale of years) obtained here may suggest that the short residence time of groundwater in some subterranean estuaries (Shaw et al, 1998; Charette and Sholkovitz, 2006) is the main cause for the lack of barite precipitation.

Sulfate is also significantly low in the hypersaline groundwater compared with the lake water (∼250 and 393 mg/L, respectively, Table 3.1, Fig. 3.5a), suggesting that gypsum also precipitates on entering the aquifer. The fast decrease of SO_4 compared to Ba (compare Fig. 3.4 and Fig. 3.5a) indicates that the precipitation of gypsum occurs prior to most of the precipitation of barite. Based on the above velocities, the calculated removal rate of SO_4 is 0.8 y^{-1}.

It should be noticed that radium and barium were not significantly removed by this faster gypsum precipitation, due to their relatively low distribution coefficients in gypsum (Ichikuni

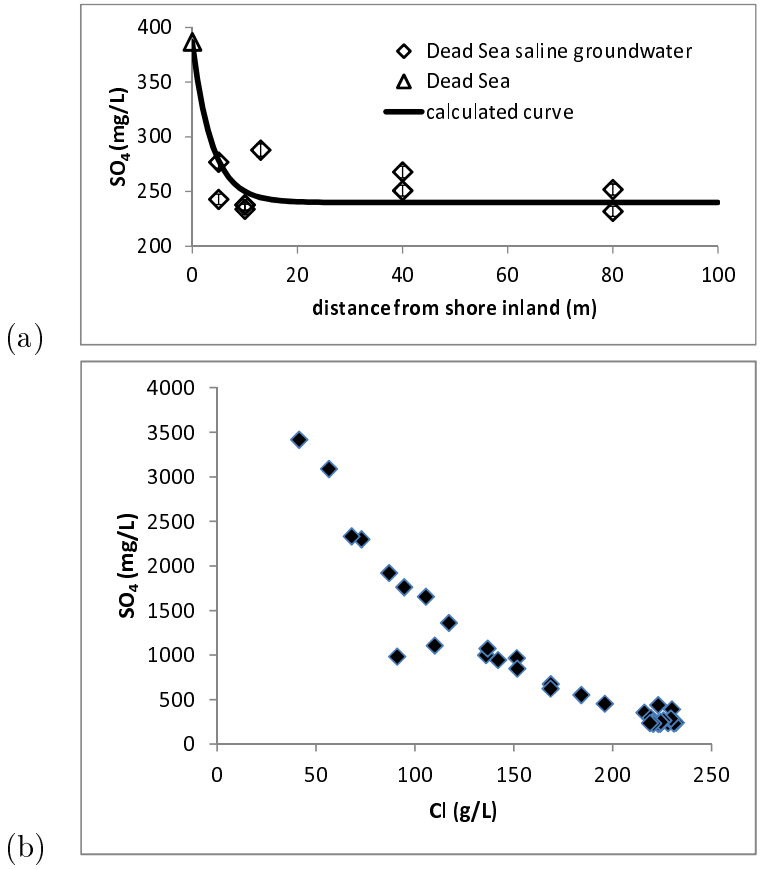


Figure 3.5: (a) Sulfate concentrations in the circulating Dead Sea water with distance from shore, (b) the relationship betewwn sulfate and salinity in groundwater of the Dead Sea coastal aquifer.

and Musha, 1978; Gnanapragasam and Lewis, 1995).

Redox-controlled reactions

Reduced conditions are common groundwater in in coastal aquifer settings (subterranean estuaries), below and at the fresh-saline water interface (Snyder et al, 2004; Sivan et al, 2005; Charette and Sholkovitz, 2006; Roy et al, 2011). These conditions affect the concentrations of certain elements, such as Mn, Fe and U (Charette and Sholkovitz, 2006; Roy et al, 2011; Sanders et al, 2012), similar to the behavior of these elements in sub-seafloor pore water (Cochran et al, 1986). Such patterns were also observed in the highly hypersaline circulated Dead Sea water, including an increase of Fe and Mn due to the dissolution of oxides and a decrease in U concentration along the saline groundwater flow path from the lake into the aquifer (Fig. 3.6). This suggests a transition to reduced conditions as the Dead Sea water flows into the aquifer. Applying similar calculations as above yields rates of the same order as for the barite precipitation, with the removal of U ($k = 0.4$ y^{-1}) being faster than the

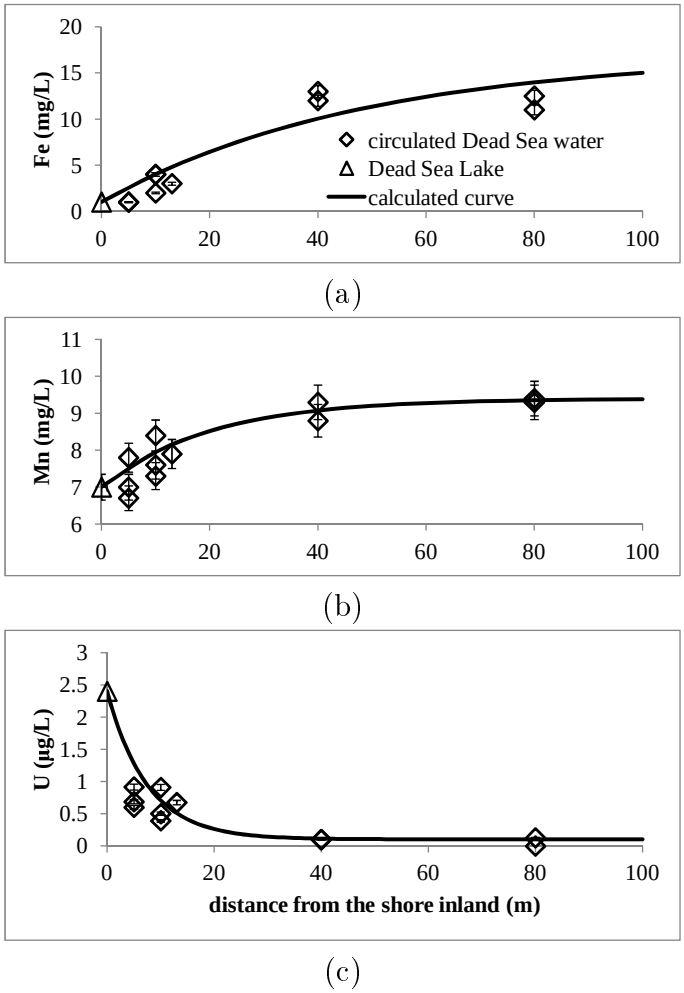


Figure 3.6: (a) Fe, (b) Mn and (c) U concentrations in the hypersaline groundwater with distance from shore, showing the contribution of Fe and Mn and the removal of U from the Dead Sea water while traveling through the aquifer.

contribution of Fe ($k = 0.06\ \mathrm{y}^{-1}$) and Mn ($k = 0.15\ \mathrm{y}^{-1}$, Fig. 3.6). In other cases, documented reduction of Fe-oxides is much faster (Cochran et al, 1986), and therefore occurs even where groundwater residence time is short (e.g. Charette and Sholkovitz, 2006). The slow rate in the Dead Sea case may be due to the bio-mediated nature of the Fe-oxides reduction, which could be significantly different under the hypersaline conditions of the Dead Sea water (Oren, 1999). Fe-oxides, which are reduced by organic carbon, could also be sensitive to the organic carbon content of the groundwater system, resulting in a very slow process on the order of thousands of years in a poor-carbon systems (Roy et al, 2011).

In common marine seafloor and coastal aquifer settings (Cochran et al, 1986; Charette and Sholkovitz, 2006), uranium is usually reduced later than or between the reduction and dissolution of the Mn and Fe oxides (Klinkhammer and Palmer, 1991; Cochran et al, 1986),

while in the Dead Sea aquifer, uranium is reacting earlier (larger k). The reason for the difference in the sequence of reduction could be either geochemical (e.g. pH) or microbiological (Cochran et al, 1986). Since the microbial halophilic community of the hypersaline environment of the Dead Sea is significantly different from any other environment (Oren, 1999), the order of reduction may also be different. Alternatively, U(VI) can be removed by adsorption onto organic matter or oxides (Kolodny and Kaplan, 1973), which is usually a fast process, at the low pH of the Dead Sea (5–6). This should be further studied.

3.3.3 Processes in the fresh-saline transition zone

Sulfate in the transition zone

The groundwater in the fresh–saline transition zone (lower Cl concentrations and densities, Fig. 3.1) next to the Dead Sea shore contains elevated concentrations of sulfate (up to $\sim$ 3400 mg/L, Table 3.1) compared with that in the circulated Dead Sea hypersaline water, and its concentration increases with decreasing salinity (Fig. 3.5b). This is apparently due to the dissolution of gypsum available in the sediment, while the water retains a degree of saturation (Ω) close to 1 (Table 3.4). The dissolution of gypsum and the increase in sulfate in the fresher groundwater also keeps the mixed water supersaturated with barite ($\Omega = 2 - 6$, Fig. 3.7, Table 3.4) and celestine (Table 3.4) even though the Ba ans Sr concentrations decrease with decreasing salinity. The supersaturation of these minerals even slightly increases with decreasing salinity (Fig. 3.7). Nevertheless, barite apparently does not precipitate from this water (Kiro et al, 2012), just from the circulated Dead Sea water, where Ω is above $\sim$ 2. This could be due to the different salinity, as well as to the short residence time of water in this zone (<2 y, with velocities of 30-300 m/y, compared with 3 m/y in the hypersaline zone, Kiro et al, 2008).

The dissolution of gypsum in the transition zone water is limited to the immediate vicinity of the lake, while farther inland sulfate concentrations are low (in a borehole 1km from lake, SO_4 concentrations were 190–500 mg/L). This is probably due to the fact that gypsum availability for dissolution is restricted to the close-to shore fresh–saline transition zone area, where Dead Sea hypersaline water has been recently circulating (prior to the lake level drop) and gypsum precipitation was taking place. Farther away from the shore, any available gypsum if occurred, has been probably already washed away.

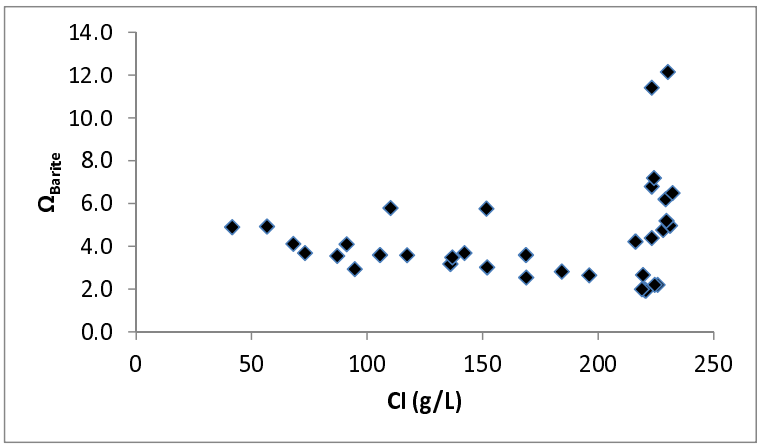


Figure 3.7: Degree of saturation of barite in the fresh–saline groundwater transition zone, calculated with PHREEQC.

Adsorption–desorption processes

It is well established that salinity affects the adsorption and desorption of several trace elements (Turner, 1996), in particular that of radium (Webster et al, 1995; Sturchio, 2001; Gonneea et al, 2008; Kiro et al, 2012). In a previous work, we found that the adsorption distribution coefficient (K) in the Dead Sea aquifer is very low, varying between 0–0.6 in the hypersaline groundwater to 6–10 in the fresh groundwater end-member. This was based on the radium data from one borehole with different salinities (Kiro et al, 2012). Examining the data from all boreholes makes it clear that radium adsorption is highly variable both in saline and fresh groundwater in the aquifer (Fig. 3.8), probably due to the variability in the content of clay minerals and Fe or Mn oxides in the aquifers. In this section we derive K in the fresh water end-member based on the activities of radium isotopes in the fresh-saline transition zone.

In the case of a short-lived radium isotope (^{224}Ra and ^{223}Ra) eq. 3.2 can be reduced to (Kiro et al, 2012):

$$C = \frac{P}{\lambda(K+1)} \tag{3.5}$$

where C[dpm/L] is the radium activity, P[dpm/(LT)] is the production rate of the radium isotope, K is the dimensionless partition coefficient and λ[1/T] is the decay constant.

While this equation cannot be used to define the definite K, it is useful for the characterization of the relationship between salinity and K. Based on the response of the ^{226}Ra distribution to the Dead Sea lake level drop, Kiro et al (2012) showed that K in the saline

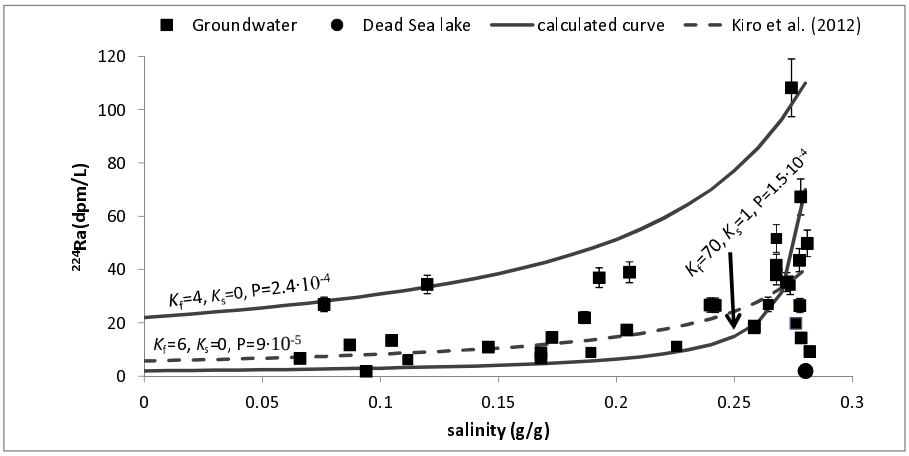


Figure 3.8: Compilation of ^{224}Ra activities and salinities in water from different boreholes at the Arugot alluvial fan aquifer. Activities increase with salinity due to the low adsorption in the hypersaline groundwater. A very similar pattern is shown by the ^{223}Ra activities (Kiro et al, 2012). The solid and dashed lines are curves calculated according to eq. 3.5 with various K_f (K_f and K_s are the maximal and minimal K values in the fresh and hypersaline groundwater, see text for further explanation).

groundwater should be less than 1, while P could be deduced from the activity of radium in the saline groundwater. Fitting the short-lived radium data (^{224}Ra and ^{223}Ra, Fig. 3.8, Table 3.2) from all boreholes to the above equation and linearly extrapolating to zero salinity yields a fresh water K between 6 and 70 (an adsorption distribution coefficient K_d between 0.6 and 7 L/Kg).

K can also be calculated using the long-lived radium isotope, ^{226}Ra. Radium (^{226}Ra) activities in the fresh-saline transition zone decrease with salinity (Fig. 3.9), which is mainly due to the mixing with low radium fresh groundwater, while its activity in the groundwater is hardly affected by the adsorption–desorption processes because ^{226}Ra is already adsorbed on the aquifer solids due to its long half-life (Kiro et al, 2012). The amount of ^{226}Ra adsorbed onto the aquifer solids can be derived from the activity of ^{222}Rn in the relevant groundwater, since the latter is produced by the disintegration of ^{226}Ra on the aquifer solids. The highest concentrations of unsupported ^{222}Rn, therefore the highest concentration of adsorbed radium, were observed in water with intermediate salinities ($\sim$ 100 gr/L Cl Fig. 3.9). The location of the peak of adsorbed radium in the mixed water zone is probably determined by the combined effect of the high radium supply by the Dead Sea circulated hypersaline water and the reduced salinity due to mixing with fresh groundwater. ^{222}Rn peak in the transition zone was also observed in Waquoit Bay (Dulaiova et al, 2008), where indeed the highest activities of ^{222}Rn coincide with high concentrations of ^{226}Ra and Mn in the sediments.

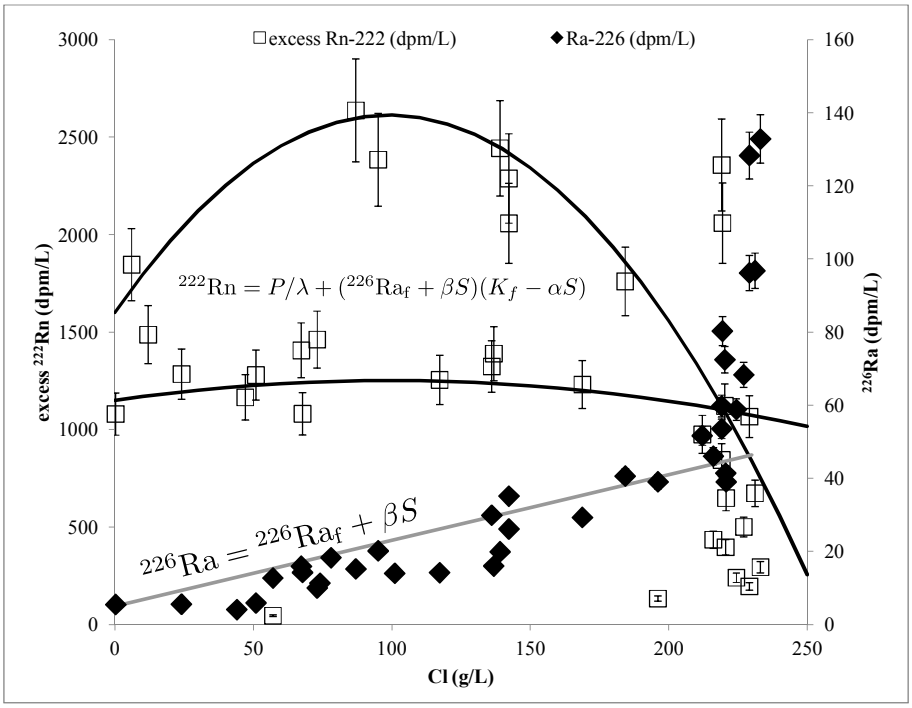


Figure 3.9: Excess ^{222}Rn over salinity (Table 3.2) in the Dead Sea aquifer groundwater. The solid curves were calculated according to eq. 3.7 so as to fit the field data (P/λ is 1100 dpm/L). The two samples with very low ^{222}Rn activity from the fresh–saline transition zone were taken close to the water table, where radon may have escaped to the atmosphere. ^{226}Ra activities are also shown together with the fitted linear relationship between ^{226}Ra and salinity in the fresh–saline transition zone ($^{226}Ra = 5 + 0.2S$, Kiro et al, 2012).

Assuming steady state, the unsupported ^{222}Rn activity in the groundwater can be defined as:

$$^{222}\mathrm{Rn} = \frac{P_{222}}{\lambda} + K \cdot {}^{226}\mathrm{Ra} \tag{3.6}$$

where λ[1/T] is the decay constant of ^{222}Rn, P_{222}[dpm/(L $\cdot$ T)] is the production rate of ^{222}Rn from the decay of supported ^{226}Ra in the solid grain and $K \cdot {}^{226}$Ra[dpm/(L $\cdot$ T)] is the production from the unsupported ^{226}Ra adsorbed onto the grain surface, where K is the dimensionless partition coefficient of radium and ^{226}Ra[dpm/L] is the activity of ^{226}Ra in the groundwater.

Assuming a linear relationship between both K and salinity (S) and ^{226}Ra and salinity (mixing) in the transition zone, as reflected in Fig. 3.9, we can define $^{226}\mathrm{Ra} = {}^{226}\mathrm{Ra_f} + \beta S$, where $^{226}\mathrm{Ra_f}$ (=5 dpm/L) is the activity of ^{226}Ra in the fresh groundwater, and β (=0.2) is the dependence of ^{226}Ra on salinity (S). The linear relationship between K and salinity is defined by $K = K_f - \alpha S$, where K_f is the partition coefficient in the fresh water and α is the dependence of K on salinity. Substituting into eq. 3.7, this yields a quadratic equation of ^{222}Rn as a function of salinity:

$$^{222}\mathrm{Rn} = \frac{P}{\lambda} + {}^{226}\mathrm{Ra_f}K_f + (\beta K_f - \alpha\,{}^{226}\mathrm{Ra_f})S - \alpha\beta S^2 \tag{3.7}$$

The calculated K_f that fits the field data from the Dead Sea aquifer (Fig. 3.9) varies between 10 and 100 (when K in the saline groundwater is assumed zero), which is similar to the range of values obtained by the short-lived radium isotopes (6-70).

The K values obtained in this study for fresh water are lower than in other studies (e.g. Krishnaswami et al, 1982; Webster et al, 1995; Sturchio, 2001; Gonneea et al, 2008) by at least an order of magnitude (e.g. ~3000, Gonneea et al, 2008). Many factors may control the radium adsorption such as the sediment content of Mn and Fe oxides, the reductive dissolution of these oxides (Gonneea et al, 2008), clay content (Webster et al, 1995) and other characteristics of the sediment. The linear relationship between the salinity and K in the fresh–saline transition zone suggests that the adsorption of radium is constrained by the availability of adsorbing sites (Kiro et al, 2012). The reduced conditions and the dissolution of Fe and Mn oxides during Dead Sea groundwater circulation (section 3.3.2)

may significantly reduce the number of adsorbing sites in the hypersaline water zone of the aquifer. However, reduced conditions are common in groundwater, in particular in coastal aquifers (e.g. Charette and Sholkovitz, 2006; Roy et al, 2011), therefore, it would be difficult to understand why the above explanation holds just for the Dead Sea aquifer. Alternatively, at the Dead Sea aquifer, the continuous lake level drop has been continuously exposing previously hypersaline water zones with relatively few adsorbing sites to the fresh–saline transition zone groundwater, which could result in relatively low K's. We also note that most K values were defined via lab experiments (e.g. Webster et al, 1995; Gonneea et al, 2008). The upscaling from lab to the field may result in K differences of an order of magnitude due to preferential flow or inhomogeneous distribution of clays or oxides (Goren et al, 2011). Nevertheless, large K's of radium in fresh groundwater were also determined in the field by Krishnaswami et al (1982). To conclude, it seems that radium K is highly sensitive to aquifer parameters, and it should be further studied both in lab and in the field.

3.4 SUMMARY

This paper discusses water ages and rates of processes involved in seawater circulation in the aquifer. The groundwater velocities were estimated both by Na/Cl ratios (unique to the Dead Sea system) and the accumulation rate of ^{228}Ra and were found to be between 1 and 6 m/y. ^{228}Ra was proved to be a useful tool for the determination of groundwater age or velocity.

During Dead Sea water circulation in the aquifer, Ba, ^{226}Ra, U and other elements are removed, while ^{228}Ra, Mn and Fe are added, all before dilution with fresh water takes place. The rate constants of the removal or contribution of certain elements were calculated. It was found that gypsum precipitation, which removes SO_4, is the fastest process ($k = 0.8$ y^{-1}), while the removal of Ba and ^{226}Ra due to barite/celestine precipitation is slower ($k = 0.22$ y^{-1}). U is removed relatively fast ($k = 0.4$ y^{-1}) and the redox-driven dissolution of Mn and Fe oxides is the slowest ($k = 0.15$ and 0.06 y^{-1}, respectively). During the follow-up dilution with fresh water, adsorption (radium) as well as gypsum dissolution takes place.

This study highlights the importance of aquifer residence times in the discussion of the geochemical processes that occur during seawater circulation in the aquifer. It was shown in other subterranean estuaries that though highly supersaturated, barite does not precipitate in pore water. In this study we show that this is a matter of residence time, and that the tens of years of Dead Sea water circulation in the aquifer are enough to allow barite precipitation. The time scales of the reduction and dissolution of Fe-oxides vary over several

orders of magnitude, from weeks to thousands of years. In the Dead Sea case, the dissolution of Fe-oxides occurs over tens of years, which is possible due to the long residence time of the Dead Sea circulated water.

Chapter 4

Modeling radium distribution in coastal aquifers during sea level changes: The Dead Sea case (GCA, 2012)

Available online at www.sciencedirect.com

SciVerse ScienceDirect

Geochimica et Cosmochimica Acta 88 (2012) 237–254

Geochimica et Cosmochimica Acta

www.elsevier.com/locate/gca

Modeling radium distribution in coastal aquifers during sea level changes: The Dead Sea case

Yael Kiro [a,b,*], Yoseph Yechieli [b], Clifford I. Voss [c], Abraham Starinsky [a], Yishai Weinstein [d]

[a] Institute of Earth Sciences, The Hebrew University, Edmond J. Safra Campus, Givat Ram, Jerusalem 91904, Israel
[b] Geological Survey of Israel, 30 Malkhe Israel Street, Jerusalem 95501, Israel
[c] U.S. Geological Survey 345 Middlefield Road, MS 496 Menlo Park, CA 94025, USA
[d] Bar-Ilan University, Department of Geography and Environment, Ramat-Gan 52900, Israel

Received 20 June 2011; accepted in revised form 14 March 2012; available online 19 May 2012

Abstract

We present a new approach to studying the behavior of radium isotopes in a coastal aquifer. In order to simulate radium isotope distributions in the dynamic flow field of the Dead Sea aquifer, a multi-species density dependent flow model (SUTRA-MS) was used. Field data show that the activity of ^{226}Ra decreases from 140 to 60 dpm/L upon entering the aquifer from the Dead Sea, and then further decreases linearly due to mixing with Ra-poor fresh water. On the other hand, an increase is observed in the activity of the shorter-lived isotopes (up to 52 dpm/L ^{224}Ra and 31 dpm/L ^{223}Ra), which are relatively low in Dead Sea water (up to 2.5 dpm/L ^{224}Ra and 0.5 dpm/L ^{223}Ra). The activities of the short lived radium isotopes also decrease with decreasing salinity, which is due to the effect of salinity on the adsorption of radium. The relationship between ^{224}Ra and salinity suggests that the adsorption partition coefficient (K) is linearly related to salinity. Simulations of the steady-state conditions, show that the distance where equilibrium activity is attained for each radium isotope is affected by the isotope half-life, K and the groundwater velocity, resulting in a longer distance for the long-lived radium isotopes. K affects the radium distribution in transient conditions, especially that of the long-lived radium isotopes. The transient conditions in the Dead Sea system, with a 1 m/yr lake level drop, together with the radium field data, constrains K to be relatively low (<10). Thus, the sharp decrease in ^{226}Ra cannot be explained by adsorption, and it is better explained by removal via coprecipitation, probably with barite or celestine.
© 2012 Elsevier Ltd. All rights reserved.

1. INTRODUCTION

There are four naturally occurring radium isotopes (the 'radium quartet'), with half-lives ranging from 3.7 days to 1600 years. Two of them, ^{226}Ra and ^{223}Ra, are the radioactive progeny of uranium isotopes (^{238}U and ^{235}U, respectively), while ^{228}Ra and ^{224}Ra are decay products of ^{232}Th. Three of the isotopes (^{226}Ra, ^{224}Ra and ^{223}Ra) disintegrate into radon isotopes (^{222}Rn, ^{220}Rn and ^{219}Rn, respectively), while ^{228}Ra decays to ^{224}Ra via ^{228}Th (and the short-lived ^{228}Ac). All four radium isotopes are produced from aquifer solids and in surface water bodies by the decay of their insoluble parents, which are adsorbed on sediment grains or on suspended material. In freshwater, radium is mainly tightly bound to the surface of sediment grains (e.g., Webster et al., 1995; Gonneea et al., 2008; Lazar et al., 2008) while in saline water the radium is much more soluble and readily undergoes ion exchange with other adsorbed cations (e.g., Krishnaswami et al., 1991; Moore, 2000; Sturchio, 2001). Several studies estimated adsorption–desorption coefficients from field data (e.g., Krishnaswami et al., 1982; Lazar et al., 2008) and from lab experiments (e.g., Webster et al., 1995; Gonneea et al., 2008). The effect of salinity on the adsorption distribution coefficient of radium was studied mainly by lab experiments

* Corresponding author at: Institute of Earth Sciences, The Hebrew University, Edmond J. Safra Campus, Givat Ram, Jerusalem 91904, Israel.
E-mail address: yael.kiro@mail.huji.ac.il (Y. Kiro).

0016-7037/$ - see front matter © 2012 Elsevier Ltd. All rights reserved.
http://dx.doi.org/10.1016/j.gca.2012.03.022

testing various salinities up to seawater salinity (35 g/L; Webster et al., 1995; Gonneea et al., 2008). In this study, the effect of salinity on adsorption was studied directly from field data up to Dead Sea salinities (340 g/L) which are significantly higher than the salinities previously tested.

Radium isotopes are commonly used as natural tracers of groundwater discharge to the ocean (e.g., Moore, 1996) and can be used for studying groundwater flow dynamics. A groundwater system adjacent to a salt water body (lake or ocean) is usually a mixed salinity groundwater system in which fresh water flows above saline water and between them there is a fresh-saline transition zone (also referred to as *subterranean estuary*). The special conditions in this environment cause chemical reactions which affect nutrients, trace metals and radioisotope budgets in coastal waters (e.g., Moore, 1996; Charette and Sholkovitz, 2002; Kelly and Moran, 2002). Since radium isotopes may be influenced by some of these chemical reactions and because they are commonly used as submarine groundwater discharge tracers, it is important to study their distribution in the coastal groundwater system. In these systems, the distribution of radium may be affected by adsorption–desorption processes, salinity, the mixture of the two water bodies, the redox state of the groundwater (Gonneea et al., 2008) and the age of the groundwater (which may be relatively young close to the sediment–water interface immediately after water enters the aquifer from the sea/lake).

Sources of radium isotopes in groundwaters are alpha recoil caused by the decay of the parent nuclide in the solid, desorption from the solid surface, dissolution of aquifer solids and *in situ* production by the decay of the dissolved parent nuclide (Krishnaswami et al., 1982; Hammond et al., 1988; Porcelli and Swarzenski, 2003; Tricca et al., 2001). Sinks of radium in groundwater may be coprecipitation with sulfate minerals (Doerner and Hoskins, 1925; Langmuir and Riese, 1985), adsorption and decay. These processes have different time scales and the effect of each one of them on radium activities in the groundwater strongly depends on the travel time of the groundwater (Tricca et al., 2001; Ku et al., 2009).

In general, modeling of solute transport in groundwater can be done by several approaches. In the case where the dissolved solids affect the flow regime, a multi-species density-dependent flow model should be used (e.g., SUTRA-MS, Hughes and Sanford, 2005). In the case of several solutes that interact in a contaminated plume, a multi-component coupled reactive transport model (which is not density-dependent) should be used (e.g., MODFLOW-MT3D). A third approach would be to combine between a density-dependent flow model and a geochemical model using the flow field calculated by the density-dependent model and then calculating the geochemical reactions (e.g., a combination between PHREEQC and any density-dependent flow model). However, this requires knowledge of the chemical processes occurring in the aquifer.

In order to simulate solutes in a coastal aquifer, only a density-dependent flow model can be used. The transport equation in these models takes into account zero- and first-order production or decay and adsorption–desorption processes based on isotherms (Voss, 1984). Only a geochemical model can describe the specific chemical reactions and can consider the reactions between several solutes in the groundwater. However, this requires a full understanding of the inhomogeneity and all chemical reactions and parameters that occur in the system (which is usually not possible). Most geochemical reactions can be described in general by the zero- and first-order production terms and by adsorption–desorption processes and therefore modeling trace elements does not always require a coupled model (which is computationally demanding) or a geochemical model and may be explained by the transport equation.

Modeling radium isotopes in coastal aquifers contributes to the understanding of processes that control the radium distribution and activities, and may be used for defining the groundwater flow field as well as the hydrological parameters. Several studies have modeled radium activities in the groundwater assuming steady-state conditions (Krishnaswami et al., 1982) and one-dimensional transient conditions (Davidson and Dickson, 1986; Tricca et al., 2001; Ku et al., 2009). However, these approaches assume constant water salinities and thus cannot be used in order to study radium distribution in coastal areas which include groundwater of various salinities and a two-dimensional flow field.

The objective of this study was to develop a method which uses groundwater flow in a dynamic variable-density flow field in order to understand the distribution of radium isotopes in coastal aquifers in general and specifically on the Dead Sea coast. This was achieved by numerical simulation using SUTRA-MS, which is a multi-species density-dependent flow model (Hughes and Sanford, 2005). This model calculates the flow field according to the water density, which is then used for calculating the radium distribution in the aquifer. It is unique in using a hydrological tool and settings in order to gain a better understanding of the geochemistry of radium in coastal aquifers and provides essential parameters for calculating mass balances in the Dead Sea lake.

1.1. The Dead Sea system

The Dead Sea is a terminal lake located in a deep pull-apart basin along the Dead Sea transform fault. The deepest point in the lake is about −720 m bmsl. It is a hypersaline lake with a current area of 620 km^2 and a drainage basin of 40,000 km^2. The lake level has been continuously dropping from −390 m in the 1930s (Klein and Flohn, 1987) to −420 m in 2007, with a steeper decline since the 1960s reaching a rate of 1 m/yr during the past few years (Lensky et al., 2005). This decline is the result of the increased utilization of water in the northern part of the basin, particularly the creation of the Israeli National Water Carrier in the 1960s and the Jordanian Jordan Valley (King Abdullah) Canal in the 1970s. The Israel Dead Sea Works and the Jordanian Arab Potash Company significantly compounded this negative balance by pumping water from the lake. Altogether, these changes in water management resulted in a decrease of the average annual inflow to the lake from 1600 to 2000 million m^3 in the early

1900s (Neumann, 1958; Klein, 1998; Salameh and El-naser, 1999) to a current 265–335 million m^3 (Lensky et al., 2005).

The chemical composition of Dead Sea water is Ca-chloridic with a low Na/Cl ratio compared to normal ocean water (0.21 today vs. 0.87, respectively). This composition is the result of the evaporation of seawater which intruded the rift valley, followed by halite precipitation (Starinsky, 1974). Other processes of water–rock interaction, such as dolomitization of carbonates in the adjacent aquifer, have further altered the original composition. The Na/Cl ratio is still decreasing due to the present precipitation of halite in the lake (Gavrieli, 1997).

The current (2011) Dead Sea salinity and density are 340 g/L and 1.24 kg/L, respectively. The Dead Sea is extremely enriched in radium relative to most natural water bodies. The ^{226}Ra activity in the Dead Sea (~140 dpm/L; adjusted after Mazor, 1962; Stiller and Chung, 1984; Chan and Chung, 1987; Chung and Craig, 2004) is 1600 times that of Pacific surface water (~0.09 dpm/L) and 400 times that of Pacific deep water (~0.35 dpm/L, Broecker et al., 1967), whereas the salinity of the Dead Sea is only 10 times that of ocean water.

There are three principal aquifers in the Dead Sea region: the Lower Cretaceous sandstone Kurnub aquifer, the Upper Cretaceous carbonate Judea aquifer and the Quaternary alluvial aquifer (Arad and Michaeli, 1967; Yechieli et al., 1995). The alluvial aquifer is in direct hydraulic contact with the lake along most of its shoreline. It mainly consists of clastic sediment deposited in fan deltas (gravel, sand and clay) and of lacustrine sediment (e.g., clastics, aragonite, gypsum and salt). Alternations between gravel and clay create several sub-aquifers that differ in their hydraulic heads and chemical composition. The alluvial aquifer is bounded on its west by normal faults, which set Cretaceous carbonate rocks of the Judea Group against Quaternary alluvial and lacustrine sediments. The freshwater recharge of the alluvial aquifer is mainly through lateral flow from the Judea Group aquifer, which is replenished in the highlands 10–30 km to the west and by flash floods. Direct recharge on this aquifer is negligible because of the arid climate in the Dead Sea region (precipitation <100 mm/yr).

The hydraulic relationship between the Dead Sea and the alluvial aquifer is expressed in a relatively rapid water level response (several days) to level changes in the Dead Sea (Yechieli et al., 1995). Groundwater levels respond to the lake level drop at different rates according to the aquifer hydraulic parameters and lake bathymetry near the coast. The groundwater level drop may reach the same rate as the Dead Sea lake level drop (Kiro et al., 2008).

The extremely high density of the Dead Sea water induces a very shallow transition zone between the fresh and saline water bodies. According to the Ghyben–Herzberg approximation, the depth of the transition zone is 4.35 times the groundwater elevation, compared to 40 times in aquifers next to the ocean (Yechieli, 2000). The depth of the transition zone in the study area (Fig. 1) is shallow as expected and relatively wide due to dispersion and the lake level drop (Fig. 2, Kiro et al., 2008).

The fresh and saline groundwater bodies respond to the Dead Sea level drop and the flow direction tends to be toward the lake. Nevertheless, simulations (Kiro et al., 2008) and geochemical data (Kiro, 2006) indicate that lake water circulation in the aquifer still occurs during the lake level drop. The Dead Sea coastal aquifer system, with its high salinity gradient and fast decline of lake and groundwater levels, provides a unique opportunity to study radium isotopes in the field along a flow path in transient conditions.

2. METHODS

2.1. Modeling radium distribution in dynamical density-dependent flow conditions

SUTRA-MS (Hughes and Sanford, 2005) was used in order to calculate the distribution of radium isotopes in the density-dependent flow field of the Dead Sea aquifer during its level drop. The flow field was calculated by coupling the flow and solute transport equations. The radium isotope distributions were calculated according to the flow field during the continuous Dead Sea lake level drop. Details about the governing equations and the numerical methods of the model are given in Voss (1984) and Hughes and Sanford (2005).

The solute mass balance equation includes zero and first order production coefficients and an equilibrium adsorption process which may behave according to a linear, Langmuir or Freundlich isotherm (Voss, 1984). An additional modification was made in order to adapt the code to the high salinity conditions of the Dead Sea, by supporting a salinity-dependent adsorption distribution coefficient (K_d).

2.2. Sample collection and Ra and Ba measurements

Samples from the Dead Sea lake were taken from a vertical profile 8 km offshore and surface water were sampled along a transect from the Dead Sea shore up to 8 km (100, 500 and 1000 m away from the shore, Fig. 1). ^{226}Ra samples were collected in 500 ml glass bottles. The short-lived radium isotope samples (20 L) were collected from surface water. Groundwater samples were collected from several boreholes, mostly 10, 80 and 150 m away from the shore inland (Table 1). All groundwater samples were filtered through a 0.45 μm filter. The volume of ^{226}Ra samples was 0.5 L and the volume of the short-lived radium isotopes was 3 L.

^{226}Ra activities were measured by counting ^{222}Rn disintegrations after incubating the water sample for at least three weeks in order to allow the ^{222}Rn to reach secular equilibrium with ^{226}Ra. Radon was then extracted via helium recycling through the water sample and adsorption onto a cooled charcoal column. The radon gas was then transferred to a counting (Lucas) cell after heating the column to 450 °C (Mathieu et al., 1988).

The short-lived radium isotopes (223 and 224) were measured by a delayed coincidence counter (RaDeCC) after adsorbing the radium onto MnO_2-coated acrylic fibers (Moore and Arnold, 1996). The short-lived daughters of the radium isotopes, ^{219}Rn and ^{220}Rn, which are produced by recoil from the Mn fibers, are swept into a scintillation

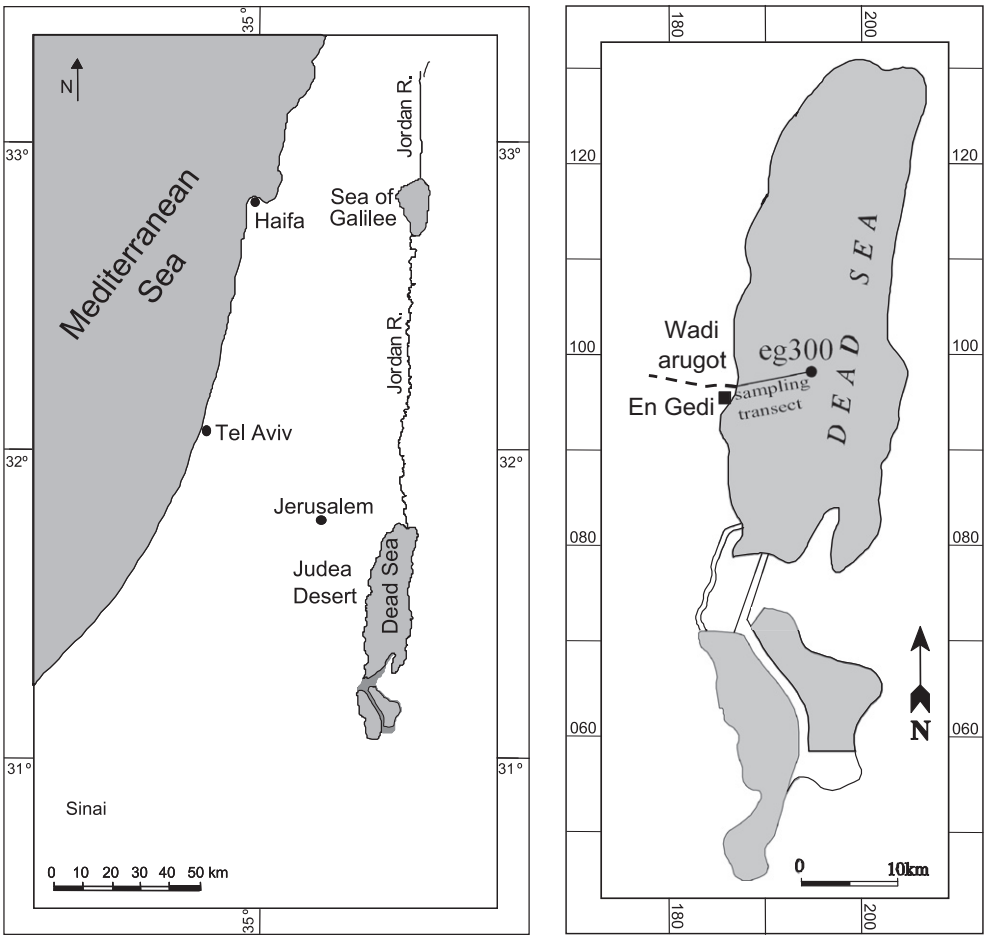


Fig. 1. Location map of the study area at the Arugot alluvial fan. The sampling transect in the Dead Sea and the location of the profile samples (eg 300) are indicated.

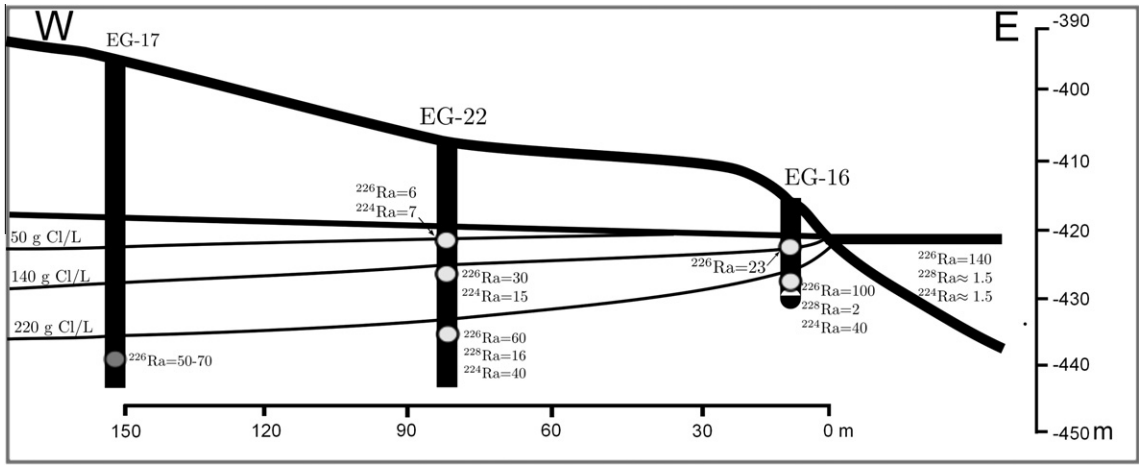


Fig. 2. Cross section of Arugot alluvial fan groundwater system including sample locations and averaged radium activities. The contours are of chloride in g/L and the activities of radium are in dpm/L.

cell where alpha decay of the radon nuclides and their polonium daughters (^{215}Po and ^{216}Po, respectively) occurs. The scintillations are translated into electronic signals, and these are sent to a delayed coincidence circuit, which electronically discriminates the paired decays of 219 and 215 (thus 223) from those of 220 and 216 (thus 224) (Giffin et al.,

Table 1
Field results, radium measurement errors are 5–10% and barium errors are 5%.

Sample location	Date	Distance from shore (m)	Elevation (m)	Depth (m)	^{226}Ra (dpm/L)	^{228}Ra (dpm/L)	^{224}Ra (dpm/L)	^{223}Ra (dpm/L)	Ba (mg/L)	Cl (g/L)
Dead Sea					145 (average)	0.9–2	0.5–2.5	0.03–0.5	4.85	224
Spring	27/8/08	10		0	18					78
EG16	21/1/08	10	−420.8	6	16		8	5	0.36	67
EG16	21/1/08	10	−421.8	7	22		26	17	1	142
EG16	1/7/04	10	−426.7	12	92				3.5	224
EG16	21/1/08	10	−426.2	11.5	101	2	39	31	2.3	224
EG11	21/1/08	80	−420.7	15.8	6		7	3	0.36	51
EG11	13/6/10	80	−424.4	19.5	14		12	5	0.5	68
EG11	22/6/09	80	−423.3	18.5	10		1.9	1.4	0.5	73
EG11	21/1/08	80	−423.9	19	29		15	8	1.2	142
EG11	16/5/05	80	−424.9	20	46				1.2	164
EG22	13/6/10	80	−427.8	22	14		11	5	0.9	117
EG22	22/6/09	80	−425.8	20	30		7	4	1	136
EG22	13/6/10	80	−426.8	21	16		9	5	1	137
EG22	13/6/10	80	−431.1	25.3	29		17	9	1	169
EG22	22/6/09	80	−423.8	28	68		18	13	1.3	212
EG22	24/3/09	80	−435.3	29.5	60	16	20	5	1.5	219
EG22	13/6/10	80	−435.3	29.5	80		19	5	1.6	219
EG22	21/1/08	80	−432.3	26.5	39		38	17	1.7	220
EG20	22/6/09	80	−469.8	64	52	27	11	6	1.5	227
EG20	13/6/10	80	−468.8	63	75	20	34	17	1.5	220
EG20	13/6/10	80	−451.5	45.7	62	33	52	26	1.5	224
EG21	13/6/10	80	−424.7	18.9	15		6	2	0.6	87
EG21	22/6/09	80	−425.8	20	20		2.5	0.9	1.0	139
EG21	13/6/10	80	−428.1	22.3	26		9	3	1.1	152
EG21	13/6/10	80	−431.4	25.6	41		11.3	5	1.3	184
EG21	22/6/09	80	−434.8	29	54	14	9	4	1.3	219
EG21	13/6/10	80	−435.4	29.6	72	29	27	9	1.4	220
EG17	18/12/05	150	−433.0	37	52				1.6	201
EG19	22/6/09	400	−446.9	59	4		2			44
EG19	22/6/09	400	−434.8	50	14		6			101
EG13	30/4/03	400	−416.5	28.6	56				1.8	200
EG6	22/6/09	600	−422.4	40	6		0.9	1.0		24
Arugot-Keshet	21/1/08	2000			6		0.8	0.7		0.25

Y. Kiro et al. / Geochimica et Cosmochimica Acta 88 (2012) 237–254

1963; Moore and Arnold, 1996). Chance coincidence of ^{224}Ra and ^{223}Ra was calculated according to Giffin et al. (1963).

Due to the high ionic strength of the Dead Sea water, the adsorption of radium on the MnO_2 fibers was found to be of low efficiency (5–15%). The adsorption efficiency was calculated by measuring ^{226}Ra on the fibers and in water using the extraction system as described above. In order to increase the adsorption efficiency, Dead Sea water was diluted 5–20 times which increased the adsorption efficiency to 30–80%. A dilution experiment on the MnO_2 fibers was done in order to test the adsorption of radium from diluted Dead Sea water, showing an increase from 28% with no dilution to almost 90% adsorption efficiency with a dilution of 14%.

Activities of ^{228}Ra were measured by gamma spectrometry after ashing the Mn fibers which reduces the sample mass by approximately 90% (Dulaiova and Burnett, 2004).

Barium concentrations were measured at the Geological Survey of Israel lab using Perkin-Elmer Sciex Elan-DRC-e ICP-MS.

3. RADIUM ACTIVITIES IN THE DEAD SEA AQUIFER

3.1. Field results

The activities of ^{226}Ra in the Dead Sea lake are relatively uniform (around 130–160 dpm/L) and in agreement with the inventory of Stiller and Chung (1984). Groundwater samples were taken during this study (2008–2010) from boreholes in the alluvial fan of the Arugot Valley (Figs. 1 and 2) with salinities that varied between Dead Sea salinity and fresh water.

All groundwater samples have significantly lower ^{226}Ra activities than Dead Sea water. Moreover, the activity of onshore groundwater with the same salinity as Dead Sea water, which is commonly interpreted as recirculated Dead Sea water (Kiro, 2006), is less than half of Dead Sea water activity (50–70 dpm/L compared with 130–160 dpm/L, Fig. 3a). Groundwater with lower salinities show mixing between the recirculated Dead Sea groundwater and fresh groundwater with very low activities (a few dpm/L, Fig. 3a). Ba concentrations in the lake and groundwater show a behavior similar to ^{226}Ra. Ba decreases from 5 mg/L in the lake to 1.5 mg/L in the saline groundwater (Fig. 3b).

Unlike the ^{226}Ra, the short-lived isotopes, ^{224}Ra and ^{223}Ra, are strongly enriched in the aquifer (up to 52 and 31 dpm/L respectively) compared with the lake (up to 2.5 and 0.5 dpm/L respectively; Fig. 4), and their activities decrease with decreasing groundwater salinity, albeit in a non-linear relation (Fig. 4a). This decrease cannot be due to dilution because the source of the short-lived radium isotopes is the aquifer sediments and not the lake water which contains low activities of these isotopes. Rather, it is seemingly caused by the increase in radium adsorption onto the solid surface with decreasing salinity.

Similar to the short-lived radium isotopes, ^{228}Ra is also derived from the aquifer sediments. ^{228}Ra activities in groundwater with Dead Sea salinity were ~2 dpm/L in a sample taken 10 m inland from the shore and 14–37 dpm/L in samples taken 80 m inland from the shore (Table 1).

3.2. ^{226}Ra and Ba removal on entering the aquifer

There are two possible mechanisms for the removal of ^{226}Ra and Ba in the aquifer: adsorption and precipitation. Barium and radium have shown to be affected by adsorption–desorption processes in coastal aquifers (Moore, 1996; Shaw et al., 1998; Gonneea et al., 2008; Michael et al., 2011). Although these studies have shown that in salt water barium and radium are released from sediments, adsorption should be considered due to the high concentrations of barium and radium in the Dead Sea. In the Dead Sea aquifer, radium may be adsorbed on manganese and iron oxides and on clays (e.g., Webster et al., 1995; Gonneea et al., 2008).

Radium has also been shown to coprecipitate with barite and celestine (which create a solid solution; Doerner and Hoskins, 1925; Langmuir and Riese, 1985; Zhu, 2004). The Dead Sea is supersaturated with barite ($\Omega \sim 10$) and celestine ($\Omega \sim 2$, Table 2). However, these minerals do not precipitate in the lake, not even after the Dead Sea water evaporates up to a degree of evaporation of 4 (Zilberman-Kron, 2008). Nevertheless, radium and barium definitely have the potential to be removed by precipitation of barite or celestine in the aquifer. Katz et al. (2009) suggested that barite precipitates from the Dead Sea water

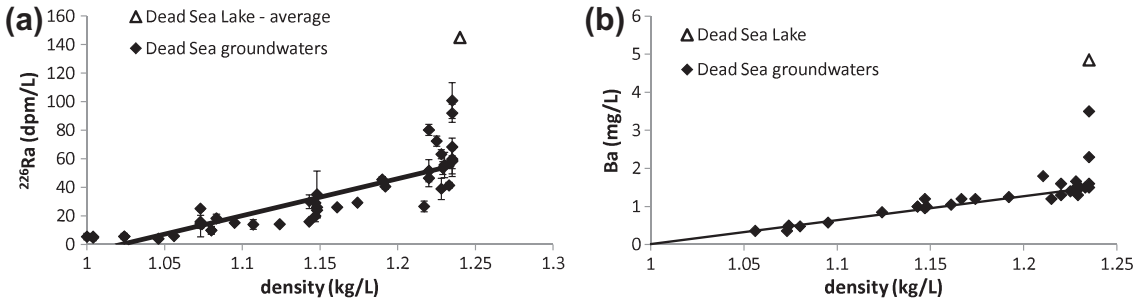


Fig. 3. (a) ^{226}Ra in the Dead Sea water and in the coastal aquifer groundwater. Groundwater with Dead Sea salinities carries significantly reduced activities compared with the lake (50–70 compared with 130–160 dpm/L). Fresher groundwater activities lie on a mixing line between the saline groundwater with the reduced activity and a low activity fresh water end member. (b) Ba in the Dead Sea water and in the coastal aquifer groundwater.

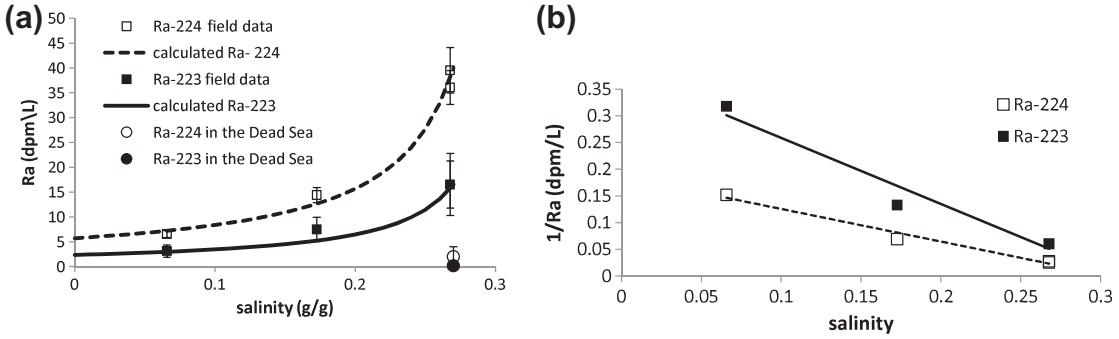


Fig. 4. (a) ^{224}Ra and ^{223}Ra activities in Dead Sea water and in groundwater with different salinities and depths sampled from boreholes located 80 m inland from the shoreline. Also shown are the best-fit curves that were calculated by Eq. (3) assuming a linear relation between salinity and *K*. ^{224}Ra and ^{223}Ra are highly enriched in the groundwater relative to the lake. (b) $1/^{224}$Ra and $1/^{223}$Ra vs. salinity in groundwater.

Table 2
Saturation degree (Ω) and distribution coefficient (D) of radium and barium in minerals. The saturation degrees were calculated from the data in Table 3 using PHREEQC with the Pitzer database.

	Ω–lake	Ω–aquifer	D–Ra	D–Ba	D–Sr
Anhydrite	1.66	1.05	800[a]		
Barite	10.00	2.04	1–2[b]		0.0001[c]
Celestine	1.99	1.20	296[c]	572[c]	
Gypsum	1.07	0.71	0.1[d]		0.21[e]

[a] At 25° (Langmuir and Riese, 1985).
[b] Based on experimental study (Rosenberg et al., 2011).
[c] Zhu (2004).
[d] Gnanapragasam and Lewis (1995).
[e] Ichikuni and Musha (1978).

due to water interaction with bottom lake sediments during earthquakes. Similarly, it is probable that barite precipitation occurs when lake water interacts with the aquifer sediments. The degree of saturation of both barite and celestine decreases after the Dead Sea water interacts with the aquifer sediments (Table 3).

Assuming the decrease of radium and barium on entering the aquifer was caused by barite precipitation, the calculated distribution coefficient of Ra in barite is 1.02 (calculation described in Rosenberg et al. (2011)), in accordance with literature values (Table 2). Alternatively, both radium and barium could precipitate with celestine, which is also supersaturated in the Dead Sea water (Table 2). The possibility of coprecipitation with gypsum is less likely due to the low distribution coefficient of radium (Table 2). However, the possibility of coprecipitation with anhydrite cannot be excluded because of the high distribution coefficient of radium in anhydrite (Table 2). Nevertheless, Rosenberg et al. (2011) show an experimental study where radium usually coprecipitates with barite.

In summary, the most likely scenario of the removal of barium and radium on entering the aquifer is coprecipitation with barite and/or celestine.

4. MODEL SETTINGS

The purpose of the model was to study radium isotope distributions in coastal aquifers in steady-state and transient conditions. The variations in salinities in these types of aquifers require a two-dimensional multi-species density-dependent flow model. Therefore, we used SUTRA-MS (Hughes and Sanford, 2005) which calculated the distribution of all four radium isotopes in the variable-density flow field of the Dead Sea aquifer. Comparison between the radium field data and simulation results provides a good estimate of parameters affecting radium distribution in coastal aquifers such as the adsorption distribution coefficient, its dependence on salinity and the production rate of the radium isotopes. The model produces the pressure, groundwater velocities, salinities and activities of all four radium isotopes in time and space.

According to Hughes and Sanford (2005), the radium mass balance equation is

Table 3
Chemical composition of Dead Sea water from the lake (Zilberman-Kron, 2008) and from the aquifer (borehole EG20, distance of 80 m) in mg/L in representative samples. The differences between lake and aquifer water in major elements is also due to changes in the lake chemistry over the past decades (Gavrieli, 1997; Kiro, 2006).

	Cl	SO_4	Mg	Ca	Na	K	Sr	Ba	Ra (dpm/L)	U (μg/L)	Fe	Density (g/cm^3)
Lake	223,741	352	51,060	18,608	33,557	7884	339	4.85	145	2.4[a]	1[b]	1.2357
Aquifer	224,260	249.8	42,924	17,173	36,339	7522	307	1.5	62	0.13	12.5	1.228

[a] Data from Haase-Schramm et al. (2004).
[b] Data from this study.

$$\frac{\partial(nS_w\rho C)}{\partial t}+\frac{\partial[(1-n)\rho_s C_s]}{\partial t} = -\nabla\cdot(nS_w\rho\mathbf{v}C)+\nabla\cdot[nS_w\rho(D_m\mathbf{I}+\mathbf{D})\cdot\nabla C] + nS_w\rho P_0 - nS_w\rho\lambda C-(1-n)\rho_s\lambda C_s \quad (1)$$

where n is the porosity, S_w is the water saturation, $\rho[M_w/L^3]$ is the water density, $C[M_{solute}/M_w]$ is the radium isotope concentration, $t[T]$ is time, $\rho_s[M_{solid}/L^3]$ is the density of the solid grain, $C_s[M_{ads}/M_{solid}]$ is the radium isotope concentration on the solid grains, $\mathbf{v}[L/T]$ is the groundwater velocity, $D_m[L^2/T]$ is the molecular diffusivity, $\mathbf{I}$ is the identity tensor, $\mathbf{D}[L^2/T]$ is the dispersion tensor, $P_0[C/T]$ is the zero-order production rate that includes alpha recoil by the decay of the parent nuclide on the solid surface, *in situ* production by the decay of the parent nuclide dissolved in the water and dissolution, and $\lambda[1/T]$ is the decay constant of the radium isotope. This equation describes the change of radium concentration in the water and on the solid grains with time as a function of advection, dispersion, production of radium by the decay of its parent nuclide and decay of radium in the water and on the solid grains.

The adsorption–desorption processes are much faster than the groundwater flow time scale (minutes compared to years; Krishnaswami et al., 1982). Therefore, an equilibrium adsorption approach was used. We used a linear adsorption isotherm in which the partitioning of radium between water and the solid grains is defined by the adsorption distribution coefficient as $C_s=\rho K_d C$ where $K_d[L^3/M]$ is the adsorption distribution coefficient which is a linear function of salinity. This reduces Eq. (1) to

$$(nS_w\rho+(1-n)\rho_s\rho K_d)\frac{\partial C}{\partial t} = -\nabla\cdot(nS_w\rho\mathbf{v}C)+\nabla\cdot[nS_w\rho(D_m\mathbf{I}+\mathbf{D})\cdot\nabla C] + nS_w\rho P_0-(nS_w\rho+(1-n)\rho_s\rho K_d)\lambda C \quad (2)$$

For the short-lived radium isotopes (^{223}Ra and ^{224}Ra) in steady-state conditions, where the flow ($\mathbf{v}$) is negligible relative to the decay and with no hydrodynamic dispersion, the equation describing radium distribution according to Eq. (2) is

$$C=\frac{P_0}{\lambda(K+1)} \quad (3)$$

where K is the dimensionless partition coefficient which is defined as $K=\frac{(1-n)\rho_s K_d}{n}$ (for the remainder of this paper we will only refer to the dimensionless K). According to ^{224}Ra field data, salinity is proportional to $1/Ra^{224}$ (Fig. 4b) while according to Eq. (3) ^{224}Ra is proportional to $1/(K+1)$. This suggests that the relation between K and salinity is approximately linear where $K=K_f-\alpha\cdot salinity$ (K_f is the value of K in the fresh water and α is the dependence of K on salinity).

The adsorption–desorption rates, and thus also K, should be similar for all of the radium isotopes because there is no fractionation effect in such masses. Since K is also defined by $K=\frac{k_1}{k_2+\lambda}$ (Krishnaswami et al., 1982, where $k_1[1/T]$ and $k_2[1/T]$ are the adsorption and desorption rates respectively), K may be different in the various isotopes if desorption is low ($k_2\leqslant\lambda$). However, this is obviously not the case in the Dead Sea hypersaline environment where the activity of the short-lived radium isotopes is a function of salinity which affects the desorption ($k_2\gg\lambda$). Therefore, K was set to the same value for all radium isotopes.

P_0 of the short-lived isotopes was calculated for various K's according to Eq. (3) using the measured concentration of the radium isotope in the saline water, and P_0 of ^{228}Ra was calculated assuming secular equilibrium with ^{224}Ra (according to $P_0(228)=P_0(224)\cdot\lambda(228)/\lambda(224)$). P_0 of ^{226}Ra was estimated by comparing ^{226}Ra field data with simulation results.

In the case of the Dead Sea coastal aquifer, most of the radium isotopes are not supported by dissolved parents, only by the decay of their parents in the aquifer sediments. Their relatively uniform distribution in the saline water and the observed trend with respect to salinity suggest that the parent nuclides of the radium isotopes in the U and Th series are uniformly distributed and contribute radium to the groundwater at a constant rate. In short time scales and for the shorter-lived radium isotopes, the value of P_0 is mainly an indication of the contribution by recoil of the parent nuclide which is a function of the geometry of the grain and the parent concentration in the solid (Tricca et al., 2001; Ku et al., 2009).

4.1. Groundwater flow field in the Dead Sea groundwater system

The radium distribution is calculated in the model according to the flow field of the water in the Dead Sea groundwater system. The mechanism that drives the saline water circulation is caused by hydrodynamic dispersion and is calculated by the hydrological model. The velocity in the fresh water is toward the Dead Sea and is much higher than in the saline circulated water. The groundwater in the transition zone also flows toward the Dead Sea. The model's flow results show that the main outflow of salts back into the Dead Sea is in the transition zone, and there is almost no outflow of pure saline water (Fig. 5a). The field data from the near-shore borehole in which ^{228}Ra is low and ^{226}Ra is relatively high suggests that these samples of saline groundwater interacted with the aquifer sediments for a relatively short time, indicating that they were taken from the saline flow path from the Dead Sea into the aquifer and not from the recirculated Dead Sea brine on its way back to the Dead Sea.

5. SIMULATIONS OF RADIUM DISTRIBUTION IN THE DEAD SEA GROUNDWATER

The boundary conditions and model parameters are summarized in Tables 4 and 5. In order to rule out the possibility of removal of radium (and barium) by adsorption as described in Section 3.2, several simulations were done with the Dead Sea lake activity at the boundary (140 dpm/L). The simulations do not simulate the precipitation of barite which is assumed to occur on the lake–aquifer boundary. For this reason, the activity of ^{226}Ra at the boundary was set to 60 dpm/L (the typical activity in the Dead Sea saline groundwater). The effect of K on the distribution of all four radium isotopes was tested in steady-state and transient

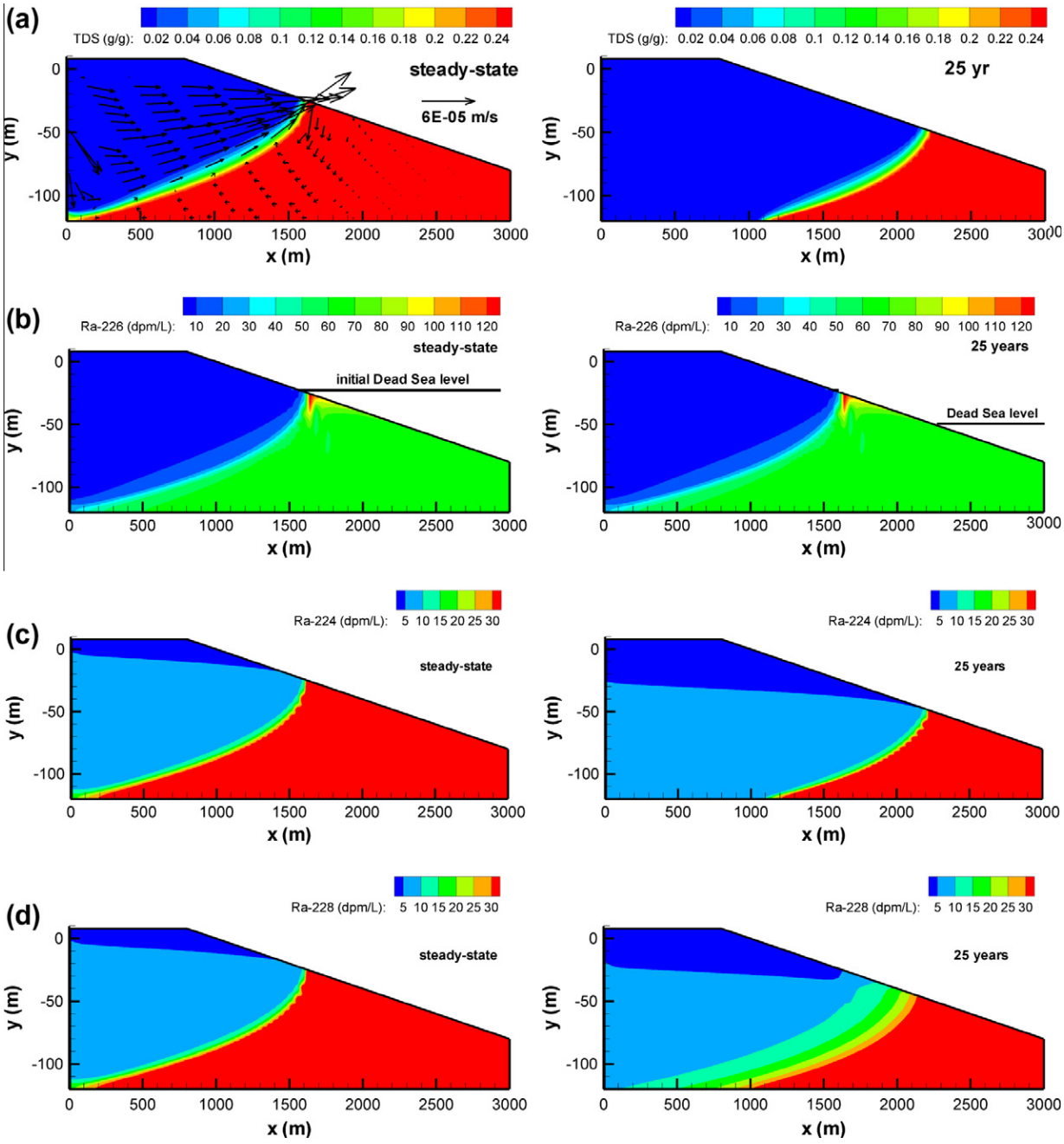


Fig. 5. Simulation results with a large K (100,000 and 15,000 in the fresh and saline water, respectively) in steady state and after 25 years, with a lake level drop of 1 m/yr. ^{226}Ra activity at the Dead Sea boundary was set to 140 dpm/L. (a) The total dissolved solids distribution (TDS) and groundwater velocities. (b) ^{226}Ra – this distribution does not change with lake level drop over 25 years and cannot explain the relation between the salinity and ^{226}Ra observed in the field. (c) ^{224}Ra. (d) ^{228}Ra. The response of ^{224}Ra distribution to the lake level drop is very fast, actually synchronous with lake level drop, while that of ^{228}Ra is slower. The simulation results for ^{223}Ra (not shown) are similar to those for ^{224}Ra due to their similar half-lives.

conditions. The relation of K with salinity was defined according to the short-lived radium isotopes and salinity relation (Fig. 4) and the maximal tested K value was 100,000 which is the maximal value reported in fresh water (Krishnaswami et al., 1982). The simulation results that are presented here are those with the minimal and maximal tested K's. The minimal K fits the field data in transient conditions and the maximal K represents a case with high adsorption which causes the decrease of ^{226}Ra from 140 to 60 dpm/L.

5.1. Steady-state conditions

The steady-state conditions produce the behavior of radium distribution in a coastal aquifer in general, and how the half-life of the radionuclide affects its distribution.

Table 4
Model boundary conditions. Values are typical of the Dead Sea region.

Boundary	Condition	TDS (g/g)	^{226}Ra (dpm/L)	^{228}Ra (dpm/L)	^{224}Ra (dpm/L)	^{223}Ra (dpm/L)
East (Dead Sea)	Specified pressure (according to the Dead Sea lake level)	0.27	140/60	0	0	0
West	Constant flux (0.5 kg/s)	0	0	0	0	0
Upper	No flow					
Lower	No flow					

Table 5
Model parameters. Hydrological parameters are from Kiro et al. (2008).

Parameter	Value
Porosity	0.2
Horizontal permeability	10^{-10} m^2
Vertical permeability	10^{-11} m^2
Longitudinal dispersivity	10 m
Transverse dispersivity	0.1 m
Dead Sea water density	1.24 kg/L
Dead Sea lake level drop	1 m/yr
^{226}Ra decay constant	-1.37×10^{-11}1/s
^{228}Ra decay constant	-3.82×10^{-9}1/s
^{223}Ra decay constant	-7.02×10^{-7}1/s
^{224}Ra decay constant	-2.19×10^{-6}1/s
Fresh water K in the high K simulations	100,000
Saline water K in the high K simulations	15,000
Fresh water K in the low K simulations	6
Saline water K in the low K simulations	0
P_0(226) in the high K simulations	1.24×10^{-5} dpm/s
P_0(228) in the high K simulations	2.29×10^{-3} dpm/s
P_0(224) in the high K simulations	1.31 dpm/s
P_0(223) in the high K simulations	0.17 dpm/s
P_0(226) in the low K simulations	8×10^{-10} dpm/s
P_0(228) in the low K simulations	1.53×10^{-7} dpm/s
P_0(224) in the low K simulations	8.77×10^{-5} dpm/s
P_0(223) in the low K simulations	1.26×10^{-5} dpm/s

The steady-state simulations are used as initial conditions for the transient simulations and highlight the effect of the transient conditions of the lake level drop. Under steady-state conditions, the parameters affecting the radium isotope distribution are the groundwater velocity, the half-life of the radium isotope, the partition coefficient (K), hydrodynamic dispersion and the constant production of radium in the water (P_0) which includes recoil, *in situ* production, and dissolution (Eq. (2)).

The distributions of the short-lived radium isotopes (^{224}Ra and ^{223}Ra) in steady-state conditions match the TDS distribution and represent the relation between salinity and adsorption (Section 3). The steady-state distributions of ^{228}Ra and ^{226}Ra are more complicated and may vary along the fresh and saline flow paths toward and from the Dead Sea, respectively (Figs. 5 and 6). Because of the higher velocities in the fresh water (Fig. 5a), and hence the low residence time, the changes in the long-lived radium isotopes is negligible compared with the changes that may occur in the saline groundwater. Hydrodynamic dispersion affects only the configuration of the radium transition zone where there are differences in radium concentration (e.g., Fig. 5) and can be estimated according to the TDS distribution (Kiro et al., 2008). However, in order to simplify the problem and study the effect of all other parameters, hydrodynamic dispersion was not taken into account in the following analysis. In order to understand the effect and significance of each parameter (ignoring the hydrodynamic dispersion), one can consider a single flow path (one-dimensional flow) with constant velocity and salinity (constant K). In this case, Eq. (2) can be re-written as:

$$\frac{\partial C}{\partial x} = \frac{P_0 - \lambda(K+1)C}{v_x} \tag{4}$$

where $v_x[L/T]$ is the velocity in the x direction. The solution of this equation is (after Krest and Harvey, 2003):

$$C = \frac{P_0}{\lambda(K+1)}\left(1 - e^{-\frac{\lambda(K+1)x}{v_x}}\right) + C_0 e^{-\frac{\lambda(K+1)x}{v_x}} \tag{5}$$

where $C_0[M_{solute}/M_w]$ is the concentration of the radium isotope at the boundary. It is clear from Eq. (5) that if the value of $\lambda(K+1)x/v_x$ is large enough, the concentration of the radium isotope is constant and equal to $P_0/\lambda(K+1)$ representing a steady state between production, adsorption and decay. It is also apparent that P_0 does not affect the general distribution pattern of the radium isotopes, just its concentration. The above equation describes both a fresh groundwater flow path toward the Dead Sea and a saline water flow path from the Dead Sea into the aquifer. Along a saline flow path, the distance between the shore and the location where the concentration is in steady state (x_{ss}) depends on the half-life of the isotope, the partition coefficient (K) and the velocity of the groundwater ($x_{ss} \propto v_x/\lambda(K+1)$). Note that the young groundwater would not be in secular equilibrium because ^{226}Ra, and in some cases ^{228}Ra, are not accumulated from the aquifer sediments at the same rate as the short-lived radium isotopes. Moreover, the main source of ^{226}Ra in the groundwater is the Dead Sea water rather than the aquifer sediments as in all other radium isotopes. This results in nonsecular equilibrium ratios between ^{226}Ra and ^{223}Ra. The steady-state results for Dead Sea water inflow into the aquifer may be summarized in three main scenarios (Fig. 6), depending on the value of $v_x/(K+1)$. In the first scenario, there is a decrease in ^{226}Ra due to adsorption and steady-state concentrations of all other three radium isotopes. This may occur at a very short distance from the shore when the velocity is low or with a large K (Fig. 6a). In the second scenario, there is almost no change in ^{226}Ra concentrations and constant concentrations of the short-lived radium isotopes (^{223}Ra and ^{224}Ra) while there is a gradual increase in ^{228}Ra reaching steady state at a

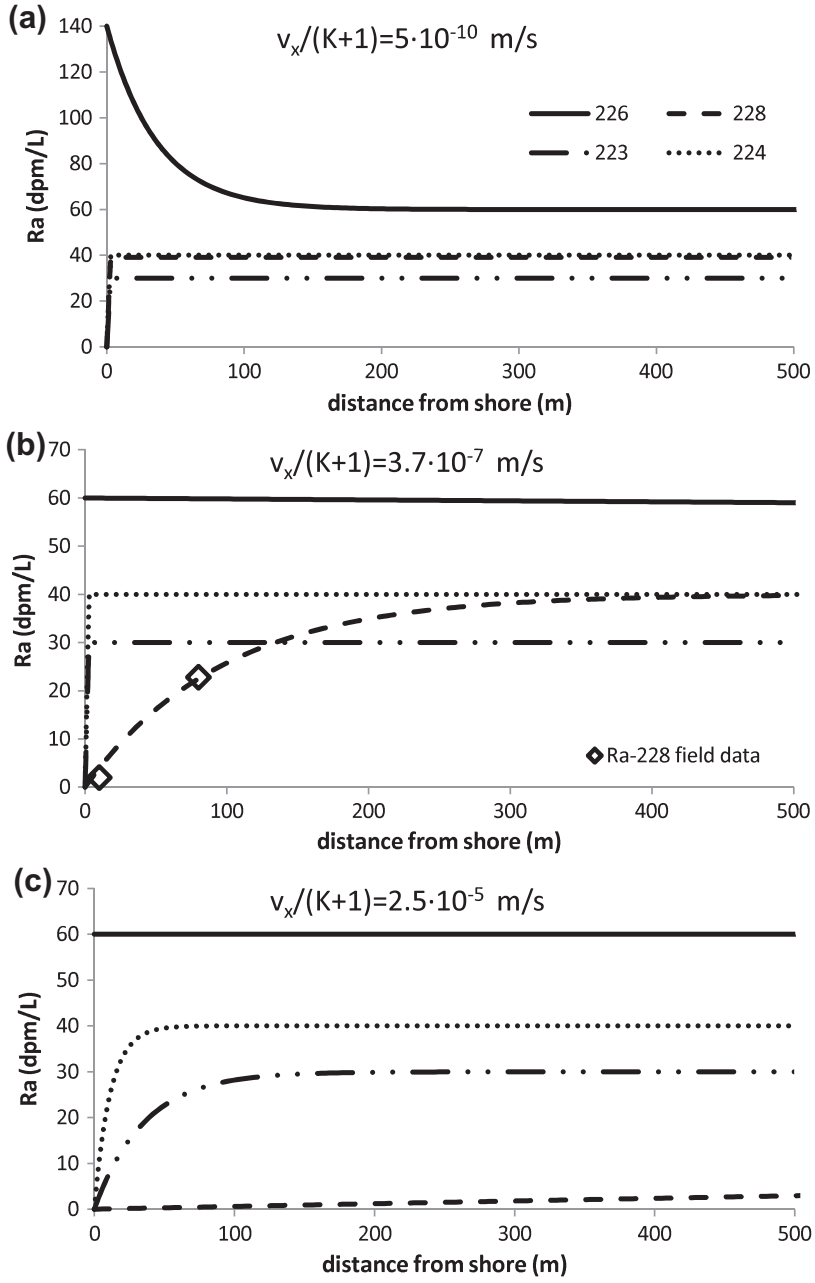


Fig. 6. Radium isotope activities in the saline water as a function of the distance from the shore inland in steady-state conditions and with different values of $v_x/(K+1)$ according to Eq. (5). In plot (a), the ^{226}Ra activity at the Dead Sea boundary was set to 140 dpm/L, while in (b) and (c) it was set to 60 dpm/L (see text, Section 5). Plot (a) fits the observed ^{226}Ra, ^{224}Ra and ^{223}Ra distributions, but not that of the ^{228}Ra. Plot (b) fits all the radium isotope observations. Plot (c) fits the observed ^{226}Ra distribution but does not fit the observed distribution of all other radium isotopes. Also shown in plot (b) are ^{228}Ra activities of two samples from the Dead Sea coastal aquifer (the 80 m sample is the averaged activity of several samples from two different boreholes, Table 1). Assuming a maximal groundwater velocity of 10^{-5} m/s, K must be lower than 100 in order to fit the observed activities.

greater distance from the shore (Fig. 6b). This occurs when $v_x/(K+1)$ is around 10^{-7} m/s. In the third scenario, there is no change in ^{226}Ra, the short-lived radium isotopes reach steady-state concentrations farther from the shore, and ^{228}Ra hardly increases (the steady-state activity should be the same as for ^{224}Ra). This may occur when the velocity is high and K is low (Fig. 6c). Assuming steady state, all three scenarios may fit the ^{226}Ra data from the Dead Sea aquifer, which is almost constant (around 60 dpm/L). The short-lived radium isotopes are already high in the saline water very close to the Dead Sea(10 m from the shore inland) and thus agree with the first two scenarios. However, the ^{228}Ra data, which show a significant increase with distance from the shore agrees only with the second scenario. This, together with the higher activities of ^{226}Ra close to the shore, also suggests that the age of the saline groundwater

increases with distance from the shore, indicating that the samples represent a flow path from the shore inland rather than the end of the saline water circulation flow path back into the lake. Therefore, the groundwater velocity of the saline water must be greater than 10^{-7} m/s in order to fit the ^{228}Ra data (Fig. 6b). Thus, in order to reduce the ^{226}Ra activity from 140 to 60 dpm/L by adsorption, K must be at least 200. An independent estimation of the velocity from previous hydrological studies (10^{-5}–10^{-7} m/s; Kiro et al., 2008) constrains the partition coefficient to relatively low values ($K < 100$) in order to fit the ^{228}Ra data (Fig. 6b) which rules out the possibility that the decrease of ^{226}Ra is due to adsorption.

5.2. The response of the radium distribution to the Dead Sea lake level drop

According to the discussion above, the steady-state conditions can only provide the ratio between the groundwater velocity and the partition coefficient and some constraints on these parameters. However, the transient conditions of the Dead Sea can be used to derive a better estimation of the partition coefficient. The steady-state simulation results were used as initial conditions for the transient simulations.

5.2.1. The effect of K on each of the radium isotope distributions

During a lake/sea level drop, the fresh–saline transition zone responds to the level drop and moves downward (Fig. 5a). Adsorption and desorption processes may cause retardation in solute transport during transient conditions resulting in a delay in their response to the lake level drop. With a constant density and porosity and for the saturated zone (describing radium distribution in each of the water bodies separately), Eq. (2) can be re-written as

$$R\frac{\partial C}{\partial t} = -\vec{\nabla}\cdot(\vec{v}C) + \vec{\nabla}\cdot[(D_m\underline{I} + \underline{\underline{D}})\cdot\vec{\nabla}C] + P_0 - R\lambda C \quad (6)$$

where $R = K + 1$ is the retardation factor which describes the response of the radium distribution to the lake level drop. It can be seen in Eq. (6) that the larger the decay constant (λ), the more the radium activity is affected by radioactive decay and the less it is affected by adsorption.

Starting with no radium along a flow path, the one-dimensional solution of a simplified case (no hydrodynamic dispersion) of the above equation is

$$C(x,t) = \begin{cases} \left(C_0 - \frac{P_0}{R\lambda}\right)e^{-\frac{R\lambda}{v_x}x} + \frac{P_0}{R\lambda} & x \leqslant \frac{v_x t}{R} \\ \frac{P_0}{R\lambda}(1 - e^{-\lambda t}) & x > \frac{v_x t}{R} \end{cases} \quad (7)$$

This solution is composed of two expressions which control different areas, one is only time dependent and the other depends only on the distance from the shore inland (along a saline groundwater flow path). The transition between the two expressions is also time dependent. According to this solution, the response rate of the radium concentration depends on its decay constant. The retardation factor ($R = K + 1$) affects the location of the transition between the two expressions of the solution. Accordingly, a large R would narrow the area controlled by the spatially-dependent expression resulting in radium concentrations calculated according to the time-dependent expression in most of the region. In this case, the response of ^{226}Ra ($t_{1/2} = 1600$ year) to any change may take up to several hundreds of years, while the response of the short-lived radium isotopes would take no more than a few days. On the other hand, a small R increases the area calculated by the spatially-dependent expression after a shorter time resulting in a faster response of ^{226}Ra.

Groundwater velocity has the opposite effect to that of R. High groundwater velocity would drive the transition between the spatially-dependent and time-dependent expressions of Eq. (7) away from the shore. We conclude from the above that the short-lived radium isotopes always respond fast and are not affected by R while the response of the long-lived radium isotope (^{226}Ra) is slow when R is large and fast when R is small.

The ^{226}Ra velocity (or response rate) is given by v_x/R. Thus, in order to obtain a response similar to the TDS response, R should be close to 1 and therefore K should be close to zero. The time response of the ^{226}Ra activity where it decreases due to adsorption is proportional only to its half-life. This is true for any other radionuclide. Therefore, in the Dead Sea system where the response of ^{226}Ra is fast, removal of ^{226}Ra due to adsorption is not possible and any simulation with K that causes a decrease of ^{226}Ra due to adsorption would respond in a time scale of thousands of years.

In the simulations where ^{226}Ra at the boundary is 140 dpm/L, a large K is required in order to reduce the ^{226}Ra activity from 140 to 60 dpm/L (Figs. 5b and 7). In this case, the decrease in activity to 60 dpm/L is due to adsorption, and therefore the salinity–activity relation is nonlinear. The ^{226}Ra distribution does not change with time throughout the whole simulation (Fig. 5b) and does not respond to the lake level drop which results in an almost constant activity of 60 dpm/L in both saline and fresh groundwater after 25 years (Fig. 7).

On the other hand, the short-lived radium isotopes respond to the lake level drop at the same rate as the salinity response (Fig. 5c) and the activity–salinity pattern remains approximately constant over time even when K is very large. As for the ^{228}Ra (with the intermediate half-life), its distribution responds to the lake level drop, though slower than that of the short-lived isotopes (Fig. 5d). A smaller K would cause a faster response of ^{226}Ra and ^{228}Ra and a fast response of the short-lived radium isotopes, similar to the case with the large K (Fig. 8).

5.2.2. Estimating the adsorption distribution coefficient using the transient conditions of the Dead Sea

The simulations show that ^{226}Ra distribution does respond to the lake level drop when K is relatively small. However, a small K cannot cause the large decrease of ^{226}Ra from 140 to 60 dpm/L upon entering the aquifer. This rules out the possibility of adsorption as a cause of ^{226}Ra (and barium) removal and supports the hypothesis of removal by coprecipitation with barite/celestine (Section 3.2). Therefore, the activity of ^{226}Ra at the boundary was set to 60 dpm/L.

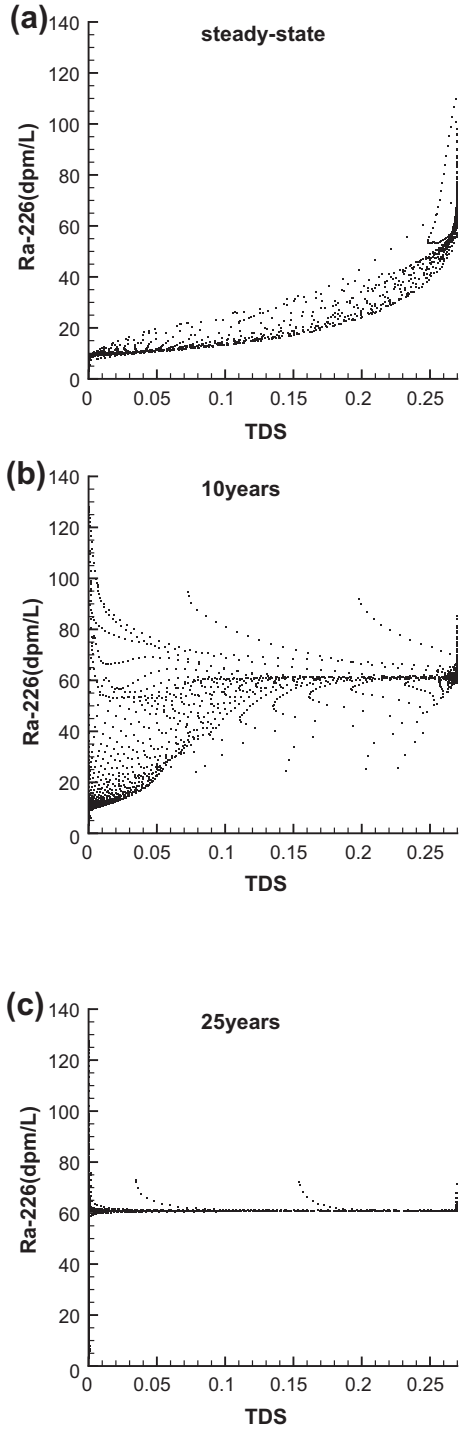


Fig. 7. The aquifer activity–salinity relationships in simulation results, shown as a scatter plot of calculated activity vs. salinity values of various points in the 2D model space. Results are for a relatively large K, with a lake level drop of 1 m/yr and where the ^{226}Ra activity at the Dead Sea boundary was set to 140 dpm/L: (a) in steady state; (b) after 10 years; (c) after 25 years. The diagrams indicate that the steady-state activity–salinity relation is not linear and that this relation varies with time during lake level drop. Note that after 25 years, the activity of ^{226}Ra shows almost no variation with salinity in disagreement with the field data.

The simulations suggest that K in the fresh water must be smaller than 10 in order to allow a relatively fast response of the ^{226}Ra distribution to the lake level drop (Fig. 8).

A rough estimation of K can also be obtained using Eq. (7). Assuming a maximal saline water velocity of 10^{-5} m/s, and assuming that the ^{226}Ra response to the lake level drop is expected after $t = 1$ year at 100 m from the shore, it follows that $K(= R - 1)$ in the saline water should be less than 1. This value of K cannot reduce the activity of ^{226}Ra from 140 to 60 dpm/L at this distance from the shore because the distance for attaining the steady-state activity ($>v_x/R\lambda$) should be around 1000 km.

The short-lived radium isotopes further constrain the possible range of K. Setting K in the fresh water to 6–10 and using a linear relation between K and salinity, K in the recirculated Dead Sea water must be 0–0.6 (Figs. 4 and 9). The salinity–activity pattern of the short-lived radium isotopes is constant over time and does not change between steady state and transient simulations (Fig. 9). On the other hand, the relationship between ^{226}Ra activity and salinity is linear in steady state, while it is complex and changes over time with lake level drop (Fig. 10) due to the retardation effect. The linearity of the field data (Fig. 3) suggests that the ^{226}Ra is not far from steady state (Fig. 10a). The linear pattern would persist for a longer period and still be observed after 10 years in the case of a lower rate of lake level drop (e.g., 0.5 m/yr, which is the average lake level drop since 1960; Fig. 11).

Previous studies (experimental and field data) show a large variability of aquifer K's (~10–100,000; Krishnaswami et al., 1982; Rama and Moore, 1996; Baraniak et al., 1999; Sturchio, 2001; Gonneea et al., 2008). These were mainly calculated for fine-grained sediments, glacial deposits, and sand and carbonate aquifers. The K obtained for fresh water in this study is at the lower end, which may be attributed to the coarser sediments in this alluvial aquifer and possibly to the preferential flow typical of this kind of aquifer, both leading to a reduced water–rock interaction. Furthermore, the groundwater in the Dead Sea aquifer may be reduced, which could increase the solubility of Mn and Fe oxides and therefore reduce the number of adsorption sites of radium.

6. THE EFFECT OF SALINITY ON ADSORPTION MECHANISMS

This study uses a K_d-based model in which K_d decreases linearly with salinity. The dependence of the adsorption on salinity is obtained directly from the short-lived radium isotope field data (Section 4). Zhu (2003) showed that some geochemical processes may not be captured by K_d-based models as opposed to geochemical models, which may represent better the relationship between K_d and salinity. However, since the geochemical processes are not all known in time and space in this study and considering the fact that the proposed barite precipitation is not included in the simulation, but rather its effect is assumed as a boundary condition, the model presented explains well the observed radium distributions and describes the adsorption–desorption processes.

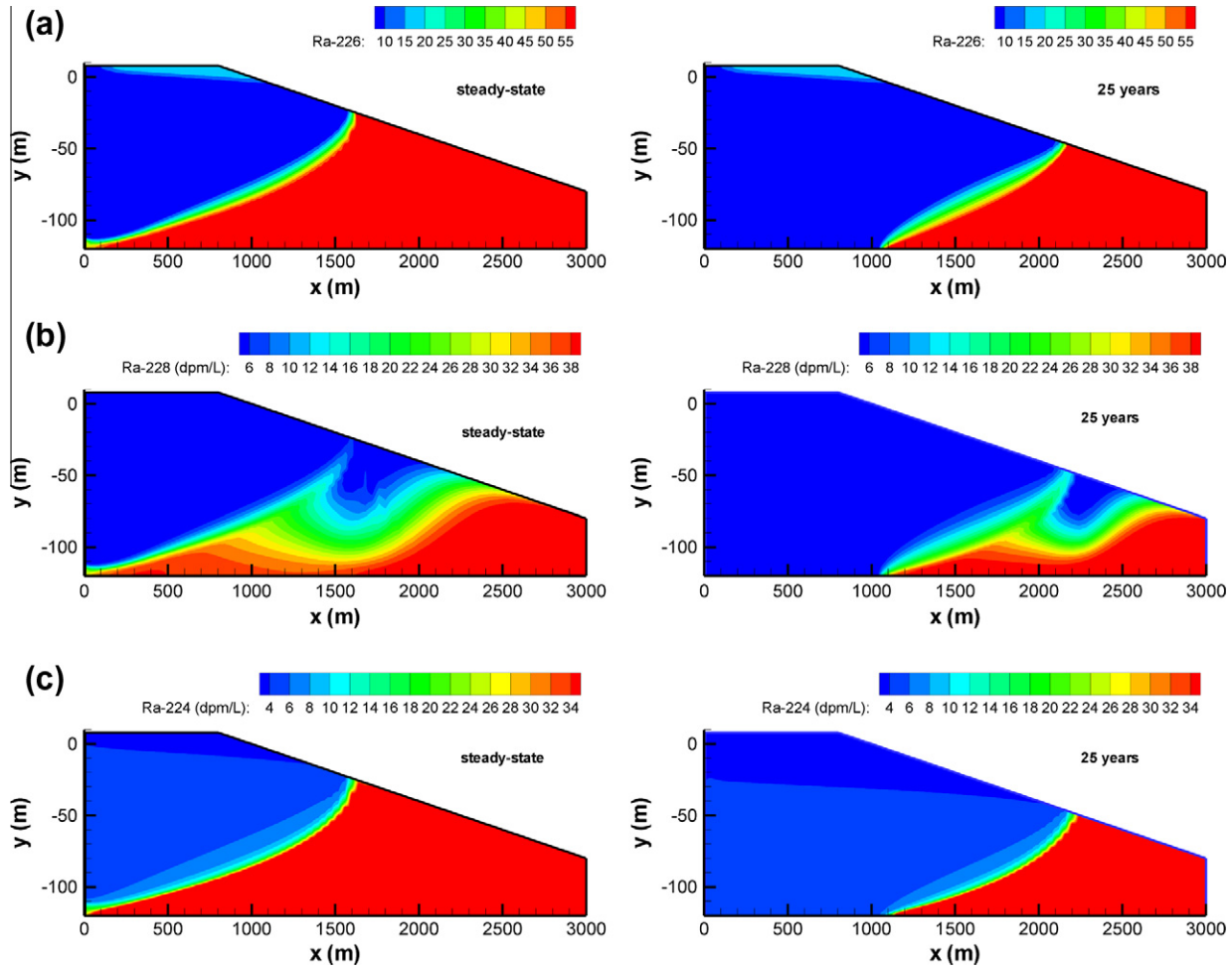


Fig. 8. Simulation results with $K = 0$ in the saline water and $K = 6$ in the fresh water, with ^{226}Ra at the Dead Sea boundary set to 60 dpm/L and lake level drop of 1 m/yr. (a) ^{226}Ra; (b) ^{228}Ra; (c) ^{224}Ra (^{223}Ra behavies similar to ^{224}Ra). These results agrees with field observations (Figs. 3 and 4a). Similar results are obtained when K is up to 0.6 and up to 10 in the saline and fresh groundwater, respectively.

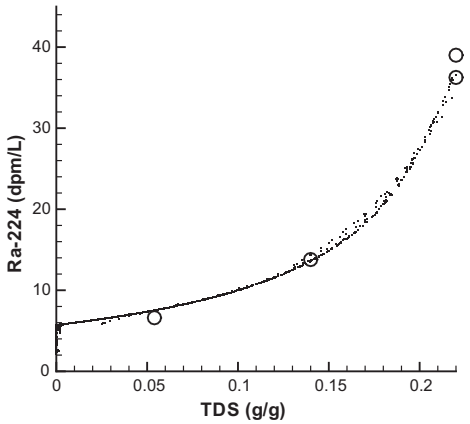


Fig. 9. ^{224}Ra activity over salinity during an entire transient simulation (0–50 years; black dots) compared with field data (circles). K is set to 0 in the saline water and 6 in the fresh water.

Several studies showed that salinity affects the adsorption and desorption of radium (e.g., Webster et al., 1995; Sturchio, 2001; Gonneea et al., 2008) and other trace metals (Turner, 1996) onto solids. Webster et al. (1995) and Gonneea et al. (2008) studied this effect up to seawater salinity, while Sturchio (2001) studied salinities up to 250 g/L. Webster et al. (1995) and Sturchio (2001) showed that $K \propto 1/salinity$, which implies that K decreases with salinity but not linearly as in the Dead Sea aquifer. An adsorption experiment with Dead Sea water diluted to variable degrees on Mn-fibers showed a non-linear behavior, similar to Webster et al.'s (1995) and Sturchio's (2001, see Section 2.2). The nonlinear decrease of K with salinity is attributed to a mechanism of cation competition over adsorption sites (Webster et al., 1995). Therefore, the linear behavior of K with salinity in the Dead Sea groundwater should be attributed to a different mechanism.

In general, there are several mechanisms that may explain the effect of salinity on radium adsorption:

1. Behavior of the electrolytic solution: (a) cation competition over adsorption sites. Due to the high salinity and ionic strength of the water, the adsorption sites are occupied by solutes other than radium (Webster et al., 1995).

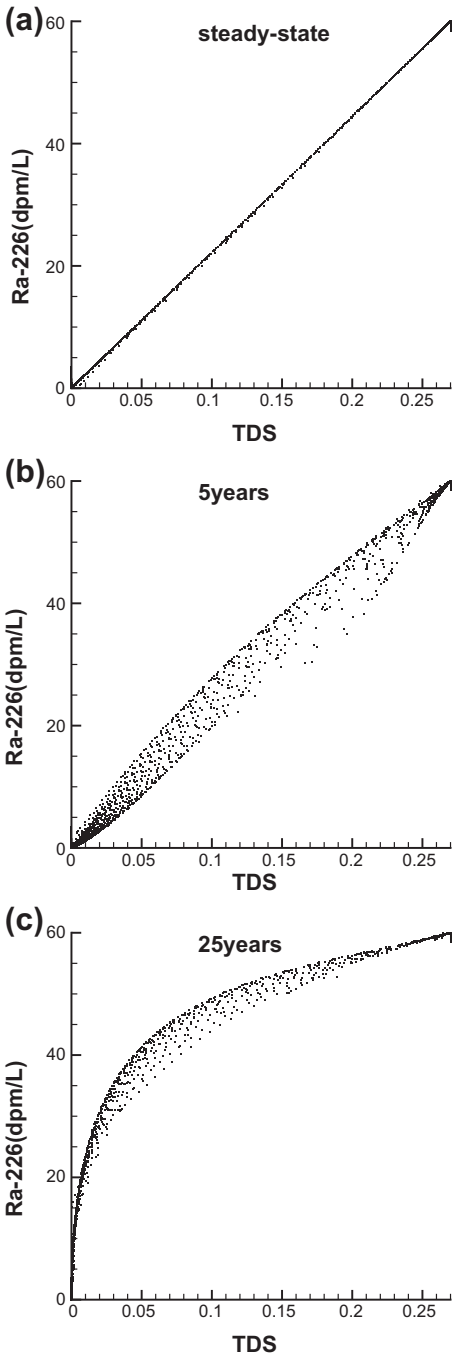


Fig. 10. Activity–salinity relations in the simulation results, shown as a scatter plot of calculated activity vs. salinity of various points in the 2D model space. Results are for $K = 0$ and $K = 6$ in saline and fresh water, respectively, and with lake level drop of 1 m/yr: (a) in steady state; (b) after 5 years; (c) after 25 years.

(b) Complexation of radium with other solutes in the water (for example Cl; Langmuir and Riese, 1985) which are less attracted to the solid surface (Turner et al., 1981). The concentration of complexes increases with salinity and may result in less radium available for adsorption.

2. Effect of saline water–rock interaction on the solid surface, which may result in a decrease in the number of sites due to clay flocculation (Whitehouse et al., 1958). Alternatively, it could be caused by the reduction of ferric oxides, which is supported by elevated concentrations of Fe in the saline groundwater compared with the lake water concentrations (Table 3).

The above mechanisms can be examined by the surface complex modeling approach (Dzombak and Morel, 1990). A reaction between the adsorbate and the solid surface can be written as: $\equiv XOH^{\circ} + M^{2+} = \equiv XOM^{+} + H^{+}$ where $\equiv XOH^{\circ}$ is a possible surface species and M^{2+} is a divalent cation. Considering the equilibrium constants for both Ra and Mg (which represent the salinity assuming a solution of Mg, Ra, chloride), the above reaction would result in:

$$K = K^{s}_{Ra} \cdot \frac{[N_S]}{([Mg]K^{s}_{Mg} + [H^{+}])} \tag{8}$$

after defining $K = \frac{[\equiv XORa^{+}]}{[Ra^{2+}]}$ and where K^{s}_{Ra} and K^{s}_{Mg} are the equilibrium constants of the reaction between the solid surface and Ra and Mg, respectively and $N_S (= \equiv XOH^{\circ} + \equiv XOMg^{+} + \equiv XORa^{+})$ is the total number of adsorbing sites. This shows that if the only change in these chemical reactions is salinity, then K (or K_d) would be proportional to $1/salinity$.

The same can be shown for complexation with another species in the solute. For example, complexation of Ra and Cl: $Ra^{2+} + Cl^{-} = RaCl^{+}$. In this case, $\frac{[Ra^{2+}]}{[Ra_{tot}]} = \frac{1}{1+K_{assoc}[Cl^{-}]}$ where $[Ra_{tot}] = [RaCl^{+}] + [Ra^{2+}]$, K_{assoc} is the association constant and Ra^{2+} is the dissolved radium in solution available for adsorption. In the case of constant concentration of the total radium ($[Ra_{tot}]$) for all salinities, the concentration of Ra^{2+} is proportional to $1/salinity$ which results in the nonlinear decrease of K with respect to salinity by the same proportion.

However, Eq. (8) also shows that the relationship between K and the concentration of adsorbing sites (N_S) is linear. It seems that the decrease of N_S is significantly higher than the salinity effect on adsorption due to the other mechanisms. The number of adsorbing sites may be affected by clay flocculation or reduction of oxides which may be affected by salinity. Clay flocculation (Whitehouse et al., 1958) and the redox potential were shown to be affected by water salinity (Millero, 1985). Moreover, the salinity or ionic strength may also affect the electric charge of the adsorbing surface which affects the apparent equilibrium constant, K^{s}_{Ra} (Dzombak and Morel, 1990). In conclusion, the linear decrease of K with salinity suggests that the main mechanism that controls the adsorption of radium is the effect of the high salinity in the Dead Sea system on the aquifer sediments rather than competition or complexation.

7. SUMMARY AND CONCLUSIONS

The interaction of Dead Sea water with the aquifer sediments has a significant effect on the activities and concentrations of radium and barium. During the Dead Sea hypersaline water circulation in the coastal aquifer, Ba

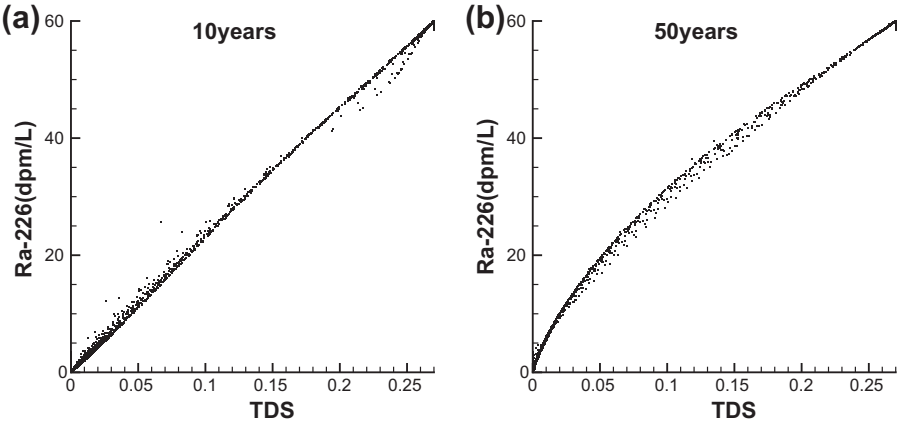


Fig. 11. Salinity–activity relations in simulation results, shown as a scatter plot of calculated activity vs. salinity values of various points in the 2D model space. Results are for the same parameters as in Fig. 7 but with a lake level drop of 0.5 m/yr. The effect of the retardation due to adsorption is smaller than with 1 m/yr level drop, and the relation is closer to linear during the lake level drop.

and ^{226}Ra are removed from the Dead Sea water and ^{228}Ra, ^{224}Ra and ^{223}Ra are added. Other elements that are affected by water–rock interaction such as uranium (which decreases in the saline groundwater) and Fe (which increases, Table 3) may also be sensitive to saline groundwater circulation. Avrahamov et al. (2010) showed that the carbonate system is also affected by saline groundwater circulation where the DIC and δ^{13}C values decrease. These chemical changes in the circulating Dead Sea water may have implications for the Dead Sea water chemistry regarding radium isotopes and other trace elements.

In order to study the behavior of radium in the dynamic groundwater system of the Dead Sea, we used a multi-species density-dependent groundwater flow model. This modeling approach can be used for any radionuclide or other trace elements and has strength in coastal groundwater systems with mixed salinities. Such environments cannot be described by a simple 1D time-dependent model which is suitable for fresh groundwater systems. Only a multi-species density-dependent flow model (such as SUTRA-MS) can describe the 2D flow field, the mixture between the fresh and saline water bodies, the effect of the salinity on K, and the transient conditions. The simulations, combined with the field data, provided new insights into the behavior of radium isotopes in coastal aquifers. In steady state, after seawater enters the aquifer, the distance at which the activity of each radium isotope attains equilibrium with the sediments is proportional to $v_x/\lambda(K+1)$. This distance increases with velocity and decreases with the decay constant and the partition coefficient. Therefore, in this case study, the activity of the short-lived radium isotopes reaches equilibrium immediately and the activity of ^{226}Ra ($t_{1/2} = 1600$ year) remains constant and does not change in the recirculated Dead Sea water along the aquifer (Fig. 6b).

In this study we use transient conditions for estimating K. In transient conditions, K affects only the long-lived radium isotopes, causing retardation of the response of ^{226}Ra and ^{228}Ra distributions to the lake level drop. The fact that no significant retardation is observed in the field constrains the value of K to be relatively low (<10), which precludes adsorption as a cause for the large decrease in ^{226}Ra on entering the aquifer. This decrease is best explained by mineral coprecipitation, probably of barite and celestine. The short-lived radium isotopes, which indicate the linear dependence of K on salinity, further constrain the range of K to be 0–0.6 in the saline water, given that K is 6–10 in the fresh water.

The study of radium geochemistry in groundwater is of great importance because of the common use of radium as a submarine groundwater discharge tracer. Flux calculations are highly dependent on end member estimations. The different sensitivity of each of the radium isotope distributions to changes in sea level (according to the adsorption distribution coefficient) may affect the concentrations of each isotope in the submerged water. In the Dead Sea case, ^{226}Ra is removed and all other radium isotopes are contributed to the groundwater and the lake water after Dead Sea water interacts with the aquifer sediments. A lake level rise may increase the amount of groundwater interacting with the sediments while a lake level drop should cause amounts of groundwater with altered composition to flow back into the lake, affecting radium and other trace element concentrations.

ACKNOWLEDGMENTS

We thank W. Sanford, A. Provost and J. Hughes for their help with SUTRA-MS. We thank H. Michael for fruitful discussions. We thank Y. Rosenberg for his code and help with calculating the activities of radium, calculations of saturation degrees, and for fruitful discussions. We thank M. Feldman and Y. Shalem for their help with lab work (^{226}Ra, ^{224}Ra and ^{223}Ra measurements). We thank B. Burnett for the ^{228}Ra analysis. We thank O. Yoffe and D. Stiber from the Geological Survey of Israel lab for the major elements and Ba analysis. We thank the reviewers and the associated editor, C. Zhu, for their many constructive comments that improved this paper significantly. We thank Y. Erel, B. Lazar and Y. Kolodny for their advice. We thank the BSF Rahamimoff Travel Grant for Young Scientists which funded the travel expenses of the first author (YK) to the USGS, the Hoffman Leadership and Responsibility Fellowship of the Hebrew University and the Rieger Foundation for the support given while work-

ing on this study. We thank the Ministry of National Infrastructure for supporting this research.

REFERENCES

Arad A. and Michaeli A. (1967) Hydrogeological investigations in the western catchment of the Dead Sea. *Israel J. Earth Sci.* **16**, 181–196.

Avrahamov N., Yechieli Y., Lazar B., Lewenberg O., Boaretto E. and Sivan O. (2010) Characterization and dating of saline groundwater in the dead sea area. *Radiocarbon* **52**(2–3), 1123–1140.

Baraniak L., Thieme M., Bernhard G. and Nitsche H. (1999) Sorption behavior of radium on sandy and clayey sediments of the upper Saxon Elbe river valley. *J. Radioanal. Nucl. Chem.* **241**(3), 511–517.

Broecker W. S., Li Y. H. and Cromwell J. (1967) Radium-226 and radon-222; concentrations in Atlantic and Pacific Oceans. *Science* **158**(3806), 1307–1311.

Chan L. H. and Chung Y. (1987) Barium and radium in the Dead-Sea. *Earth Planet. Sci. Lett.* **85**(1–3), 41–53.

Charette M. A. and Sholkovitz E. R. (2002) Oxidative precipitation of groundwater-derived ferrous iron in the subterranean estuary of a coastal bay. *Geophys. Res. Lett.* **29**(10), 1–4.

Chung Y. and Craig H. (2004) Radium redux in the Dead Sea: profiles and transient Ra/Ba models. *Earth Planet. Sci. Lett.* **218**(3–4), 291–299.

Davidson M. R. and Dickson B. L. (1986) A porous flow model for steady state transport of radium in groundwater. *Water Resour. Res.* **22**(1), 34–44.

Doerner H. and Hoskins W. (1925) Co-precipitation of radium and barium sulfates. *J. Am. Chem.* **47**(3), 662–675.

Dulaiova H. and Burnett W. C. (2004) An efficient method for γ-spectrometric determination of radium-226, 228 via manganese fibers. *Limnol. Oceanogr. Methods* **2**, 256–261.

Dzombak D. A. and Morel F. (1990) *Surface Complexation Modeling: Hydrous Ferric Oxide*. John Wiley & Sons Inc., 401pp.

Gavrieli I. (1997) Halite deposition from the Dead Sea; 1960–1993. In *The Dead Sea; the Lake and its Setting*, vol. 36 (eds. T. M. Niemi, Z. Ben-Avraham and J. R. Gat). Oxford University Press, pp. 161–170.

Giffin C., Kaufman A. and Broecker W. S. (1963) Delayed coincidence counter for assay of actinon and thoron. *J. Geophys. Res.* **68**, 1749–1757.

Gnanapragasam E. K. and Lewis B. a. G. (1995) Elastic strain energy and the distribution coefficient of radium in solid solutions with calcium salts. *Geochim. Cosmochim. Acta* **59**(24), 5103–5111.

Gonneea M. E., Morris P. J., Dulaiova H. and Charette M. A. (2008) New perspectives on radium behavior within a subterranean estuary. *Mar. Chem.* **109**, 250–267.

Haase-Schramm A., Goldstein S. L. and Stein M. (2004) U–Th dating of Lake Lisan (late Pleistocene Dead Sea) aragonite and implications for glacial East Mediterranean climate change. *Geochim. Cosmochim. Acta* **68**(5), 985–1005.

Hammond D. E., Zukin J. G. and Teh-Lung K. (1988) The kinetics of radioisotope exchange between brine and rock in a geothermal system. *J. Geophys. Res.* **93**(B11), 13175–13186.

Hughes J. D. and Sanford W. E. (2005) SUTRA-MS a version of SUTRA modified to simulate heat and multipile-solute transport. Open-File Report 2004-1207, U.S. Geological Survey.

Ichikuni M. and Musha S. (1978) Partition of strontium between gypsum and solution. *Chem. Geol.* **21**, 359–363.

Katz A., Agnon A. and Marco S. (2009) Earthquake-induced barium anomalies in the Lisan Formation, Dead Sea Rift valley, Israel. *Earth Planet. Sci. Lett.* **286**(1–2), 219–229.

Kelly R. P. and Moran S. B. (2002) Seasonal changes in groundwater input to a well-mixed estuary estimated using radium isotopes and implications for coastal nutrient budgets. *Limnol. Oceanogr.* **47**, 1796–1807.

Kiro Y. (2006) The effect of the Dead Sea level drop in the past 50 years on the groundwater system in the alluvial aquifer in its vicinity. M.Sc., The Hebrew University.

Kiro Y., Yechieli Y., Lyakhovsky V., Shalev E. and Starinsky A. (2008) Time response of the water table and saltwater transition zone to a base level drop. *Water Resour. Res.* **44**, 1–15.

Klein M. (1998) Water balance of the upper Jordan River basin. *Water Int.* **23**(4), 244–248.

Klein C. and Flohn A. (1987) Contribution to the knowledge in the fluctuations of the Dead Sea level. *Theor. Appl. Climatol.* **38**, 151–156.

Krest J. M. and Harvey J. W. (2003) Using natural distributions of short-lived radium isotopes to quantify groundwater discharge and recharge. *Limnol. Oceanogr.* **48**(1), 290–298.

Krishnaswami S., Graustein W. C., Turekian K. K. and Dowd J. F. (1982) Radium, Thorium and radioactive lead isotopes in groundwaters: application to the in situ determination of adsorption–desorption rate constants and retardation factors. *Water Resour. Res.* **6**, 1663–1675.

Krishnaswami S., Bhushan R. and Baskaran M. (1991) Radium isotopes and ^{222}Rn in shallow brines, Kharaghoda (India). *Chem. Geol.* **87**(2), 125–136.

Ku T., Luo S., Goldstein S., Murrell M., Chu W. and Dobson P. (2009) Modeling non-steady state radioisotope transport in the vadose zone – a case study using uranium isotopes at Peña Blanca, Mexico. *Geochim. Cosmochim. Acta* **73**(20), 6052–6064.

Langmuir D. and Riese a. (1985) The thermodynamic properties of radium. *Geochim. Cosmochim. Acta* **49**(7), 1593–1601.

Lazar B., Weinstein Y., Paytan A., Magal E., Bruce D. and Kolodny Y. (2008) Ra and Th adsorption coefficients in lakes – Lake Kinneret (Sea of Galilee) "natural experiment". *Geochim. Cosmochim. Acta* **72**, 3446–3459.

Lensky N. G., Dvorkin Y., Lyakhovsky V., Gertman I. and Gavrieli I. (2005) Water, salt, and energy balances of the Dead Sea. *Water Resour. Res.* **41**, W12418.

Mathieu G., Biscaye P., Lupton R. and Hammond D. (1988) System for measurement of ^{222}Rn at low levels in natural waters. *Health Phys.* **55**(6), 989–992.

Mazor E. (1962) Radon and radium content of some Israeli water sources and a hypothesis on underground reservoirs of brines, oils and gases in the Rift Valley. *Geochim. Cosmochim. Acta* **26**, 765–786.

Michael H. a., Charette M. a. and Harvey C. F. (2011) Patterns and variability of groundwater flow and radium activity at the coast: A case study from Waquoit Bay, Massachusetts. *Mar. Chem.* **127**(1–4), 100–114.

Millero F. J. (1985) The effect of ionic interactions on the oxidation of metals in natural waters. *Geochim. Cosmochim. Acta* **49**(I), 547–553.

Moore W. S. (1996) Large groundwater inputs to coastal waters revealed by ^{226}Ra enrichments. *Nature* **380**, 612–614.

Moore W. S. (2000) Determining coastal mixing rates using radium isotopes. *Cont. Shelf Res.* **20**, 1993–2007.

Moore W. S. and Arnold R. (1996) Measurement of ^{223}Ra and ^{224}Ra in coastal waters using a delayed coincidence counter. *J. Geophys. Res.* **101**(1), 1321–1329.

Neumann J. (1958) Tentative energy and water balances for the Dead Sea. *Bull. Res. Counc. Israel* **7G**, 137–163.

Porcelli D. and Swarzenski P. W. (2003) The behavior of U- and Th-series nuclides in groundwater. In *Uranium-series Geochemistry* (eds. B. Bourdon, G. M. Henderson, C. C. Lundstorm and

S. P. Turner). The Mineralogical Society of America, Washington, pp. 317–361 (Chapter 8).

Rama and Moore W. S. (1996) Using the radium quartet evaluating groundwater input and water exchange in salt marshes. *Geochim. Cosmochim. Acta* **60**(23), 4645–4652.

Rosenberg Y., Metz V., Oren Y., Volkman Y. and Ganor J. (2011) Co-precipitation of radium in high ionic strength systems: 2. Kinetic and ionic strength effects. *Geochim. Cosmochim. Acta* **75**(19), 5403–5422.

Salameh E. and El-naser H. (1999) Does the actual drop in Dead Sea level reflect the development of water sources within its drainage basin? *Acta Hydroch. Hydrob.* **27**, 5–11.

Shaw T. J., Moore W. S., Kloepfer J. and Sochaski M. A. (1998) The flux of barium to the coastal waters of the southeastern USA: the importance of submarine groundwater discharge. *Geochim. Cosmochim. Acta* **62**(18), 3047–3054.

Starinsky A. (1974) Interaction between calcium chloride brines and sedimentary rocks. Ph.D., The Hebrew University, Jerusalem.

Stiller M. and Chung Y. (1984) Radium in the Dead Sea: a possible tracer for the duration of meromixis. *Limnol. Oceanogr.* **29**(3), 574–586.

Sturchio N. (2001) Radium geochemistry of ground waters in Paleozoic carbonate aquifers, midcontinent, USA. *Appl. Geochem.* **16**(1), 109–122.

Tricca A., Wasserburg G. J., Porcelli D. and Baskaran M. (2001) The transport of U- and Th-series nuclides in a sandy unconfined aquifer. *Geochim. Cosmochim. Acta* **65**(8), 1187–1210.

Turner A. (1996) Trace-metal partitioning in estuaries: importance of salinity and particle concentration. *Mar. Chem.* **54**(96), 27–39.

Turner D. R., Whitfield M. and Dickson A. G. (1981) The equilibrium speciation of dissolved components in freshwater and seawater at 25 °C and 1 atm pressure. *Geochim. Cosmochim. Acta* **45**, 855–881.

Voss C. I. (1984) SUTRA: finite-element simulation model for saturated–unsaturated, fluid-density-dependent groundwater flow with energy transport or chemically-reactive single-species solute transport. Investigations Report 84-4369.

Webster I. T., Hancock G. J. and Murray A. S. (1995) Modelling the effect of salinity on radium desorption from sediments. *Geochim. Cosmochim. Acta* **59**(12), 2469–2476.

Whitehouse U. G., Jeffrey L. M. and Debbrecht J. D. (1958) Differential settling tendencies of clay minerals in saline waters. *Clays Clay Miner.* **7**, 1–79.

Yechieli Y. (2000) Fresh-saline groundwater interface in the western Dead Sea area. *Ground Water* **38**(4), 615–623.

Yechieli Y., Ronen D., Berkovitz B., Dershowitz W. and Hadad A. (1995) Aquifer characteristics derived from the interaction between water levels of a terminal lake (Dead Sea) and an adjacent aquifer. *Water Resour. Res.* **31**, 893–902.

Zhu C. (2003) A case against Kd-based transport models: natural attenuation at a mill tailings site. *Comput. Geosci.* **29**(3), 351–359.

Zhu C. (2004) Coprecipitation in the barite isostructural family: 1. binary mixing properties 1. *Geochim. Cosmochim. Acta* **68**(16), 3327–3337.

Zilberman-Kron T. (2008) The origin and geochemical evolution of brines in the sinkholes along the Dead Sea coast. M.Sc., The Hebrew University.

Associate editor: Chen Zhu

Chapter 5

Radon and radium in the hydrological system of the Dead Sea

5.1 INTRODUCTION

Groundwater concentrations of radionuclides were shown to be significantly affected by water–rock interaction (e.g. Rama and Moore, 1984; Davidson and Dickson, 1986; Tricca et al, 2001). In particular, radon and radium isotopes are usually enriched in groundwater as a result of the disintegration of their parent nuclides in the host aquifer solids (e.g. Krishnaswami et al, 1982).

Previous studies have shown that the concentration of these radionuclides in water are affected by the U and Th concentrations of the aquifer rock, the travel time of the groundwater, recoil, dissolution and adsorption–desorption processes (e.g. Davidson and Dickson, 1986; Tricca et al, 2001). In this study, we try to apply radium isotopes in order to understand flow dynamics and estimate the age and velocities of the groundwater.

There are four naturally occurring radium isotopes (the 'radium quartet'), with half-lives ranging from 3.7 days to 1600 years. Two of them, ^{226}Ra and ^{223}Ra, are the radioactive progeny of uranium isotopes (^{238}U and ^{235}U, respectively), while ^{228}Ra and ^{224}Ra are decay products of ^{232}Th. Three of the isotopes (^{226}Ra, ^{224}Ra and ^{223}Ra) disintegrate into radon isotopes (^{222}Rn, ^{220}Rn and ^{219}Rn, respectively), while ^{228}Ra decays to ^{224}Ra via ^{228}Th (and the short-lived ^{228}Ac). All four radium isotopes are produced from aquifer solids and in surface water bodies by the decay of their insoluble parents. In freshwater, radium is mainly tightly bound to the surface of sediment grains (e.g., Webster et al, 1995; Gonneea et al, 2008; Lazar et al, 2008) while in saline water the radium is much more soluble and readily undergoes ion exchange with other cations (e.g., Krishnaswami et al, 1991; Sturchio, 2001).

5.1.1 The behavior of radon and radium isotopes in groundwater

Due to the relatively short half-life of radon and radium isotopes, groundwater activities represent water–rock interaction processes rather than the origin of the groundwater, which may be represented by conservative elements. Therefore Ra and Rn can be used to characterize processes and the kinetics involved.

Processes responsible for radium input to the groundwater are: a) alpha recoil by the decay of the parent nuclide (Th) in the aquifer solids, b) desorption from the solid surface, c) dissolution or recrystallization and d) decay of the parent nuclide in the solution. Radium sinks include a) radioactive decay, b) adsorption (Krishnaswami et al, 1982) and c) co-precipitation (e.g. Kiro et al, 2012).

As for radon, which is a dissolved gas, the main sources include: a) decay of dissolved ^{226}Ra and b) alpha recoil by the decay of ^{226}Ra which may be supported by the parent nuclide in the source rock (Krishnaswami et al, 1982), adsorbed (unsupported) on the solid surface (Moise et al, 2000) due to its relatively high mobility in certain conditions, such as high salinities (Webster et al, 1995) and temperatures (Rama and Moore, 1996), or produced from a surface coating enriched in ^{232}Th and ^{230}Th (Tricca et al, 2001), while the main sinks are radioactive decay and loss to the pore space above groundwater level due to degassing.

In a close water–rock system, the total concentration of radium and radon in the solids and water is in secular equilibrium with the ^{238}U, ^{235}U and ^{232}Th. Radium will be partitioned between the solid surface and the groundwater according to the adsorption partition coefficient (K) and the ^{226}Ra/^{223}Ra and ^{224}Ra/^{228}Ra ratios in the water would represent values around secular equilibrium (Davidson and Dickson, 1986). ^{224}Ra/^{228}Ra ratio in secular equilibrium is 1, while ^{226}Ra/^{223}Ra activity ratio is 21 according to the natural abundance of ^{238}U and ^{235}U. Due to the effect of recoil and the number of alpha decay steps, the secular equilibrium ratios of ^{224}Ra/^{228}Ra may reach 1.5, $\frac{^{226}\mathrm{Ra}/^{223}\mathrm{Ra}}{21}$ may reach twice the ^{238}U/^{234}U ratio and ^{226}Ra/^{228}Ra ratio may reach twice the U/Th ratio in the solid (Davidson and Dickson, 1986). The deviation of these isotope activities from secular equilibrium is an indication of the rate of water–rock processes, the age of the groundwater and groundwater flow paths and mechanisms.

The adsorption of radium onto aquifer solids is highly sensitive to salinity (Webster et al, 1995; Sturchio, 2001; Gonneea et al, 2008; Kiro et al, 2012), even though it is also a function of mineralogy (clay and oxides content) and of the redox state of the groundwater (Gonneea et al, 2008; Kiro et al, 2012). Of all radium isotopes, ^{226}Ra is the main isotope to be affected by adsorption–desorption processes, due to its longer half-life.

High activities of radon are common in groundwater and considered to be a relatively large fraction (∼5%) of the radon produced in the aquifer rock by the decay of ^{238}U and its daughters (Tricca et al, 2001), considering ^{222}Rn is in secular equilibrium with its parent nuclides and taking into account the water–rock ratio. In the Dead Sea groundwater, the activities of radon may even exceed the expected produced radon in the rock (> 100%, Moise et al, 2000). Several models and hypotheses explain these high activities. Krishnaswami et al (1982) interpret the high activities of radon as production by alpha recoil from the parent nuclide (supported ^{226}Ra) in the rock, while Moise et al (2000) explained its high activities due to the high content of adsorbed ^{226}Ra on the solids and Tricca et al (2001) suggested contribution by surface coating enriched in ^{232}Th and ^{230}Th.

The contribution of radon or radium isotopes to the groundwater depends on the time scale of the different processes and the isotope half-life. Alpha recoil is a very significant process for the short-lived isotopes which are produced relatively fast by their parent nuclides, while a radium-rich source (e.g. the Dead Sea brine) is significant for ^{226}Ra ($t_{1/2}$=1600 yr) which decays slowly relative to the other isotopes (Kiro et al, 2012). Adsorption and desorption processes considered to be relatively fast (seconds to hours, Krishnaswami et al, 1982) compared to the groundwater flow time scale and decay, while contribution by dissolution is a slower process and depends on the degree of saturation of the dissolved minerals.

The objective of this research is to use the Dead Sea hydrological system as a natural field lab for studying the behavior of radon and radium isotopes in a system with a large salinity range, different lithologies and diverse hydrological mechanisms. This study details the different groundwater sources in the Dead Sea groundwater system that vary from fresh water to hypersaline water and the application of radium and radon to understand groundwater flow dynamics, velocities and ages.

5.1.2 The Dead Sea hydrological and geochemical system

The Dead Sea is a terminal lake located in a deep pull-apart basin along the Dead Sea transform fault. The lake level has been continuously dropping from -390m in the 1930's (Klein and Flohn, 1987) to -427m at present (2013), reaching a rate of more than 1 m/y. This decline is the result of the increased utilization of fresh water in the northern part of the basin and the increased evaporation by the Israel Dead Sea Works and the Jordanian Arab Potash Company. Altogether, these changes in water management resulted in a decrease of the average annual inflow to the lake from 1600–2000 million m^3 in the early 1900's (Neumann, 1958; Klein, 1998; Salameh and El-Naser, 1999) to a current 265–335 million m^3 (Lensky

et al, 2005).

The composition of the Dead Sea water is Ca-chloride with a low Na/Cl ratio compared to normal ocean water (0.21 today vs. 0.86, respectively). This composition is the result of the evaporation of seawater that intruded the rift valley, followed by halite precipitation. Other water–rock interactions, such as dolomitization of carbonates, have further altered the original composition (Starinsky, 1974). The Na/Cl ratio is still decreasing due to the present precipitation of halite in the lake (Gavrieli, 1997).

The current Dead Sea salinity and density are 340 g/L and 1.24 kg/L, respectively. It is extremely enriched in radium relative to most natural water bodies. The ^{226}Ra activity in the Dead Sea (∼147 dpm/L; Kiro et al, 2012) is 1,600 times that of Pacific surface water (∼0.09 dpm/L) and 400 times that of Pacific deep water (∼0.35 dpm/L, Broecker et al, 1967).

The water sources to the Dead Sea are the Jordan River (∼100 million m^3/y), fresh and brakish grounadwater and brines discharging along the western shore (∼100 million m^3/y) and perennial streams on the eastern catchment of the Dead Sea (∼100 million m^3/y), which are mainly fed by groundwater (Lensky et al, 2005; Fig. 2.1). Almost all water sources to the Dead Sea, except the Jordan River are groundwater-based, therefore contain relatively high activities of radium. The main source of water at the western Dead Sea is the Ein Feshkha springs, which are brackish and discharge at a relatively constant salinity (∼2 g Cl/L, ∼60 million m^3/y). Kane, Samar and Ein Gedi springs (Fig. 2.1) are fresh water springs (< 0.5 g Cl/L). These springs, including Ein Feshkha, are the result of rain water infiltration at the highlands of the Judea mountains. This fresh groundwater mixes with Dead Sea water close to the shore, so the groundwater discharging on the shore and groundwater in boreholes have various salinities. Ein Qedem springs are thermal brines (∼120 g Cl/L) in which the discharge is relatively low (∼10 million m^3/y) but they are a major source of dissolved constituents due to their high salinity. The temperature of these brines is around 45°C, which indicates that the groundwater comes from at least 0.5km depth (Gavrieli et al, 2001; Stern, 2010).

The streams on the eastern catchment of the Dead Sea originate from springs some of which are thermal (up to 65°C), and a small amount is stems from floods (Salameh, 1996). The main sources of water are found in Wadi Mujib, Wadi Hasa and Wadi Zarqa Ma'in (Fig. 2.1). At present, most of these water sources are dammed and utilized.

There are three principal aquifers on the west side of the Dead Sea: the Lower Cretaceous sandstone Kurnub aquifer, the Upper Cretaceous carbonate Judea aquifer and the Quater-

nary alluvial aquifer (Arad and Michaeli, 1967; Yechieli et al, 1995). The alluvial aquifer is in direct hydraulic contact with the lake along most of its shoreline. It mainly consists of clastic sediment deposited in fan deltas (gravel, sand and clay) and of lacustrine sediments (e.g., clastics, aragonite, gypsum and halite). Alternations between gravel and clay create several sub-aquifers that differ in their hydraulic heads and chemical composition. The alluvial aquifer is bounded on its west by normal faults, which set Cretaceous carbonate rocks of the Judea Group against Quaternary alluvial and lacustrine sediments. The freshwater recharge of the alluvial aquifer is mainly through lateral flow from the Judea Group aquifer, which is replenished in the highlands 10–30km to the west and by flash floods. Direct recharge on this aquifer is negligible because of the arid climate in the Dead Sea region (precipitation $<$100 mm/y). On the east side of the Dead Sea the geology is different and the groundwater aquifers are divided into three complexes: the deep sandstone aquifer complex, the upper Cretaceous aquifer complex and the shallow aquifer complex. The sandstone aquifer contains two units, the Paleozoic Disi group and the Jurassic-Lower Cretaceous Kurnub and Zerka group, which both outcrop along the Dead Sea Rift valley. The Cretaceous complex consists of limestone, dolomite, marl and chert (Salameh, 1996).

The hydraulic relationship between the Dead Sea and the alluvial aquifer is expressed in a relatively rapid water level response (several days) to level changes in the Dead Sea (Yechieli et al, 1995). Groundwater levels respond to the lake level drop at different rates according to the aquifer hydraulic parameters and lake bathymetry near the coast. The groundwater level drop may reach the same rate as the Dead Sea lake level drop (Kiro et al, 2008).

The extremely high density of the Dead Sea water induces a very shallow transition zone between the fresh and saline water bodies. According to the Ghyben-Herzberg approximation, the depth of the transition zone is 4.35 times the groundwater elevation, compared to 40 times in aquifers next to the ocean (Yechieli, 2000). The transition zone is also relatively wide due to hydrodynamic dispersion and the lake level drop (Kiro et al, 2008). In fact, often there is no fresh water zone in the alluvial aquifer near the lake (up to $\sim$100m) and relatively high salinities were found at the water table up to a few hundreds of meters from the shore inland.

Dead Sea water circulates beneath the transition zone due to density differences and hydrodynamic dispersion, also during the lake level drop (Kiro et al, 2008). Water–rock interaction during the circulation affects several trace element concentrations. One of the main processes is precipitation of barite, which removes Ba and ^{226}Ra from the Dead Sea water, causing a decrease in Ba and ^{226}Ra from 5 and $\sim$147 to 1.5 mg/L and $\sim$60 dpm/L,

respectively (Kiro et al, 2012).

5.2 METHODS

Water samples were taken from the main water sources around the Dead Sea (Fig. 2.1, Table 5.1). The water sources to the Dead Sea included the Jordan River, groundwater and brines discharging along the western shore of the Dead Sea and springs brines and streams at the eastern catchment of the Dead Sea. Circulated Dead Sea water and the fresh–saline transition zone were studied from boreholes. Groundwater samples of various salinities were collected from several depths in boreholes mainly at Wadi Arugot alluvial fan area (Fig. 2.1). Sampling took place after pumping three times the borehole volume in order to clean the borehole and obtain a representative sample of the aquifer's water.

Water samples for major elements were collected in plastic bottles, and samples for trace elements were collected in 125ml LDPE bottles after running through a 0.45μ filter and acidified to pH$\sim$2. Water samples for ^{226}Ra and ^{222}Rn analysis were sampled in 0.5L vacuumed glass bottles, while water samples for short-lived radium isotopes (^{228}Ra, ^{223}Ra and ^{224}Ra) were collected in 3-20L plastic containers, followed by running the water through 0.45μ filter and extracting the radium onto MnO_2-coated acrylic fibers (Moore and Arnold, 1996).

Major and trace element concentrations were measured using Perkin Elmer Optima 3300 ICP-AES for cations, Dionex ICS-2000 Ion Chromatograph for anions and Perkin Elmer Sciex Elan-DRC-e ICP-MS for the trace elements.

^{222}Rn was extracted via helium bubbling and was adsorbed onto a cooled charcoal column. The radon gas was then transferred to a counting (Lucas) cell after heating the column to 450°C (Mathieu et al, 1988). ^{226}Ra was measured after incubation for at least three weeks in order to allow the ^{222}Rn to reach secular equilibrium with the ^{226}Ra.

The short-lived radium isotopes (223 and 224) were measured by a delayed coincidence counter (RaDeCC, Moore and Arnold, 1996). Chance coincidence of ^{224}Ra and ^{223}Ra was calculated according to Giffin et al (1963).

^{228}Ra was also measured by the delayed coincidence counter (RaDeCC), following the procedure of Moore (2008). It was measured on the same fibers used for determining the ^{224}Ra. The samples were measured at least twice ($>$ 1 month and $>$ 6 months) after the first measurement of ^{224}Ra to allow for the growth of ^{228}Th from the adsorbed ^{228}Ra. ^{228}Ra concentration was calculated according to the growth rate of ^{228}Th as described in Moore (2008). Additionally, some of the samples were measured for ^{228}Ra by γ spectrometry

following the procedure of Dulaiova and Burnett (2004).

The adsorption efficiency of radium on the MnO_2-coated fibers was calculated by comparing the activity of ^{226}Ra adsorbed on the fibers and that in water of the same sample, both measured with the extraction system (above). The adsorption of radium from Dead Sea water and the brines, was found to be of low efficiency (5–15%), which is due to the very high ionic strength of the water. Therefore, the saline water was diluted by 5 to 20 times, which increased the adsorption efficiency to 30–80%. Nevertheless, it was still quite variable and the efficiency was determined for each sample. The activity (of all isotopes) was corrected accordingly.

5.3 RESULTS

Water was sampled from all main water bodies in the Dead Sea hydrological system (Fig. 2.1), including springs on the western Dead Sea coast: Ein Feshkha (EF), Ein Qedem (EQ), Kane and Samar springs (K), and streams on the eastern catchment of the Dead Sea (EC) including Wadi Mujib, Wadi Hasa, Wadi Zarqa Ma'in, Wadi Karak and Wadi Ibn Hammad (Fig. 2.1). All samples were analyzed for radon and radium isotopes (see section 3.2). Circulated Dead Sea water (CDS) and groundwater from the fresh-saline transition zone (TZG) were sampled mainly from boreholes at the Wadi Arugot alluvial fan.

All groundwaters contain relatively high activities of ^{222}Rn and radium isotopes, while the highest activities of radium occur in the hypersaline groundwater of CDS and EQ brines, reaching ^{226}Ra activities of hundreds dpm/L and ^{223}Ra, ^{224}Ra and ^{228}Ra activities of tens dpm/L (Figures 5.1, 5.2). and the highest activities of ^{222}Rn occur in EQ and EF groundwaters (Table 5.1).

5.3.1 ^{228}Ra/^{226}Ra and ^{224}Ra/^{223}Ra ratios

Radium isotope ratios are shown in Figures 5.3 and 5.4 and in Table 5.1. The water sampled at the eastern shore are distinct from western groundwater in their radium isotope signature with only a small overlap (Fig. 5.3). While the average ^{228}Ra/^{226}Ra and ^{224}Ra/^{223}Ra in the eastern groundwater are 0.76 and 8.6, respectively, the ratios in the western groundwater are much lower (0.15 and 2.4 respectively). Some of the western groundwater (Ein Feshkha, Kane and Samar springs and the Ein Qedem brines) have even lower ^{228}Ra/^{226}Ra ratios, at EF and K groundwater it is 0.05 and at EQ it is 0.03 (Table 5.1).

The relationship between ^{228}Ra/^{226}Ra and ^{224}Ra/^{223}Ra ratios is another way to show the difference between the groundwater groups. The EC, CDS and TZG groups are mainly above

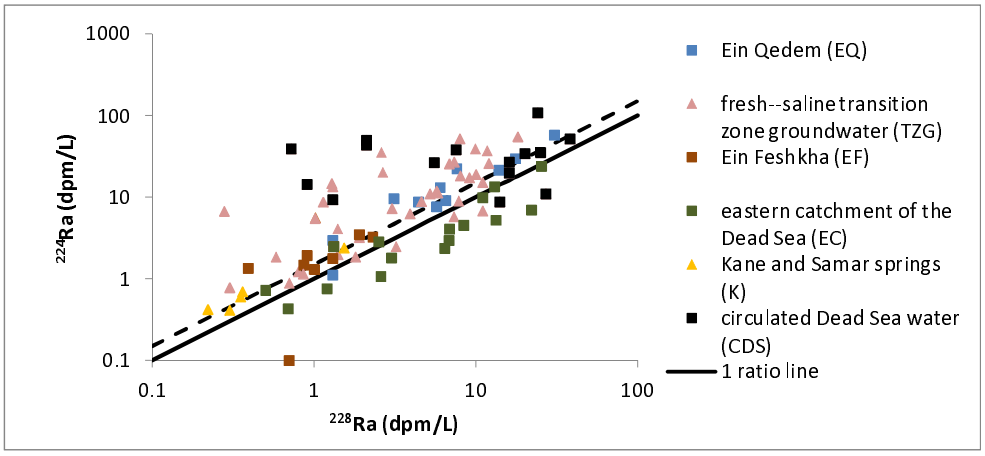


Figure 5.1: The relationship between ^{228}Ra and ^{224}Ra activities in the Dead Sea groundwater

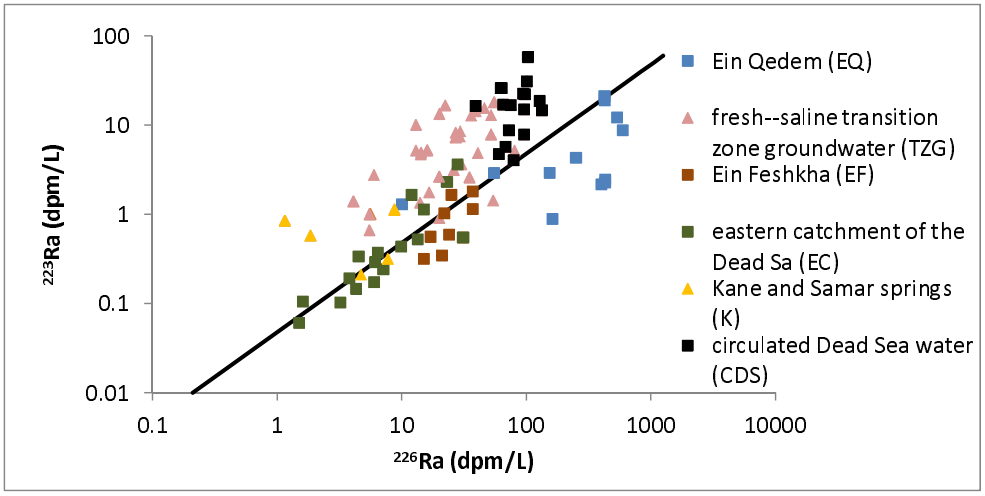


Figure 5.2: The relationship between ^{226}Ra and ^{223}Ra activities in the Dead Sea groundwater.

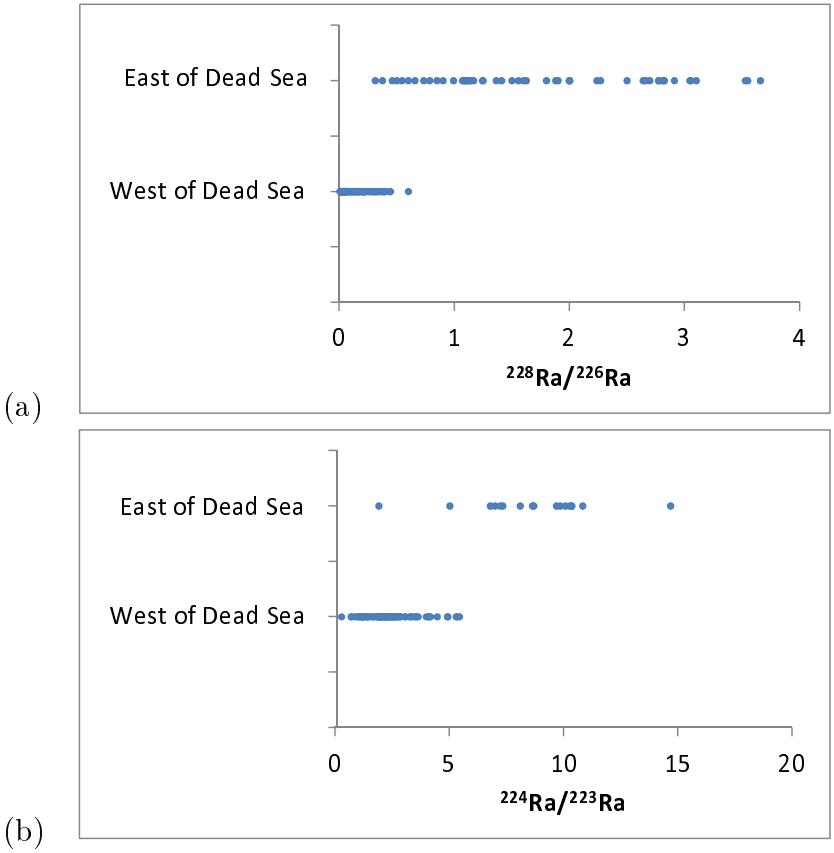


Figure 5.3: ^{228}Ra/^{226}Ra and ^{224}Ra/^{223}Ra ratios in groundwater around the Dead Sea. The eastern catchment consists of crystalline and sand rock with relatively high Th/U ratio, while the western catchment consists of carbonate rocks with much lower Th/U. This is represented by the ^{228}Ra/^{226}Ra and ^{224}Ra/^{223}Ra ratios.

the secular equilibrium line (^{224}Ra/^{228}Ra=1–1.5, ^{226}Ra/^{223}Ra=21) with low ^{224}Ra/^{223}Ra ratio relative to ^{228}Ra/^{226}Ra ratio, while EF, EQ and K groups lie on or slightly beneath the secular equilibrium line (Fig. 5.4).

5.3.2 ^{226}Ra/^{223}Ra and ^{224}Ra/^{228}Ra ratios

The relationship between ^{226}Ra and ^{223}Ra and between ^{224}Ra and ^{228}Ra in the groundwater samples are shown in figures 5.2 and 5.1, together with the secular equilibrium line. Each groundwater group lies in a distinctive area of these two plots (above, on or below the secular equilibrium lines). Only the K and EF groundwater groups lie on both ^{226}Ra/^{223}Ra and ^{224}Ra/^{228}Ra ratio secular equilibrium lines, while the EQ group lies on the ^{224}Ra/^{228}Ra equilibrium line and below the ^{226}Ra/^{223}Ra line and EC group lies on the ^{226}Ra/^{223}Ra line and below the ^{224}Ra/^{228}Ra secular equilibrium line. The TZG and CDS groundwater groups are above both secular equilibrium lines (e.g lower ratio than secular equilibrium).

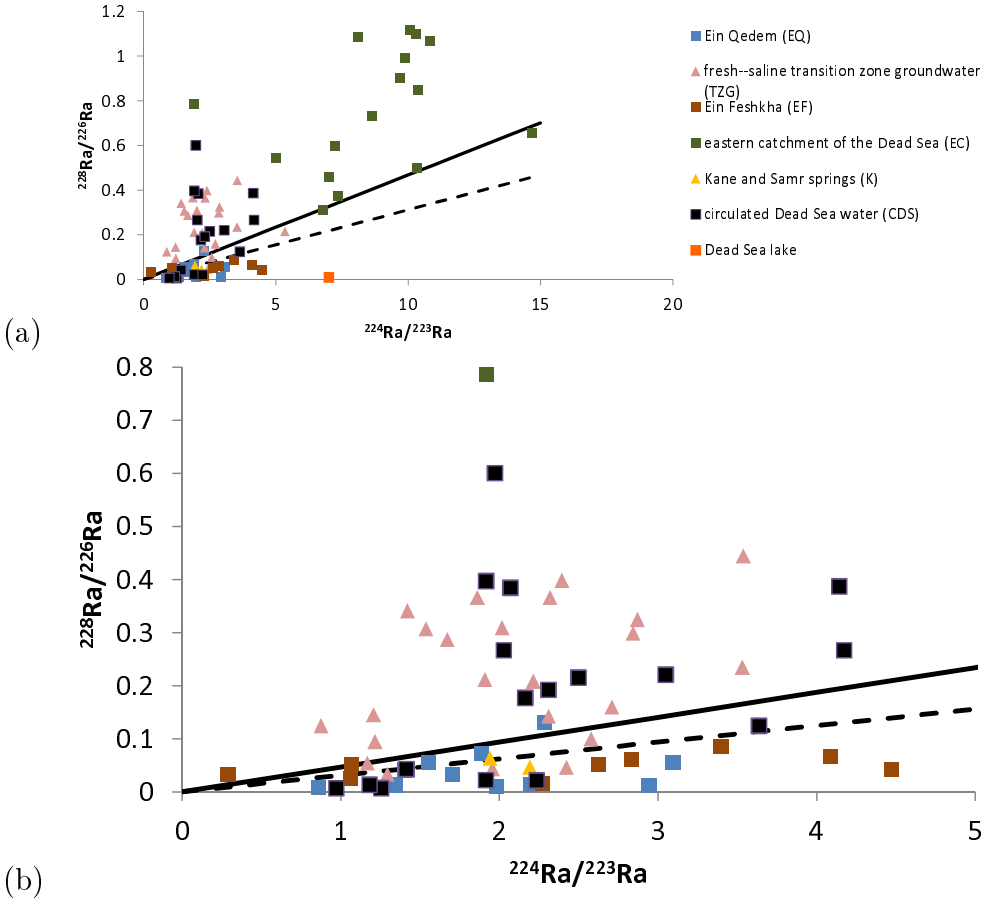


Figure 5.4: (a) ^{228}Ra/^{226}Ra vs. ^{224}Ra/^{223}Ra ratio in groundwater around the Dead Sea. The solid (^{224}Ra/^{228}Ra=1) and dashed (^{224}Ra/^{228}Ra=1.5) lines are calculated according to secular equilibrium with U and Th in the aquifer rock. (b) the same data enlarged.

5.3.3 ^{226}Ra, ^{223}Ra and ^{222}Rn relationship

The isotopic composition of groundwater from the western shore is plotted on a ternary diagram of ^{222}Rn, ^{223}Ra and ^{226}Ra, which are all the progenies of uranium (Fig. 5.5). ^{222}Rn and ^{223}Ra are both short-lived isotopes and reach equilibrium with the aquifer sediments after several weeks. Their expected activity equilibrium ratio in the case of no radium adsorption, based on ^{238}U/^{235}U natural abundance ratio, is 21.

It is apparent that all groundwater groups are very variable in their radionuclide ratios. The large variation in each groundwater group occurs mainly along the red of grey adsorption–desorption (K) change lines (section 5.4.4, Fig. 5.5).

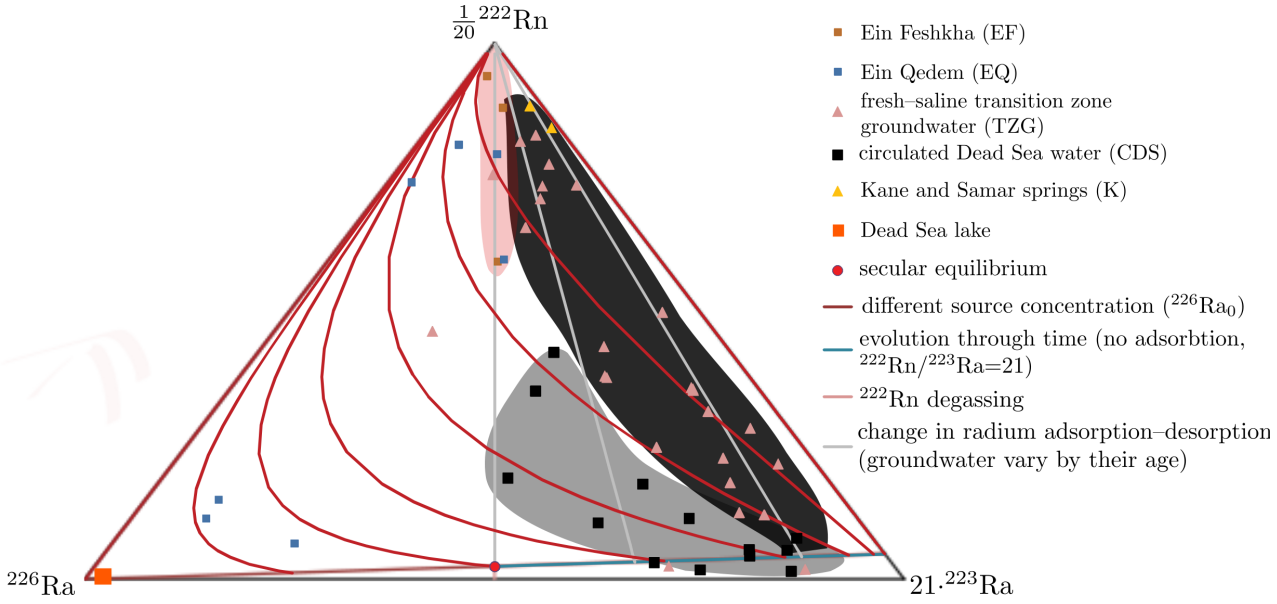


Figure 5.5: A ternary diagram of ^{226}Ra, ^{223}Ra and ^{222}Rn with plotted groundwater samples demonstrating processes affecting the relationship between these three isotopes. The secular equilibrium ratio is marked by the red dot, while The grey and red lines represent the change in the relationship between the three isotopes as a function of K (adsorption–desorption) according to equations 5.4.4, 5.4.4 and 5.4.4. Each of the grey lines differs by groundwater age (where ^{226}Ra$_0$=0), while each of the red lines differs by their initial ^{226}Ra$_0$ in young groundwater (t=0). The different fields emphasize the different groundwater groups.

5.3.4 ^{222}Rn in the Dead Sea system groundwaters

Most groundwater around the Dead Sea contain extremely high activities of ^{222}Rn (Salameh, 1996; Moise et al, 2000, Table 5.1). EF, EQ and EC groundwaters reach ^{222}Rn activities of 60,000 dpm/L, while the TZG and K groups contain lower activities up to 3500 dpm/L.

The lowest ^{222}Rn activities in this system occur at the CDS groundwater with activities of hundreds dpm/L.

Table 5.1: Radium and radon activities and ratios in water around the Dead Sea. The samples are organized according to the groundwater groups as it appears in the table. Radium and radon measurement errors are 5–10% and Ba and U errors are 5%. Other data of the samples are in Appendix C.

Sample	Location	date	Cl (g/L)	Ba (mg/L)	U (μg/L)	^{226}Ra	^{228}Ra	^{224}Ra	^{223}Ra	excess ^{222}Rn (dpm/L)	^{224}Ra/^{223}Ra	^{224}Ra/^{228}Ra	^{226}Ra/^{223}Ra	^{228}Ra/^{226}Ra
	Arugot alluvial fan (TZG, CDS)													
yk1	EG16	21/01/08	67	0.36		14.4								
yk2	EG16	21/01/08	67			25.2								
yk3[a]	EG16	21/01/08	67			16.0		7.6	5.2	1407	1.5		3.1	
yk4	EG16	21/01/08	142			35.2				2289				
yk5	EG16	21/01/08	142	1		24.0								
yk6[a]	EG16	21/01/08	142			22.2	6.8	25.7	16.7	2059	1.5	3.8	1.3	0.31
yk7	EG16	21/01/08	224	2.3		58.4								
yk8	EG16	21/01/08	224			58.9				241				
yk9[a]	EG16	21/01/08	224			100.9	0.7	39.3	31.4		1.3	55	3.2	0.01
yk11[a]	EG11	21/01/08	51	0.36		6.0	0.3	6.7	2.8	1280	2.4	24	2.1	0.05
yk12[a]	EG11	21/01/08	142	1.2		29.1	1.3	14.7	7.5		2.0	11	3.9	0.04
yk13[a]	EG22	21/01/08	221	1.66		39.1	7.5	38.2	16.5	650	2.3	5.1	2.4	0.19
yk14[a]	Arugot-Keshet	21/01/08	0.25			5.5	0.3	0.78	0.7	1081	1.2	2.6	8.2	0.05
yk42[a]	Spring	27/08/08	78			18.3				2980				
EG22-29.5m[a]	EG22	24/03/09	219	1.5		60	16	19.9	4.8	2358	4.2	1.2	13	0.27
ES	Ein Shulamit	24/03/09				7.7								
yk110A[a]	EG20	22/06/09	227	1.5		68	27	11.1	5.8	449	1.9	0.4	12	0.40
yk111A[a]	EG21	22/06/09	139	0.96		20	3.2	2.5	0.9	2426	2.7	0.8	22	0.16
yk112[a]	EG21	22/06/09	219	1.3		79	14	8.8	4.1	769	2.2	0.6	19	0.18
yk113[a]	EG11	22/06/09	73	0.48		54	1.8	1.9	1.4	1452	1.3	1.0	38	0.03
yk115	EG6	22/06/09				5.6	0.7	0.9	1.0	2614	0.9	1.3	5.5	0.13
yk118[a]	EG19	22/06/09	44			4.1	1.4	2.0	1.4	1872	1.4	1.4	2.9	0.34
yk119[a]	EG19	22/06/09	101			35	7.3	5.7	2.6	3428	2.2	0.8	13	0.21
yk120	AR2	22/06/09	12			52	11	15.1	7.9	1435	1.9	1.4	6.6	0.21
yk121	AR2	22/06/09	11			27	12	25.8	7.3	798	3.5	2.2	3.7	0.44
yk122[a]	EG22	22/06/09	136	0.48		30	11	6.8	3.7	1294	1.9	0.6	8.2	0.37
yk123[a]	EG22	22/06/09	212	1.3		52	8	18.2	13.1	932	1.4	2.3	4.0	0.15
yk240[a]	EG11	13/06/10	68	0.5	0.7	14.3	5.7	11.8	5.0	1082	2.4	2.1	2.9	0.40
yk241[a]	EG22	13/06/10	137	1	0.2	16	4.6	8.8	5.3	1390	1.7	1.9	3.0	0.29
yk242[a]	EG22	13/06/10	169	1.2	0.09	29.4	9.1	17.3	8.6	1232	2.0	1.9	3.4	0.31
yk243[a]	EG22	13/06/10	219	1.6	0.07	80.3	10	18.9	5.2	2060	3.6	1.9	15	0.12
yk244[a]	EG22	13/06/10	117	0.85	0.27	14.2	5.2	11.0	4.7	1255	2.3	2.1	3.0	0.37
yk245[a]	EG20	13/06/10	224	1.5	0.12	63.3	38	51.7	26.3		2.0	1.4	2.4	0.60
yk246[a]	EG20	13/06/10	220	1.5	0.13	75	20	34.2	16.9	397	2.0	1.7	4.4	0.27
yk247[a]	EG21	13/06/10	87	0.58	0.54	16.6	3.9	6.2	1.8	2638	3.5	1.6	42.4	0.23
yk248[a]	EG21	13/06/10	152	1.05	0.17	26.1	7.8	9.0	3.2	48	2.8	1.2	8.3	0.30

Continued on next page

Table 5.1 – *Continued from previous page*

Sample	Location	date	Cl (g/L)	Ba (mg/L)	U (μg/L)	^{226}Ra	^{228}Ra	^{224}Ra	^{223}Ra	excess ^{222}Rn (dpm/L)	^{224}Ra/^{223}Ra	^{224}Ra/^{228}Ra	^{226}Ra/^{223}Ra	^{228}Ra/^{226}Ra
yk249[a]	EG21	13/06/10	184	1.25	0.11	40.7	5.8	11.3	4.9	1760	2.3	1.9	8.3	0.14
yk250[a]	EG21	13/06/10	220	1.4	<0.05	72.5	16[b]	27.0	8.9	1122	3.0	1.7	8.2	0.22
yk291[a]	spring	05/07/10	74	0.51	3.6	14	3.02	7.3	1.4	3815	5.3	2.4	10	0.22
yk400[b]	EG24	13/06/11	148	1.2	1.2	27	4.6	22.1	8.3		2.7	4.8	3.3	0.17
yk401[b]	EG24	13/06/11	230	4.1	0.6	96	1.3	9.3	7.9		1.2	7.2	12	0.01
yk402[b]	EG25	13/06/11	82	0.5	1.4	13	1.3	13.5	5.2		2.6	10	2.5	0.10
yk410[b]	EG25	13/06/11	151	0.9	0.7	36	11.7	37.0	12.9		2.9	3.2	2.8	0.33
yk411[b]	EG25	13/06/11	229	2.8	0.7	96	17.3	26.8	15.1	1067	1.8	1.5	6.4	0.18
yk412[b]	EG25	13/06/11	95	0.6	1.3	20	3.3	34.5	13.5	2385	2.6	10.5	1.5	0.17
yk413[b]	EG24	13/06/11	216	2.2	1.4	46	9.9	39.1	15.6	436	2.5	3.9	2.9	0.22
yk414[b]	EG24	13/06/11	229	3.5	0.9	128	5.5	26.6	18.8	196	1.4	4.8	6.8	0.04
yk415[b]	EG24	13/06/11	233	4	0.7	133	0.9	14.4	14.8	295	1.0	16	9.0	0.01
yk416[b]	EG23	13/06/11	196	1.3	1.1	39	8.4	26.7	14.4	134	1.9	3	2.7	0.22
yk417[b]	EG23	13/06/11	228	3.2	0.9	94	2.1	43.6	22.8		1.9	21	4.1	0.02
yk418[b]	EG23	13/06/11	223	3.1	0.5	103	19.9	67.9	58.5		1.2	3	1.8	0.19
yk419[b]	EG23	13/06/11	231	3.3	0.4	97	2.1	49.9	22.3	674	2.2	24	4.3	0.02
yk420[b]	EG26	13/06/11	57	0.4	2.1	13	2.8	27.0	10.2	46	2.7	9.64	1.3	0.22
yk421[b]	EG26	13/06/11	226	1.4	<0.1	65	25	35.3	17.1		2.1	1.4	3.8	0.38
yk422[b]	EG26	13/06/11	220	1.4	<0.1	62	24	108.3	26.1		4.1	4.5	2.4	0.39
	Einot-Qedem (EQ)		120		0.03-0.12[d]									
yk52		27/07/08				261.8				11021				
yk53		27/07/08				14.9				641				
yk61		03/11/08				400	4.4	8.7	2.2	1151	4.0	2.0	184	0.01
yk62		03/11/08				471.1				704				
yk64		03/11/08				161.6	1.3	1.1	0.9	633	1.2	0.9	180	0.01
yk185		21/09/09				429	6	13.2	2.5	27548	5.3	2.2	173	0.01
yk186		21/09/09									3.1	1.4	8.8	0.25
yk189		21/09/09				515	7.3			14914				0.01
yk190		21/09/09				594	7.6	22.4	8.8	1132	2.5	2.9	67	0.01
yk193		21/09/09									2.3	2.3	6.9	0.14
yk194		21/09/09				430.3	5.7	7.6	2.3		3.3	1.3	187	0.01
yk195		21/09/09				425.9		32.0	19.0		1.7		22	
EQ101		17/11/09				55	3.1	9.6	2.9	3454	3.3	3.1	19	0.06
EQ102		17/11/09				250	13.8	21.4	4.3	29342	4.9	1.6	58	0.06
EQ103		17/11/09				423	30.5	57.6	21.2	66821	2.7	1.9	20	0.07
EQ104		17/11/09				536	17.5	29.8	12.3		2.4	1.7	44	0.03
	Jordan River													
jordan1		18/05/09				6				9.7				
jordan2		18/05/09				2				9.9				
jordan3		18/05/09				3.1				9.2				
jordan4		18/05/09				1.2				31				
yk390[f]	Baptism site	24/02/11				3.2	1.06	2.1	0.4		5.4	2.0	8.1	0.33
	Ein Feshkha (EF)		2		1.96[c]									
EQ105		17/11/09				25	1.3	1.8	1.7	8836	1.1	1.4	15	0.05
EQ106		17/11/09				21	0.7	0.1	0.4		0.3	0.1	60	0.03
yk310		04/10/10	8.83			31	1.3	2.5	0.6		4.5	1.9	56	

Continued on next page

Table 5.1 – *Continued from previous page*

Sample	Location	date	Cl (g/L)	Ba (mg/L)	U (μg/L)	^{226}Ra	^{228}Ra	^{224}Ra	^{223}Ra	excess ^{222}Rn (dpm/L)	^{224}Ra/^{223}Ra	^{224}Ra/^{228}Ra	^{226}Ra/^{223}Ra	^{228}Ra/^{226}Ra
yk311		04/10/10	81	0.072		114								
yk312		04/10/10	2.1			22	1.9	3.5	1.0		3.4	1.8	21	0.09
yk313		04/10/10	5.4	0.3		37	0.9	1.9	1.8	2198	1.1	2.1	20	0.02
yk314		04/10/10	2.2	0.4		17	0.9	1.5	0.6		2.6	1.6	30	0.05
yk315		04/10/10		0.04		37	2.3	3.3	1.2		2.8	1.4	32	0.06
yk316	Spring in the Dead Sea	04/10/10				166		6.7	1.4		4.9		121	
yk317		04/10/10	2.0		2.4	15	1	1.3	0.3		4.1	1.3	47	0.07
yk318		04/10/10	21	0.8		50				6790				
yk391		24/02/11				24	0.4	1.4	0.6	11321	2.3		40	
yk392[f]		24/02/11				28.4	0.12			64000				
	Samar and Kane Springs (K)				1.33[c]									
yk350	Samar Spring	08/11/10	39	1		8.7	1.5	2.4	1.1		2.1	1.6	7.7	0.17
yk351	Samar Spring	08/11/10	2.8	0.5		7.7	0.4	0.7	0.3		2.2	1.7	24	0.05
yk352	Samar Spring	08/11/10	4.8	0.4		10.1								
yk353	Samar Spring	08/11/10	2.5	0.15		3.3								
yk354	Samar Spring	08/11/10	4.0	0.27		2.1								
yk355	Samar Spring	08/11/10	53.0	4.1		12.1								
yk356	Kane Spring	08/11/10	1.2	0.15	1.01[c]	4.7	0.3	0.4	0.2		1.9	1.4	22	0.06
yk357	Samar Spring	08/11/10	2.0	0.37		3.1								
yk393	Samar Spring	24/02/11				1.85	0.2	0.4	0.6	2125	0.7	2.1	3.2	0.11
yk394	Samar Spring	24/02/11				1.15	0.4	0.6	0.9	2050	0.7	1.5	1.3	0.35
	Eastern Catchment, Jordan (EC)													
yk300	Wadi Hudeira	23/09/10	0.10			1.1	0.6	0.5	0.1		5.0	0.9	11	0.55
yk301	Wadi Ibn-Hamad	23/09/10	0.12	0.0648		6.4	6.9	4.1	0.4		10.8	0.6	17	1.08
yk302	Wadi Ibn-Hamad	23/09/10	0.13	0.0674		4.5	7.8	3.0	0.3		8.7	0.4	13	1.73
yk303	Wadi Hasa	25/09/10	0.10	0.0698		7.1	6.4	2.4	0.2		9.7	0.4	29	0.90
yk304	Wadi Mujib	25/09/10	0.13	0.0168		9.9	8.4	4.5	0.4		10.4	0.5	23	0.85
yk305	Wadi Zarka Ma'in	25/09/10	0.77	0.0604		13.4	13.3	5.2	0.5		9.9	0.4	25	0.99
yk360	Wadi Hanzira	15/12/10	0.14	0.04		1.7								
yk361	Wadi Fifa	15/12/10	0.09	0.1		39								
yk362	Wadi Hasa	15/12/10	0.13	0.09		17				16384[e]				
yk363	Wadi Karak	16/12/10	0.16	0.08		3.2	1.2	0.8	0.1		7.3	0.6	31	0.40
yk365	Spring	16/12/10	202	6.8		28	21.9	7.0	3.6		1.9	0.3	7.7	0.78
yk366[f]	Wadi Mujib	16/12/10	0.41	0.07		6.1	6.8	3.0	0.3		10.1	0.4	21	1.11
yk367[f]	Wadi Zarka Ma'in	16/12/10	0.73	0.08		15	11	9.9	1.1		8.6	0.9	13	0.73
yk368	Zarka Ma'in	16/12/10	0.72	0.12		12	13	13.5	1.7	31635[e]	8.1	1.0	7.2	1.08
yk369	Zarka Ma'in	16/12/10	0.77	0.09		31								
yk370	Zarka Ma'in	16/12/10	0.71	0.1		22								
yk371	Zarka Ma'in	16/12/10	0.67	0.095		39								
yk372	Wadi El-Hidan	16/12/10	0.12	0.055		6.6								
yk373	Wadi Mujib	17/12/10	0.11	0.08		1.5	0.7	0.4	0.1		7.0	0.6	24	0.47

Continued on next page

Table 5.1 – *Continued from previous page*

Sample	Location	date	Cl (g/L)	Ba (mg/L)	U (μg/L)	^{226}Ra	^{228}Ra	^{224}Ra	^{223}Ra	excess ^{222}Rn (dpm/L)	^{224}Ra/^{223}Ra	^{224}Ra/^{228}Ra	^{226}Ra/^{223}Ra	^{228}Ra/^{226}Ra
yk374	Wadi Ibn-Hamad	17/12/10	0.13	0.09		5.1								
yk375	Wadi Ibn-Hamad	17/12/10	0.11	0.07		6	3	1.8	0.2		10.3	0.6	34	0.50
yk376	Wadi Ibn-Hamad	17/12/10	0.13	0.09		8.5				13098[e]				
yk377	Wadi Ibn-Hamad	17/12/10	0.13	0.075		3.8	2.5	2.8	0.2		14.7	1.1	20	0.66
yk378	Wadi Wadia	17/12/10	0.09	0.12		23	25	23.9	2.3	6349[e]	10.3	1.0	10	1.09
yk379	Wadi Wadia	17/12/10	0.10	0.06		11								
yk380	Spring, Dead Sea	17/12/10	12	0.135		1.6	0.5	0.7	0.1		6.8	1.4	15	0.31
yk381	Zara	17/12/10				4.3	2.6	1.1	0.1	56610[e]	7.2	0.4	29	0.60
yk116	Darga2	22/06/09	6			5.5	0.8	1.2	1.0	1841	1.2	1.5	5.4	0.15
yk117	Darga2	22/06/09	47			55	24	38.5	18.1	1199	2.1	1.6	3.0	0.44
yk-Ar	Arugot Wadi - flood					3.8								
yk-dg	Darga Wadi -flood					6.6								
yk290	EG3	05/07/10	83	0.5	<0.05	20	1.9	3.2	2.7	1166	1.2	1.7	7.5	0.10
yk340	Borehole - Mishash fm.	03/11/10	161			1231				2736				
yk341	Borehole - Mishash fm.	03/11/10	161			1358				2115				

[a] Kiro et al (2012) [b] data from chapter 3 [c] Kronfeld et al (1991) [d] Haase-Schramm et al (2004)
[e] Salameh (1996), ^{222}Rn of Wadi Hasa is from Afra thermal spring. [f] measured by γ-spectrometry

5.4 DISCUSSION

5.4.1 Radium isotope composition and Th/U ratio of the aquifer rocks

The variability observed in the radium isotopes ratios reflects the different Th/U ratio of the aquifer rocks. However, due to their different half-lives, the ^{228}Ra/^{226}Ra ratio averages longer periods of water–rock interaction and does not necessarily reflect the local rock composition, while the ^{224}Ra/^{223}Ra ratio attains secular equilibrium with the aquifer rocks after several weeks.

Due to the large displacement along the Dead Sea transform (left lateral, 105 km, Garfunkel, 1981), the lithology on both flanks of the Dead Sea rift is very different, with mainly Late Cretaceous carbonates exposed on its west, while Early Cretaceous sandstones (overlain by carbonates) being exposed on its eastern flank. With typical sandstones ^{232}Th/^{238}U activity ratio of 1–1.5 (Gascoyne, 1992), the ^{228}Ra/^{226}Ra ratio of 0.76 is compatible with the expected ratio between ^{228}Ra/^{226}Ra in water and ^{232}Th/^{238}U in the rock, which is affected by the accumulation of preceding nuclides in the U-series (Davidson and Dickson, 1986). On the other hand, the ^{228}Ra/^{226}Ra ratios in the western Dead Sea springs and brines (EF, EQ and K, 0.03–0.05) are just 20–30% the ^{232}Th/^{238}U activity ratio measured in the Late

Cretaceous rocks (0.16, Haliva, 2004). These low ratios could be related to the presence of aragonite layers with very low $^{232}Th/^{238}U$ ratio in the coastal alluvial aquifer (down to 0.01, Haase-Schramm et al, 2004) or may be due to the different lithology and location of U and Th in the different rocks. The water–rock interaction may be very different in the sandstone and in the carbonate aquifer in terms of the availability of U- and Th-series radionuclides, adsorption–desorption processes and dissolution, which should be more significant in carbonates.

5.4.2 The source of ^{222}Rn to the Dead Sea system groundwater

The high activities of unsupported ^{222}Rn in the Dead Sea groundwaters require an additional source of ^{222}Rn to the uranium in the sediments. Taking U concentration of 1–2 ppm in the carbonate rocks of the alluvial aquifer and porosity of 0.2, the activity of ^{222}Rn equivalent to the activity in groundwater that could be produced in the aquifer is 6,000–12,000 dpm/L. These activities are a maximum estimate, since usually just a minor amount of radon is effectively ejected to the pore space fluid (up to 10%, Krishnaswami et al, 1982; Tricca et al, 2001; Weinstein et al, 2007a). In the Dead Sea system, the activities in EF and EQ groundwaters reach more than 60,000 dpm/L (Table 5.1), which is 1–2 orders of magnitude higher than the estimated contribution of ^{222}Rn above, and the TZG and K groundwater with thousands dpm/L are also significantly higher than can be effectively supplied by the local rocks. The amount that can be supplied by the local alluvial aquifer rocks is evident by radon activities in the CDS (hundreds dpm/L, Table 5.1), due to its hypersalinity and almost no adsorption of radium (Kiro et al, 2012). This suggest that higher activities of radon found in other groundwater probably originated from other sources, such as adsorbed ^{226}Ra.

On the eastern catchment, ^{222}Rn data is available only for the thermal springs (Salameh, 1996, Table 5.1). ^{222}Rn activities varies between ∼6,000–60,000 dpm/L while expected activities are significantly lower (3,000–6,000 dpm/L assuming U concentration of 0.5–1 ppm in the country sandstone rock) Unlike next to the Dead Sea, groundwater from a similar sandstone aquifer in southern Jordan, the Disi aquifer, contains only ∼400–700 dpm/L ^{222}Rn (Vengosh et al, 2009), which is around 10-20% of the ^{222}Rn produced in the sandstone rocks as it was found in other aquifers (e.g. Krishnaswami et al, 1982; Tricca et al, 2001; Weinstein et al, 2007a).

These high activities of ^{222}Rn requires an additional unsupported (by ^{238}U and its daughters in the solid) source of ^{222}Rn to the groundwater. Since Th is immobile and is less likely

to travel long distances from the host rock, the likely source of ^{222}Rn is adsorbed ^{226}Ra, which may be very mobile in certain conditions.

Both salinity (Webster et al, 1995; Sturchio, 2001; Gonneea et al, 2008; Kiro et al, 2012) and temperature (Rama and Moore, 1996) may affect radium adsorption, where in high salinity and/or temperature, radium is more mobile and therefore brines or thermal groundwater may contain higher activities of radium. Therefore, thermal springs in which temperature decreases during upflow or mixing between saline Ra-rich brines and fresh water may cause adsorption of ^{226}Ra along their flow path and contribution of high ^{222}Rn.

The young and fresh groundwater (K and sample ES, Table 5.1) contains up to several thousands dpm/L of ^{222}Rn which suggests much less adsorbed ^{226}Ra. Even these activities of ^{222}Rn, as well as ^{226}Ra activities are significantly high compared to the groundwater from the same aquifer (Judea) above the rift valley (^{222}Rn=800 and ^{226}Ra=0.16 dpm/L Moise et al, 2000. This may be due to the alternation of the carbonate rocks by interaction between the Dead Sea brine and the rocks (Starinsky, 1974), which included dolomitization and precipitation of oxides, that may have had concentrated more uranium due to adsorption or co-precipitation of oxides near the Dead Sea rift valley.

To conclude, the activities of radon and radium isotopes in the Dead Sea groundwater seem to be relatively high, which may be due to the Dead Sea brine being a terminal lake that interacted with the rocks. The significantly high ^{222}Rn activities are probably due to ^{226}Ra adsorption and occur mainly in thermal springs and where salinity changes, while the low activities of ^{222}Rn in the circulated Dead Sea water (CDS) are due to the lack of radium adsorption in the hypersaline groundwater.

5.4.3 Groundwater age and secular equilibrium ratios of radium isotopes

Generally, secular equilibrium ratios (^{224}Ra/^{228}Ra=1–1.5, ^{226}Ra/^{223}Ra$\sim$21) of the radium isotopes in groundwater do not occur in any case. ^{224}Ra/^{228}Ra secular equilibrium ratio is obtained faster, due to the shorter half-life of ^{228}Ra, and is therefore more common. For example, in K and EQ groups, most of the groundwater samples are far from ^{226}Ra/^{223}Ra secular equilibrium ratio (Fig. 5.2), while they lie on the secular equilibrium line of ^{228}Ra/^{224}Ra (Fig. 5.1). The TZG and CDS groundwater groups are considered to be the youngest groundwater in this system, and are represented by non secular equilibrium ratios in both ^{224}Ra/^{228}Ra and ^{226}Ra/^{223}Ra.

The non-secular relationship between ^{228}Ra/^{226}Ra and ^{224}Ra/^{223}Ra ratios in the Dead Sea system (Fig. 5.4) probably reflect the time of water–rock interaction with the present

aquifer rock. CDS and TZG groundwater are very young and are depleted in both ^{226}Ra and ^{228}Ra compared to ^{223}Ra and ^{224}Ra (Figures 5.1 and 5.2), while the EC, EF and EQ groups probably represent a flow path through different rock types. The EC groundwater is depleted in ^{224}Ra (^{224}Ra/^{228}Ra<1 Fig. 5.1), which may indicate a source rock richer in Th, while the EQ group is depleted in ^{223}Ra compared to ^{226}Ra (Fig. 5.2), indicating a source rock richer in U (see section 5.4.6).

^{224}Ra/^{228}Ra ratios lower than 1 in groundwater were also explained by ejection losses of ^{228}Th (Krishnaswami et al, 1982) or by recoil back into the grain (Porcelli and Swarzenski, 2003). However, groundwater from the sandy Disi aquifer in Jordan have ^{224}Ra/^{228}Ra ratios of ∼1–2 and secular equilibrium ratio of ^{226}Ra/^{223}Ra (Vengosh et al, 2009) suggesting that the mechanism which cause the low ^{224}Ra/^{228}Ra ratio is groundwater flow through different rock types rather than processes that are controlled by the decay of the U series.

Considering a single flow path of groundwater in a homogeneous sediment and neglecting hydrodynamic dispersion, the concentration of a radionuclide in time and space is (Kiro et al, 2012):

$$C(x,t) = \begin{cases} \left(C_0 - \frac{P}{R\lambda}\right) e^{-\frac{R\lambda}{v_x}x} + \frac{P}{R\lambda} & x \le \frac{v_x t}{R} \\ \frac{P}{R\lambda}\left(1 - e^{-\lambda t}\right) & x > \frac{v_x t}{R} \end{cases} \tag{5.1}$$

where C[dpm/L] is the concentration of the radium isotope, C_0[dpm/L] is the concentration this isotope at the beginning of the flow path ($x = 0$), P[dpm/(LT)] is the production rate, λ[1/T] is the decay constant, $R(= K + 1)$ is the retardation factor, v_x[L/T] is the groundwater velocity, x[L] is the distance from the beginning of the flow path and t[T] is time.

Secular equilibrium ratios are reached, when both involved isotopes attain steady-state activities of $\frac{P}{\lambda R}$, which is obtained at a distance larger than $v_x/(\lambda R)$ and after a time that is proportional to $1/\lambda$. Therefore, secular equilibrium ratios suggest that the water equilibrate with the relevant aquifer rocks for a period larger than $1/(\lambda R)$, when the λ is the smaller amongst the two isotopes.

At very low K's ($R \sim 1$), secular equilibrium ratio of ^{226}Ra/^{223}Ra is obtained after 10,000 years and may be translated directly to groundwater age. In cases where K is large, according to equation 5.1, most of the groundwater will behave according to the time-dependent term in the equation (detail discussion in Kiro et al, 2012) until it reaches steady-state after 10,000

years. Therefore, in these cases, secular equilibrium activities suggest, that the flow path of the groundwater exists 10,000 years, but the groundwater age (which is defined by the time water entered the aquifer) can be much younger, strongly depending on K value.

EF and EQ groundwater groups were dated by ^{14}C to ∼3000 and 15,000 years (Yechieli et al, 1996), respectively. ^{14}C ages of water of mixed salinities are dictated mainly by the fresh groundwater end member. The ^{226}Ra/^{223}Ra ratio in both groups is in or above secular equilibrium (Figures 5.2, 5.5). In the case of the EQ brines, there is probably no mixing between two end members and the isotopic ratio of radium is expected to be in secular equilibrium. The EF groundwater is brackish, with relatively constant salinity (∼2 g Cl/L, Table 5.1), which is probably the result of mixing of fresh meteoric water with an ancient brine. In this case, in which two end members mix, assuming high adsorption–desorption partition coefficient (∼1000 see section 5.4.5) the secular equilibrium ratio suggests that the mixing between the fresh groundwater and the brine occurred thousands of years ago. In cases of high adsorption (large R), the ^{226}Ra distribution would be according to the time-dependent term, because $t_{1/2} < \frac{Rx}{v_x}$ (where $t_{1/2}$[T] is the isotopes half-life, $R \sim 1000$, $x \sim 1000$m, and $v_x = 10$m/y), and therefore the time to attain secular equilibrium depends only on the isotope half-life. Note that if the adsorption–desorption of radium between the brine end member and the rock is very low, the mixing time determination is not accurate, and the brine end member's age should be at least 10,000 years.

Groundwater that is affected by recent mixing between two end members due to the lake level drop, such as the K and TZG groundwater, contains ^{226}Ra/^{223}Ra ratios that are not in secular equilibrium, while the EC groundwater contain secular equilibrium ratios, suggesting a relatively constant flow path of groundwater over the past 10,000 years.

The Dead Sea basin has hosted several water bodies during its geological history (Stein, 2001), which have probably penetrated to the adjacent aquifer rocks, and are evident by the ancient brines found in the aquifer (Yechieli et al, 1996). The secular equilibrium ratio of ^{226}Ra/^{223}Ra at the fresh and brackish groundwater around the Dead Sea suggests that the hydrological system of the Dead Sea, where meteoric water flows through the aquifer to the Dead Sea basin, has not change much during the past 10,000 years.

5.4.4 The mass balances of ^{226}Ra, ^{223}Ra and ^{222}Rn

The local activity of a certain radon or radium isotope in the groundwater can be expressed by its mass balance:

$$\frac{\partial C}{\partial t} = -\lambda \cdot C + \frac{P}{(K+1)} \tag{5.2}$$

where C[dpm/L] is the radionuclide activity, t[T] is time, λ[1/T] is the decay constant, P[dpm/(LT)] is the production rate of the radionuclide from the solid and K is the adsorption–desorption partition coefficient.

The ^{226}Ra mass balance equation and its solution are defined as:

$$^{226}\mathrm{Ra} = \frac{P}{\lambda_{226}(K+1)} \cdot \left(1 - e^{-\lambda_{226} t}\right) + ^{226}\mathrm{Ra}_0 \cdot e^{-\lambda_{226} t} \tag{5.3}$$

while the solution for ^{223}Ra and ^{222}Rn (assuming secular equilibrium), are :

$$^{223}\mathrm{Ra} = \frac{P}{21 \cdot \lambda_{226}(K+1)} \tag{5.4}$$

$$^{222}\mathrm{Rn} = \frac{P}{\lambda_{226}} + K \cdot ^{226}\mathrm{Ra} \tag{5.5}$$

where ^{226}Ra, ^{223}Ra and ^{222}Rn are the activities in [dpm/L], P[dpm/(L $\cdot$ T)] is the production rate of ^{226}Ra that mainly includes alpha recoil and dissolution, λ_{226}[1/T] is the ^{226}Ra decay constant and $^{226}\mathrm{Ra}_0$ [dpm/L] is the initial concentration of ^{226}Ra in the groundwater at $t = 0$.

The production rates of these three isotopes are related according to secular equilibrium ratios and natural abundant ratio of ^{238}U and ^{235}U. The dimensionless partition coefficient is defined as $K = C_s/C$ where C_s[dpm/L] is the activity of the adsorbed radium expressed as equivalent concentration in water, and C[dpm/L] is the activity in the water. The contribution of ^{222}Rn to the groundwater is assumed to be both by the decay of supported (by ^{238}U and its daughters in the solid) and unsupported adsorbed ^{226}Ra.

The various Dead Sea groundwater composition are plotted on a ternary diagram of ^{226}Ra, ^{223}Ra and ^{222}Rn (Fig. 5.5). The red curves show compositional changes with K for young ($t \sim 0$) groundwater and for various initial ^{226}Ra concentration ($^{226}\mathrm{Ra}_0$), while the

grey lines demonstrate the change in composition with K in groundwater with different ages (i.e. each line represents a different groundwater age), for $^{226}Ra_0$=0.

The distribution of the different groundwater samples on the ternary diagram suggests that the main cause of the variability in each of the groundwater groups is caused by adsorption–desorption changes, while the differences between the groundwater groups are mainly due to their age or to source activity ($^{226}Ra_0$) differences. This indicates the sensitivity of K to different parameters and heterogeneity of the aquifer sediments.

5.4.5 The adsorption of radium

Radium adsorption could be roughly calculated according to the ^{222}Rn activities, assuming that its main source is the adsorbed ^{226}Ra ($\frac{P}{\lambda_{226}} << K \cdot {}^{226}Ra$), as discussed above (section 5.4.2). In this case $K \cong {}^{222}Rn/{}^{226}Ra$ resulting in $K \sim 1500$, $K \sim 1300$, $K \sim 40$ and $K < 100$ at EF, K EQ and TZG groundwater groups, respectively. The K of TZG and CDS groundwater groups were estimated independently to be up to 100 in the fresh end member of the TZG and 0.6 in the CDS groundwater (Kiro et al, 2012, section 3.3.3).

The adsorption of radium is sensitive to salinity (Webster et al, 1995; Sturchio, 2001; Gonneea et al, 2008; Kiro et al, 2012), which is obvious in the Dead Sea groundwater system, where the CDS and EQ hypersaline groundwater contain the highest activities of radium. The K in the hypersaline groundwater of the CDS groundwater can be down to zero (i.e. no adsorption, Kiro et al, 2012), which is also indicated by the $^{222}Rn/^{223}Ra$ ratio of the CDS samples that lie on the secular equilibrium line (Fig. 5.5).

However, the Mn and Fe oxides content and the redox-state of the groundwater has also shown to be important factors in radium adsorption (Gonneea et al, 2008). Although the aquifer medium of most of the different groundwater groups at the western Dead Sea is similar, K in fresh groundwater varies by two orders of magnitude. The higher estimations are consistent with K obtained in previous studies (e.g. Gonneea et al, 2008) and where a relatively high content of Mn and Fe oxides was found in the sediments (up to ~5% and 1.7%, respectively Kronfeld et al, 1991). The lower K's in the Dead Sea system may be explained by the lower oxides (Mainly Mn) content (up to 1% Mn and ~3% Fe, Y. Neumeier, personal communication) of the aquifer sediments and the reduced environment (Kiro et al, 2012) including the EQ groundwater group, which has also relatively low K (even relative to its high salinity) and flows in a reduced environment (Stern, 2010).

Table 5.2: Radium isotopic ratios in EQ groundwaters and the estimated velocity. K is estimated according to ^{222}Rn as described in section 5.4.5.

^{226}Ra/^{223}Ra	^{224}Ra/^{228}Ra	estimated $v_x(K+1)$ (m/d)
∼180	0.9–2.2	∼ 0.5
∼20–70	1.4–2.9	∼ 500

5.4.6 The thermal brine of Ein Qedem

The Ein Qedem (EQ) hot brines may be used as a case study of the effect of water–rock interaction on radium isotopes. These brines discharge over several kilometers along the Dead Sea shore from the alluvial aquifer and their chemical composition and temperature is quite constant (up to 48°C), indicating an ascent from at least 0.5km depth (Stern, 2010). However, the activities of radium vary between different springs which are represented by the different samples (Table 5.1), probably due to the different groundwater velocities and adsorption along the flow path. U-rich rocks are abundant in phosphorite layers as found in the Mishash Formation, as well as in aragonite layers that precipitated from the lake (Haase-Schramm et al, 2004).

The activities of radium are high (^{226}Ra is usually > 400, Table 5.1) and the groundwater is at least 10,000 years old (section 5.4.3). The high ^{226}Ra/^{223}Ra ratio suggests that the source of the groundwater interacted with sediments that are richer in uranium than the alluvial sediments, which contributed the high ^{226}Ra to the groundwater, and in which the ^{223}Ra has decayed during the ascent of the groundwater.

The EQ groundwater is divided according to radium isotopic ratios into two groups (^{226}Ra/^{223}Ra∼180 and ∼20–70, Table 5.2), which are caused by the different groundwater velocities of each spring, assuming a uniform source. The activity of radium along a flow path can be described as follows (after Davidson and Dickson, 1986):

$$C(x) = \frac{P}{\lambda(K+1)}\left(1 - e^{-\frac{\lambda(K+1)x}{v_x}}\right) + C_0 e^{-\frac{\lambda(K+1)x}{v_x}} \tag{5.6}$$

where C[dpm/L] is the radium activity in groundwater, v_x[L/T] is velocity along the flow path, λ[1/T] is the decay constant, P[dpm/(L · T)] is the production rate of the radium isotope from the aquifer solids, $x[L]$ is the distance along the flow path, C_0[dpm/L] is the activity of the radium isotope at the beginning of the flow path, and K is the dimensionless adsorption partition coefficient.

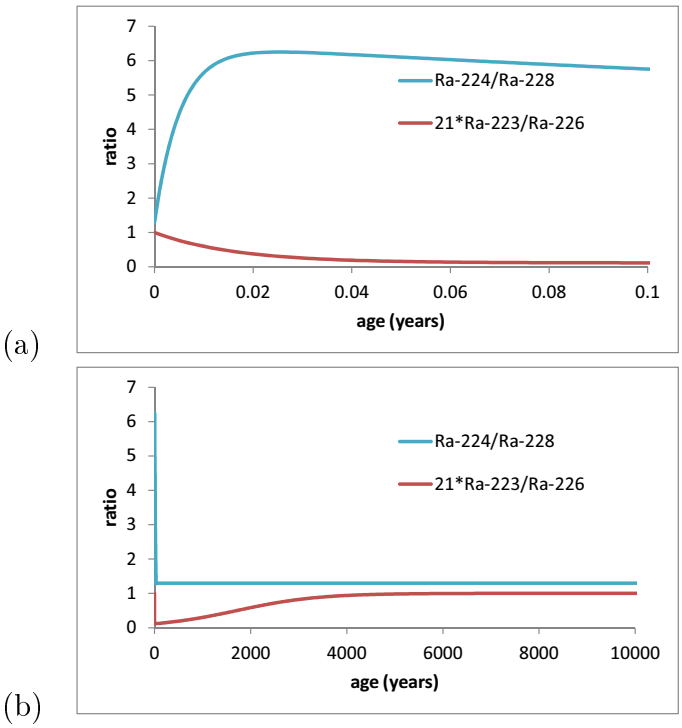


Figure 5.6: $^{226}Ra/^{223}Ra$ and $^{224}Ra/^{228}Ra$ ratios with time along a flow path. (a) ratios after a short time, (b) ratios until attaining steady state.

According to this equation, $^{226}Ra/^{223}Ra$ and $^{224}Ra/^{228}Ra$ ratios can be calculated as a function of time at a specific distance (x) and a certain velocity (Fig. 5.6). These plots show that any combination of deviation from secular equilibrium is possible considering the $^{226}Ra/^{223}Ra$ and $^{224}Ra/^{228}Ra$ ratios. After a very short time (a few days), the short lived radium isotopes (^{223}Ra and ^{224}Ra) hardly decay and the ratios retain in secular equilibrium. After longer periods (a few weeks), ^{224}Ra builds up (or decays, depends on the isotopic composition of the alluvial aquifer sediments relative to the source rock) slightly faster than ^{223}Ra. After even longer periods (tens of years), the difference between the two ratios (in terms of deviation from secular equilibrium) increases due to the larger difference between ^{228}Ra and ^{226}Ra half-life. The $^{224}Ra/^{228}Ra$ ratio attains equilibrium within 30 years, while the $^{226}Ra/^{223}Ra$ may take up to 10,000 years (Fig. 5.6). Samples where $^{226}Ra/^{223}Ra$ =21 suggest a very fast ascent (at least 500 m/d), which does not allow the ^{223}Ra in the water to decay. The slightly lower half-life of ^{224}Ra (relative to ^{223}Ra) allows $^{224}Ra/^{228}Ra$ ratio to exceed 2, while $^{226}Ra/^{223}Ra$ remains close to secular equilibrium.

In the EQ group, lower ^{226}Ra usually coincides with lower activities of the other radium isotopes (keeping the isotopic ratios). This is probably due to local adsorption which reduces the activity of radium and decreases the distance where secular equilibrium attains (Kiro

et al, 2012). This local adsorption is probably possible due to the lake level drop and change of groundwater flow paths.

5.5 SUMMARY AND CONCLUSIONS

The different groundwater bodies around the Dead Sea with their wide range of salinity, age, groundwater flow mechanisms and interaction with different rock types provide new insights on the behavior of radon and radium isotopes in groundwater. The largest variations are in the adsorption distribution coefficient (K), which is due to the sediments heterogeneity, difference in adsorption site concentrations and the large variations in the groundwater salinity.

$^{226}Ra/^{223}Ra$ ratio can be used to estimate groundwater age or the age of the groundwater system. For brines, where K is low, the secular equilibrium ratio indicate a groundwater age of thousands of years. The abundant secular equilibrium ratios of $^{226}Ra/^{223}Ra$ in fresh and brackish groundwater around the Dead Sea suggest that the hydrological system around the Dead Sea has not changed significantly at least 10,000 years. Complex groundwater flow mechanisms such as at EQ (Ein Qedem groundwater) results in deviations from secular equilibrium in very old groundwater which indicate and constrain the velocity of the ascent and groundwater flow. All other groundwater groups (TZG, CDS and K) has non secular equilibrium $^{226}Ra/^{223}Ra$ ratios because they are relatively young or because of the recent mixture with the Dead Sea brines and fresh groundwater due to the lake level drop.

The ancient groundwater bodies, both in the western Dead Sea shore (EF and EQ) and in the hot springs in the eastern catchment contain high activities of ^{226}Ra and significantly high activities of ^{222}Rn. Long periods of water–rock interaction extract more ^{226}Ra to the groundwater which is then available for adsorption and contribution of ^{222}Rn.

Chapter 6

The role of long-term aquifer seawater circulation in elemental mass balances: a lesson from the Dead Sea

6.1 INTRODUCTION

Seawater circulation in coastal aquifers, a major component of submarine groundwater discharge (SGD), has been recently recognized as a process affecting trace element and nutrient mass balances of coastal areas (e.g. Simmons, 1992; Moore et al, 2008). SGD was shown to contribute Ca, Ba and Sr to the Bengal Basin in the same order of magnitude as river fluxes (Basu et al, 2001; Dowling et al, 2003). It was also suggested that groundwater involved in water–rock interaction affects oceanic $^{87}Sr/^{86}Sr$ (Stein et al, 2000; Cochran et al, 2010). Estimates of SGD vary over several orders of magnitude (a few to 10^6 m^3/y per meter shoreline) due to the natural spatial variability in hydrological, geological and climatological parameters (Burnett et al, 2001; Taniguchi et al, 2002; Gallardo and Marui, 2006). In particular, seawater circulation could vary considerably depending on the studied scale from wave setup and tidal-driven short-term circulation (Robinson et al, 1998; Li et al, 1999), through seasonal (Michael et al, 2005), and up to the multi-annual dispersive circulation along the fresh–saline water interface (Cooper, 1959). Determining the circulation type and time scale is highly important to the characterization of water–rock interaction and to the assessment of its impact on oceanic mass balances. In particular, while the short-term wave or tidal circulations are mainly related to adsorption–desorption and redox processes (e.g. Charette and Sholkovitz, 2006), the multi-year dispersive circulation could involve the precipitation and dissolution of various minerals and may have a greater potential to affect certain ele-

ment budgets on a global scale. However, in an oceanic settings it is difficult to differentiate between the different types of circulation. The absence of waves and tides, together with the long-term behavior of the radium isotopes (^{226}Ra and ^{228}Ra) in the Dead Sea groundwater described in this paper, provide a unique opportunity to quantify this circulation.

The objective of this paper is to highlight the importance of the long-term seawater circulation for elemental mass balance of saline water bodies. In this study, we use an antithetic behavior of two radium isotopes during Dead Sea water circulation in the aquifer, where ^{226}Ra ($t_{1/2}$=1600 yr) decreases and ^{228}Ra ($t_{1/2}$=5.75 yr) increases, in order to construct the radium mass balance of the Dead Sea and calculate the extent of the circulation.

6.1.1 Radium isotopes

There are four naturally occurring radium isotopes (^{226}Ra, ^{228}Ra, ^{223}Ra and ^{224}Ra), with half-lives ranging between several days to 1600 years. They are an integral part of the U and Th decay chains and due to their relatively high solubility they are enriched in groundwater and commonly used as SGD tracers (e.g. Moore, 1996; Moore et al, 2008).

Their sources in natural water include the decay of their radioactive parents (Th isotopes), dissolution and desorption from the solid surface, while their sinks include radioactive decay, co-precipitation with minerals and adsorption (Krishnaswami et al, 1982; Tricca et al, 2001; Kiro et al, 2012).

6.1.2 The Dead Sea system

The Dead Sea is highly enriched in radium isotopes (^{226}Ra, ^{228}Ra), which are 2–3 orders of magnitude higher than in the ocean (Stiller and Chung, 1984; Somayajulu and Rengarajan, 1987), compared with its salinity, which is only 10 times higher. The chemical composition of the Dead Sea is Ca-chloridic, which is the result of the evaporation of seawater, followed by halite precipitation and dolomitization of carbonates in the adjacent aquifer (Starinsky, 1974).

The Dead Sea water mass balance underwent significant changes during the past 50 years due to anthropogenic intervention. This includes a drastic reduction in the Jordan River input and an enhanced evaporation due to potash salt production, which caused a sharp lake level drop (reaching 1 m/y) and an increase in the Dead Sea water salinity. The latter resulted in an overturn during the winter of 1979 and a change in the Dead Sea regime from meromictic (permanently stratified) to monomictic (Steinhorn, 1985).

Studies of the meromictic Dead Sea from the late 1970's (Stiller and Chung, 1984; Chan

and Chung, 1987; Somayajulu and Rengarajan, 1987; Chung and Craig, 2004) showed that the upper water mass contained higher activities of ^{226}Ra and ^{228}Ra than the lower water mass, which was attributed to the input from Ra-rich sources around the lake (Figures 2.1, 6.1). The ^{226}Ra mass balance was used to determine the age of the Dead Sea meromictic structure (200-340 years, Stiller and Chung, 1984; Chan and Chung, 1987; Chung and Craig, 2004).

The alluvial aquifer adjacent to the Dead Sea is in direct hydraulic contact with the lake along most of its shoreline. It mainly consists of clastic fan delta deposits (gravel, sand and clay) intercalated with lacustrine sediments (e.g. clay, aragonite, gypsum and salt). Direct recharge by precipitation is negligible (precipitation <100 mm/y), and the main recharge is by lateral flow from the adjacent aquifers, including the Cretaceous carbonate aquifer on the Dead Sea western side and the carbonate and sandy aquifers on its eastern side (2–3 km from the lake), which is replenished at the highlands 10–30km away.

The fresh–saline transition zone in the Dead Sea alluvial aquifer is very shallow due to the high density of the Dead Sea water. According to the Ghyben–Herzberg approximation, the depth of the transition zone in the Dead Sea coastal aquifer is 4.35 times the groundwater elevation, compared to 40 times in aquifers next to the ocean (Yechieli, 2000).

The hydraulic relationship between the Dead Sea and the alluvial aquifer is manifested in a relatively rapid water level response (several days) to lake level changes (Yechieli et al, 1995), with the response time varies according to the aquifer hydraulic parameters and lake bathymetry near the coast. In some cases, the water table drop may reach the same rate as the lake level drop (Kiro et al, 2008). The fresh–saline transition zone also responds to the lake level drop by deepening and enhancing the fresh water flow to the lake. Nevertheless, the Dead Sea water circulation, which is the subject of this study, persists during lake level drop (Kiro et al, 2008).

6.2 METHODS

All main water sources around the Dead Sea (Wadi Mujib, Wadi Zarqa Ma'in, Wadi Hasa, Ein Feshkha and Ein Qedem, Fig. 2.1) and groundwater from boreholes (mainly Wadi Arugot) were sampled (Fig. 2.1) and analyzed for major and trace elements and for radium isotopes. Dead Sea water was sampled along a vertical profile 8 km offshore (Fig. 2.1, eg300 - 31.5030°N/35.4712°E; water depth of ∼300m) and surface water was sampled along a transect between Wadi Aqugot and eg300 (Fig. 2.1).

Water samples for major elements were collected in plastic bottles, and samples for trace

elements were collected in 125ml LDPE bottles after running through 0.45μm filters and acidified to pH ~2. Water samples for ^{226}Ra analysis were sampled in 0.5L vacuumed glass bottles, while water samples for ^{228}Ra were collected in 3-20L plastic containers, followed by filtration (0.45μm filters) and the adsorption of the radium onto MnO_2-coated acrylic fibers (Moore and Arnold, 1996). The adjustment of the method for adsorbing radium on the MnO_2-fibers from the hypersaline Dead Sea water is detailed in Kiro et al (2012).

^{226}Ra was measured using a modified emanation technique and Lucas cells (Mathieu et al, 1988). Some of the samples were measured for ^{228}Ra by gamma spectrometry in Florida State University following the procedure of Dulaiova and Burnett (2004). Other samples were measured several times by a delayed-coincidence counter (Moore and Arnold, 1996), as to follow the buildup of the ^{228}Th by the decay of ^{228}Ra, following the procedure of Moore (2008). All water sources were measured by the delayed-coincidence counter, and some of them were also measured by gamma spectrometry, as indicated in D and E. Ba, U and Fe were measured by a Perkin-Elmer Sciex Elan-DRC-e ICP-MS.

6.3 RESULTS AND DISCUSSION

6.3.1 Radium in the Dead Sea

Currently, ^{226}Ra concentration is uniform throughout the mixed lake (147 ± 17 dpm/L, Fig. 6.1, Table 6.1). Its calculated inventory of $19 \cdot 10^{15}$ dpm (based on the current lake volume of $127 \cdot 10^9$ m^3) is similar to the inventory calculated for the meromictic lake in the 1970's (Stiller and Chung, 1984). On the other hand, the present day inventory of ^{228}Ra seems to be higher than that calculated for the meromictic lake, $1.9 \cdot 10^{14}$ dpm based on average activity of 1.5 ± 0.6 dpm/L (Table 6.1, Fig. 6.1) and $1.3 \cdot 10^{14}$ dpm calculated from the 1970's ^{228}Ra profile of Somayajulu and Rengarajan (1987), respectively.

The meromictic lake profiles, from 1978, show higher activities of radium in the upper water mass than in the lower one (Fig. 6.1). This suggest that the main contribution of radium to the Dead Sea is from relatively shallow sources. At present, the ^{226}Ra and ^{228}Ra profiles are almost uniform due to the monomictic structure of the lake, with some increase in ^{226}Ra towards the lake floor (Fig. 6.1, June 2009) attributed to the contribution of radium from the bottom sediments.

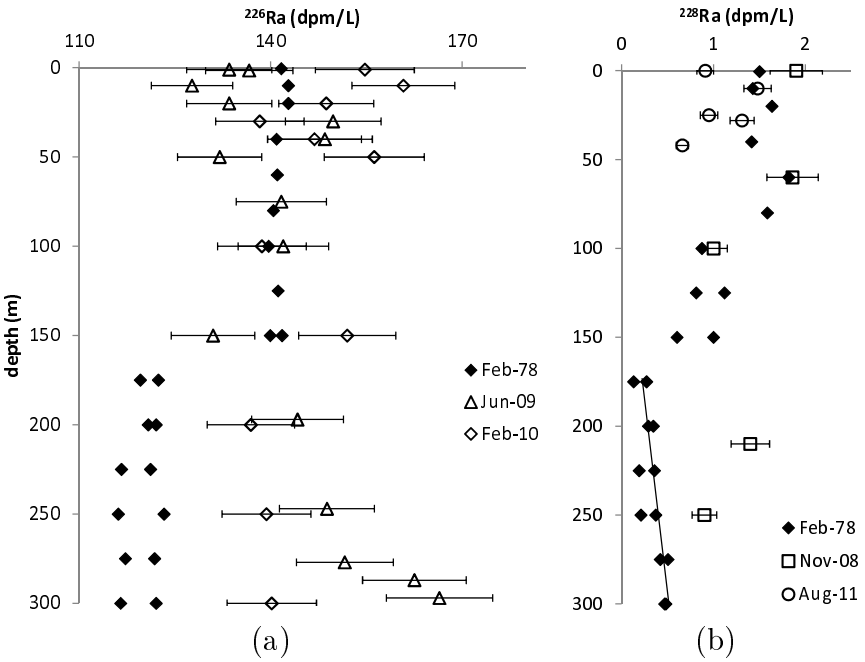


Figure 6.1: Profiles of (a) ^{226}Ra and (b) ^{228}Ra in the Dead Sea at the 1978 during the meromictic period of the Dead Sea and at present. The 1978 data of ^{226}Ra and ^{228}Ra is taken from Stiller and Chung (1984) and Somayajulu and Rengarajan (1987), respectively.

Table 6.1: Average concentrations of trace elements and radium isotopes in the circulated Dead Sea water and in the lake. n is the number of radium samples (D and E), and the error is the standard deviation of the samples' activity. Analytical error on trace element and ^{226}Ra measurements are up to 5%, while ^{228}Ra analytical error is up to 10%.

	Cl (g/L)	^{226}Ra (dpm/L)	n	^{228}Ra (dpm/L)	n	Ba (mg/L)	Fe (mg/L)	U (μg/L)
Dead Sea lake (present)	220	147 ± 17	136	1.5 ± 0.6	20	5	1	2.4[a]
Circulate Dead Sea water	224	60 ± 14	14	22 ± 8	10	1.5	12	0.1

[a] Haase-Schramm et al, 2004

6.3.2 Dead Sea Water Circulation in the Aquifer

Figure 6.2 shows a cross section of the fresh–saline transition zone as observed through boreholes in the alluvial fan aquifer at Wadi Arugot (Fig. 2.1). Dead Sea water penetrates the aquifer due to density differences, mixes with terrestrial groundwater and flows in the fresh–saline transition zone back toward the Dead Sea. Accordingly, the total groundwater flow to the Dead Sea, including both terrestrial and circulated groundwater components, is larger than the flow into the aquifer, while the salt budget is balanced.

The flow of Dead Sea water into the aquifer is manifested by the gradual increase and build up of ^{228}Ra ($t_{1/2}$=5.75 y) from 1–2 dpm/L in the lake to steady-state concentrations of 20–40 dpm/L in the groundwater at a distance of 40–80 meters from the shore inland (Fig. 6.2). Assuming no significant adsorption of radium take place in the hypersaline groundwater (Kiro et al, 2012), the distribution of ^{228}Ra mainly represents a balance between its production from the aquifer and its decay. Assuming a homogeneous aquifer, steady-state concentrations should be attained after 30 years. In this case, the groundwater residence time in the Dead Sea coastal aquifer is on the scale of tens of years. The flow patterns and similar residence times of the Dead Sea water in the aquifer are also predicted by hydrological simulations (Kiro et al, 2008).

While ^{228}Ra increases, ^{226}Ra and Ba gradually decrease during lake water circulation, from lake concentrations of ∼147 dpm/L and 5 mg/L to ∼60 dpm/L and 1.5 mg/L, respectively (Table 6.1, Fig. 6.2). The removal of Ba and ^{226}Ra is attributed to the precipitation of barite or celestine, both being highly supersaturated in the Dead Sea (Kiro et al, 2012). The gradual decrease in both elements along the hypersaline flow path indicate that it occurs in a time scale of years. ^{228}Ra also co-precipitates with barite. However, it mainly occurs while ^{228}Ra activities are relatively low (close to the lake water), while the contribution by recoil and desorption is much higher, which implies a net accumulation effect (Fig. 6.2).

The concentrations of Ba and ^{226}Ra in the transition zone groundwater lie on a mixing line between hypersaline water with decreased concentration of Ba and ^{226}Ra (1.5 mg/L and ∼60 dpm/L) and Ba- and Ra-poor fresh water (Fig. 6.3), indicating that the mixing between the two water bodies and the return flow to the Dead Sea occur only after the completion of the barite/celestine precipitation (at least tens of years).

In summary, the Dead Sea coastal aquifer is a sink for ^{226}Ra and Ba and a source of ^{228}Ra in a relatively long term process of Dead Sea water circulation in the aquifer. In this paper we recalculate the Dead Sea radium mass balance, taking into account the circulation in the aquifer, which allows the determination of the extent of circulation.

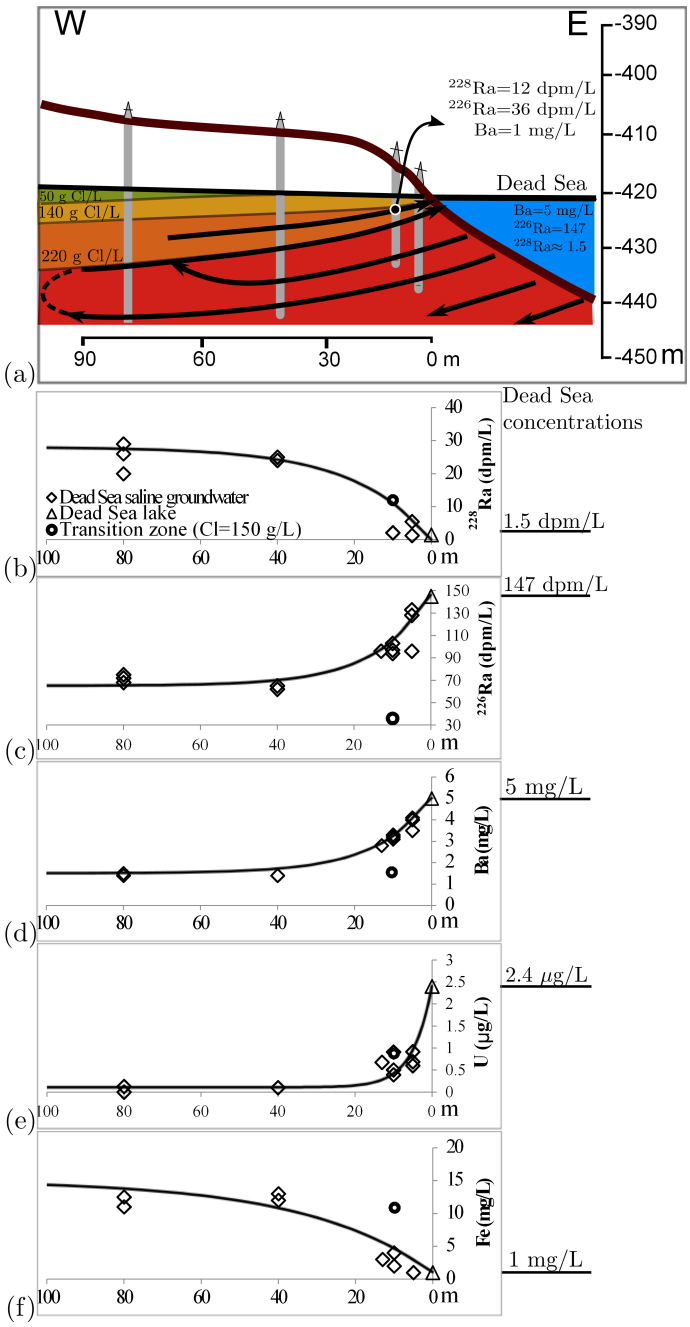


Figure 6.2: (a) A cross section, showing the fresh-saline transition zone in the Dead Sea aquifer and the direction of groundwater flow in this system. (b)-(f) Concentrations of ^{226}Ra, ^{228}Ra, Ba, U and Fe in the circulated Dead Sea water (~220 g Cl/L) along a flow path from the Dead Sea into the aquifer. The concentrations of each element in the fresh–saline transition zone is also shown. Note that the saline water flows back into the Dead Sea after dilution with terrestrial groundwater at the fresh–saline transition zone and therefore the concentrations are lower than the actual end-member of the circulated Dead Sea water.

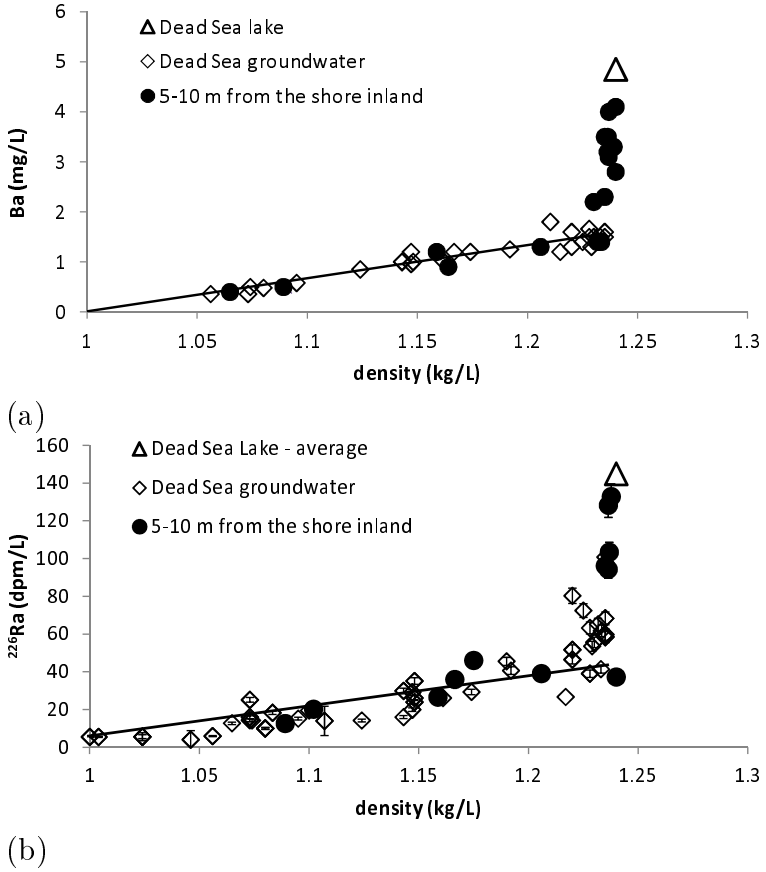


Figure 6.3: (a) Ba and (b) ^{226}Ra versus density at the fresh–saline transition zone in the aquifer (modified after Kiro et al, 2012).

Table 6.2: Radium and barium in the main water sources of the Dead Sea.

Source	Discharge (10^6m^3/y)	^{226}Ra (dpm/L)	^{228}Ra (dpm/L)	Ba (mg/L)	^{226}Ra (10^{12} dpm/y)	^{228}Ra (10^{12} dpm/y)	Ba (10^9 mg/y)
Jordan River	1000-1600[a]	0.5–2[b]	0.01–0.1[c]	0.05–0.16[b]	0.5–2.3	0.01–0.16	50–260
Ein Feshkha	54-100[d]	17–50	0.5–1	0.2–1.5	0.9–5	0.08–0.4	11–150
Ein Qedem	8-15[d]	300–500	10–21[e]	1	2.4–7.5	0.08–0.3	8–15
East Dead Sea catchment	90-220[f]	6–14	7–29	0.02–0.08	0.5–3	0.65–6.4	2–18

[a] Values before 1964 (Neumann, 1958; Klein, 1998; Salameh and El-Naser, 1999).
[b] Values in Lake Kinneret (Sea of Galilee) and the Jordan River (Stiller and Chung, 1984; Lazar et al, 2008).
[c] Calculated from ^{226}Ra/^{228}Ra ratio in Lake Kinneret and nearby saline springs (Moise et al, 2000).
[d] Values from Israel Hydrological Service.
[e] Moise et al (2000).
[f] Minimum value is the discharge to the northern Dead Sea basin, while the maximum value is the discharge to both northern and the southern basins (including Wadi Hasa, Salameh and El-Naser, 1999).

6.3.3 Radium Mass Balance in the Dead Sea

The activities of radium measured in the late 1970's represent the natural state of the Dead Sea before the lake level started dropping and affecting mass balances. For this reason, we first calculate the radium mass balance based on the 1970's activities and mid 20^{th} century water fluxes. The present Dead Sea activities are then used to examine the impact of lake level drop on the circulation in the aquifer.

Sources of radium to the Dead Sea

The sources of radium and barium to the Dead Sea are detailed in Tables 6.2, 6.3 and 6.4.

Water sources The main sources of ^{226}Ra are the saline springs (e.g. Ein Qedem) and brackish water springs (Ein Feshkha) on the west coast of the Dead Sea (Fig. 2.1), while the main water sources of ^{228}Ra are on the eastern catchment of the Dead Sea (Table 6.2). Barium is contributed mainly from the Jordan River and Ein Feshkha springs (Table 6.2).

Sediment sources Lake bottom sediments and suspended load also contribute radium to the Dead Sea due to the decay of thorium and to the desorption of radium in the hypersaline environment of the Dead Sea (Li and Chan, 1979).

The flux of radium from the suspended load (S, Table 6.4) may be calculated according to a precipitation rate of 1.5 mm/y (Bartov et al, 2006) with a Dead Sea area of $\sim 700 \cdot 10^6$ m^2 (Stanhill, 1994), sediment density of 2000 kg/m^3, and averaged concentrations of U and Th in the detritus of 4.1 and 4.4 ppm, respectively (Haliva, 2004; Haase-Schramm et al, 2004). Assuming ^{226}Ra and ^{228}Ra concentrations are in secular equilibrium with ^{238}U and ^{232}Th, respectively, and a recoil fraction of $\sim$5% according to $f = 3L/4r$ (Kigoshi, 1971),

Table 6.3: Model parameters and output.

Symbol	Parameter	Units	Value	Source
Input:				
V_{DS}	Volume of the Dead Sea	[m^3]	$1.46 \cdot 10^{11}$	Stiller and Chung (1984)
λ	Decay constant	[1/y]		
^{226}Ra			$4.33 \cdot 10^{-4}$	
^{228}Ra			0.12	
Ra_{DS}	Radium activity in the Dead Sea	[dpm/m^3]		
^{226}Ra			134000*	Calculated from inventory (Stiller and Chung, 1984).
^{228}Ra			920*	Inventory calculated from profile (Somayajulu and Rengarajan, 1987).
Ra_c	Radium activity in circulated Dead Sea water	[dpm/m^3]		This study
^{226}Ra			60000	
^{228}Ra			$20000 - 40000$	
F_G	SGD (non circulated water)	[$10^6 m^3$/y]		Estimated according to evaporation (Lensky et al, 2005).
fresh			50 ± 50	
brine (Ein-Qedem type)			25 ± 25	
Output:				
F_c	Flux of Dead Sea water circulation in the aquifer	[$10^6 m^3$/y]	320 ± 60	
F_G	SGD (non circulated water)	[$10^6 m^3$/y]		
fresh			$0 - 60$	
brine (Ein Qedem type)			43 ± 14	
K	Adsorption–desorption partition coefficient		$0 - 0.2$	

*Averaged activities
Uncertainties reported in 3σ.
Radium activities in the Dead Sea lake and Dead Sea volume are from the late 1970's and represent the undisturbed case.

Table 6.4: Sources and sinks of radium in the Dead Sea. Model parameters, tested values and most probable values. Sinks are marked with a minus sign.

Symbol	Parameter	Tested values (input) (10^{12} dpm/y)		Most probable values (output) (10^{12} dpm/y)		Remarks
		^{226}Ra	^{228}Ra	^{226}Ra	^{228}Ra	
$\sum F_i Ra_i$	Radium flux through water sources	21 ± 11	2.3 ± 1.5	30 ± 6	3 ± 1	Water fluxes from Salameh and El-Naser (1999), Lensky et al (2005) and the Israel Hydrological Service (Table 6.2). Radium concentrations are from Moise et al (2000) and this study.
I	Radium recoil and diffusion from bottom sediments	0.25 ± 0.03	1.8 ± 0.2	2.6±0.8*	2 ± 0.6*	The average contribution from bottom sediments of ^{228}Ra was estimated according to activities in the lower water mass (Somayajulu and Rengarajan, 1987). ^{226}Ra was estimated according to the world's average flux (Broecker and Peng, 1982).
S	Radium in suspended load	2.25±0.2	0.1±0.01	N.A.	N.A.	^{226}Ra contribution was taken from Chan and Chung (1987) and the average contribution from sediments entering the Dead Sea was estimated from U and Th concentrations (Haase-Schramm et al, 2004; Haliva, 2004) and a sedimentation rate of 1.5 mm/y (Bartov et al, 2006).
P	Precipitation rate	0–(−1)	0–(−0.007)	0–(−1)	0–(−0.004)	Chan and Chung (1987), ^{228}Ra precipitation rate was calculated from ^{226}Ra/^{228}Ra in the lake.
$F_C(Ra_{DS} - Ra_c)$	Circulation	N.A.	N.A.	-23 ± 5	12 ± 2	This study.
$\lambda V_{DS} Ra_{DS}$	Radioactive decay	N.A.	N.A.	−8.5	−16	This study.
$\lambda V_{DS} Ra_{DS} K$	Adsorption (scavenging)	N.A.	N.A.	0–(−1)	0–(−2.5)	This study.

Uncertainties reported in 3σ.
*$I + S$

where f is the fraction of radium recoiled from the ^{238}U and ^{232}Th, L(=900Å) is the recoil length, and r(=2–4μm, Haliva, 2004) is the grain radius, the averaged fluxes of ^{226}Ra and ^{228}Ra will be around $0.3 \cdot 10^{12}$ and $0.1 \cdot 10^{12}$ dpm/y, which are negligible compared to the other sources. Nevertheless, Chan and Chung (1987) have estimated that the desorptive flux of ^{226}Ra is $1.5 - 3 \cdot 10^{12}$ dpm/y by comparing ^{226}Ra in surface sediments of the Dead Sea and the Jordan River. This may be due to the relatively long half-life of ^{226}Ra which may accumulate near the grain surface area.

In our treatment of the contribution by the suspended load, we use the dimensionless adsorption partition coefficient (K) instead of the kinetic constants, which describes the effective partitioning of radium between the water and the sediment surface and is defined as $K = Ra_s/Ra_{DS}$ where Ra_s[dpm/L] is the activity of radium adsorbed on the solid surface expressed as equivalent concentration in water and Ra_{DS}[dpm/L], is the activity of radium in the Dead Sea water. We use this K instead of the kinetic constants in order to avoid dealing separately with adsorption and the desorption.

The average flux of ^{228}Ra from the bottom sediments (I) was calculated assuming that the only source of ^{228}Ra to the deep water of the meromictic lake was the bottom sediments and the only sink was its radioactive decay. Taking the 1970's average activity of ^{228}Ra in the lower water mass, 0.3 dpm/L (Somayajulu and Rengarajan, 1987), with a water volume of $49.11 \cdot 10^9$ m^3 (Stiller and Chung, 1984), yields an inventory of $1.5 \cdot 10^{13}$ dpm and a flux of $1.8 \cdot 10^{12}$ dpm/y. ^{226}Ra contribution from the sediments is demonstrated in the increase in its activity next to the lake floor (Fig. 6.1, June-09 profile). It was determined according to the world's average flux from the ocean floor (Broecker and Peng, 1982) as 0.25 dpm/y with an uncertainty of 10%.

Sinks of radium in the Dead Sea

The major sink of ^{228}Ra in the Dead Sea is its radioactive decay. On the other hand due to its longer half-life, Dead Sea water circulation in the aquifer is a dominant factor in the removal of ^{226}Ra. Another sink is the co-precipitation with minerals (gypsum and aragonite) in the lake, which may remove up to 10^{12} dpm/y ^{226}Ra (Stiller and Chung, 1984; Chan and Chung, 1987), while is insignificant in the ^{228}Ra balance (Table 6.4).

Mass balance calculation

The new radium data of the Dead Sea sources (Table 6.2) clearly shows that an additional process, which contributes ^{228}Ra and removes ^{226}Ra, is required in order to settle the mass

Table 6.5: Input and output by decay of radium in the Dead Sea

	Input from water sources (10^{12} dpm/y)	Output by decay (10^{12} dpm/y)
^{226}Ra	$10-32$	8
^{228}Ra	$0.8-3.8$	16

balance for both ^{226}Ra and ^{228}Ra (Table 6.5).

Taking into account all sources and sinks, the radium mass balance in the Dead Sea is:

$$(1+K)\frac{\partial V_{DS}Ra_{DS}}{\partial t} = \sum F_i Ra_i + I + S + F_c Ra_c - F_c Ra_{DS} - P - \lambda(1+K)V_{DS}Ra_{DS} \quad (6.1)$$

Parameter notation is given in Tables 6.3 and 6.4.

Assuming an approximate uniform volume of the Dead Sea before the 1970's, the solution of the mass balance equation is:

$$Ra_{DS}(t) = \frac{\sum F_i Ra_i + I + S + F_c Ra_c - P}{\lambda(1+K)V_{DS} + F_c}\left(1 - e^{-\left(\lambda + \frac{F_c}{V_{DS}(1+K)}\right)t}\right) \quad (6.2)$$

In steady state, the amount of seawater circulating in the aquifer is:

$$F_c = \frac{\sum F_i Ra_i + S + I - P - V_{DS}\lambda(1+K)Ra_{DS}}{Ra_{DS} - Ra_c} \quad (6.3)$$

This equation was solved for both ^{226}Ra and ^{228}Ra using the values summarized in tables 6.3 and 6.4. The volumes of Dead Sea water circulating in the aquifer (F_c) and the radium adsorption coefficient (K) in the lake were calculated using a Monte Carlo method taking into account the uncertainty in all parameters involved. $\sum F_i Ra_i$[dpm/y] includes all water sources (Table 6.2) into the Dead Sea including sublacustrine groundwater discharge (F_G[m^3/y], Table 6.3) which was estimated by water and energy mass balance to be up to 100 million m^3/y, taking into account the evaporation rate (Stanhill, 1994; Lensky et al, 2005) and the water sources before human intervention (Salameh and El-Naser, 1999). The flux of sublacustrine brine (Ein Qedem type), also a part of F_G, was estimated to be no more than 50 million m^3/y (coastal discharge of these brines is ca. 10 m^3/y). Radium was assumed to be uniformly distributed, while a normal distribution was assumed for the flux of water, the flux from sediments (I and S) and the co-precipitation (P).

The model also constrains the distribution of all input parameters by eliminating all implausible results (which occur if one of the parameters is negative).

Our calculations indicate that the volume of saline water circulating in the aquifer in steady state is 320 (σ1=22) million m^3/y (Table 6.3), which is ca. 2 million m^3/y per km

shoreline. This method yields relatively small errors due to the antithetic behavior of the two radium isotopes during circulation despite the uncertainty in the parameters. Hydrological simulations (Kiro et al, 2008) suggest that steady-state velocities of Dead Sea water in the aquifer were around 15–150 m/y (Kiro et al, 2008). Considering an effective shore length (where circulation occurs, mainly at the alluvial fans) of 50 km and a reasonable circulation zone 50 m thick (Kiro et al, 2008), it yields a circulation flux of 40–400 million m^3/y, in agreement of the Ra-calculated fluxes. Note that the discharge value of circulated water is related to the flow of seawater into the aquifer, while the flow back into the sea includes both the circulated water and the terrestrial water, which are mixed in the fresh–saline transition zone. The calculations' output also supports the conclusion of Lensky et al (2005) by constraining the volume of sublacustrine groundwater discharge (F_g, Table 6.3) to no more than 100 million m^3/y.

In order to locate the circulation and verify that it is related to coastal processes, we repeated the radium balance calculations (Eq. 6.3) separately for the upper and lower water masses of the 1970's meromictic lake. Water mass volumes were taken from Stiller and Chung (1984), while sources and sinks were assumed as in Tables 6.3, 6.4. Most sources in the tables are only of the upper water mass, while the input from the bottom sediments is assumed to be only of the lower water mass. The calculations reveal that most of the circulation (90%) is shallow (coastal), associated with the fresh–saline transition zone.

This further implies that the ^{228}Ra in the lower water mass before 1979 was mainly contributed by diffusion from the bottom sediments and may serve as a large-scale estimation for ^{228}Ra flux from the Dead Sea bottom sediments. Divided by the lake area ($\sim 700 \cdot 10^6$), this flux is estimated by $\sim$2500 dpm/m^2/y, which is on the same order of magnitude as fluxes calculated for seafloor fine-grain sediments (Moore et al, 2008).

Historical versus contemporary radium mass balance in the Dead Sea

The time to attain steady-state activity of a specific radioactive isotope in an open water body increases with its half-life, the decrease in the volume of seawater circulation in the aquifer, the volume of the water body and the adsorption distribution coefficient of the isotope in the lake (eq. 6.2). Therefore, the relatively short-lived ^{228}Ra reaches steady state after 30 years, while attaining steady state for the long-lived ^{226}Ra is expected to be much longer, strongly depending on the circulation/lake volume ratio. Thus, the present concentrations of ^{226}Ra and Ba (stable) in the lake are similar to those of the 1970's, representing the undisturbed case of the Dead Sea, while the current ^{228}Ra activity is different from that in the 1970's due

Table 6.6: Inventory and fluxes of several trace elements, based on the concentrations in table 6.1, due to Dead Sea water circulation in the aquifer.

Element	Inventory (mg)	Circulation (mg/y)
Ba	$7 \cdot 10^{14}$	10^{12}
U	$3.5 \cdot 10^{11}$	$7 \cdot 10^{8}$
Fe	$1.5 \cdot 10^{14}$	$-4 \cdot 10^{12}$

to the lake level drop and changes in the water mass balance.

^{228}Ra may have decreased in the lake as the result of the decrease of external ^{228}Ra sources due to the drastic reduction in general flow to the lake. However, the increase in the averaged ^{228}Ra activity (from 0.9 to 1.5 dpm/L) in the lake probably represent the increase in the flux of the circulated Dead Sea water (Kiro et al, 2008), which contain high activities of ^{228}Ra.

6.4 IMPLICATIONS

6.4.1 The Dead Sea trace element mass balances

The effect of the circulation of Dead Sea water in the aquifer on the radium isotopes is illustrated in Fig. 6.4. Besides radium, it is also expected to affect the concentrations of other trace elements in the lake such as Ba (sink), U (sink) and Fe (source, Fig. 6.2, Table 6.6). The decrease in U and increase in Fe are related to the anoxic conditions in the aquifer, similar to the redox-driven removal of U in the Waquoit Bay subterranean estuary, which has been suggested to be a major oceanic sink of U (Charette and Sholkovitz, 2006). Indeed, anoxic conditions were found in the Dead sea coastal aquifer (Avrahamov et al., pers. comm.).

This is also relevant to paleoclimate interpretations, which are often based on trace elements in lacustrine sediments (e.g. Haskell et al, 1996) such as U and Sr in the Dead Sea basin water bodies (Stein et al, 1997; Haase-Schramm et al, 2004).

6.4.2 Long-term circulation in coastal aquifers

This study demonstrates the importance of lake water and seawater circulation in the aquifer for elemental mass balances, which should be considered in both present and paleo-budgets. Seawater circulation in the aquifer and its associated water–rock interaction were intensively studied in a few locations (e.g. Charette and Sholkovitz, 2006; Roy et al, 2011). However, its impact on oceanic mass balances is not clear, since its extent is debatable (e.g. Li et al, 1999; Smith, 2004) and difficult to determine due to the involvement of driving factors like

waves and tides (Robinson et al, 1998), which may occur throughout the whole continental shelf and may involve very large volumes of water (e.g. Moore et al, 2008). However, these mechanisms involve short-term circulation and may be quite limited in terms of water–rock interaction. The Dead Sea system provides a unique opportunity to isolate and quantify the long-term seawater circulation due to the absence of tides and to the very limited wave activity. The water fluxes determined in this study should not be unique to the Dead Sea system, but rather are very relevant globally to other coastal systems.

The extent of the long-term dispersive circulation is mainly a function of the hydrological parameters (Kiro, 2006; Kiro et al, 2008). Although the density differences affect the fresh–saline transition zone slope and shape, it does not affect the saline water velocity during circulation and therefore the high density of the Dead Sea does not need to be taken into consideration when implying the calculated circulation in other coastal systems. Other changes in hydraulic parameters, which may be more related to the coastal sediment type, are covered by the large variability (lacustrine to fluviatile) along the Dead Sea shores.

Multiplying our calculated seawater circulation flux by an estimated global coastline of 350,000-1,600,000km (CIA World Fact Book and the World Resources Institute) results in a discharge of $7 - 32 \cdot 10^{11}$ m^3/y to the oceans. This value is still 1–2 orders of magnitude lower than the Atlantic shelf-wide SGD of Moore et al (2008), but is of the same order of magnitude as that of oceanic ridge hydrothermal systems (Elderfield and Schultz, 1996), and due to its relatively long residence time in the aquifer (years) it could have a significant impact on oceanic mass balances of certain elements.

For example, it has been suggested that mass balances of oceanic $^{87}Sr/^{86}Sr$ ratios and other elements should be reevaluated by considering fresh SGD (Basu et al, 2001). Similarly, considering the larger water volumes, and the water–rock interactions involved (e.g. dolomitization, Stein et al, 2000), $^{87}Sr/^{86}Sr$ ratios and their variations along the geological history could be significantly affected by seawater circulation in the aquifer.

It should be noted that the long-term circulation may also include water exchange due to long-term sea or lake level fluctuations, which would increase the volume of water interacting with the aquifer sediments and flowing back into the lake/sea. Sea level rise causes seawater intrusion into the aquifer, while sea level drop causes an outflow of the saline water back into the lake (Kiro et al, 2008). This mechanism is relevant for both Dead Sea fluctuations and global sea level changes.

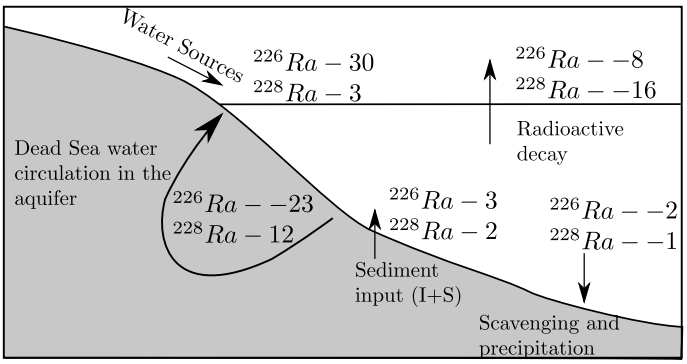


Figure 6.4: A summary of the sources and sinks (10^{12} dpm/y) of radium in the Dead Sea. Water sources include all sources mentioned in Table 6.2.

6.5 CONCLUSIONS

In this paper we show that seawater circulation along the fresh–saline water interface actually involves relatively large volumes of water, which significantly affects trace element mass balances in the Dead Sea and as may well do in oceanic systems. It is suggested that while other short-term circulation types (e.g. tidal- or wave-induced) may only involve the adsorption-desorption or redox-driven mechanisms, the dispersive seawater circulation is a more profound one, since it allows enough time for other water–rock interactions to occur and may as well be an important factor in global oceanic mass balances. The method of using two components where one is increasing and the other is decreasing during aquifer seawater circulation was shown to be a promising and robust method for estimating seawater circulation in the aquifer, yielding relatively small errors. This method can be applied in other oceanic settings where two elements behave antithetically, like the Dead Sea radium isotopes (e.g. U and Fe).

Chapter 7

Summary and conclusions

This study deals with the Dead Sea–aquifer interaction, including both the geochemical and hydrological processes. The Dead Sea water circulates in the aquifer due to dispersive mixing and density differences between the fresh groundwater and the Dead Sea water. Compared to other circulation types, this is a relatively long-term and large-scale mechanism, which is the main one in the Dead Sea hydrological system due to the absent of tides and to insignificant waves. This makes the Dead Sea an excellent field laboratory to study this type of circulation, providing new insights in to coastal aquifer processes and their possible input to oceanographic mass balances.

The hypersaline water of the Dead Sea is supersaturated with barite and celestine, which appears to precipitate during Dead Sea water circulation in the aquifer, removing Ba, Sr and ^{226}Ra (by co-precipitation) from the Dead Sea. The precipitation time-scale is of several years (k=0.22 y^{-1}). Gypsum also precipitates during the Dead Sea water circulation, causing the sulfate to decrease by ∼100 mg/L from 393 to ∼250 mg/L, however, its precipitation is much faster than that of the barite/celestine (k=0.8 y^{-1}). Redox-controlled reactions also occur, contributing Mn and Fe by dissolution of oxides and removing U by reduction and adsorption. These types of reactions and behavior are typical to oceanic settings, both in pore water and in subterranean estuaries. However, the sequence of the element reduction in the Dead Sea is different, with a relatively fast removal of U (k=0.4 y^{-1}) and a slower contribution of Mn and Fe (k= 0.15 and 0.06 y^{-1}, respectively), while in regular oceanic settings (coastal or deep sea), U is reduced later than or between the reduction of Mn and Fe. The difference between the Dead Sea and oceanic settings may be related to either geochemical or to differences in the microbe communities involved.

The activities of the short-lived radium isotopes (^{228}Ra, ^{224}Ra and ^{223}Ra) are high in the

circulated Dead Sea water due to their relatively fast production from the aquifer sediments. ^{224}Ra and ^{223}Ra (with the half-lives of several days) are high in all of the circulated Dead Sea water, while ^{228}Ra ($t_{1/2}$=5.75 y) gradually increases, allowing the estimation of the circulating water velocity, which was found to be ∼1–6 m/y for the past few decades.

The circulated Dead Sea water flows back into the lake after mixing with fresh groundwater in the fresh–saline transition zone. The mixing occurs only after several years when the discussed geochemical reactions occur, which is indicated by the fact that all samples (including those that are from near shore boreholes) lie on a mixing line between fresh water (with low ^{226}Ra and Ba) and the reduced concentrations of Ba and ^{226}Ra of the circulated Dead Sea water.

During the flow of the circulated Dead Sea water back into the lake, at the fresh–saline transition zone, gypsum is dissolved, causing an increase of the sulfate concentration with decreasing salinity. ^{223}Ra, ^{224}Ra and ^{222}Rn, all with half-lives of several days, are affected by the adsorption of radium, suggesting a linear relationship between the adsorption partition coefficient (K) and salinity, where K decreases with salinity.

Simulations with a multi-species density-dependent flow model (SUTRA-MS) show that the adsorption does not affect the response of the short-lived radium isotopes distributions to the change of the Dead Sea lake level, making them a useful tool for defining the relationship between radium adsorption and salinity in transient conditions. On the other hand, the distribution of the long-lived ^{226}Ra during the transient conditions of the Dead Sea level drop is very sensitive to adsorption. A simulation of ^{226}Ra during the Dead Sea level drop indicates that K must be considerably low (lower than 0.6 in the circulated Dead Sea water and up to 100 in the fresh groundwater). This K could not cause the significant decrease in ^{226}Ra between the lake and the circulated Dead Sea water (∼147 and ∼60 dpm/L, respectively). Therefore, it is suggested that ^{226}Ra is removed by barite (or celestine) precipitation after entering the aquifer.

The obtained K is much lower then in other studies and also compared with other locations in the Dead Sea vicinity (e.g. Ein Feshkha). However, most of the other estimations were done in lab experiments rather than directly from field data. Preferential flow and inhomogeneous distribution of clays and oxides may cause an apparent higher K in the lab. Moreover, many factors, such as redox state of the groundwater, the Mn and Fe oxides content and salinity, affect K suggesting that the range of K (of radium) in nature is larger.

The isotopic ratios of radium in groundwaters around the Dead Sea is affected by the Th/U ratio of the rocks. The groundwater flow mechanism and their age. The ^{226}Ra/^{223}Ra

ratio can be used as a groundwater dating tool of brines (where K is low) or of the groundwater system. The relatively abundant secular equilibrium $^{226}Ra/^{223}Ra$ ratio in the Dead Sea groundwater suggests that the hydrological system of the Dead Sea has not changed significantly at least 10,000 years. All groundwater around the Dead Sea contain very high activities of ^{222}Rn, which can not be explained by the U content of the aquifer rocks but rather produced from adsorbed ^{226}Ra.

The antithetic behavior of ^{226}Ra and ^{228}Ra during the Dead Sea water circulation in the aquifer, where ^{226}Ra is removed by barite precipitation and ^{228}Ra is contributed to the Dead Sea provides a robust method for quantifying the annual volume of Dead Sea water circulating in the aquifer. Detailed radium mass balance calculations suggest that the steady-state circulation volume is 320 million m^3/y. These large volumes probably affect the mass balances of trace elements in the Dead Sea, e.g. ^{226}Ra, ^{228}Ra, Ba, U and Fe.

This study emphasizes the importance of the relationship between the geochemical and circulation time-scales to the assessment of the actual contribution of seawater circulation to oceanic budgets. The extent of circulation is $\sim$2 million m^3/y per km shoreline, which falls in the range of SGD assessment from other oceanic settings. However, the Dead Sea-derived volumes are only for the long-term dispersive circulation, which has a greater potential to affect the composition of groundwater and may also affect oceanic budgets of trace elements.

Appendices

Appendix A

SGD estimates from different studies

Table A.1: SGD estimates from different studies. SGD units presented here are discharge per meter shoreline. In case that the value of discharge per meter shoreline is not mentioned implicitly in the study, the values were estimated by flux multiplied by the discharge distance from shore or by total discharge divided by the shoreline length. In case that several methods occur in the same study or there are several or a range of estimates, averaged values are presented.

Study	SGD (m^3/y per m shore-line)	Shore -line length (km)	Distance from shore (m)	water depth (m)	Location	SGD type	Method	measured or reported value in study	Remarks
Robinson, 1996	1				Chesapeake Bay, VA		numerical modeling		from Burnett et al, 2001
Robinson, 1996	2				Chesapeake Bay, VA		Darcy's law		from Burnett et al, 2001
Whiting and Childers, 1989	6		1–2	2–10	saltmarsh estuaries		seepage meters, water balance, salinity budget, hydraulic dynamics	1.3–6.6 m/y	from Taniguchi et al, 2002
Gallagher et al, 1996	39		5–9	1	Chesapeake Bay, VA	65% circulated seawater	seepage meters	0.63 $L/m^2/h$	from Taniguchi et al, 2002
Fanning et al, 1981	79	10	20000, area: 85 km^2	12–13	West FL	thermal springs	flowmeter	25 L/s	from Taniguchi et al, 2002
Tsunogai et al, 1996	100		12000, area: 2 km^2	1000	Sagami Bay, Japan		heat Flow, chemical composition	310–500 m^3/d	from Taniguchi et al, 2002
Boldovski, 1996	132				Kamchatka Peninsula				fractured rock aquifer
Sellinger, 1995	164				Lake Michigan		numerical modeling, water budget		from Burnett et al, 2001
Martin et al, 2007	168		22		Indian River Lagoon, FL	fresh	seepage meters, salinity	0.02–0.9 m^3/d per m shoreline	
Uchiyama et al, 2000	168				Kashima Coast, Japan		modeling		from Gallardo and Marui, 2006
Henry et al, 1989	200				Nankai Wedge, Japan	thermal discharge along trenches	temperature	100 m/y	condiuits of 2 m diameter
Bokuniewicz, 1980	438		30	1.3	Great South Bay, NY		seepage meters	40 l/m^2/d	from Taniguchi et al, 2002
Kroeger et al, 2007	438				Tampa Bay, FL	fresh	Darcy's law		
Taniguchi, 2000	450		5	1	South of Osaka Bay, Japan		seepage meters, numerical modeling	44–136 m/y	from Taniguchi et al, 2002
Mulligan and Charette, 2006	584		kilometers		Cape Cod, MA	total, most saline	Rn	5.6 m^3/d per m shoreline	
Zimmermann et al, 1985	700		25	1.5	East Coast of FL		seepage meters, piezometers	24–32 m/y	from Taniguchi et al, 2002
Reay et al, 1992	812		0–50		Chesapeake Bay, VA		seepage meters	0.02–3.69 l/m^2/h	from Taniguchi et al, 2002
Rasmussen, 1998	1018		<500	0.5–2	NE coastal Gulf of Mexico, FL		seepage meters, numerical modeling	0.37–3.7 m/y	from Taniguchi et al, 2002

Continued on next page

Table A.1 – *Continued from previous page*

Study	SGD (m^3/y per m shore-line)	Shore-line length (km)	Distance from shore (m)	water depth (m)	Location	SGD type	Method	measured or reported value in study	Remarks
Kroeger et al, 2007	1059				Tampa Bay, FL	fresh	water budget		
Burnett et al, 2006	1132				Cockburn Sound, Australia		seepage meters, Rn, Ra isotopes, modeling		
Charette et al, 2003	1424	1	area: 0.9 km^2		Great Sippewissett Marsh, Cape Cod, MA		Radium isotopes	3900 m^3/d	
Mulligan and Charette, 2006	1460		kilometers		Cape Cod, MA	fresh	Darcy's law, seepage meter		
Lewis, 1987	1805		meters	1.5	Barbados, West Indies		Seepage meters, piezometers	268–454 m/y	from Taniguchi et al, 2002
Weinstein et al, 2007a	1825				Dor, Israel	fresh	Rn		
Kaleris et al, 2002	1935				Baltic Sea		modeling		from Gallardo and Marui, 2006
Kamermans et al, 2002	1936				Zanzibar Island		modeling		from Gallardo and Marui, 2006
Shaban et al, 2005	1954	174			Lebanon coast		temperature, remote sensing	340cot 10^6 m^3/y	from Gallardo and Marui, 2006
Dead Sea	2000				Dead Sea	circulated	Ra isotopes		
Mulligan and Charette, 2006	2044		kilometers		Cape Cod, MA	total	Rn		
Kroeger et al, 2007	2044				Tampa Bay, FL	total	Rn		$\sim 50 - -80\%$ is saline
Swarzenski et al, 2007	2190		1450000		Tampa Bay, FL		Rn, Ra isotopes		
Dulaiova et al, 2006	2190				West Neck Bay, NY		Rn, Ra isotopes		
Johannes and Hearn, 1985	2200		50	5	Perth, Australia		salinity, hydrology	$4.8{\cdot}10^4$ m^3/d	from Taniguchi et al, 2002
Swarzenski et al, 2006	2555				Dor, Israel		Rn		
Povinec et al, 2008	2555				Ubatuba, Brazil		^{226}Ra		
Langevin, 2003	2701	50			Biscayne Bay, FL		modeling	$3.7 \cdot 10^5$ m^3/d	
Fischer et al, 1964	3000	2.4	<300		HI Island		thermal image analysis	millions gallons/d	from Taniguchi et al, 2002
Hussain et al, 1999	3942	1600			Chesapeake Bay, VA	fresh	Rn, Ra isotopes	200 m^3/s	
Burnett et al, 2006	4015				Shelter Island		seepage meters, Rn, Ra isotopes, modeling		
Valiela et al, 1990	4331		35–200		coastal bays of New England		salinity, Seepage meters	2–4 L/m^2/y	from Taniguchi et al, 2002
Kamermans et al, 2002	4380				Kenya, Southern Coast		modeling		from Gallardo and Marui, 2006
Cable et al, 1997	4450		<500	0.5–2	NE Gulf of Mexico, FL		seepage meters	8.9 m/y	from Taniguchi et al, 2002
Taniguchi et al, 2006	6360		300		Sicily		seepage meters	12.1 L/min/m^2	
Lambert and Burnett, 2003	7358				NE Gulf of Mexico, FL		Rn	100m	200m offshore

Continued on next page

Table A.1 – *Continued from previous page*

Study	SGD (m^3/y per m shore-line)	Shore -line length (km)	Distance from shore (m)	water depth (m)	Location	SGD type	Method	measured or reported value in study	Remarks
Burnett et al, 2006	7665			40	Mauritius		seepage meters, Rn		
Taniguchi et al, 2008	7665		7000		Yellow River		seepage meters		
Moore, 2003	7884	0.1			NE Gulf of Mexico, FL		Rn, Ra isotopes, seepage meters		200m offshore
Kim et al, 2003	9868	152			Jeju Island, South Sea of Lorea	fresh	seepage meters, Ra isotopes, nutrients	shoreline 152 km	
Taniguchi et al, 2003a	10512	0.1			NE Gulf of Mexico, FL		seepage meters	100m	200m offshore
Cable et al, 1996a	11800		<500		NE Gulf of Mexico, FL		seepage meters		from Taniguchi et al, 2002
Bugna et al, 1996	11826		<500	0.5–2	NE Gulf of Mexico, FL		seepage meters	10–80 $ml/m^2/min$	from Taniguchi et al, 2002
Giblin and Gaines, 1990	13149		1000, area: 1.4^2	<2	Cape Cod, MA		seepage meters, water balance, salinity budget, hydraulic dynamics	0.79–8.9 m^3/d	from Taniguchi et al, 2002
Schwartz, 2003	13560	50			Delaware estuary		Rn	14–29 m^3/s	from Gallardo and Marui, 2006
Vanek and Lee, 2012	15000		<200	2	Laholm Bay, Sweeden		seepage meters, water balance, salinity budget, hydraulic dynamics	75 m/y	from Taniguchi et al, 2002
Cable et al, 1997	19640		area: 7 km^2	0.5–2	NE Gulf of Mexico, FL		seepage meters	1.04–18.6 m/y	from Taniguchi et al, 2002
Elhatip, 2003	23360	1			Ovacif-Silifke, Turkey	springs	hydrochemical techniques	$6.4 \cdot 10^4$ m^3/d	
Garrison et al, 2003	32873	1	area: 1.44 km^2		Kahana Bay, Oahu	16% fresh	Rn	90000000 L/d	
Moore, 1996	34219	320			North and South Carolina		^{226}Ra	$3{\cdot}10^{10}$ L/d	recalculated in Moore et al (2008) $1.2 \cdot 10^5$
Simmons, 1992	38599		15000		Keys, FL		seepage meters		from Taniguchi et al, 2002
Martin et al, 2007	42705		22		Indian River Lagoon, FL	marine	seepage meters, salinity	117 m^3/d per m shoreline	
Martin et al, 2007	42705				Indian River Lagoon, FL	marine	seepage meters, Rn		
Lamontagne et al, 2008	50458				Adelaide, Australia		^{226}Ra, ^{228}Ra		
Kim et al, 2005	59585	3860	$4{\cdot}10^5$ km^2		Yellow Sea	brackish	^{226}Ra, ^{228}Ra	$2.3{\cdot}10^{11}$ m^3/y	
Burnett et al, 2006; Burnett and Dulaiova, 2006	91250				Donnalucata, Sicily		seepage meters, Rn, Ra isotopes		
Hwang et al, 2005	94900	100			Yeoja Bay, Korea		nutrients, Ra isotopes	$2.6{\cdot}10^7$ m^3/d	from Gallardo and Marui, 2006
Kim et al, 2003	98684	152	152000		Jeju Island, South Sea of Korea	circulated	seepage meters, Ra isotopes, nutrients		

Continued on next page

Table A.1 – *Continued from previous page*

Study	SGD (m^3/y per m shore-line)	Shore -line length (km)	Distance from shore (m)	water depth (m)	Location	SGD type	Method	measured or reported value in study	Remarks
Ollivier et al, 2008	104223	166			Gulf of Lion		^{226}Ra, ^{228}Ra	0.24–$4.5{\cdot}10^{10}$ L/d	
Windom and Niencheski, 2003	114063	200			Patos Lagoon, Brazil		hydrochemistry	$6.25 \cdot 10^7$ m^3/d	from Gallardo and Marui, 2006
Garcia-Solsona et al, 2008	127750	1			Venice Lagoon	circulated	Ra isotopes	$3.5{\cdot}10^9$ L/d	major flux is circulated
Windom et al, 2006	130000		hundreds of km		Brazil		Ra isotopes		
Simmons, 1992	175565		37000		Wilmington, NC		seepage meters		from Taniguchi et al, 2002
Corbett et al, 1999	214500		<30000	<2	Keys and Florida Bay, FL		seepage meters	3.6–10.7 m/y	from Taniguchi et al, 2002
Kim et al, 2008	219000		area: 120 km^2		Korea		Ra isotopes, nutrients	$6{\cdot}10^6$ m^3/d	
Dowling et al, 2003	300000	500		200	Bengal Basin		trace elements, modeling	$1.5{\cdot}10^{11}$ m^3/y	
Moore et al, 2008	350000				Atlantic		^{228}Ra		Also deeper contribution of SGD
Moore, 2006	365000				Sicily		^{226}Ra		
Cable et al, 1996b	525960		30000, area: 620 km^2	0.5–2	NE Gulf of Mexico, FL		Rn, Ra isotopes	180–710 m^3/s	from Taniguchi et al, 2002
Taniguchi et al, 2008	608820		7000		Yellow River	total, 1% fresh	seepage meters		7% from yellow river discharge
Piekarek-Jankowska, 1995				<50	Puck Bay, Baltic Sea		nutrient, isotope	0.15 m/y	from Taniguchi et al, 2002
Taniguchi et al, 1998				150	Tokyo Bay, Japan		groundwater temperature, depth profile	0.03–0.42 m/y	from Taniguchi et al, 2002
Deming et al, 1992				600	North Slope of AK		heat flow	0.07 m/y	from Taniguchi et al, 2002
Simmons, 1992			37000	10–33	Keys, FL		seepage meters	10.8 l/m^2/d	inflow of salt water into the aquifer
Brooks, 1961			4000	38	Crescent, FL		salinity	42 m^3/s	from Taniguchi et al, 2002
Lee, 1977					lakes	fresh	seepage meters	0.01–$2.58{\cdot}10^{--6}$ m/s	
Hay, 1984					Baffin Island, Canada		remote acoustic imaging	0.34 m^3/s	from Taniguchi et al, 2002
Taniguchi and Iwakawa, 2004					Osaka Bay, Japan	fresh	seepage meters, hydraulic gradient and conductivity	$1.37{\cdot}10^{-8}$ m/s	
Taniguchi and Iwakawa, 2004					Osaka Bay, Japan	total	seepage meters	$6{\cdot}10^{-8}$ m/s	4–29% is fresh

Continued on next page

Table A.1 – *Continued from previous page*

Study	SGD (m^3/y per m shore-line)	Shore -line length (km)	Distance from shore (m)	water depth (m)	Location	SGD type	Method	measured or reported value in study	Remarks
Taniguchi et al, 2005					Suruga Bay, Japan		seepage meters, water balance	$4.7{\cdot}10^{-7}$– $1.8{\cdot}10^{-5}$ m/s	14.7 % is fresh
Taniguchi et al, 2003b					Western Australia		temperature	$3.6 \cdot 10^{-3}$ – $-9 \cdot 10^{-3}$ m/d	from Gallardo and Marui, 2006
Oliveira et al, 2003					Sao Paulo, Brazil		Rn, Ra isotopes	0.023–0.048 md	from Gallardo and Marui, 2006
Capone and Bautista, 1985					Great South Bay, NY		sediment chemistry	10–50 L/m^2/d	from Gallardo and Marui, 2006

Appendix B

^{228}Ra mass balance in the groundwater including co-precipitation with barite

The complete mass balance equation of ^{228}Ra includes the co-precipitation of ^{228}Ra with barite:

$$\frac{\partial C}{\partial t} = -\nabla \cdot \mathbf{v}C + \nabla \cdot \mathbf{D}\nabla C - \lambda(K+1)C + P - S \tag{B.1}$$

where C[dpm/L] is ^{228}Ra activity in groundwater, t[T] is time, $\mathbf{v}$[L/T] is velocity, $\mathbf{D}$[L^2/T] is dispersion, λ[1/T] is the decay constant, P[dpm/(L $\cdot$ T)] is the production rate of ^{228}Ra from the aquifer solids by recoil and dissolution, S[dpm/(L $\cdot$ T)] is the precipitation rate and K is a dimensionless adsorption partition coefficient given by $K = C_s/C$ where C_s[dpm/L] is the activity of ^{228}Ra on the solid surface expressed as equivalent concentration in water.

The precipitation rate of ^{228}Ra can be defined by the precipitation rate of ^{226}Ra (eq. 3.3) according to the ^{226}Ra/^{228}Ra ratio in the water:

$$S = S_6 \frac{C}{C_6} = k(C_6 - C_{sat_6})\frac{C}{C_6} \tag{B.2}$$

where S_6[dpm/L $\cdot$ T] is the precipitation rate of ^{226}Ra, C_6[dpm/L] is the activity of ^{226}Ra and C_{sat_6}[dpm/(L $\cdot$ T)] is the activity of ^{226}Ra in saturation.

Substituting the precipitation rate of ^{228}Ra and the ^{226}Ra solution (eq. 3.4) in the steady-state one dimensional mass balance equation (neglecting hydrodynamic dispersion) yields:

$$v\frac{\partial C}{\partial x} = -\lambda(K+1)C + P - k\left(1 - \frac{C_{sat_6}}{(C_{0_6} - C_{sat_6})e^{-\frac{k}{v}x} + C_{sat_6}}\right)C \tag{B.3}$$

where C_{0_6}[dpm/L] is the initial activity of ^{226}Ra in the Dead Sea lake.
The non-elementary solution of the above equation where $C(0) = 0$ is:

$$C\left(x\right) = \frac{P}{v_x}\int_0^x \frac{\mathrm{e}^{\frac{l(K+1)z}{v_x}}}{\left(\mathrm{e}^{-\frac{kz}{v_x}}C_{0_6} - \mathrm{e}^{-\frac{kz}{v_x}}C_{sat_6} + C_{sat_6}\right)}dz \cdot \tag{B.4}$$

$$\left(C_{0_6}\,\mathrm{e}^{-\frac{x(k+lK+l)}{v_x}} - \mathrm{e}^{-\frac{x(k+lK+l)}{v_x}}C_{sat_6} + \mathrm{e}^{-\frac{l(K+1)x}{v_x}}C_{sat_6}\right) \tag{B.5}$$

Considering the calculated velocities and precipitation rates, the effect of barite precipitation on ^{228}Ra activities is negligible (Fig. 3.3).

Appendix C

Additional data of samples

Table C.1: Groundwater samples parameters and major element concentrations.

Sample	Location	date	Temp. °C	EC (mS/cm)	pH	Elev. (m)	depth (m)	Water table elev. (m)	Na (g/L)	K (g/L)	Ca (g/L)	Mg (g/L)	Sr (g/L)	Cl (g/L)	SO_4 (g/L)	Br (g/L)	Na/Cl (eq./eq.)	Ca/Mg (eq./eq.)	Br/Cl (eq./eq.)	TDS (g/L)	R.E %
	Arugot alluvial fan																				
yk1	EG16	21/01/08				-420.8	6.05	-420.8													
yk2	EG16	21/01/08				-420.8	6.05	-420.8													
yk3	EG16	21/01/08	23.9			-420.8	6.05	-420.8	14	2	6	12	0.11	67		1.6	0.313	0.311	0.010	102	-0.4
yk4	EG16	21/01/08	23.9			-421.8	7.05	-421.8	28	5	11	26	0.20	142		5.8	0.303	0.259	0.018	217	-1.1
yk5	EG16	21/01/08	24.3			-421.8	7.05	-421.8													
yk6	EG16	21/01/08	24.3			-421.8	7.05	-421.8													
yk7	EG16	21/01/08	23.9			-426.2	11.5	-426.2													
yk8	EG16	21/01/08	23.3			-426.2	11.5	-426.2	34	8	17	44	0.32	224		5.8	0.233	0.239	0.011	334	-1.6
yk9	EG16	21/01/08	24.9			-426.2	11.5	-426.2													
yk11	EG11	21/01/08	27.1			-420.7	19	-420.4													
yk12	EG11	21/01/08	27.8			-423.9	18.5	-420.4													
yk13	EG22	21/01/08	26.3			-432.3	26.5	-420.2	38	7	17	42	0.30	221		5.6	0.268	0.245	0.011	331	-1.3
yk42	Spring	27/08/08	34				0		17	2	6	13	0.12	78	1.2	1.7	0.328	0.302	0.010	119	-1.5
EG22-29.5m	EG22	24/03/09				-435.3	29.5		38	7	16	41	0.30	219	0.0	5.7	0.269	0.242	0.012	328	-1.5
ES	Ein-Shulamit	24/03/09							0.044	0.003	0.06	0.026	0.0005	0.08	0.03	0.0002	0.859	1.283	0.001	0.47	1.2
yk110A	EG20	22/06/09	27.6			-469.9	64	-421.7	38	8	17	44	0.32	227		5.3	0.259	0.237	0.010	342	-0.8
yk111A	EG21	22/06/09	31.5			-425.9	20	-422.1	30	5	11	24	0.20	139		2.9	0.336	0.275	0.009	213	0.0
yk112	EG21	22/06/09	31			-434.9	29	-422.1	39	8	17	42	0.31	219		5.1	0.271	0.238	0.010	331	-0.6
yk113	EG11	22/06/09	32.8			-423.4	18.5	-421.9	16	2	7	13	0.12	73		1.6	0.338	0.315	0.009		0.1
yk115	EG6	22/06/09	34.3			-422.4	40	-411.1													
yk118	EG19	22/06/09	36.6			-437.9	50	-415.4	10	1	4	7	0.08	44	0.73	1.0	0.367	0.383	0.010	69	-1
yk119	EG19	22/06/09	34.2			-446.9	59	-415.4	22	3	9	16	0.18	101	0.96	2.2	0.340	0.347	0.010	155	-1.1
yk120	AR2	22/06/09	37.5			-411.6	47	-405.5	2.9	0.5	1.1	1.7	0.02	12	0.40	0.3	0.378	0.405	0.009	19	-1.2
yk121	AR2	22/06/09	36.5			-409.6	45	-405.5	2.8	0.5	1.1	1.6	0.02	11	0.40	0.2	0.384	0.409	0.009	18	-1.2
yk122	EG22	22/06/09	32.9			-425.8	20	-421.6	29	4	11	24	0.21	136	1.50	3.0	0.334	0.285	0.010	210	0.4
yk123	EG22	22/06/09	32.2			-433.8	28	-421.6	39	7	16	40	0.29	212	1.00	5.0	0.285	0.241	0.010	320	-1
yk240	EG11	13/06/10	31		6.25	-424.4	19.5	-422.8	10	2	5	9	0.09	46	2.72	0.8	0.350	0.321	0.008	75	
yk241	EG22	13/06/10	35.1		5.83	-426.8	21	-422.5	28	4	10	23	0.19	137	1.07	3.1	0.319	0.269	0.010	206	-1.9
yk242	EG22	13/06/10	34.4		5.68	-431.1	25.3	-422.5	33	5	13	30	0.23	169	0.68	3.9	0.300	0.264	0.010	254	-1.4
yk243	EG22	13/06/10	32.6		5.25	-435.3	29.5	-422.5	38	7	17	41	0.30	219	0.30	5.4	0.268	0.244	0.011	328	-1.4
yk244	EG22	13/06/10	33.8		6.02	-427.8	22	-422.5	25	4	9	20	0.16	117	1.36	2.6	0.326	0.279	0.010	177	-1.1
yk245	EG20	13/06/10	31.5		5.47	-451.6	45.7	-422.6	36	8	17	43	0.31	224	0.25	5.5	0.250	0.243	0.011	334	-1.8
yk246	EG20	13/06/10	31.2		5.47	-468.9	63	-422.6	36	8	17	43	0.31	220	0.23	5.5	0.252	0.245	0.011	330	-1.1
yk247	EG21	13/06/10	33.8		6.29	-424.8	18.9	-423.0	19	3	7	15	0.13	87	1.92	2.0	0.331	0.299	0.010	132	-0.8
yk248	EG21	13/06/10	34.7		5.84	-428.2	22.3	-423.0	32	5	12	26	0.21	152	0.85	3.5	0.327	0.269	0.010	131	-0.4
yk249	EG21	13/06/10	34.6		5.65	-431.5	25.6	-423.0	36	6	14	32	0.25	184	0.55	4.4	0.304	0.270	0.011	278	-1.5
yk250	EG21	13/06/10	33.2		5.45	-435.5	29.6	-423.0	38	7	17	42	0.31	220	0.25	5.5	0.268	0.239	0.011	330	-1.2
yk291	spring	05/07/10					0		17	2	6	12	0.11	74	2.10	1.6	0.364	0.321	0.010	115	-0.7
yk400	EG24	13/06/11	27.7			-424.6	2.8	-424.4	29	4.9	12	27	0.22	148		3.4	0.306	0.268	0.010		
yk401	EG24	13/06/11	28.2		6	-439.8	18	-424.4	31	8.2	19	49	0.36	230		6	0.209	0.233	0.012		
yk402	EG25	13/06/11	26.9		6.45	-424.1	2.75	-424.1	18	2.8	6.7	14	0.12	82		1.8	0.331	0.297	0.010		
yk410	EG25	13/06/11	31.4		5.95	-425.9	4.5	-424.4	30	5	12	27	0.21	151	0.97	3.5	0.304	0.276	0.010		

Continued on next page

Table C.1 – *Continued from previous page*

Sample	Location	date	Temp. °C	EC (mS/cm)	pH	Elev. (m)	depth (m)	Water table elev. (m)	Na (g/L)	K (g/L)	Ca (g/L)	Mg (g/L)	Sr (g/L)	Cl (g/L)	SO_4 (g/L)	Br (g/L)	Na/Cl (eq./eq.)	Ca/Mg (eq./eq.)	Br/Cl (eq./eq.)	TDS (g/L)	R.E %
yk411	EG25	13/06/11	29.9		5.74	-431.4	10	-424.4	33	7	19	46	0.32	229	0.29	5.8	0.225	0.247	0.011		
yk412	EG25	13/06/11	31.2		6.27	-424.9	3.5	-424.4	20	3	8	16	0.13	95	1.76	2.1	0.318	0.306	0.010		
yk413	EG24	13/06/11	31.7		5.85	418.5	3.25	-424.6	32	7	18	43	0.31	216	0.36	5.4	0.231	0.254	0.011		
yk414	EG24	13/06/11	33.4		5.73	411.8	10	-424.6	32	8	19	47	0.33	229	0.28	6.1	0.215	0.248	0.012		
yk415	EG24	13/06/11	32.1		5.85	402.8	19	-424.6	31	8	20	48	0.34	233	0.24	6.1	0.206	0.247	0.012		
yk416	EG23	13/06/11	31.5		5.7	-426.2	6.32	-424.6	38	6	15	36	0.26	196	0.46	4.7	0.295	0.259	0.011		
yk417	EG23	13/06/11	32.8		5.58	-429.8	10	-424.6	33	8	19	47	0.33	228	0.24	6.0	0.222	0.248	0.012		
yk418	EG23	13/06/11	31.4		5.68	-434.3	14.5	-424.6	31	7	19	47	0.33	223	0.24	6.1	0.215	0.250	0.012		
yk419	EG23	13/06/11	30.7		5.8	-439.3	19.5	-424.6	31	7	20	47	0.33	231	0.23	6.3	0.210	0.250	0.012		
yk420	EG26	13/06/11	32.7		6.36	-424.4	17.8	-423.8	12	2	5	9	0.08	57	3.09	1.3	0.338	0.363	0.010		
yk421	EG26	13/06/11	31.2			-436.6	30	-423.8	37	7	17	43	0.30	226	0.27	5.7	0.254	0.246	0.011		
yk422	EG26	13/06/11	29.2			-441.6	35	-423.8	37	7	18	43	0.30	220	0.25	5.7	0.262	0.247	0.011		
	Einot-Qedem																				
yk52		27/07/08	43.5				0														
yk53		27/07/08	43.2				0														
	Jordan River																				
yk390	Baptism site	24/02/11	15.7	8.25			0														
	Ein-Feshkha																				
yk311		04/10/10				-423.0			8	3	7	18	0.12	81			0.155	0.223			
yk313		04/10/10				-423.0			1.35	0.18	0.47	0.8	0.006	5.38	0.14	0.1	0.387	0.359	0.009	8.5	-2
yk314		04/10/10				-423.0			0.62	0.07	0.26	0.3	0.003	2.18	0.11	0.04	0.439	0.515	0.008	3.8	-1.7
yk318		04/10/10				-423.0			4.47	0.75	1.72	3.7	0.03	21	0.24	0.57	0.321	0.286	0.012	33	-1.4
yk391		24/02/11	24.3	4.31																	
yk392		24/02/11	23.4	3.31																	
	Samar and Kane Springs																				
yk350	Samar Spring	08/11/10							20	0.40	1.1	2	0.020	39	0.65	0.28	0.773	0.334	0.003		
yk351	Samar Spring	08/11/10							0.65	0.11	0.3	0.48	0.005	3	0.20	0.06	0.358	0.379	0.010		
yk352	Samar Spring	08/11/10							1.23	0.17	0.43	0.74	0.007	5	0.28	0.10	0.395	0.355	0.009		
yk353	Samar Spring	08/11/10							0.54	0.12	0.28	0.46	0.004	3	0.34	0.06	0.333	0.363	0.010		
yk354	Samar Spring	08/11/10							1.15	0.16	0.42	0.59	0.007	4	0.52	0.07	0.445	0.435	0.008		
yk355	Samar Spring	08/11/10							12	1.70	3.8	8.7	0.080	53	1.05	1.64	0.350	0.266	0.014		
yk356	Kane Spring	08/11/10							0.32	0.05	0.15	0.21	0.002	1	0.22	0.03	0.406	0.433	0.009		
yk357	Samar Spring	08/11/10							0.45	0.10	0.19	0.33	0.003	2	0.12	0.04	0.357	0.355	0.010		
	Eastern Catchment, Jordan																				
yk300	Wadi Hudeira	23/09/10	30						0.08	0.01	0.03	0.02	0.001	0.12	0.08		1.028	0.958			
yk301	Wadi Ibn-Hamad	23/09/10							0.09	0.01	0.04	0.02	0.001	0.13	0.09		1.091	1.061			
yk302	Wadi Ibn-Hamad	23/09/10							0.07	0.01	0.04	0.02	0.001	0.10	0.07		1.141	1.179			
yk303	Wadi Hasa	25/09/10							0.07	0.01	0.05	0.03	0.001	0.13	0.13		0.842	1.033			
yk304	Wadi Mujib	25/09/10							0.42	0.05	0.09	0.04	0.003	0.77	0.21		0.835	1.436			
yk305	Wadi Zarka Ma'in	25/09/10							0.19	0.01	0.08	0.04	0.002	0.35	0.23		0.846	1.244			
yk360	Wadi Hanzira	15/12/10	15.2	0.854					0.08	0.00	0.05	0.05	0.001	0.15	0.13		0.756	0.687		0.55	-0.6
yk361	Wadi Fifa	15/12/10	15.4	0.63					0.06	0.01	0.08	0.03	0.001	0.09	0.09	0.0003	1.028	1.470	0.001	0.52	2.1
yk362	Wadi Hasa	15/12/10	18.6	0.862					0.08	0.01	0.07	0.03	0.001	0.13	0.14		0.890	1.314		0.53	-0.6
yk363	Wadi Karak	16/12/10	14						0.10	0.01	0.06	0.04	0.002	0.16	0.16		0.904	0.953		0.59	-0.9
yk365	Spring	16/12/10	18.7						66	5.2	10.5	25	0.188	202		3.2	0.505	0.259	0.007	311	-1.5
yk366	Wadi Mujib	16/12/10	17	1.97					0.22	0.02	0.11	0.04	0.002	0.41	0.27	0.0013	0.839	1.594	0.001	1.17	-1.9

Continued on next page

Table C.1 – *Continued from previous page*

Sample	Location	date	Temp. ∘C	EC (mS/cm)	pH	Elev. (m)	depth (m)	Water table elev. (m)	Na (g/L)	K (g/L)	Ca (g/L)	Mg (g/L)	Sr (g/L)	Cl (g/L)	SO_4 (g/L)	Br (g/L)	Na/Cl (eq./eq.)	Ca/Mg (eq./eq.)	Br/Cl (eq./eq.)	TDS (g/L)	R.E %
yk367	Wadi Zarka Ma'in	16/12/10	23.4	2.9					0.43	0.05	0.10	0.03	0.003	0.73	0.20	0.0029	0.902	1.784	0.002	1.62	0.8
yk368	Zarka Ma'in	16/12/10	40.5	2.42					0.40	0.05	0.10	0.03	0.003	0.72	0.21	0.0026	0.863	2.021	0.002	1.59	-1.8
yk369	Zarka Ma'in	16/12/10	60	0.36					0.45	0.05	0.12	0.03	0.003	0.77	0.20	0.0029	0.899	2.348	0.002	1.69	2.0
yk370	Zarka Ma'in	16/12/10	35						0.41	0.05	0.10	0.03	0.003	0.71	0.19	0.0029	0.903	2.070	0.002	1.59	-1.2
yk371	Zarka Ma'in	16/12/10	65						0.39	0.04	0.10	0.03	0.003	0.67	0.17	0.0028	0.898	2.134	0.002	1.48	0.4
yk372	Wadi El-Hidan	16/12/10							0.09	0.01	0.05	0.04	0.001	0.12	0.11	0.0009	1.092	0.918	0.003	0.53	1.4
yk373	Wadi Mujib	17/12/10							0.07	0.01	0.08	0.03	0.001	0.11	0.18	0.0006	0.983	1.798	0.002	0.56	1.5
yk374	Wadi Ibn-Hamad	17/12/10	21.1						0.10	0.01	0.04	0.02	0.001	0.13	0.09	0.0004	1.205	1.130	0.001	0.47	1.7
yk375	Wadi Ibn-Hamad	17/12/10	17.5	0.00099					0.08	0.01	0.04	0.02	0.001	0.11	0.08	0.0005	1.115	1.274	0.002	0.43	-0.8
yk376	Wadi Ibn-Hamad	17/12/10	31.7	0.2					0.08	0.01	0.05	0.02	0.001	0.13	0.06	0.0013	0.949	1.213	0.005	0.44	-0.6
yk377	Wadi Ibn-Hamad	17/12/10	34.9	0.582					0.08	0.01	0.05	0.02	0.001	0.13	0.06	0.0011	0.938	1.318	0.004	0.45	-1.5
yk378	Wadi Wadia	17/12/10	29.8	0.605					0.05	0.01	0.04	0.02	0.001	0.09	0.08	0.0004	0.901	1.404	0.002	0.36	-1.8
yk379	Wadi Wadia	17/12/10	24.2	0.2					0.06	0.01	0.04	0.02	0.001	0.10	0.07	0.0005	0.977	1.274	0.002	0.37	1.8
yk380	Spring, Dead Sea	17/12/10	27.3	18.6					3.00	0.42	2	1.8	0.024	12	2.1	0.23	0.386	0.674	0.009	22	0.3
yk381	Zara	17/12/10	27																		
yk116	Darga2	22/06/09	35.4				33		1.4	0.38	0.54	0.94	0.009	6.1	0.20	0.13	0.368	0.348	0.010	10	0.2
yk117	Darga2	22/06/09	34.9				53		9.9	1.97	4.07	7.9	0.070	47	0.50	1.1	0.326	0.313	0.010	72	-0.3
yk290	EG3	05/07/10							24	2.35	8.5	11	0.150	83	3.3	1.8	0.451	0.458	0.010		

Continued on next page

Table C.2: Concentrations of trace elements in the Dead Sea groundwater.

Sample	Location	date	Mn (mg/L)	Fe (mg/L)	Ni (μ/L)	Cu (μ/L)	Zn (μ/L)	Pb (μ/L)	Th (μ/L)	Si (mg/L)	Rb (mg/L)	Li (mg/L)
yk240	EG11	13/06/2010	2	2	< 20	< 20	< 10	< 0.5				
yk241	EG22	13/06/2010	3.9	5	< 20	< 20	< 10	< 0.5				
yk242	EG22	13/06/2010	5.3	7.5	< 20	< 20	< 10	< 0.5				
yk243	EG22	13/06/2010	9.4	19	< 20	< 20	20	< 0.5				
yk244	EG22	13/06/2010	3.2	3.5	< 20	< 20	< 10	< 0.5				
yk245	EG20	13/06/2010	9.5	11	< 20	< 20	20	< 0.5				
yk246	EG20	13/06/2010	9.4	11	< 20	< 20	20	< 0.5				
yk247	EG21	13/06/2010	2.3	3	< 20	< 20	< 10	< 0.5				
yk248	EG21	13/06/2010	4.4	6.4	< 20	< 20	< 10	< 0.5				
yk249	EG21	13/06/2010	5.5	7.4	< 20	< 20	< 10	< 0.5				
yk250	EG21	13/06/2010	9.3	12.5	< 20	< 20	20	< 0.5				
yk291	spring	05/07/2010	1.85	3	< 20	< 20	< 10	1.9				
yk400	EG24	13/06/2011	5.3					0.8	<0.1	4	1.3	11
yk401	EG24	13/06/2011	6.7					1.4	<0.1	15	1.9	17
yk402	EG25	13/06/2011	2.1					<0.1	<0.1	0	0.7	6.0
yk410	EG25	13/06/2011	4.3	11				7	<5		1.0	7.9
yk411	EG25	13/06/2011	7.9	3				12	<5		1.4	12.5
yk412	EG25	13/06/2011	2.3	11				7			0.6	5.2
yk413	EG24	13/06/2011	6.7	7				8			1.3	10.9
yk414	EG24	13/06/2011	7.8	<1				10			1.4	12.9
yk415	EG24	13/06/2011	7	<1				8			1.4	12.7
yk416	EG23	13/06/2011	6.5	13				6			1.1	9.0
yk417	EG23	13/06/2011	8.4	2				10			1.4	12.1
yk418	EG23	13/06/2011	7.3	4				4			1.3	11.7
yk419	EG23	13/06/2011	7.6	4				5			1.4	12.2
yk420	EG26	13/06/2011	1.5	2				7			0.4	2.9
yk421	EG26	13/06/2011	9.3	13				4			1.3	11.1
yk422	EG26	13/06/2011	8.8	12				4			1.3	10.6
yk290	EG3	05/07/2010	0.44	<0.1	< 20	< 20	< 10	2				

Appendix D

^{226}Ra and ^{228}Ra activities in the Dead Sea

Location	Sampling date	^{226}Ra (dpm/L)	s.d.	^{228}Ra (dpm/L)	s.d.	Distance from shore (km)	Depth (m)	Sample name
Arugot	21/01/2008	134	17.4	0.3	0.03	0	0	yk10
Arugot	18/02/2008	142	10.9			0	0	yk21
Arugot	18/02/2008	112	30.0			0	0	yk23
Arugot	18/02/2008	142	14.2			0	0	yk24
Arugot	18/02/2008	124	12.3			0	0	yk25
eg300	27/02/2008	129	25.6	1.4	0.14	8	0	yk31
eg300	27/02/2008	132	29.1			8	300	yk32
eg300	27/02/2008	172	17.2			8	40	yk33
eg300	27/02/2008	130	6.5			8	150	yk34
Arugot	27/02/2008	135	6.7	1.8	0.18	1	0	yk35
Arugot	27/02/2008	141	16.4			0.5	0	yk36
Arugot	27/02/2008	159	15.1	2.2	0.22	0.1	0	yk37
Arugot	27/02/2008	160	16	1.9	0.19	0	0	yk38
Arugot	27/07/2008	166	13.3			0	0.5	yk40
Arugot	27/07/2008	124	6.0			0	0.5	yk41
Arugot	27/07/2008	135	17.9			0	0.5	yk43
Arugot	27/07/2008	130	33.1			0	0.5	yk44
Arugot	27/07/2008	146	8.8			0	0.5	yk45
Arugot	27/07/2008	137	0.0			0	0.5	yk47
Arugot	27/07/2008	140	18.6			0	0.5	yk48
Arugot	27/07/2008	149	14.9			0	0.2	yk49
Arugot	27/07/2008	139	13.9			0	1	yk50
Zeelim	27/07/2008	152	7.7			0	0.3	yk51a
Zeelim	27/07/2008	163	16.2			0	0.3	yk51b
Ein Qedem	27/07/2008	137	11.9			0	0.2	yk55
Ein Qedem	27/07/2008	143	12.5			0	0.1	yk56
Arugot	03/11/2008	162	8.3	1.8	0.18	0	0	yk60
Arugot	03/11/2008	153	9.2			0	0	yk60c
Ein Qedem	03/11/2008	154	9.2			0	0	yk65
eg300[a]	11/11/2008	141	8.5	1.9	0.57	8	0.5	yk70

Continued on next page

Table D.1 – *Continued from previous page*

Location	Sampling date	^{226}Ra (dpm/L)	s.d.	^{228}Ra (dpm/L)	s.d.	Distance from shore (km)	Depth (m)	Sample name
eg300	11/11/2008	162	9.7			8	20	yk71
eg300	11/11/2008	148	10.4			8	50	yk72
eg300	11/11/2008	159	8.0			8	50	yk72
eg300	11/11/2008	154	7.4			8	50	yk72b
eg300	11/11/2008	167	13.3			8	150	yk73
eg300	11/11/2008	167	8.3			8	150	yk73B
eg300	11/11/2008	141	7.7			8	75	yk74
eg300	11/11/2008	140	8.4			8	260	yk75
eg300	11/11/2008	161	12.9			8	260	yk75B
eg300	11/11/2008	178	8.9	1.9	0.19	8	60	yk76
eg300	11/11/2008	172	10.3	1.4	0.14	8	210	yk77
eg300	11/11/2008	141	10.2			8	240	Yk78
eg300	11/11/2008	156	7.4	0.9	0.09	8	250	yk79
eg300	11/11/2008	141	14.1	1.0	0.10	8	100	yk80
Arugot	11/11/2008	148	16.2			1	0	yk81
Arugot	11/11/2008	128	9.0			0.5	0.5	yk82
Arugot[a]	11/11/2008	143	12.9	2.2	0.44	0.1	0	yk83
Arugot	11/11/2008	132	7.9			0	0	yk84
Dead Sea station	12/02/2009	129	11.6			4	0.4	yk90
eg300	12/02/2009	151	10.6			8	0.5	yk91
eg300	12/02/2009	162	11.4			8	0.5	yk92
eg300	12/02/2009	138	9.7			8	20	yk93
eg300	12/02/2009	147	8.8			8	40	yk94
eg300	12/02/2009	138	8.3			8	150	yk95
eg300	12/02/2009	143	8.6			8	300	yk96
Arugot	12/02/2009	144	11.5			1	0.5	yk97
Arugot	12/02/2009	124	9.9			1	0.5	yk98
Arugot	12/02/2009	136	8.2			0.5	0.5	yk99
Arugot	12/02/2009	146	13.2			0.5	0.5	yk100
Arugot	12/02/2009	136	12.2			0.1	0.5	yk101
Arugot	12/02/2009	127	11.5			0.1	0.5	yk102
Arugot	24/03/2009	184	11.0			0	0	DS
Arugot	24/03/2009	224	11.2			0	0	090324DSA
eg300	29/06/2009	166	8.5			8	297	yk130
eg300	29/06/2009	163	11.4			8	287	yk131
eg300	29/06/2009	152	9.1			8	277	yk132
eg300	29/06/2009	149	7.4			8	247	yk133
eg300	29/06/2009	144	1.9			8	197	yk134
eg300	29/06/2009	131	0.7			8	150	yk135
eg300	29/06/2009	142	6.2			8	100	yk136
eg300	29/06/2009	142	9.9			8	75	yk137
eg300	29/06/2009	132	4.0			8	50	yk138
eg300	29/06/2009	149	7.3			8	40	yk139
eg300	29/06/2009	150	7.5			8	30	yk141
eg300	29/06/2009	134	10.7			8	20	yk142
eg300	29/06/2009	128	8.9			8	10	yk143
eg300	29/06/2009	134	1.0			8	1	yk144
eg300	29/06/2009	137	6.1	1.0	0.10	8	1.5	yk145
Dead Sea station	29/06/2009	134	2.1	2.1	0.21	4	0.5	yk146A

Continued on next page

Table D.1 – *Continued from previous page*

Location	Sampling date	^{226}Ra (dpm/L)	s.d.	^{228}Ra (dpm/L)	s.d.	Distance from shore (km)	Depth (m)	Sample name
eg300	29/06/2009	144	2.5	1.5	0.15	0.1	1	yk147
eg300	04/08/2009	144	11.3			8	250	yk170
eg300	04/08/2009	149	6.3			8	300	yk171
eg300	04/08/2009	146	8.8			8	280	yk172
eg300	04/08/2009	134	8.1			8	40	yk173
eg300	04/08/2009	156	3.4			8	150	yk174
eg300	04/08/2009	132	4.4			8	10	yk175
eg300	04/08/2009	153	12.2			8	1	yk176
eg300	04/08/2009	153	9.2			8	20	yk177
eg300	04/08/2009	158	4.8			8	30	yk178
Ein Qedem	12/09/2010	159	12.7	1.3	0.13	0	0	yk191
Ein Qedem	12/09/2010	130	17.0			0	0	yk192
eg300	09/02/2010	137	11.0			8	200	yk200
eg300	09/02/2010	139	12.5			8	250	yk201
eg300	09/02/2010	144	17.3			8	300	yk202
eg300	09/02/2010	140	11.2			8	300	yk202
eg300	09/02/2010	147	11.7			8	40	yk203
eg300	09/02/2010	156	9.4			8	50	yk204
eg300	09/02/2010	139	5.5			8	100	yk205
eg300	09/02/2010	152	9.1			8	150	yk206
eg300	09/02/2010	155	6.2	2.3	0.23	8	1	yk207
eg300	09/02/2010	161	8.0			8	10	yk208
eg300	09/02/2010	149	7.4			8	20	yk209
eg300	09/02/2010	138	6.9			8	30	yk210
Arugot	09/02/2010	171	8.4			1	0.5	yk211
Arugot	09/02/2010	142	8.5	1.9		0.5	0.5	yk212
Arugot	09/02/2010	70	13.4	1.6		0.1	0.5	yk213
Lido	10/05/2010	148	7.5			0.1	10	yk220
Ein Feshkha	10/05/2010	190	0.7			0.1	10	yk221
Ein Feshkha	10/05/2010	112	5.6			0.5	10	yk222
Lido	10/05/2010	129	6.3			0.5	10	yk223
Lido	10/05/2010	161	7.9			0.5	1	yk224
Lido	10/05/2010	189	8.7			0.5	2	yk225
Lido	10/05/2010	152	7.1			0.5	5	yk226
Lido	10/05/2010	155	7.2			0.5	7	yk227
Lido	10/05/2010	135	6.3			0.5	10	yk228
Lido	10/05/2010	134	6.3			0.5	20	yk229
Lido	10/05/2010	132	6.5			0.5	37	yk230
Lido	10/05/2010	126	6.1			0.5	1	yk231
Lido	10/05/2010	163	8.1			0.5	3	yk232
Arugot	21/06/2010	161	8.0			8	200	YK260
eg300	21/06/2010	130	6.1			8	250	YK261
eg300	21/06/2010	157	7.8			8	290	YK262
eg300	21/06/2010	145	6.9			8	300	YK263
eg300	21/06/2010	162	7.9			8	50	YK264
eg300	21/06/2010	129	6.1			8	75	yk265
eg300	21/06/2010	131	6.5			8	130	yk266
eg300	21/06/2010	167	7.9			8	150	yk267
eg300	21/06/2010	148	6.9			8	0	yk268

Continued on next page

Table D.1 – *Continued from previous page*

Location	Sampling date	^{226}Ra (dpm/L)	s.d.	^{228}Ra (dpm/L)	s.d.	Distance from shore (km)	Depth (m)	Sample name
eg300	21/06/2010	138	6.3			8	10	yk269
eg300	21/06/2010	152	7.5			8	20	yk270
eg300	21/06/2010	128	5.8			8	30	yk271
Arugot	21/06/2010	173	8.1			0.5	0	yk272
Arugot	21/06/2010	151	7.5			1	0	yk273
Arugot	21/06/2010	159	8.0			0.1	0	yk274
Ein Feshkha	04/10/2010	156	6.9			0	0	yk316
eg300	11/10/2010	154	7.2	1.1	0.11	8	8	yk320
eg300	11/10/2010	140	6.2			8	200	yk322
eg300	11/10/2010	149	6.7			8	250	yk323
eg300	11/10/2010	164	7.6			8	280	yk324
eg300	11/10/2010	178	8.1			8	0	yk325
eg300	11/10/2010	136	6.3			8	50	yk326
eg300	11/10/2010	149	6.7			8	75	yk327
eg300	11/10/2010	148	6.8			8	150	yk328
eg300	11/10/2010	141	6.5			8	100	yk329
eg300	11/10/2010	149	6.8			8	40	yk330
eg300	11/10/2010	153	7.0			8	30	yk331
Ein Feshkha	25/01/2011	150	7.5			250	40	EFA 250 40m
eg300	04/08/2011	166	8.3	0.9	0.09	8	0	yk440
eg300	04/08/2011	138	6.9	1.3	0.13	8	28	yk441
eg300	04/08/2011	188	9.5	1.0	0.10	8	25	yk442
eg300	04/08/2011	182	9.0	1.5	0.15	8	10	yk443
eg300	04/08/2011	141	7.1	0.7	0.07	8	42	yk444

[a] ^{228}Ra measured in γ-spectrometry

Appendix E

^{226}Ra and ^{228}Ra activities in circulated Dead Sea water

Location	Sampling date	^{226}Ra (dpm/L)	s.d.	^{228}Ra (dpm/L)	s.d.	Distance from shore (km)	Depth (m)	Sample name
MAZOR2		62	7.5				55	MAZOR2-55m
EG16		92	6.4			10	12	EG16-12m
EG15	30/06/2004	75	8.3			20	20	040630EG15-20
EG17[a]	18/12/2005	52	6.2			150	37	051218EG17-37m
EG16	21/01/2008	58	4.7			10	11.5	yk7
EG16	21/01/2008	59	9.3			10	11.5	yk8
EG16[a]	21/01/2008	101	12.5	1[b]	1	10	11.5	yk9
EG22[a]	21/01/2008	39	7.5	8	0.8	80	26.5	yk13
EG22[a]	24/03/2009	60	6.6	16[b]	6.4	80	29.5	EG22-29.5m
EG21[a]	22/06/2009	79	3.95	14	1.4	80	29	yk112
EG20[a]	22/06/2009	68	3.6	27[b]	2.16	80	64	yk110A
EG21[a]	13/06/2010	73	3.6	16[c]	5.2	80	29.6	yk250
EG20[a]	13/06/2010	63	3	38	3.8	80	45.7	yk245
EG20[a]	13/06/2010	75	3.7	20	2	80	63	yk246
sinkhole in the eastern Dead Sea	16/12/2010	28	1.4	22	0.22	120		yk365
EG24	21/03/2011	96	4.8	1	0.13	5	4.5	yk401
EG24	13/06/2011	128	6.4	6	0.55	5	10	yk414
EG24	13/06/2011	133	6.7	1	0.09	5	19.5	yk415
EG23	13/06/2011	94	4.7	2	0.21	10	10	yk417
EG23	13/06/2011	103	5.2			10	14.5	yk418
EG23	13/06/2011	97	4.9	2	0.21	10	19	yk419
EG26	13/06/2011	65	3.3	25	2.5	40	30	yk421
EG26	13/06/2011	62	3.1	24	2.4	40	35	yk422

[a] Kiro et al (2012) [b] ^{228}Ra measured by γ-spectrometry [c] section 3

Bibliography

Anati D.A., Stiller M., Shasha S. and Gat J.R. (1987) Changes in the thermo-haline structure of the Dead Sea; 1979-1984. *Earth and Planetary Science Letters* **84(1)**, 109–121.

Arad A. and Michaeli A. (1967) Hydrogeological investigations in the western catchment of the Dead Sea. *Israel Journal of Earth Sciences* **16**, 181–196.

Assaf G. and Nissenbaum A. (1977) The evolution of the upper water mass of the Dead Sea, 1819–1976. In *Proc. Symp. on Desertic Terminal Lakes* (ed. D.C. Green), Utah State University, pp. 61–72.

Avrahamov N., Yechieli Y., Lazar B., Lewenberg O., Boaretto E. and Sivan O. (2010) Characterization and dating of saline groundwater in the dead sea area. *Radiocarbon* **52(2-3)**, 1123–1140.

Bartov Y., Bookman R. and Enzel Y. (2006) Current depositional environments at the Dead Sea margins as indicators of past lake levels. In *New Frontiers in Dead Sea Paleoenvironmental Research* (eds. Y. Enzel, A. Agnon and M. Stein), The Geological Society of America, pp. 127–140.

Basu A.R., Jacobsen S.B., Poreda R.J., Dowling C.B. and Aggarwal P.K. (2001) Large groundwater strontium flux to the oceans from the Bengal Basin and the marine strontium isotope record. *Science* **293**, 1470–1473.

Bokuniewicz H. (1980) Groundwater seepage into Greal South Bay, New York. *Estuarine and coastal marine science* **10**, 437–444.

Boldovski N. (1996) Ground-water flow in the coastal zone of the East-Sikhote-Alin volcanic belt. In *Groundwater discharge in the coastal zone: proceedings of an international symposium.*

Broecker W.S., Li Y.H. and Cromwell J. (1967) Radium-226 and radon-222; concentrations in Atlantic and Pacific Oceans. *Science* **158(3806)**, 1307–1311.

Broecker W.S. and Peng T.H. (1982) *Tracers in the Sea.* Eldigio Press, New York, 690 pp..

Brooks H.K. (1961) The submarine spring off Crescent Beach, Florida. *Quarterly Journal Florida Academy of Science* **24(1)**, 22–134.

Bugna G.C., Chanton J.P., Young J.E., Burnett W.C. and Cable P.H. (1996) The importance of groundwater discharge to the methane budgets of nearshore and continental shelf waters of the northeastern Gulf of Mexico. *Geochimica et Cosmochimica Acta* **60(23)**, 4735–4746.

Burnett W.C., Aggarwal P.K., Aureli A., Bokuniewicz H., Cable J.E., Charette M.a., Kontar E., Krupa S., Kulkarni K.M., Loveless A., Moore W.S., Oberdorfer J.a., Oliveira J., Ozyurt N., Povinec P., Privitera a.M.G., Rajar R., Ramessur R.T., Scholten J., Stieglitz T., Taniguchi M. and Turner J.V. (2006) Quantifying submarine groundwater discharge in the coastal zone via multiple methods. *Science of the total environment* **367(2-3)**, 498–543.

Burnett W.C. and Dulaiova H. (2003) Estimating the dynamics of groundwater input into the coastal zone via continuous radon-222 measurements. *journal of environmental radioactivity* **69(1-2)**, 21–35.

Burnett W.C. and Dulaiova H. (2006) Radon as a tracer of submarine groundwater discharge into a boat basin in Donnalucata, Sicily. *Continental Shelf Research* **26(7)**, 862–873.

Burnett W.C., Taniguchi M. and Oberdorfer J. (2001) Measurement and significance of the direct discharge of groundwater into the coastal zone. *Journal of Sea Research* **46**, 109–116.

Cable J., Burnett W., Chanton J., Corbett D. and Cable P. (1997) Field Evaluation of Seepage Meters in the Coastal Marine Environment. *Estuarine, Coastal and Shelf Science* **45(3)**, 367–375.

Cable J.E., Bugna G.C., Burnett W.C. and Chanton J.P. (1996a) Application of ^{222}Rn and CH_4 for assessment of groundwater discharge to the coastal ocean **41(6)**, 1347–1353.

Cable J.E., Burnett W.C., Chanton J.P. and Weatherly G.L. (1996b) Estimating groundwater discharge into the northeastern Gulf of Mexico using radon-222. *Earth and Planetary Science Letters* **144**, 591–604.

Capone D.G. and Bautista M.F. (1985) A groundwater source of nitrate in nearshore marine sediments. *Nature* **313**, 214–216.

Chan L.H. and Chung Y. (1987) Barium and radium in the Dead Sea. *Earth and Planetary Science Letters* **85(1-3)**, 41–53.

Charette M.A. and Sholkovitz E.R. (2002) Oxidative precipitation of groundwater-derived ferrous iron in the subterranean estuary of a coastal bay. *Geophysical Research Letters* **29(10)**, 1–4.

Charette M.A. and Sholkovitz E.R. (2006) Trace element cycling in a subterranean estuary: Part 2. Geochemistry of the pore water. *Geochimica et Cosmochimica Acta* **70**, 811–826.

Charette M.a., Splivallo R., Herbold C., Bollinger M.S. and Moore W.S. (2003) Salt marsh submarine groundwater discharge as traced by radium isotopes. *Marine Chemistry* **84(1-2)**, 113–121.

Christy A.G. and Putnis A. (1993) The kinetics of barite dissolution and precipitation in water and sodium chloride brines at 44-85°C. *Geochimica et Cosmochimica Acta* **57**, 2161–2168.

Chung Y. and Craig H. (2004) Radium redux in the Dead Sea: profiles and transient Ra/Ba models. *Earth and Planetary Science Letters* **218(3–4)**, 291–299.

Cochran J.K., Carey A.E., Sholkovitz E.R. and Surprenant L.D. (1986) The geochemistry of uranium and thorium in coastal marine sediments and sediment pore waters. *Geochimica et Cosmochimica Acta* **50**, 663–680.

Cochran J.K., Kallenberg K., Landman N.H., Harries P.J., Weinreb D., Turekian K.K., Beck A.J. and Cobban W.A. (2010) Effect of diagenesis on the Sr, O, and C isotope composition of late Cretaceous mollusks from the Western Interior Seaway of North America. *American Journal of Science* **310(2)**, 69–88.

Cooper H.H. (1959) A hypothesis concerning the dynamic balance of fresh water and salt water in a coastal aquifer. *Journal of Geophysical Research* **64**, 461–467.

Corbett D.R., Chanton J., Burnett W., Dillon K., Rutkowski C. and Fourqurean J. (1999) Patterns of groundwater discharge into Florida Bay. *Limnology and Oceanography* **44**, 1045–1055.

Davidson M.R. and Dickson B.L. (1986) A porous flow model for steady state transport of radium in

groundwater. *Water Resources Research* **22(1)**, 34–44.

Deming D., Sass J.H., Lachenbruch A.H. and De Rito R.F. (1992) Heat flow and subsurface temperature as evidence for basin-scale ground-water flow, north slope of Alaska. *Geological Society of America Bulletin* **104(5)**, 528–542.

Dowling C., Poreda R.J. and Basu A.R. (2003) The groundwater geochemistry of the Bengal Basin: weathering, chemsorption, and trace metal flux to the oceans. *Geochimica et Cosmochimica Acta* **67(12)**, 2117–2136.

Dulaiova H., Burnett W., Chanton J., Moore W., Bokuniewicz H., Charette M. and Sholkovitz E. (2006) Assessment of groundwater discharges into West Neck Bay, New York, via natural tracers. *Continental Shelf Research* **26(16)**, 1971–1983.

Dulaiova H. and Burnett W.C. (2004) An efficient method for γ -spectrometric determination of radium-226 ,228 via manganese fibers. *Limnology and Oceanography-Meth.* **2**, 256–261.

Dulaiova H., Gonneea M., Henderson P. and Charette M. (2008) Geochemical and physical sources of radon variation in a subterranean estuary – Implications for groundwater radon activities in submarine groundwater discharge studies. *Marine Chemistry* **110(1-2)**, 120–127.

Elderfield H. and Schultz A. (1996) Mid-ocean ridge hydrothermal fluxes and the chemical composition of the ocean. *Annual Review of Earth and Planetary Sciences* **24**, 291–224.

Elhatip H. (2003) The use of hydrochemical techniques to estimate the discharge of Ovacik submarine springs on the Mediterranean coast of Turkey. *Environmental Geology* **43**, 714–719.

Fanning K.A., Byrne R.H., Ii J.A.B., Betzer P.E.R., Moore W.S., Elsinger R.J. and Pyle T.E. (1981) Geothermal springs of the west Florida continental shelf: evidence for dolomitization and radionuclide enrichment. *Earth and Planetary Science Letters* **52**, 345–354.

Fischer W.A., Moxham M., Polcyn F. and Setting G. (1964) Infrared surveys of Hawaiian volcanoes. *Science* **146**, 733–741.

Gallagher D.L., Dietrich A.M., Reay W.G., Hayes M.C. and Simmons G.M. (1996) Ground water discharge of agricultural pesticides and nutrients to estuarine surface water. *Ground Water Monitoring & Remediation* **16**, 118–129.

Gallardo A.H. and Marui A. (2006) Submarine groundwater discharge: an outlook of recent advances and current knowledge. *Geo-Marine Letters* **26**, 102–113.

Garcia-Solsona E., Masqué P., Garcia-Orellana J., Rapaglia J., a.J. Beck, Cochran J., Bokuniewicz H., Zaggia L. and Collavini F. (2008) Estimating submarine groundwater discharge around Isola La Cura, northern Venice Lagoon (Italy), by using the radium quartet. *Marine Chemistry* **109(3-4)**, 292–306.

Garfunkel Z.V.I. (1981) Internal structure of the Dead Sea leaky transform (rift) in relation to plate kinematics. *Tectonophysics* **80**, 81–108.

Garrison G.H., Glenn C.R. and McMurtry G.M. (2003) Measurement of submarine groundwater discharge in Kahana Bay, O'ahu, Hawai'i. *Limnology and Oceanography* **48(2)**, 920–928.

Gascoyne M. (1992) Geochemistry of the actinides and their daughters. In *Uranium-series disequilibrium: applications to earth, marine and environmental sciences* (eds. M. Ivanovich and R. Harmon), Oxford University Press, USA, chap. 2, 2nd edn., p. 910.

Gavrieli I. (1997) Halite deposition from the Dead Sea; 1960–1993. In *The Dead Sea; the Lake and its Setting* (eds. T.M. Niemi, Z. Ben-Avraham and J.R. Gat), Oxford University Press, vol. 36, pp. 161–170.

Gavrieli I., Yechieli Y., Halicz L., Spiro B., Bein A. and Efron D. (2001) The sulfur system in anoxic subsurface brines and its implication in brine evolutionary pathways: The Ca-chloride brines in the Dead Sea area. *Earth and Planetary Science Letters* **186**, 199–213.

Giblin A.E. and Gaines A.G. (1990) Nitrogen inputs to a marine embayment: the importance of groundwater. *Biogeochemistry* **10**, 309–328.

Giffin C., Kaufman A. and Broecker W.S. (1963) Delayed coincidence counter for assay of actinon and thoron. *Journal of Geophysical Research* **68**, 1749–1757.

Gilboa G. (1963) Methods for determining radium and radon in water sources. M.sc., Technion Israel Institute of Technology, Haifa.

Gnanapragasam E.K. and Lewis B.A.G. (1995) Elastic strain energy and the distribution coefficient of radium in solid solutions with calcium salts. *Geochimica et Cosmochimica Acta* **59(24)**, 5103–5111.

Gonneea M.E., Morris P.J., Dulaiova H. and Charette M.A. (2008) New perspectives on radium behavior within a subterranean estuary. *Marine Chemistry* **109**, 250 – 267.

Goren O., Gavrieli I., Burg A. and Lazar B. (2011) Cation exchange and $CaCO_3$ dissolution during artificial recharge of effluent to a calcareous sandstone aquifer. *Journal of Hydrology* **400(1-2)**, 165–175.

Haase-Schramm A., Goldstein S.L. and Stein M. (2004) U-Th dating of Lake Lisan (late Pleistocene Dead Sea) aragonite and implications for glacial East Mediterranean climate change. *Geochimica et Cosmochimica Acta* **68(5)**, 985–1005.

Haliva A. (2004) Mineralogy, Petrography and isotopic composition of fine-grain detritial sediments of the Dead Sea. M.sc., The Hebrew University.

Haskell B.J., Engstrom D.R. and Fritz S.C. (1996) Late Quaternary paleohydrology in the North American Great Plains inferred from the geochemistry of endogenic carbonate and fossil ostracodes from Devils Lake, North Dakota, USA. *Palaeogeogr. Palaeoecol.* **124**, 179–193.

Hay A.E. (1984) Remote acoustic imaging of the plume from a submarine spring in an Arctic Fjord. *Science* **225**, 1154–1156.

Henry H.R. (1964) Effect of dispersion on salt encroachment in coastal aquifers. In *Sea water in coastal aquifers*, Water-supply paper 1613-C, pp. C70–C84.

Henry P., Lallemant S.J., Pichon X.L.E. and Lallemand S.E.N. (1989) Fluid venting along Japanese trenches: tectonic context and thermal modeling. *Tectonophysics* **160**, 277–291.

Holtzman R., Shavit U., Segal-Rozenhaimer M. and Gavrieli I. (2005) Quantifying ground water inputs along the lower Jordan River. *Ground Water* **34**, 897–906.

Hughes J.D. and Sanford W.E. (2005) SUTRA-MS a version of SUTRA modified to simulate heat and multipile-solute transport. Open-File Report 2004-1207, U.S. Geological Survey.

Hussain N., Church T.M. and Kim G. (1999) Use of ^{222}Rn and ^{226}Ra to trace groundwater discharge into the Chesapeake Bay. *Marine Chemistry* **65**, 127–134.

Hwang D.w., Lee Y.w. and Kim G. (2005) Large submarine groundwater discharge and benthic eutrophica-

tion in Bangdu Bay on volcanic Jeju Island , Korea. *Limnology and Oceanography* **50(5)**, 1393–1403.

Ichikuni M. and Musha S. (1978) Partition of strontium between gypsum and solution. *Chemical Geology* **21**, 359–363.

Johannes R.E. and Hearn C.J. (1985) The effect of submarine groundwater discharge on nutrient and salinity regimes in a coastal lagoon off Perth, western Australia. *Estuarine, Coastal and Shelf Science* **21**, 789–800.

Kaleris V., Lagas G., Marczinek S. and Piotrowski J. (2002) Modelling submarine groundwater discharge: an example from the western Baltic Sea. *Journal of Hydrology* **265(1-4)**, 76–99.

Kamermans P., Hemminga M.A., Tack J.F., Mateo M.A., Marbà N., Mtolera M., Stapel J., Verheyden A. and Daele T.V. (2002) Groundwater effects on diversity and abundance of lagoonal seagrasses in Kenya and on Zanzibar Island (East Africa). *Marine Ecology Progress Series* **231**, 75–83.

Kelly R.P. and Moran S.B. (2002) Seasonal changes in groundwater input to a well-mixed estuary estimated using radium isotopes and implications for coastal nutrient budgets. *Limnology and Oceanography* **47**, 1796–1807.

Kigoshi K. (1971) Alpha-recoil thorium-234: dissolution into water and the Uranium-234/Uranium-238 disequilibrium in nature. *Science* **173(3991)**, 47–48.

Kim G., Lee K.K., Park K.S., Hwang D.W. and Yang H.S. (2003) Large submarine groundwater discharge (SGD) from a volcanic island. *Geophysical Research Letters* **30(21)**, 2098.

Kim G., Ryu J.w. and Hwang D.w. (2008) Radium tracing of submarine groundwater discharge (SGD) and associated nutrient fluxes in a highly-permeable bed coastal zone, Korea. *Marine Chemistry* **109**, 307 – 317.

Kim G., Ryu J.W., Yang H.S. and Yun S.T. (2005) Submarine groundwater discharge (SGD) into the Yellow Sea revealed by ^{228}Ra and ^{226}Ra isotopes: implications for global silicate fluxes. *Earth and Planetary Science Letters* **237(1-2)**, 156–166.

Kiro Y. (2006) The effect of the Dead Sea level drop in the past 50 years on the groundwater system in the alluvial aquifer in its vicinity. M.sc., The Hebrew University.

Kiro Y., Yechieli Y., Lyakhovsky V., Shalev E. and Starinsky A. (2008) Time response of the water table and saltwater transition zone to a base level drop. *Water Resources Research* **44**, 1–15.

Kiro Y., Yechieli Y., Voss C.I. and Starinsky A. (2012) Modeling radium distribution in coastal aquifers during sea level changes : The Dead Sea case. *Geochimica et Cosmochimica Acta* **88**, 237–254.

Klein C. and Flohn A. (1987) Contribution to the knowledge in the fluctuations of the Dead Sea level. *Theoretical and Applied Climatology* **38**, 151–156.

Klein M. (1998) Water balance of the upper Jordan River basin. *Water International* **23(4)**, 244–248.

Klinkhammer G.P. and Palmer M.R. (1991) Uranium in the oceans: where it goes and why. *Geochimica et Cosmochimica Acta* **55**, 1799–1806.

Kolodny Y. and Kaplan I.R. (1973) Deposition of uranium in the sediment and interstitial water of an anoxic fjord. In *Proceedings of symposium on hydrogeochemistry and biogeochemistry*, The Clarke Company, Tokyo, pp. 418–442.

Krest J.M. and Harvey J.W. (2003) Using natural distributions of short-lived radium isotopes to quantify

groundwater discharge and recharge. *Limnology and Oceanography* **48(1)**, 290–298.

Krishnaswami S., Bhushan R. and Baskaran M. (1991) Radium isotopes and ^{222}Rn in shallow brines, Kharaghoda (India). *Chemical Geology* **87(2)**, 125–136.

Krishnaswami S., Graustein W.C., Turekian K.K. and Dowd J.F. (1982) Radium, Thorium and radioactive lead isotopes in groundwaters: application to the insitu determination of adsorption–desorption rate constants and retardation factors. *Water Resources Research* **6**, 1663–1675.

Kroeger K.D., Swarzenski P.W., Greenwood W.J. and Reich C. (2007) Submarine groundwater discharge to Tampa Bay: Nutrient fluxes and biogeochemistry of the coastal aquifer. *Marine Chemistry* **104(1-2)**, 85–97.

Kronfeld J., Ilani S. and Strull A. (1991) Radium precipitation and extreme ^{238}U-series disequilibrium along the Dead Sea coast, Israel. *Applied Geochemistry* **6**, 355–361.

Krumgalz B.S., Hecht A., Starinsky A. and Katz A. (2000) Thermodynamic constraints on Dead Sea evaporation: can the Dead Sea dry up? *Chemical Geology* **165(1-2)**, 1–11.

Lambert M.J. and Burnett W.C. (2003) Submarine groundwater discharge estimates at a Florida coastal site based on continuous radon measurements. *Biogeochemistry* **66(1/2)**, 55–73.

Lamontagne S., La Salle C.L., Hancock G.J., Webster I.T., Simmons C.T., Love A.J., James-Smith J., Smith A.J., Kampf J. and Fallowfield H.J. (2008) Radium and radon radioisotopes in regional groundwater, intertidal groundwater, and seawater in the Adelaide Coastal Waters Study area: Implications for the evaluation of submarine groundwater discharge. *Marine Chemistry* **109(3-4)**, 318–336.

Langevin C.D. (2003) Simulation of submarine ground water discharge to a marine estuary: Biscyne Bay, Florida. *Ground Water* **41(6)**, 758–771.

Langmuir D. and Riese A. (1985) The thermodynamic properties of radium. *Geochimica et Cosmochimica Acta* **49(7)**, 1593–1601.

Lazar B., Weinstein Y., Paytan A., Magal E., Bruce D. and Kolodny Y. (2008) Ra and Th adsorption coefficients in lakes – Lake Kinneret (Sea of Galilee) "natural experiment". *Geochimica et Cosmochimica Acta* **72**, 3446–3459.

Lee C.H. and Cheng R.T.S. (1974) On seawater encroachment in coastal aquifers. *Water Resources Research* **10(5)**, 1039–1043.

Lee D.R. (1977) A device for measuring seepage flux in lakes and estuaries. *Limnology and Oceanography* **22**, 140–147.

Lensky N.G., Dvorkin Y., Lyakhovsky V., Gertman I. and Gavrieli I. (2005) Water, salt, and energy balances of the Dead Sea. *Water Resources Research* **41**, W12418.

Lewis J.B. (1987) Measurements of groundwater seepage flux onto a coral reef: spatial and temporal variations. *Limnology and Oceanography* **32(5)**, 1165–1169.

Li L., Barry D.A., Stagnitti F. and Parlange J.U. (1999) Submarine groundwater discharge and associated chemical input into a coastal sea. *Water Resources Research* **35**, 3253–3259.

Li Y.H. and Chan L.H. (1979) Desorption of Ba and ^{226}Ra from river-borne sediments in the Hudson Estuary. *Earth and Planetary Science Letters* **43**, 343–350.

Longuet-Higgins M. (1983) Wave set-up, percolation and undertow in the surf zone. *Proceedings of the royal society A* **390**, 283–291.

Marine I.W. (1979) The use of naturally occurring helium to estimate groundwater velocities for studies of geologic storage of radioactive waste. *Water Resources Research* **15(5)**, 1130–1136.

Martin J.B., Cable J.E., Smith C., Roy M. and Cherrier J. (2007) Magnitudes of submarine groundwater discharge from marine and terrestrial sources: Indian River Lagoon, Florida. *Water Resources Research* **43(5)**, W05440.

Mathieu G., Biscaye P., Lupton R. and Hammond D. (1988) System for measurement of ^{222}Rn at low levels in natural waters. *Health Physics* **55(6)**, 989–992.

Matmon D. (1995) Simulations of groundwater flow between the Mediterranean Sea and the Jordan Rift Valley. M.sc., The Hebrew University.

Mazor E. (1962) Radon and radium content of some Israeli water sources and a hypothesis on underground reservoirs of brines, oils and gases in the Rift Valley. *Geochimica et Cosmochimica Acta* **26**, 765–786.

Michael H.A., Mulligan A.E. and Harvey C.F. (2005) Seasonal oscillations in water exchange between aquifers and the coastal ocean. *Nature* **436**, 1145–1148.

Moise T., Starinsky A., Katz A. and Kolodny Y. (2000) Ra isotopes and Rn in brines and ground waters of the Jordan-Dead Sea Rift Valley: enrichment, retardation, and mixing. *Geochimica et Cosmochimica Acta* **64**, 2371–2388.

Mook W.G. (1980) Carbon-14 in hydrogeological studies. In *Handbook of environmental isotope geochemistry* (eds. P. Fritz and J.C. Fontes), Elsevier Scientific Publishers, pp. 49–74.

Moore W.S. (1996) Large groundwater inputs to coastal waters revealed by ^{226}Ra enrichments. *Nature* **380**, 612–614.

Moore W.S. (1999) The subterranean estuary: a reaction zone of ground water and sea water. *Marine Chemistry* **65**, 111–125.

Moore W.S. (2000) Determining coastal mixing rates using radium isotopes. *Continental Shelf Research* **20**, 1993–2007.

Moore W.S. (2003) Sources and fluxes of submarine groundwater discharge delineated by radium isotopes. *Biogeochemistry* **66(1/2)**, 75–93.

Moore W.S. (2006) Radium isotopes as tracers of submarine groundwater discharge in Sicily. *Continental Shelf Research* **26(7)**, 852–861.

Moore W.S. (2008) Fifteen years experience in measuring ^{224}Ra and ^{223}Ra by delayed-coincidence counting. *Marine Chemistry* **109**, 188–197.

Moore W.S. and Arnold R. (1996) Measurement of ^{223}Ra and ^{224}Ra in coastal waters using a delayed coincidence counter. *Journal of Geophysical Research* **101(1)**, 1321–1329.

Moore W.S., Sarmiento J.L. and Key R.M. (2008) Submarine groundwater discharge revealed by ^{228}Ra distribution in the upper Atlantic Ocean. *Nature geoscience* **1(5)**, 309–311.

Mulligan A.E. and Charette M.A. (2006) Intercomparison of submarine groundwater discharge estimates from a sandy unconfined aquifer. *journal of hydrology* **327(3-4)**, 411–425.

Neumann J. (1958) Tentative energy and water balances for the Dead Sea. *Bulletin of the Research Council of Israel* **7G**, 137–163.

Oliveira J., Burnett W.C., Mazzilli B.P., Braga E.S., Farias L.a., Christoff J. and Furtado V.V. (2003) Reconnaissance of submarine groundwater discharge at Ubatuba coast, Brazil, using ^{222}Rn as a natural tracer. *Journal of environmental radioactivity* **69(1-2)**, 37–52.

Ollivier P., Claude C., Radakovitch O. and Hamelin B. (2008) TIMS measurements of ^{226}Ra and ^{228}Ra in the Gulf of Lion, an attempt to quantify submarine groundwater discharge. *Marine Chemistry* **109**, 337 – 354.

Oren A. (1999) Microbiological studies in the Dead Sea: future challenges toward the understanding of life at the limit of salt concentrations. *Hydrobiologia* **405**, 1–9.

Piekarek-Jankowska H. (1995) Hydrochemical effects of submarine groundwater discharge to the Puck Bay (southern Baltic Sea, Poland). *Geographia Polonica* **67**, 103–120.

Plummer L.N., Michel R.L., Thurman E.M. and Glynn P.D. (1993) Environmental tracers for age dating young ground water. In *Regional ground-water quality* (ed. W.L. Alley), Van Nostrand Reinhold, New York, pp. 255–294.

Porcelli D. and Swarzenski P.W. (2003) The behavior of U- and Th-series nuclides in groundwater. In *uranium-series geochemistry* (eds. B. Bourdon, G.M. Henderson, C.C. Lundstorm and S.P. Turner), The Mineralogical society of America, Washington, chap. 8, pp. 317–361.

Povinec P.P., Bokuniewicz H., Burnett W.C., Cable J., Charette M., Comanducci J., Kontar E.A., Moore W.S., Oberdorfer J.A., Oliveira J.D., Peterson R., Stieglitz T. and Taniguchi M. (2008) Isotope tracing of submarine groundwater discharge offshore Ubatuba, Brazil: results of the IAEA – UNESCO SGD project. *Jouranl of Environmental Radiouactivity* **99**, 1596–1610.

Rama and Moore W.S. (1984) Mechanism of transport of U-Th series radioisotopes solids into ground water. *Geochimica et Cosmochimica Acta* **48(2)**, 395–399.

Rama and Moore W.S. (1996) Using the radium quartet evaluating groundwater input and water exchange in salt marshes. *Geochimica et Cosmochimica Acta* **60(23)**, 4645–4652.

Rasmussen L.L. (1998) Groundwater flow, tidal mixing and haline convection in coastal sediment. M.sc., Florida State University.

Reay W.G., Gallagher D.L. and Simmons G.M. (1992) Groundwater discharge and its impact on surface water quality in a Chesapeake Bay inlet. *Water Resources Bulletin* **28(6)**, 1121–1134.

Reimers C.E., Stecher III H.A., Taghon G.L., Fuller C.M., Huettel M., Rusch A., Ryckelynck N. and Wild C. (2004) In situ measurements of advective solute transport in permeable shelf sands. *Continental Shelf Research* **24(2)**, 183–201.

Reznik I.J., Gavrieli I., Antler G. and Ganor J. (2011) Kinetics of gypsum crystal growth from high ionic strength solutions: A case study of Dead Sea – seawater mixtures. *Geochimica et Cosmochimica Acta* **75(8)**, 2187–2199.

Reznik I.J., Gavrieli I. and Ganor J. (2009) Kinetics of gypsum nucleation and crystal growth from Dead Sea brine. *Geochimica et Cosmochimica Acta* **73(20)**, 6218–6230.

Robinson C., Gibbes B. and Li L. (2006) Driving mechanisms for groundwater flow and salt transport in a

subterranean estuary. *Geophysical Research Letters* **33(L03402)**, 1–4.

Robinson M., Gallagher D. and Reay W. (1998) Field observations of tidal and seasonal variations in ground water discharge to tidal estuarine surface water. *Ground Water Monitoring & Remediation* **18**, 83–92.

Robinson M.A. (1996) A finite element model of submarine ground water discharge to tidal estuarine waters. Ph.d, Virginia Polytechnic Institute.

Rosenberg Y.O., Metz V. and Ganor J. (2011) Co-precipitation of radium in high ionic strength systems: 1. Thermodynamic properties of the Na-Ra-Cl-SO_4-H_2O system – Estimating Pitzer parameters for $RaCl_2$. *Geochimica et Cosmochimica Acta* **75(19)**, 5389–5402.

Roy M., Martin J.B., Smith C.G. and Cable J.E. (2011) Reactive-transport modeling of iron diagenesis and associated organic carbon remineralization in a Florida (USA) subterranean estuary. *Earth and Planetary Science Letters* **304(1-2)**, 191–201.

Salameh E. (1996) *Water quality degradation in Jordan*. Friedrich Ebert Stiftung and Royal Society for the Conservation of Nature, Amman, 179 pp..

Salameh E. and El-Naser H. (1999) Does the actual drop in Dead Sea level reflect the development of water sources within its drainage basin? *Acta Hydrochimica Et Hydrobiologica* **27**, 5–11.

Sanders C.J., Santos I.R., Barcellos R. and Silva Filho E.V. (2012) Elevated concentrations of dissolved Ba, Fe and Mn in a mangrove subterranean estuary: consequence of sea level rise? *Continental Shelf Research* **43**, 86–94.

Schwartz M. (2003) Significant groundwater input to a coastal plain estuary: assessment from excess radon. *Estuarine, Coastal and Shelf Science* **56(1)**, 31–42.

Sellinger C.E. (1995) Groundwater flux into a portion of eastern Lake Michigan. *Journal of great lakes research* **21(1)**, 53–63.

Shaban A., Khawlie M., Abdallah C. and Faour G. (2005) Geologic controls of submarine groundwater discharge: application of remote sensing to north Lebanon. *Environmental Geology* **47**, 512–522.

Shalev E., Lyakhovsky V. and Yechieli Y. (2007) Is advective heat transport significant at the Dead Sea basin? *Geofluids* **1**, 292–300.

Shalev E. and Yechieli Y. (2007) The effect of Dead Sea level fluctuations on the discharge of thermal springs. *Israel Journal of Earth Sciences* **56**, 19–27.

Shaw T.J., Moore W.S., Kloepfer J. and Sochaski M.A. (1998) The flux of barium to the coastal waters of the southeastern USA: The importance of submarine groundwater discharge. *Geochimica et Cosmochimica Acta* **62(18)**, 3047–3054.

Shellenbarger G.G., Monismith S.G., Genin A. and Paytan A. (2006) The importance of submarine groundwater discharge to the nearshore nutrient supply in the Gulf of Aqaba (Israel). *Limnology and Oceanography* **51(4)**, 1876–1886.

Simmons G.M. (1992) Importance of submarine groundwater discharge (SGWD) and seawater cycling to the material flux across sediment/water interfaces in marine environments. *Marine Ecology. Progress Series* **84**, 173–184.

Sivan O., Yechieli Y., Herut B. and Lazar B. (2005) Geochemical evolution and timescale of seawater intrusion

into the coastal aquifer of Israel. *Geochimica et Cosmochimica Acta* **69(3)**, 579–592.

Smith A.J. (2004) Mixed convection and density-dependent seawater circulation in coastal aquifers. *Water Resources Research* **40(W08309)**, 1–16.

Snyder M., Taillefert M. and Ruppel C. (2004) Redox zonation at the saline-influenced boundaries of a permeable surficial aquifer: effects of physical forcing on the biogeochemical cycling of iron and manganese. *Journal of Hydrology* **296(1-4)**, 164–178.

Somayajulu B.L.K. and Rengarajan R. (1987) Ra-228 in the Dead-Sea. *Earth and Planetary Science Letters* **85(1–3)**, 54–58.

Stanhill G. (1994) Changes in the rate of evaporation from the Dead SEa. *International Journal of climatology* **14**, 465–471.

Starinsky A. (1974) Interaction between calcium chloride brines and sedimentary rocks. Ph.d, The Hebrew University, Jerusalem.

Stein M. (2001) The sedimentary and geochemical record of Neogene-Quaternary water bodies in the Dead Sea basin – inferences for the regional paleoclimatic history. *Journal of Paleolimnology* **21**, 271–282.

Stein M., Starinsky A., Agnon A., Katz A., Raab M., Spiro B. and Zak I. (2000) The impact of brine–rock interaction during marine evaporite formation on the isotopic Sr record in the oceans: evidence from Mt. Sedom, Israel. *Geochimica et Cosmochimica Acta* **64(12)**, 2039–2053.

Stein M., Starinsky A., Katz A., Goldstein S.L., Machlus M. and Schramm A. (1997) Stontium isotopic, chemical, and sedimentological evidence for the evolution of Lake Lisan and the Dead Sea. *Geochimica et Cosmochimica Acta* **61(18)**, 3975–3992.

Steinhorn I. (1985) The disappearance of the long-term meromictic stratification of the Dead Sea. *Limnology and Oceanography* **30(3)**, 451–472.

Steinhorn I., Assaf G., Gat. J.R., Nishri A., Nissenbaum A., Stiller M., Beyth M., Neev D., Garber R., Friedman G.M. and Weiss W. (1979) The Dead Sea: deepening of the mixolimnion signifies the overture to overturn of the water column. *Science* **206**, 55–56.

Stern O. (2010) Geochemistry, hydrology and paleo-hydrology of Ein Qedem spring system. M.sc., The Hebrew University, Jerusalem.

Stiller M. and Chung Y. (1984) Radium in the Dead Sea: A possible tracer for the duration of meromixis. *Limnology and Oceanography* **29(3)**, 574–586.

Sturchio N. (2001) Radium geochemistry of ground waters in Paleozoic carbonate aquifers, midcontinent, USA. *Applied Geochemistry* **16(1)**, 109–122.

Swarzenski P.W., Burnett W.C., Greenwood W.J., Herut B., Peterson R., Dimova N., Shalem Y., Yechieli Y. and Weinstein Y. (2006) Combined time-series resistivity and geochemical tracer techniques to examine submarine groundwater discharge at Dor Beach, Israel. *Geophysical Research Letters* **33**, 1–6.

Swarzenski P.W., Reich C., Kroeger K.D. and Baskaran M. (2007) Ra and Rn isotopes as natural tracers of submarine groundwater discharge in Tampa Bay, Florida. *Marine Chemistry* **104(1-2)**, 69–84.

Taniguchi M. (2000) Submarine groundwater discharge in Osaka Bay, Japan. In *Proceedings of the Japan Association of Hydrology and Water Resources*, Kyoto, pp. 186–187.

Taniguchi M., Burnett W.C., Cable J.E. and Turner J.V. (2002) Investigation of submarine groundwater discharge. *Hydrological Processes* **16**, 2115– 2129.

Taniguchi M., Burnett W.C., Dulaiova H., Kontar E.a., Povinec P.P. and Moore W.S. (2006) Submarine groundwater discharge measured by seepage meters in sicilian coastal waters. *Continental Shelf Research* **26(7)**, 835–842.

Taniguchi M., Burnett W.C., Smith C.F., Paulsen R.J., O'rourke D., Krupa S. and Christoff J.L. (2003a) Spatial and temporal distributions of submarine groundwater discharge rates obtained from various types of seepage meters at a site in the northeastern Gulf of Mexico. *Biogeochemistry* **66**, 35–53.

Taniguchi M., Ishitobi T., Chen J., Onodera S., Miyaoka K., Burnett W.C., Peterson R., Liu G. and Fukushima Y. (2008) Submarine groundwater discharge from the Yellow River Delta to the Bohai Sea, China. *Journal of Geophysical Research – Oceans* **113(C06025)**, 1–11.

Taniguchi M., Ishitobi T. and Saeki K. (2005) Evaluation of time-space distributions of submarine ground water discharge. *Ground water* **43(3)**, 336–342.

Taniguchi M. and Iwakawa H. (2004) Submarine groundwater discharge in Osaka Bay, Japan. *Limnology* **5(1)**, 25–32.

Taniguchi M., Sakura Y. and Ishii T. (1998) Estimations of saltwater–fresh water interfaces and groundwater discharge rates in coastal zones from borehole temperature data. In *Proceeding of Japanese Association of Groundwater Hydrology Meeting*, Tokyo, pp. 86–89.

Taniguchi M., Turner J.V. and Smith A.J. (2003b) Evaluations of groundwater discharge rates from subsurface temperature in Cockburn Sound, western Australia. *Biogeochemistry* **66(1/2)**, 111–124.

Tricca A., Wasserburg G.J., Porcelli D. and Baskaran M. (2001) The transport of U- and Th-series nuclides in a sandy unconfined aquifer. *Geochimica et Cosmochimica Acta* **65(8)**, 1187–1210.

Tsunogai U., Ishibashi J., Wakita H., Gamo T., Masuzawa T., Nakatsuka T., Nojiri Y. and Nakamura T. (1996) Fresh water seepage and pore water recycling on the seafloor: Sagami Trough subduction zone, Japan. *Earth and Planetary Science Letters* **138(1-4)**, 157–168.

Turner A. (1996) Trace-metal partitioning in estuaries: importance of salinity and particle concentration. *Marine Chemistry* **54(96)**, 27–39.

Uchiyama Y., Nadaoka K., Rke P., Adachi K. and Yagi H. (2000) Submarine groundwater discharge into the sea and associated nutrient transport in a sandy beach. *Water Resources Research* **36(6)**, 1467–1479.

Valiela I., Costa J., Foreman K., Teal J.M., Howes B. and Aubrey D. (1990) Transport of groundwater-borne nutrients from watersheds and their effects on coastal waters. *Biogeochemistry* **10**, 177–197.

Vanek V. and Lee D.R. (2012) Mapping submarine groundwater discharge areas- an example from Laholm Bay, southwest Sweden. *Limnology and Oceanography* **36(6)**, 1250–1262.

Vengosh A., Hirschfeld D., Vinson D., Dwyer G., Raanan H., Rimawi O., Al-zoubi A., Akkawi E., Marie A., Haquin G., Zaarur S., Ganor J., Hirschfeld D., Vinson D., Dwyer G., Raanan H. and Rimawi O. (2009) High Naturally Occurring Radioactivity in Fossil Groundwater from the Middle East High Naturally Occurring Radioactivity in Fossil Groundwater from the Middle East. *Environmental Science & Technology* **43**, 1769–1775.

Voss C.I. (1984) SUTRA: Finite-element simulation model for saturated-unsaturated, fluid-density-

dependent groundwater flow with energy transport or chemically-reactive single-species solute transport. Water-Resources Investigation Report 84-4369, U.S. Geological Survey.

Webb J. and Theodor J. (1972) Wave-induced circulation in submerged sands. *Journal of the marine biological association of the United Kingdom* **52**, 903–914.

Webster I.T., Hancock G.J. and Murray A.S. (1995) Modelling the effect of salinity on radium desorption from sediments. *Geochimica et Cosmochimica Acta* **59(12)**, 2469–2476.

Weinstein Y., Burnett W.C., Swarzenski P.W., Shalem Y., Yechieli Y. and Herut B. (2007a) Role of aquifer heterogeneity in fresh groundwater discharge and seawater recycling: An example from the Carmel Coast, Israel. *Journal of Geophysical Research* **112(C12016)**, 1–12.

Weinstein Y., Shalem Y., Burnett W.C., Swarzenski P.W. and Herut B. (2007b) Temporal variability of submarine groundwater discharge: assessments via radon and seep meters ,the southern Carmel Coast, Israel. In *A new focus on groundwater–seawater interactions*, IAHS-AISH publication, pp. 125–133.

Whiting G.J. and Childers D.L. (1989) Subtidal advective water flux as a potentially important nutrient input to southeastern U.S.A.saltmarsh estuaries. *Estuarine, Coastal and Shelf Science* **28**, 417–431.

Windom H. and Niencheski F. (2003) Biogeochemical processes in a freshwater-seawater mixing zone in permeable sediments along the coast of Southern Brazil. *Marine Chemistry* **83(3-4)**, 121–130.

Windom H.L., Moore W.S., Niencheski L.F.H. and Jahnke R.A. (2006) Submarine groundwater discharge: A large, previously unrecognized source of dissolved iron to the South Atlantic Ocean. *Marine Chemistry* **102**, 252 – 266.

Yechieli Y. (2000) Fresh–saline groundwater interface in the western Dead Sea area. *Ground Water* **38(4)**, 615–623.

Yechieli Y., Gavrieli I., Berkowitz B. and Ronen D. (1998) Will the Dead Sea die? *Geology* **26(8)**, 755–758.

Yechieli Y., Kafri U. and Sivan O. (2009) The inter-relationship between coastal sub-aquifers and the Mediterranean Sea, deduced from radioactive isotopes analysis. *Hydrogeology Journal* **17(2)**, 265–274.

Yechieli Y., Ronen D., Berkovitz B., Dershowitz W. and Hadad A. (1995) Aquifer characteristics derived from the interaction between water levels of a terminal lake (Dead Sea) and an adjacent aquifer. *Water Resources Research* **31**, 893–902.

Yechieli Y., Ronen D. and Kaufman A. (1996) The source and age of groundwater brines in the Dead Sea area, as deduced from ^{36}Cl and ^{14}C. *Geochimica et Cosmochimica Acta* **60**, 1909–1916.

Yechieli Y., Shalev E. and Hemo H. (2007a) Geochemical monitoring of groundwater in borholes in the Dead Sea region – sinkholes project. Trgsi/18/2007, Geological Survey of Israel, Jerusalem.

Yechieli Y., Shalev E. and Hemo H. (2007b) Groundwater levels in boreholes in the Dead Sea region – sinkholes project. Trgsi/09/2007, Geological Survey of Israel, Jerusalem.

Zilberman-Kron T. (2008) The origin and geochemical evolution of brines in the sinkholes along the Dead Sea coast. M.sc., The Hebrew University.

Zimmermann C.F., Montgomery J.R. and Carlson P.R. (1985) Variability of dissolved reactive phosphate flux rates in nearshore estuarine sediments: effects of groundwater flow. *Estuaries* **8**, 228–236.

המלח לא השתנה לפחות 10,000 שנה.

ההתנהגות ההפוכה של ^{226}Ra ו ^{228}Ra במהלך הצירקולציה של מי ים המלח באקוויפר, בה ^{226}Ra מסולק ו ^{228}Ra נתרם למי האגם, מהווה שיטה חדשנית ואמינה להערכת הספיקה של הצירקולציה באקוויפר. מאזן המסה הכולל את שני האיזוטופים הללו מאפשר חישוב של הנפח השנתי של הצירקולציה של מי ים המלח באקוויפר (320 מלמ״ש או ~2 מיליון מ״ק לק״מ חוף). נפח זה הינו משמעותי ויכול להשפיע באופן ניכר על ריכוזי יסודות קורט בים המלח. העובדה שנפח הצירקולציה יכול להגיע לערך כה גבוה, מצביעה על החשיבות הפוטנציאלית של התהליך למאזני מסה של יסודות מסויימים, באגמים מלוחים ובאוקיינוס.

הסדר של קבועי הקצב של הסילוק או התרומה של היסודות השונים בריאקציות הגיאוכימיות הוא:

$$k_{SO_4} > k_U > k_{Ba} = k_{Sr} = k_{Ra} > k_{Mn} > k_{Fe}$$.

לאיזוטופים קצרי החיים של רדיום (223 ו 224) ו ^{222}Rn זמן מחצית חיים של מספר ימים כך שהם מגיעים לשיווי משקל עם הסדימנט תוך מספר שבועות. ריכוזי האיזוטופים קצרי החיים של רדיום באקוויפר עולים עם המליחות באופן לא לינארי, בעוד שהקשר בין הרדון למליחות מבוטא ע"י פולינום ממעלה שנייה כאשר האקטיביות המקסימלית של רדון (~2500 התפרקויות לדקה) נמצאת באמצע טווח המליחויות. הקשר בין המליחות לאיזוטופים קצרי החיים מתקבל ע"י קשר לינארי בין מקדם הספיחה (*K*) לבין המליחות. בעוד שהאיזוטופים קצרי החיים של רדיום מהווים מדד לקשר בין המליחות והספיחה בלבד, הקשר הלינארי בין המליחות לאיזוטופ ארוך החיים של הרדיום (^{226}Ra), יחד עם ירידת המפלס המתמשכת של ים המלח, מכתיבים את הערך של *K*.

על מנת להבין את ההתנהגות של האיזוטופים של רדיום במערכת מי תהום חופית, הורצו סימולציות במודל זרימה המונעת ע"י שינויים בצפיפויות ואשר ניתן להריץ בו מספר מומסים (SUTRA-MS). המודל חישב את התפוצה של האיזוטופים השונים של רדיום בזמן ובמרחב בתנאים של ירידת המפלס של ים המלח. ההשפעה של *K* על האיזוטופים השונים של רדיום מושפעת מזמן מחצית החיים באופן בו האיזוטופים קצרי החיים אינם מושפעים כלל מהערך של K בעוד שהתגובה של האיזוטופ ארוך החיים, ^{226}Ra, מעוכבת כאשר מקדם העיכוב (*R=K+1*) גדול. הקשר הלינארי בין ^{226}Ra למליחות מחייב תגובה מהירה של ^{226}Ra לירידת המפלס של ים המלח ולכן הוא מהווה אילוץ לגבי הערך המוחלט של *K*. מהסימולציות מתקבל כי הערך המקסימלי של *K* במים המלוחים הוא 0.6 ולפי הקשר בין המליחות לאיזוטופים קצרי החיים מתקבל כי הערך המקסימלי של *K* במים המתוקים הוא 100. ערכים אלו לא יכולים לגרום לירידה המשמעותית של ^{226}Ra בין מי ים המלח באגם ובאקוויפר ולכן הסימולציות תומכות במסקנה כי ^{226}Ra מסולק ע"י שקיעת בריט או צלסטין.

בהשוואה למחקרים אחרים ולמי תהום במקומות אחרים באזור ים המלח (לדוגמא עין פשחה), מקדם הספיחה (*K*) המתקבל במים המתוקים במחקר זה נמוך יותר. גורמים רבים משפיעים על הערך של *K*, כגון מצב חימצון חיזור, ריכוז תחמוצות ברזל ומנגן ומליחות המים. הערך של *K* תלוי במקום שבו נעשתה המדידה (במעבדה או בשדה). ברב המחקרים ההערכות נעשו לפי מדידות במעבדה שבהן הערך של *K* לעיתים קרובות גבוה יותר מזה הנמדד בשדה. המחקר הנוכחי מראה כי טווח הערכים של *K* של רדיום בטבע הוא ככל הנראה גדול יותר מזה שנקבע במחקרים קודמים.

סקר מפורט של מקורות הרדיום לים המלח מראה כי ההרכב האיזוטופי של רדיום במי התהום מושפע מיחס אורניום לתוריום בסדימנטים השונים, גיל המים ומנגנון הזרימה. יחס $^{226}Ra/^{223}Ra$ נמצא במספר מעיינות סביב ים המלח (עין פשחה, עין קדם ומי התהום בצד המזרחי של ים המלח) בשיווי משקל סקולרי (21) ומרמז על כך שמערכת מי התהום סביב ים

תקציר מורחב

צירקולציה של מי ים באקוויפר חופי הוא מרכיב עיקרי בספיקות תת ימיות. תהליך זה נחשב היום כתהליך חשוב המשפיע על ריכוזי יסודות קורט ונוטריינטים באזורים חופיים. הערכות של ספיקות תת ימיות נעות על כמה סדרי גודל (10^6–1 מ״ק/שנה למטר חוף). ההערכות השונות רגישות ליחסי המים המתוקים והמלוחים, ולקני המידה של הצירקולציה בזמן ובמרחב. צירקולציה של מי ים באקוויפר יכולה להיות מונעת ע״י גלים וגיאות ושפל (מנגנון קצר טווח), ע״י שינויים עונתיים במפלס האוקיינוס או במערכת מי התהום (מנגנון בקנה מידה עונתי) או ע״י הפרש הצפיפויות בין המים המלוחים למתוקים וערבוב דיספרסיבי בין גופי המים המתוקים והמלוחים (מנגנון ארוך טווח). באוקיינוס, רוב המנגנונים מתרחשים ביחד ולכן קשה להבחין במדידה של ספיקות תת ימיות, בתרומה ובהשפעה של המנגנונים השונים.

במחקר זה, ים המלח משמש מעבדה טבעית ללימוד צירקולציה ארוכת טווח בגלל העדר מנגנוני הצירקולציה האחרים המונעים ע״י גיאות ושפל וגלים. במהלך צירקולציה של מי ים המלח באקוויפר האלוביאלי, מתרחשים מספר תהליכים גיאוכימיים בקצבים שונים, החל מתהליכים מהירים יחסית של ספיחה ושחרור ועד לתהליכים איטיים של המסה והשקעת של מינרלים. קיימת חשיבות רבה לקשר בין סקלת הזמן של הצירקולציה ושל התהליך הגיאוכימי בזמן האינטראקציה בין המים לסלע. לתהליך בו זמן שהות ארוך של מי האגם באקוויפר, יש פוטנציאל רב יותר לשנות את הרכב המים.

מעקב אחרי יחסי נתרן לכלור היורדים במי האגם בעשרות השנים האחרונות בגלל שקיעת הליט מאפשר הערכה של מהירות כניסת מי ים המלח לאקוויפר. גם ריכוז ה ^{228}Ra עולה עם הזמן במים שבאקוויפר. מי ים המלח חודרים לאקוויפר עם אקטיביות נמוכה של ^{228}Ra (~1 התפרקויות לדקה) ומקבלים ^{228}Ra מהסדימנטים של האקוויפר עד שהאקטיביות מגיעה לערך של שיווי משקל סקולרי (~27 התפרקויות לדקה). מקצב ההצטברות של ^{228}Ra ניתן להעריך את מהירות חדירת מי ים המלח לתוך האקוויפר (1 – 6 מטר לשנה).

למרות שמי ים המלח במצב של על רוויה לבריט ($\Omega \cong 12$) וצלסטין ($\Omega \cong 2.5$), מינרלים אלו אינם שוקעים בו. לעומת זאת, במהלך הצירקולציה של מי ים המלח באקוויפר, ריכוזי היסודות השונים מעידים על כך שמינרלים אלו שוקעים בעקבות המגע עם הסדימנט. ריכוז הבריום יורד מ 5 ל 1.5 מ״ג בליטר, ריכוז הסטרונציום יורד מ 350 ל 300 מ״ג בליטר וריכוז ^{226}Ra יורד מ 145 ל 60 התפרקויות לדקה לליטר. ירידה בריכוז האורניום באה לעיתים קרובות באסוציאציה עם עליה בריכוזי המנגן והברזל בגלל תנאים מחזרים. במי ים המלח שבאקוויפר ריכוז האורניום יורד מ 2.4 ל 0.1 מיקרוגרם לליטר בעוד שריכוז הברזל עולה מ 1 ל 13 מ״ג לליטר וריכוז המנגן עולה מ 7 ל 9 מ״ג לליטר.

קצבי הריאקציות הגיאוכימיות (שקיעת בריט וגבס וריאקציות המונעות ע״י חימצון-חיזור) במהלך האינטרקציה בין מי ים המלח לסלעי האקוויפר הוערכו על בסיס מהירות הזרימה של המים המלוחים (ע״י מאזן מסה חד ממדי) לאורך קו הזרימה שלהם מן הים לתוך האקוויפר.

משרד האנרגיה והמים
המכון הגיאולוגי

יחסי גומלין בין ים המלח לאקוויפר – תובנות ממערכת הרדיום

יעל קירו

עבודה זו הוגשה כחיבור לקבלת תואר "דוקטור לפילוסופיה" לסינאט האוניברסיטה העברית, ירושלים

העבודה נעשתה בהדרכתם של:
פרופ' אברהם סטרינסקי, המכון למדעי כדור הארץ, האוניברסיטה העברית, ירושלים
דר' יוסף יחיאלי, המכון הגיאולוגי, ירושלים
דר' ישי וינשטיין, המחלקה לגיאוגרפיה וסביבה, אוניברסיטת בר-אילן, רמת-גן

דוח מס' GSI/10/2013 ירושלים, תמוז תשע"ג, יוני 2013